MOLECULAR MODELING AND ATOMISTIC SIMULATIONS OF THE STRUCTURAL AND OPTICAL PROPERTIES OF POLYCARBONATES

Thesis submitted to the

UNIVERSITY OF PUNE

for the degree of

DOCTOR OF PHILOSOPHY

in

CHEMISTRY

by

M. S. Sulatha

Division of Polymer Chemistry

National Chemical Laboratory

PUNE - 411 008

INDIA

December 2004

CONTENTS

Chapter 7: Atomistic Simulations of the Orientational Birefringence of Polycarbonates in the Glassy State

ABSTRACT

This thesis presents molecular modeling and atomistic simulations studies of a series of polycarbonates. A systematic investigation of the conformational features of the repeat units, the single chains and the bulk amorphous glassy state of these polymers is presented. Optical properties of these polycarbonates such as the polarizability, optical anisotropy and birefringence and a new understanding of their relationship with chemical structure constitute the focus of this study.

Conformational analysis of the bisphenyl and carbonate fragments of bisphenol A polycarbonate (BPAPC) and four structurally modified polycarbonates, (i) polycarbonate based on 1,1'-bis(4-hydroxyphenyl)cyclohexane, BPCPC; (ii) polycarbonate based on 1,1'-bis(4-hydroxyphenyl)-3,3,5-trimethylcyclohexane, TMCPC; (iii) polycarbonate based on 1,1'-bis(3-methyl-4-hydroxyphenyl)cyclohexane, DMBPC; and (iv) dimethyl bisphenol polycarbonate, DMPC, have been performed to study structure at the segmental level (repeating unit). The presence of a cylcohexyl group at the C_α carbon leads to heterogeneity of the phenyl rings of the bisphenyl fragment. The equatorial phenyl ring undergoes unrestricted rotations as in the case of BPAPC, where as for the axial phenyl ring, rotational mobility is hindered due to 1,3-diaxial interactions. The cyclohexyl substituent does not have a major influence on the conformational characteristics of the carbonate group. The conformational characteristics about the C_α carbon remains almost similar irrespective of *ortho* methyl substituents on the phenyl rings, but interacts strongly with the carbonate group resulting in almost perpendicular orientation of the phenyl rings with respect to the carbonate group. RIS models were formulated for all the five polycarbonates. The averaged chain dimensions, $\langle R^2\rangle/M$, $\langle S^2\rangle/M$, C_n, of substituted polycarbonates are found to be lower than that of BPAPC.

An extension of the valence optical scheme-rotational isomeric state method (VOS-RIS) applicable to calculation of polarizability tensors and optical anisotropy (γ^2) of molecular fragments constituting substituted polycarbonate chains is presented. The theoretical approach utilizes experimentally derived anisotropic polarizability tensors of molecular groups in order to be able to account for induction effects and interdependence of backbone conformational states. Presence of a cyclohexylidene group at the bisphenyl C_α carbon significantly lowers γ^2 due to the low intrinsic polarizability of the cycloaliphatic

substituent and due to the conformational states of backbone phenylene rings. Optical anisotropy of the bisphenyl containing methyl substituents on phenyl rings is lower than the value for the unsubstituted bisphenyl. Among the structures investigated here, the repeat unit containing cyclohexylidene group at C_α and methyl groups on phenylene rings, leads to the polycarbonate that shows the lowest optical anisotropy. Quantitatively, cyclohexylidene at C_α is more effective in lowering the optical anisotropy than methyl groups on backbone phenylene rings. Calculated $\langle\gamma^2\rangle/x$ of the repeat units follows a linear behavior with respect to experimentally observed stress-optical coefficient of these polycarbonates in the melt (C_m). Calculated $\langle\gamma^2\rangle/x$ of these structurally modified polycarbonate chains are all lower than that of BPAPC, and the relative trend in $\langle\gamma^2\rangle/x$ is similar to that observed for C_m and C_g (glassy state) from experiments in literature. A detailed understanding of structure-property relationship is provided.

Ab initio geometry optimizations of bisphenyl and carbonate fragments corresponding to BPAPC and four structurally modified polycarbonates were performed. Optimized geometries were then used to calculate the polarizabilities of these molecules. Calculations did not take into account the solvent effect and the absolute values of the derived mean-squared optical anisotropy of DPP and DPC were much higher than the condensed phase experimental values. Optical anisotropy of the different bisphenyl fragments derived from the ab initio calculations followed a similar trend as the results obtained from the RIS/VOS scheme and the experimentally derived group polarizabilities.

Molecular dynamics simulations of bulk amorphous BPAPC and four structurally modified polycarbonates with full atomistic description are reported here. Structural modification of the BPAPC repeat unit by aliphatic groups in the polycarbonates studied lowers the cohesive energy density and solubility parameter. Short distances for some of the atom pairs derived from the radial distribution function of BPAPC are found to be in agreement with reported data from NMR measurements in literature. The peak positions of the calculated neutron scattering curves are in agreement with the experimental data leading to a correct prediction in the trend of average interchain distances for different polycarbonates. The distance between the neighboring chains calculated from the scattering curves indicate a relatively open structure for TMCPC due to the bulky trimethylcyclohexylidene substituent. Correlations between the neighbouring phenyl rings

show a weak preference for a parallel alignment of phenyl rings at distances in the range 3.5-6 Å for BPAPC. For all polycarbonates studied in this work, the distribution of the neighbouring rings is found to be completely random at distances greater than 6 Å. Fractional free volume analysis along with the neutron scattering curves indicate higher spatial distance between the neighbouring chains in TMCPC and higher free volume as compared to BPAPC. New and detailed level of fundamental insights into the relationship between polymer chemical structure and the glassy condensed structure is brought forth.

Novel atomistic simulations of uniaxial tensile deformation of BPAPC and two substituted polycarbonates DMPC and DMBPC which includes calculation of optical birefringence of bulk glassy samples is reported here. Orientation behaviour of phenylene and carbonate groups are analyzed in detail. The main chain vectors tend to preferentially align towards the stretching direction as the deformation progresses in all three polycarbonates. Orientation function of the phenylene rings vary in a similar fashion in all three polycarbonates where as a much higher reorientation towards the stretching direction is observed in the case of DMPC and DMBPC. This is thought to be due to the presence of *ortho*-methyl groups on the phenylene rings in these polycarbonates. Intermolecular packing distribution of the phenylene ring and carbonate planes were estimated in the oriented samples of BPAPC. There is an enhanced tendency for the phenylene and carbonate planes to align parallel to each other with an increase in deformation and this is seen at shorter distances as well as till about 10 Å. The torsion distributions of the oriented samples are found to be not very different from that of the undeformed samples although a clear tendency for the increase in the population of the *trans*, *trans* conformation of the carbonate groups is the molecular response that facilitates structure evolution during bulk deformation. Stretching of the polymer chain which leads to increased end-to-end chain distance is observed in all three polycarbonates. Birefringence of the atomistically simulated oriented polycarbonates is calculated using an approach that employs the polarizability anisotropy as well as the orientation function. Calculated values of the birefringence for BPAPC samples compares well with the experimentally reported value. The calculated birefringence for BPAPC at a draw ratio of 2 falls within 8% of the experimental value. Calculated birefringence values for DMPC and DMBPC are lower than that of BPAPC and in agreement with the experimental stress-optical behaviour of these polymers in the glassy state.

GLOSSARY

α	Polarizability
$\langle\gamma^2\rangle$	Mean squared optical anisotropy
BPC	1,1-Diphenyl cyclohexane
BPAPC	Bisphenol A polycarbonate
BPCPC	Polycarbonate based on 1,1'-bis(4-hydroxyphenyl)cyclohexane
CED	Cohesive energy density
C_g	Stress-optical coefficient in the glassy state
C_m	Stress-optical coefficient in the melt state
C_n	Characteristic ratio
DFT	Density functional theory
DMBPC	Polycarbonate based on 1,1'-bis(3-methyl-4-hydroxyphenyl)cyclohexane
DMCYX	1,1-Dimethyl cyclohexane
DMDPC	Dimethyl diphenyl carbonate
DMPC	Dimethyl bisphenol polycarbonate
DPC	Diphenyl carbonate
DPP	Diphenyl propane
DRS	Depolarized Rayleigh Scattering
FFV	Fractional free volume
HF	Hartree-Fock
MC	Monte Carlo
MD	Molecular dynamics
MM	Molecular Mechanics
n	Refractive index
Δn	Birefringence
NMR	Nuclear Magnetic Resonance
Δn°	Intrinsic birefringence
$\langle P_2\rangle$	Orientation function
P_i	Probability
PC	Polycarbonate

PCFF	Polymer consistent force-field
QC	Quantum chemical
$\langle R^2 \rangle$	Mean squared end-to-end distance
RIS	Rotational Isomeric State Method
RMMC	RIS Metropolis Monte Carlo Method
SANS	Small Angle Neutron Scattering
$\langle S^2 \rangle$	Mean squared radius of gyration
TDHF	Time dependent Hartree-Fock method
T_g	Glass transition temperature
TMC	3,3,5-Trimethyl-1,1-diphenyl cyclohexane
TMCPC	Polycarbonate based on 1,1'-bis(4-hydroxyphenyl)-3,3,5-trimethylcyclohexane
TMPC	Tetramethyl bisphenol polycarbonate
VOS	Valence Optical Scheme
WAXD	Wide Angle X-ray Diffraction

List of Tables

List of Figures

Chapter 1: Introduction

1.1. Molecular Modeling of Polymers

An important goal in material science is the determination of quantitative relationships between structure of a material and its properties at the microscopic, mesoscopic and macroscopic scale. For polymers, it becomes desirable from a fundamental point of view and technological standpoint to be able to relate macroscopic properties to physical microstructure and ultimately to the chemical structure at the atomistic level of the chain molecule. Computer simulations provide precise insights to the structure at the macromolecular scale and play an ever-expanding role in understanding material behaviour and for the investigation of the physical properties of polymeric systems. Molecular modeling and computer simulations have been extraordinarily successful in the several sub-disciplines that form the basis of contemporary polymer science and examples as such are several.[1-5] This chapter provides an overview of various simulation techniques as applied to study chain behaviour in dilute solution and in the condensed phase of synthetic amorphous polymers. The introduction to the application of molecular simulation methods to polymers in general is followed by a comprehensive evaluation of the literature, wherein, investigations and general status of the understanding of physical properties and behaviour of polycarbonates is brought forth.

1.1.1. Single chains in dilute solution

One of the most interesting aspects of macromolecules is their ability to explore and occupy an enormous variety of spatial arrangements (conformations and configurations).[6-10] Macromolecular chains exhibit a very large number of conformations, which can be energetically realised by rotations about single bonds constituting the chain backbone. Many of the unique macroscopic properties of polymeric phases are dictated by this conformational variability of the chains. Important properties of polymers such as rubber elasticity, amorphous and crystalline morphology, glass-transition temperature, optical properties, dipole moment, viscoelasticity and mechanical properties are affected and significantly influenced by conformational behaviour and conformationally dependent molecular

properties of the chains. Considering the properties of individual chains in the melt, it turns out that this physical situation is nearly identical to the case of an isolated chain operating under theta conditions, for which the non-bonded interaction along the chain is truncated. Under this condition, a quantification of the statistics of the enormous number of conformations for a long macromolecular chain is possible by statistical models and concepts such as the Rotational Isomeric State method (RIS). The theoretical interpretation, understanding and prediction of single chain conformational properties of polymers is conveniently provided by the RIS formalism. RIS method was first applied to macromolecules by Volkenstein.[6] The formalism was recasted into compact form and extended comprehensively to the treatment of polymers with wide range of structural differences in a pioneering manner by Flory.[8,9]

RIS method presents an extremely efficient way of providing a sufficiently accurate quantitative description of the conformations of macromolecules, neglecting the effects of excluded volume.[8] According to RIS theory, each rotatable skeletal (backbone) bond is assumed to occur in one of a small number of discrete rotational energy states. A spatial configuration can then be specified by the particular sequence of rotational states adopted by the skeletal bonds of the chain. The choice of rotational state for a given skeletal bond depends on the relative energies of the rotational states available to that bond. Thus the average conformations of the chains and their conformation dependent properties, which are calculable from the equations of statistical mechanics, depend on the relative energies of these rotational states taken collectively. The RIS model basically contains information about the correlation of adjacent torsion angles which is expressed by means of statistical weight matrices. By splitting the RIS parameters into entropic and energetic terms, even the temperature dependence of the statistical properties can be calculated. RIS theory has been applied to study the population of different conformers, averaged chain dimension of polymers like the squared end-to-end distance ($<R^2>$), squared radius of gyration ($<S^2>$), persistence length (a), characteristic ratio (C_n), molecular dipole moment ($<\mu>$), molecular optical anisotropy ($<\gamma^2>$), optical configuration parameter etc. RIS method has been applied till date to a large variety of polymers and has been looked upon as a versatile method for predicting conformational properties of macromolecular chains having a wide variety of

architectures such as linear, branched, star and cyclic encompassing compositional and stereo-chemical variability.[10,11]

Mean-squared dipole moments of a wide variety of polymers have been estimated by this method along with knowledge of the dipole moment associated with the individual bond vectors. Calculations have been performed for polymers for which the dipole moment arises (i) entirely from the main chain bonds;[12] (ii) from substituents that are rigidly attached to the main chain[13,14] and (iii) from polar side chain substituents that can have multiple conformations.[15,16] The RIS method for the calculation of mean-squared optical anisotropy, $\langle\gamma^2\rangle$, of organic molecules[8,17] and oligomers in solution has shown promise and has been applied to several polymers in the past such as poly(ethylene),[18] poly(oxyethylene),[19] atactic polystyrene as a function of stereo-chemical composition,[20] aliphatic esters,[21] aromatic esters and poly(*p*-oxybenzoate),[22] and several other systems.[10] Optical anisotropy of bisphenol A polycarbonate (BPAPC) also has been calculated using the RIS method wherein the polarizability tensors of the phenyl and carbonate group were derived from scattering measurements of model compounds. The comparison with experimental data was quite satisfactory (calculated $<\gamma^2>/x$ was 111 Å^6 as compared to experimental value of 120 ± 5 Å^6 as measured for x = 10.7 or M_n=2700 g/mol).[23,24] Several reports have come out in the past three decades on the use of RIS method to calculate $<\gamma^2>$ of polymer chains and their validation using experimental measurements in solution. In all of these cases, either good or excellent agreement of the theoretical calculations with experimental observations can be noted. The aforementioned reports and studies show clearly the effectiveness of the use of tensorial sum of constitutive properties for organic molecules and the predictive power of this theoretical approach when coupled with the RIS framework for the case of chain molecules. For all of these polymers the use of mutually consistent polarizability parameters for their small fragments and the allowance for inductive effects of substitution and neighbouring groups have been exemplified and shown to be important in order that it is possible to successfully reproduce experimental data through such calculations.

By the RIS Metropolis Monte Carlo method (RMMC),[25] recently developed by Honeycutt, the polymer chain conformations are generated using the Monte Carlo technique. In this method the chain conformations are not restricted to discrete energy states, but are generated using potential energy functions (force-fields) directly. The generated polymer chain conformations are then used to calculate conformationally averaged single chain dimensions. In principle this method is not used to obtain bond level conformational states, which can be obtained otherwise by conformational energy analysis. However, RMMC simulations provide an effective method for the calculation of overall chain dimensions. The discrete RIS formalism is superior to the RMMC formalism when accurate conformational energies are available from experiments, obviating the need for a force-field based continuum Monte Carlo simulation of conformationally averaged unperturbed single chain properties. However, the RMMC method, employed with a reasonably well parameterized force-field, is especially useful for implementation on complicated polymer structures for which conformational analysis and derivation of statistical weights can some times not be straightforward to perform. The general advantages offered by the RMMC method over the conventional RIS method can be summed up as: (1) derivation of the statistical weights for novel polymer structures and new polymers are not required for use in RMMC simulations, (2) use of the RMMC method for polymers with any type of architecture is possible in a more tractable manner without extensive parameterizations.

The RMMC method was first implemented for polyethylene, poly(dimethylsiloxane), poly(ethylene oxide), bisphenol A polycarbonate, poly(ethylene terephthalate), and, poly(ethylene) stars with 3 and 4 arms, using COMPASS force-field.[25] Bicerano reported the chain dimensions and intrinsic viscosity of some liquid crystalline polymer chains containing dihydroxy-α-methylstilbene by this method.[26] The calculated intrinsic viscosity showed a similar exponential variation with molecular weight as experimentally observed, but were larger than the observed values by roughly a factor of 6 over the entire M_w range. Sundholm and co-workers studied the rigid-rod polymers of p-phenylene terephthalates[27] and Lee et al. have looked at BPAPC.[28] Blomqvist et al. studied the chain properties of polyesters with isolated carboxyl groups, as well as for poly(methyl acrylate), poly(methyl methacrylate), poly(vinyl acetate) and for some aliphatic main-chain polyesters having alkyl chains of

various lengths between the carboxyl groups.[29] Their calculated characteristic ratios, using torsion states from ab initio calculations on small fragments into the re-optimized PCFF force-field, agreed well with experimental data. Also, the dependence of the calculated characteristic ratios for PMMA with different tacticities followed the experimentally observed behaviour. In a later work, Blomqvist,[30] reported RMMC studies on chain properties of poly(L-lactic acid), poly(L,D-lactic acid) and poly(glycolic acid), comprising strongly interacting polar carboxyl groups, using the modified PCFF force-field from ab initio calculations of torsion potentials. Chain dimensions and dipole moments of terephthalate polyesters having cycloaliphatic rings in the chain backbone were reported recently using RMMC simulations by Sulatha et al.[31] The diol unit in these polyesters were based on 1,4-cyclohexanedimethanol and 2,2,4,4-tetramethylcyclobutanediol. Different configurations of the polyester chains were studied, in which the diol units are in an all *trans* as well as a mixture of *trans* and *cis* configurations. Polyesters having the all *trans* tetramethylcyclobutylene linkages exhibited highly extended chain conformations with relatively higher values of characteristic ratio and persistence length thereby indicating rigidity of the chain backbone when compared to other polyesters having cyclohexylene linkages in the backbone. Incorporation of *cis* isomers resulted in a decrease in chain dimensions for these polyesters.

1.1.2. Modeling of bulk amorphous state structure

Polymers are characterized by a hierarchy of different length and time scales.[5] Therefore polymer simulations also have to deal with the problem of broad length and time scales. The dimensions characteristic of polymers vary from a few Angstroms (Å) corresponding to the length of covalent bonds (of the order of 1 Å), interatomic distances, repeat unit lengths, persistence length (of the order of 10 Å) and to those for the chain end-to-end distances which are typically of the order of few 100 Å. In order to simulate polymeric bulk condensed phase, one should consider a simulation system containing many such chains and ensure that the finite size of the periodic box (dimensions less than 100 Å usually) do not contribute to any artifacts to the simulations. Difficulties are encountered with the time scales

in particular, which span an extremely wide range. Typical range that would have to be considered easily exceeds ten decades in time.

On the microscopic level, relaxation properties and dynamics are dominated by local oscillations of bond angles and lengths for which the typical simulation time constant is about 10^{-13} s. Typical reorientation rates of torsions is approximately 10^{-11} s. On the semi-macroscopic level the behaviour is dominated by the overall diffusion of the chains or the relaxation of the overall conformation of the chains which requires typically several decades of time greater than those required for rotational motions about individual bonds. These times which depend on chain length and temperature, can easily reach seconds. For eg. in the case of BPAPC, considering the entangled melt viscosity, at a temperature of 50 K above the T_g for a chain having 100 repeat units, the chain relaxation times are of the order of 10^{-3} s. Working with a molecular dynamics time step of integration of one or two orders of magnitude smaller than the fastest relevant oscillation period, one would have to propagate the melt simulation over 10^{12} to 10^{13} steps for only one system at one temperature. These kinds of simulations with all structural details of the system are beyond today's computer capability. Simulations of fully atomistic models of a sufficiently large system over time scales for which thermal equilibration could be reached at practically relevant temperatures is currently not possible. One of the challenges in computer simulation of polymers is to devise methods that allow investigations of properties from the microscopic to macroscopic range by capturing the effect of chemical structure of macromolecules to the overall behaviour of the material.

Polymer simulations fall into the broad groups of minimum energy methods and ensemble methods. The ensemble sampling are distinguished according to the techniques of ensemble creation as Monte Carlo (stochastic, MC), and molecular dynamics methods (deterministic, MD).[32-44] There are many composite methods that have been developed in recent years, which attempt to combine the advantages of more than one type of method in a single simulation strategy. Minimum energy methods generate static configurations from which equilibrium, thermodynamic and mechanical properties of realistic systems can be deduced in cases where entropy does not play a significant role. This is believed to be the case for glassy materials, for which these techniques have provided a wealth of important

information in the past two decades. In spite of some very successful attempts to study entropy-dependent material properties, such as the solubility and diffusion of small guest molecules into polymer matrices, the minimum energy methods alone cannot properly address the effects of thermal motion on important polymer properties and also are unable to provide accurate estimates for the partition function. Earlier investigations also made use of Monte Carlo techniques applied to schematic models of polymers built on a lattice. With increased computer capabilities in recent years, the use of more computationally intensive methods has become feasible, allowing simulations of more realistic off-lattice models of bulk polymers by brownian and molecular dynamics as well as Monte Carlo methods.

In the field of polymer simulations, molecular coarse-graining methods have begun to play a larger role more recently.[5] Coarse-graining, a method to extend time and length scales at the loss of atomic detail, is commonly used for relaxing long chains. It consists of building mesoscopic chains of polymers by replacing a part of or entire repeat unit by coarse particles. The number of interactions required to be computed is considerably reduced. Moreover, the higher frequency motions are removed and the time step can be increased by an order of magnitude, allowing further reduction in computation time. It is therefore possible to simulate a coarse-grained system for nearly 10,000 times longer than an atomistic system. This allows the relaxation of chains of a relatively large degree of polymerization in a dense system. Thus, once the chains are relaxed with the coarse-grained model, atomistic details are reintroduced in a procedure known as inverse mapping, which is followed by a short equilibration simulation, needed to relax the local degrees of freedom. Recent developments in polymer simulations specifically with respect to the accessible time and distance scales have been reviewed.[5] Attempts by various researchers in trying to develop efficient schemes for coarse-graining of polymeric structures have been summarized in the review that throws light on how to combine the different simulation strategies and tools for understanding and predicting the properties of polymeric materials.[5]

1.1.2.1. Molecular models of amorphous polymers in the glassy state

Existing methods for the generation of bulk amorphous polymers are briefly reviewed here. Models of amorphous structures have to be generated that are (i) thermodynamically

acceptable, (ii) that have an appropriate distribution of torsion angles, (iii) a physically acceptable distribution of unoccupied volume, among other essential criteria. The original pioneering atomistic simulation of a polymer condensed phase with full structural details, known as the 'Amorphous cell method', was developed by Theodorou and Suter.[45] This method serves as a microscopic representation of the polymeric glassy state.[45] The method consists of generating an initial guess for the structure of the glass by Metropolis Monte Carlo algorithm from the appropriate rotational isomeric state model using periodic boundary conditions to remove surface artifacts. This is followed by total potential energy minimization of the resulting structure by a quasi-Newton method. The system represents an amorphous crystal in which a single polymer chain interacts with its own periodic images for the representation of a condensed interchain system. In a crystalline material the bulk of the system usually consists of replicas of a single structure represented by a leading term in the partition function, while in an amorphous material there are many coexisting structures of similar importance with corresponding terms in the partition function having similar magnitude. Therefore an ensemble of configurations needs to be sampled to be able to obtain structural information representative of a glassy phase. The amorphous cell method has been widely used in simulations, of amorphous polymer structures in the glassy state. Nevertheless, this method has a disadvantage of promoting severe atomic overlaps during initial stages of structure generation and relaxation. This method also becomes difficult to successfully implement in cases of polymers containing aromatic rings and bulky groups. Furthermore, only chain configurations that pack into the periodic box are selected which can potentially influence chain statistics to some extent.

Among other methods developed and employed by investigators, Rigby and Roe have performed MD simulations of short-chain molecules representing polyethylene in the supercooled liquid region and studied the formation of glassy state which occurs as the temperature is lowered at constant average pressure.[46] Boyd and Pant have described a method of generating polymeric glasses from well equilibrated polymeric liquids.[47] In this scheme, reptation Monte Carlo method is employed during the equilibration of polymer liquids (melt state) at different temperatures. These samples are then locally relaxed by structure energy minimization to generate polymeric glasses. Clarke and co-workers have

described a method known as the phantom chain growth (PCG) for growing amorphous samples of polymer melts which can be subsequently relaxed at a specified temperature and pressure using molecular dynamics.[48] Here, the probability of the successive torsion angles in the chain is related only to the immediate torsion angles as in the RIS formalism. Long-range interactions are incorporated once the structure is generated and subsequently allowed to relax to mechanical equilibrium. Another method lies in generating structures with lower densities which are then condensed step by step during NPT-MD simulation to experimental densities of polymer systems.[49]

Another method for generating polymer glass structures involves placing the monomer randomly in a periodic box and then 'polymerizing' the monomers to form the chain. In this method, introducing chemical bonds between the monomers results in highly strained bond lengths and valence angles that require several stages of minimization and annealing to relax the resulting chain structure. During the amorphous structure generation in this procedure, problems arise in cases where specific monomer sequences or tacticities have to be assigned along any chain.[50] Kotelyanskii et al. have presented a new technique for generating atomistic models of amorphous polymer phase that employs a trajectory generated by self-avoiding walk on a completely occupied cubic lattice. This trajectory then becomes the chain backbone and is populated with specific chemical units.[51] This particular method enables gaussian chain statistics and the control of chain tacticity and monomer sequence while avoiding severe overlaps between atoms in the structure. The method has been implemented to simulate atactic poly(styrene) phase. A new approach has been presented by Muller et al. recently for generating good and acceptable atomistically detailed starting configurations of polymers.[5,52] This approach combines an explicit steepest-descent search algorithm in the space of generalized coordinates with an adaptive scheme for gradually incorporating the effect of the non-bonded interactions between the chains and their hard surrounding. For the specific polymer, the number of discrete states for the torsion angle is specified according to the corresponding RIS model, which also gives valuable information about the correlation of two adjacent torsion angles along the backbone chain. The results obtained for PE systems were very encouraging and it is postulated that this algorithm along with the novel parallel rotation (ParRot) move constitutes a very efficient methodology for

generating initial guess structures for atomistic simulations. The method provides a greater flexibility in the choice of input parameters to account for the local energy configurations, and also the input for torsional correlations along the chain backbone can be derived with the help of a force-field.

1.1.2.2. Molecular dynamics simulation methods

The molecular dynamics method, one of the popular methods for polymer simulations, has been used to simulate the polymer bulk phase in the canonical, NPT and grand-canonical ensembles. The main advantage with MD methods is the realistic treatment of molecular motion, which allows the convenient study of dynamic properties and temperature effects of structural properties. This method has found wide applications in examining chain dynamics, glass transition, diffusion of gaseous penetrants through polymer melts and in several other phenomena.[1-4] Focus has also been on the prediction of time-averaged thermodynamic properties of polymer melts and in studies of their volumetric behaviour.

MD simulations of PE melts have been investigated, among them is one of the pioneering studies by Rigby and Roe.[46,53] They employed a fully vibrational n-alkane chain model which included torsional and non-bonded intersegmental interactions. In order to slow down the bond length vibrations, the bonds were made soft by using a spring constant for bond length stretching weakened by a factor of seven in comparison to the realistic value. Short-range order and reorientational motion of individual bonds were investigated. MD simulations of melts of $C_{44}H_{90}$ have been studied using united atom[54] as well as atomistic representations of the chain.[55]

Despite major advances, MD simulations have not proved adequate for the thermal equilibration of long-chain melts. MD studies of polymer melts usually rely on the generation of initial structures that are close to thermal equilibrium, which for melts of long chains in itself is a complex problem. This is because of the fact that the longest relevant relaxation time of a chain molecule rise rapidly with chain length, making the equilibration times of entangled, truly polymeric systems inaccessible in dynamics simulations. Because of the

current computer limitations however, the integration of the equations of motion can follow the temporal evolution of a complex polymeric system for a few nanoseconds at the most. While this is satisfactory for the study of certain fast relaxation processes, majority of the important dynamics processes in polymeric materials are in the microsecond to millisecond to second range, thus rendering MD unsuitable for the study of many polymer dynamic properties. The time and length scales associated with the relaxation of long polymer chains are out of reach of a fully atomistic molecular dynamics simulation.

1.1.2.3. Monte Carlo methods

Monte Carlo methods provide an important alternative to minimum energy methods and MD, since they are in principle capable of providing the partition function, and thus entropy dependent material properties. Being purely stochastic, these methods do not provide explicit real time information. However, MC methods can in principle be calibrated using a variety of appropriate criteria and techniques.[39] An important advantage of MC methods is that the MC moves can be biased to place different emphasis on different degrees of freedom. Significant advances in polymer MC simulations have been made especially by the introduction of new sampling techniques that have tremendously enhanced the efficiency of lattice polymer simulations, which were originally quite inefficient at high chain densities.[5] MC simulations proceed by generating a Markov chain of configurations that samples the probability distribution of the statistical mechanical ensemble of interest. It is the explicit construction of the Markov chain of random system configurations, where random numbers are used, which have given the Monte Carlo method its name.[39] This method addresses the problem of calculating thermal averages along the lines of statistical thermodynamics, by constructing a random walk through the configuration space of the considered model system. The desired physical properties are then obtained as time-averages along this stochastic trajectory in phase space. Information can also be derived on dynamical (time-displaced) correlation functions along this Markov chain of configurations.

Since the relaxation time needed to equilibrate the configurations of long flexible chains increases strongly with chain length, it is necessary to perform coarse-graining along the chain, by which many details of the local chemical structure is lost. The basic unit now is

not the chemical monomer but rather a group of successive monomers, the length of which is taken as fixed. The simplified models can be broadly classified as lattice and off-lattice models.[39] Freely jointed chain represents an off-lattice model where each polymer is modeled by a succession of *N* rigid bonds of length *l* jointed together at arbitrary angles. The steps of the MC procedure then consist of rotation of beads with a transition probability. This is an extremely unrealistic model for polymers wherein chains are allowed to come close to each other. But in reality there is a volume region excluded from occupation by monomers of other chains. The pearl-necklace model represents a crude way of taking such an excluded volume interaction into account. By varying the ratio between the diameter of the hard spheres attached to the beads and the bond length *l*, effective strength of the excluded volume interaction can be varied. Another alternative off-lattice model is the bead-spring model where two neighbouring beads are no longer kept at a fixed distance apart. On the average the distance between the beads *l*, is maintained via a harmonic potential. This model has to be complemented by a Lennard-Jones type of potential to account for excluded volume interactions at short distances. Both pearl-necklace and bead-spring models have proven useful for the simulation of polymer melts.[39]

Lattice simulations provide access to slower relaxations than those accessible in conventional MD simulations of the fully atomistic models of the same system in continuous space. The discretization on a lattice simplifies the conformational space, because a single occupied site, or bead represents several atoms from the fully atomistic representation, which leads to reduction in the number of elementary particles and degrees of freedom. The number of attempted moves provides a natural time scale for the expression of the dynamics. Introduction of many new sampling techniques has enhanced tremendously the efficiency of lattice polymer simulations, which were quite inefficient at high chain densities. A simple lattice model of polymers is the self-avoiding random walk of *N* steps on a lattice. The beads are situated at lattice sites, the bonds usually have the length of the lattice spacing. Since each lattice site can at most be occupied by only one bead, the walk cannot intersect itself and thus an excluded volume interaction is automatically included. Lattice-based MC polymer simulations of model systems, such as self avoiding random walks are simple to implement,

and often provide a startling variety of fundamental information on polymer static and dynamic behaviour in dense phases.[5,39]

The main drawback of lattice-based simulations is that the lattice representation cannot emulate in detail realistic polymer structures and most of these simulations seek general trends in physical properties shared by all flexible chain molecules.

Bond fluctuation method attempts to bridge the gap between lattice models and chemically realistic polymer structures.[56-61] Here an effective monomer does not occupy a single lattice site only but a whole group of neighbouring lattice sites. In such a case the bond connecting two neighbouring beads typically is larger than the lattice spacing and hence the bond length is not a constant and can be made fluctuating. A simple cubic lattice is used where each effective monomer blocks all eight corners of the cube from further occupation. The precise definition of the lattice spacing between the monomers takes into account the excluded volume interactions. The above described athermal bond fluctuation model which is not specific to any polymeric material provides not only a good general description of the polymer chains as a whole, but also the internal dynamics of chains on length scales in between the coil size and effective bond length. To built in chemical and geometrical structural details of a specific polymer on to the lattice bond fluctuation model, mapping procedure is employed wherein chemical details are forced from continuum space on to the lattice. Mapping ratio and the associated details are specific to the polymer structure. All fast vibrational motions are neglected and chemical structural details of less than about a few Å are disregarded in the mapping process. The structure and geometry of the repeat units is built into the model by means of choosing effective potentials for the bond lengths and angles between them. The torsional transitions are modeled by random hopping moves of the monomers on the lattice. Such mapping procedure and simulations using the bond fluctuation model were applied to PE and BPAPC.[57,60] In the case of BPAPC melts,[57] the model yielded a static structure factor qualitatively in agreement with experiments, but was unspecific with respect to quantitative details. This coarse-grained model successfully predicted the glass transition for BPAPC and followed the Vogel-Fulcher law. Similar coarse-grained models of chemically different polycarbonate have met with less success in reproducing the differences between the chemical structures and properties.[61] One of the drawbacks of the lattice

description of polymers with the bond fluctuation model is the lack of explicit inclusion of intermolecular forces other than the excluded volume. In simulations concerning polymer crystallization or liquid crystalline order, lattice artifacts are observed with this model. Also the inverse mapping procedure that reintroduces the chemical details of the polymer structure on to the coarse-grained models has not yet been implemented for this model.

With the objective of providing an efficient method for simulation of dense multi-chain polymer systems, a new high-coordination lattice model for RIS chains has been formulated by Mattice and co-workers.[5,62-72] The lattice is a coarse-grained model of the tetrahedral lattice and is named as the second nearest neighbour diamond lattice, 2nnd lattice, as only every second site of the lattice is occupied. The unit cell is a distorted cube with a coordination number of 12, which makes it more flexible than a cubic lattice with coordination number 6. Polymer chains having approximately tetrahedral bond angles and torsions near 180º and ±60º can be mapped on to the lattice. Simulations using the single bead moves are performed for isolated chains that behave as random walks, non-reversal random walks and self-avoiding random walks. Short-range interactions are incorporated by means of an extended statistical weight matrix to determine the probabilities of the different states on the 2nnd lattice. Long-range interactions are taken into account by using the lattice representation of the second virial coefficient. Simulations have been performed for PE and poly(oxyethylene) as isolated chains under theta conditions and for PE in the melt. Cohesive energy per monomer for PE melt derived from the simulations were in fair agreement with those derived from experiments. Reintroduction of the atomistic details has also been performed using the reverse mapping procedure for PE melts. 2nnd lattice simulations have been employed for PE and PP melts, cyclic PE, surface energies of PE melts and also studies concerning the cohesion and complete mixing of two thin films.

In contrast with MD, the MC moves may be tailored to achieve efficient sampling. Much effort has been directed to the development of efficient phase-space sampling methods for MC simulations. Over the years, several moves specific to chain molecules have been developed and employed effectively in simulations, including reptation, continuum configuration bias and concerted rotation. The first two of these accelerate the diffusion of the center of mass of the chain while the last improves the sampling of local fluctuations in

chain structure. The simplest off-lattice move of a single torsion angle at a time represents the pivot algorithm. In the reptation or slithering snake algorithm, one end of the chain is randomly chosen, removed it from there and added at the other chain end in a random direction.[73-76] This has been used successfully in the simulation of short alkane chains in continuum space, but is very ineffective for the treatment of long chains, since it relies on the existence of a relatively large concentration of chain ends.

The concerted-rotation method (CONROT) consists of moving seven consecutive middle torsion angles in the chain, keeping both residues of the chain around this moving unit fixed in space.[77-79] This sampling method has been employed in the simulation of polyethylene and polypropylene melts, but was found to be not more efficient than the molecular dynamics of the same systems. End-bridging Monte Carlo algorithm (EBMC) have been successfully applied in the simulation of polydisperse polymer melts.[80] The end-bridging move alters the connectivity of the bulk polymer by bridging a chain end to an interior segment on another chain with a trimer. Parallel-rotation (ParRot) algorithm[52] represents a powerful off-lattice sampling technique that permits changing torsion angles that are deep inside long chains in a dense system. In principle, MC moves can be made to tunnel through the energetic barriers in the configurational space of the polymer, circumventing the limitations of the dynamic algorithms. This feature has been exploited within lattice polymer simulations in moves that alter chain connectivity greatly enhancing the sampling efficiency. Such moves allow for structural fluctuations in highly dense lattice polymers, which cannot thermally equilibrate by other means. They have also been employed effectively in simple off-lattice models.

The configuration-bias-monte-carlo method (CBMC)[81-83] have also been applied for a variety of model systems, because of the intuitive use of available unoccupied volume. This method also relies on a high concentration of chain ends. Similar to the reptation algorithm, CBMC becomes inefficient in the treatment of long chains in a dense system.

1.1.3. Simulations of the deformation of amorphous polymers

This section presents an overview on the atomistic simulation of the deformation of amorphous polymers, which have been reported in literature. The attention is focussed on the deformation of polymers in the glassy state along with a few pertinent reports on the simulation of orientation and birefringence of polymeric melt state. Atomistic simulation of deformation of glassy polymers have been applied to a variety of polymeric structures with majority of these studies focussing on the calculation of mechanical properties and some on the elucidation of specific structural events that occur during deformation.

Methods for the atomistic simulation of the deformation of polymers were developed by Theodorou and Suter and applied to atactic poly(propylene) (*a*-PP) in one of the early pioneering works.[84-86] It was demonstrated that elastic constants of well-relaxed amorphous polymer glasses could be estimated theoretically by subjecting the simulated structures to a series of deformations of small strain. Estimates of elastic constants were obtained by two different approaches. The first was based on changes in the total potential energy of the structures with applied small-strain increments and the second approach was based on the volume-average change in the atomic-level stress tensors. The elastic constants predicted by these two approaches were closely similar and gave good agreement with experimental data. They also explored the microscopic mechanisms of small strain elastic deformation and the associated structural changes. Results indicated that deformation in the glassy bulk is accompanied by concerted displacement of chain segments approximately 10 bonds long.[84,85] Stress-strain behavior of PP was also investigated in which strain was applied beyond the yield point which was found to be at about 5% strain.[86] Plastic deformation of PP was subsequently performed by Mott, Argon, and Suter.[87] The major conclusion was that plastic deformation of PP is dilatant in early stages and is associated with complex and cooperative conformational rearrangements. From a detailed analysis of the simulation results, they showed that in a typical flexible-chain glassy polymer local plastic relaxations occur in quite large clusters on the order of 1-10 nm in size.

Deformation simulations by molecular mechanics approach has the limitation of requiring experimental densities and neglects both entropy contributions and local volume

fluctuations which can be significant in condensed phase polymers such as glasses and melts. To overcome this problem, constant stress molecular dynamics was employed by Brown and Clarke to study uniaxial tension of simple polyethylene like model (representing amorphous linear PE) and to explore the relation between polymer structure and strain hardening.[88,89] Simulations were performed on sets of samples of the same model polymer with different correlation lengths and fractions of conformers at the same temperature and pressure. Results suggested that an increase in the fraction of *trans* states and an increase in the persistence length would independently contribute to strain hardening. They found that in particular, chains which are either more extended or contains a higher fraction of *trans* conformers to begin with would be harder to deform**.** It should be noted here that the molecular dynamics approach is limited by an inherently short simulation time scale.

Atomistic simulations of deformations have been applied to a variety of polymers, details of which will not be described here. It is suffice to know that most of the simulation studies reported to date have focussed on determining the mechanical properties of the polymers and also in some cases mechanism of deformation as explored by changes in the conformational distributions and population.[84-96] Efforts have also been placed on developing better simulation protocols for polymer deformation. Conditions of constant volume usually used in deformation simulations lead to an increase of pressure with strain and to a concomitant increase in shear stress. If simulations are performed at constant pressure, by contrast, the shear stress remains constant up to the largest strains investigated. One such attempt by Utz et al. who introduced an algorithm (similar to Berendsens thermostat) for simulation of constant pressure plastic deformation which allows the study of volume changes associated with the plastic deformation of glassy solids. The method was applied to plane strain compression of a binary Lennard-Jones glass.[97]

1.1.4. Simulations of optical birefringence of amorphous polymers

This section describes the various attempts to predict the optical birefringence and orientation of polymeric materials by means of molecular simulations. Gao and Weiner have carried out MD simulations of a rubbery PE system and reported values for the birefringence and stress-optical coefficient in the melt.[98] Freely rotating chain model was used where the monomers

are treated as united atoms and the simulations were performed at a temperature of 172 K. A given time-dependent deformation was imposed on the model PE melt by subjecting the simulation cell to a constant volume elongation at a strain rate (0.01 ps^{-1}). Polarizability values for the C-C and C-H bonds were used in calculating the anisotropic refractive index of the PE system. From the ratio of the deviatoric part of the refractive index to the deviatoric part of the stress tensor, stress optical coefficient was calculated as a function of time. The stress tensor was expressed as a sum of a term proportional to the orientation of the PE chain backbone plus a term due to fluctuation of the local stress in the intrinsic frame. The value of the stress-optical coefficient in the regime where the fluctuation term becomes negligible, was 3.6×10^{-9} Pa^{-1}. The experimental value for high-density PE melts of narrow molecular weight distribution at 423 K has been reported to be 2.3×10^{-9} Pa^{-1}.

Tensile stress and birefringence in both real and model amorphous polymer melts during constant rate uniaxial elongational flow have been reported by Kroger et al.[99] Non-equilibrium MD simulations with a multi-bead anharmonic spring model were invoked to provide insight into the molecular mechanisms underlying the breakdown of the stress-optical law at high enough rates, where deviations from linear behaviour becomes pronounced. Chemical details were not taken into account in the model. These simulations were performed at constant bead density and at constant volume. Distinct contributions to the stress and alignment of segments are calculated from bead trajectories.

Equilibrium and non-equilibrium MD have been applied on model polymeric melts to investigate the entropy character of the atomic level stress in polymeric melts and the stress-optical coefficient.[100] Simulations were performed on model systems consisting of a dense collection of molecules represented by a pearl necklace type model. Simulations were performed on short molecules. Atomic level stress is defined in intrinsic coordinates with a mobile frame tied to a generic bond. By summing up the contributions due to the intrinsic stress corresponding to each atom in the system, a global stress was derived. Ratio of the global stress to the average measure of the bond orientation was related to the macroscopic stress-optical coefficient. The results derived from these calculations remained unchanged with variation of model parameters like stiffness of the non-bonded and bonded interatomic potential, cutoff radius of the non-bonded potential and the bond length. These simulations

were able to reproduce many aspects of the stress-optical behaviour of polymers. Here also, the system simulated was a model polymer with no chemical details.

Mavrantzas and Theodorou have employed EBMC method to study uniaxially oriented PE configurations representative of a melt subjected to steady-state elongational flow at various strain rates.[101] The calculated stress, free energy, internal energy and entropy were compared to simple rheological models. In a subsequent study, they calculated the birefringence of uniaxially stretched PE melt by sampling a large number of well equilibrated uniaxially stretched polymer configurations.[102] Birefringence was calculated from the anisotropy in bond orientation induced in long chain systems by the application of a tensorial field which orients the chains. Data was obtained for the volumetric behaviour, structure and chain conformation of the melts at 450 K and pressure ranging from 1 to 800 atm. A coordinate system was assigned to each methylene group of the stretched structures obtained from MC simulations which allowed the calculation of a bond order parameter. From the bond polarizabilities of the C-C and C-H bonds and the order parameter of the methylene groups, an average polarizability tensor in the lab reference frame was determined. Assuming valence optical scheme the configurational average of the polarizability tensor of the melt is determined by transforming the local, bond-fixed coordinate frame to the laboratory frame. Clausius-Mossoti equation is then used to calculate the anisotropic refractive index of the deformed melt. Both birefringence and stress were calculated as a function of the applied field which represents a steady-state elongational flow. A linear relationship was found between birefringence and stress for both C78 and C200 systems. Subsequently from the ratio of the anisotropic birefringence to the anisotropic stress tensor, the stress-optical coefficient in the melt state is calculated. The calculated values are $(3.15 \pm 0.20) \times 10^{-9}$ Pa^{-1} (C_{78} system) and $(2.35 \pm 0.10) \times 10^{-9}$ Pa^{-1} (C_{200} system). The experimentally measured value for high molecular weight, linear high density PE melts is 2.3×10^{-9} Pa^{-1} which agrees well with the value calculated for C_{200} simulated melt.

1.2. Status of Structure-Property Understanding in Polycarbonates

Polycarbonates represent an important class of polymers that have attracted a large amount of research attention because of their excellent properties. A vast literature exists on various

aspects of synthesis, properties and understanding the physical properties of these polymers. These details have been summarized by LeGrand and Bendler.[103] Here a few important aspects of structure-property relations in polycarbonates is described briefly.

Bisphenol A polycarbonate is characterized by good impact resistance and high glass and melting temperatures, along with other useful properties, and has been widely investigated over past four decades. One of the goals of research in the field of polycarbonates has been to synthesize new polycarbonate materials that have even better properties than BPAPC. Much of the attention has been devoted to structural modification of the bisphenol monomer by using different kinds of chemical substitutions. It is known that restricting the rotational mobility of the phenylene rings in the bisphenol moiety has a marked effect on the heat resistance properties. Substituents on the *ortho* position of the phenylene rings sterically interact with the carbonyl oxygen of the carbonate group. T_g is lowered when one substituent is placed on each phenylene ring (as in 3,3'-disubstituted bisphenol). In the case where two substituents are placed on each phenylene ring (as in 3,3',5,5'-tetra-substituted bisphenol) there is an enhancement in T_g. Another strategy to improve the heat resistance has been by replacing the isopropylidene group of bisphenol A by cycloaliphatic rings. One such example is the polycarbonate based on spirobiindane bisphenol (SBIPC, T_g=230 ºC) where the spiro fused structure prevents any phenylene ring rotation. Polycarbonate based on the bisphenol of 3,3,5-trimethylcyclohexane (TMCPC, T_g=239 ºC) is another such example. Substantial increase in T_g is also observed when various substituents are placed at different positions of the aliphatic cyclohexane ring. Poly (ester carbonates) represent another class by itself where the incorporation of aromatic ester moieties enhances the heat distortion temperature without significantly lowering the ductility.

In optical applications such as compact disks, BPAPC is widely used as an optical data storage material. High birefringence renders BPAPC not ideally suited for demanding future needs and several new polycarbonates have been synthesized and investigated with an aim of attaining lower birefringence than BPAPC. SBIPC is one such candidate which result in very low birefringence although the material is brittle. Polycarbonates having cycloaliphatic substituents at the isopropylidene carbon (C_α carbon) are known to lower the birefringence and stress-optical coefficients. Low birefringence is also seen in

polycarbonates where the isopropylidene methyl groups are replaced by phenylene rings. In another route, aliphatic content of the polycarbonate is increased because the aliphatic groups are known not to contribute to birefringence. Bisphenols that have substituents on both the isopropylidene carbon and the *ortho* position of the phenyl rings have been used to synthesize polycarbonates having lower birefringence. With regard to low refractive index, polycarbonates with fluorine substituents have been studied. Gas transport properties of different polycarbonates have also been reported. These mentioned reports represent only a few examples with respect to the structure-property understanding in polycarbonates. Huge amount of literature exist on the synthesis of new polycarbonate homopolymers, copolymers, blends etc, which have been accumulated in the past four decades. Much effort is still needed to fully comprehend the relation between the structure and its associated properties in these polymers. The work presented in the subsequent chapters of this thesis represents such an effort to derive structure-property understanding of the optical properties of a series of substituted polycarbonates by molecular simulation methods.

1.3. Modeling and Simulation of Polycarbonates

1.3.1. Single chain conformational properties

Conformational features of BPAPC have been the focus of considerable research since the pioneering work by Williams and Flory.[104] Various calculation methods utilized for investigations on the conformational characteristics of BPAPC and the significant results have also been summarized.[10,11] The RIS model formulated by Flory et al.[104] is based on molecular mechanics calculations on model compounds diphenyl propane (DPP) and diphenyl carbonate (DPC) wherein the structural data was taken from tables of interatomic distances and the rotational barriers and the electrostatic interactions were neglected. However, the calculated mean squared end-to-end distance, $\langle R^2 \rangle$, in their work compared favorably well with the experimental data for BPAPC from intrinsic viscosities of fractionated samples.[105,106] Rotational flexibility of the BPAPC chains and different energetically possible conformations of the chains have also been investigated by means of conformational energy calculations.[107,108] It has been noted that the polymer has low intramolecular rotational barriers and that for a 180° flip to occur, cooperative motion of the

adjacent ring is necessary in order for the system to follow a relatively low energy rotation path. Laskowski et al.[109] calculated $\langle R^2 \rangle$ from a two-state RIS model derived from ab initio calculations on DPP, DPC (STO-3G basis set) and phenyl formate (6-31G* basis set). The variation of $\langle R^2 \rangle$ with temperature was also reported in their study.

Hutnik et al.[110] developed a classical force field for BPAPC which was used to formulate a four-state RIS model from calculations done on DPC and DPP. The electrostatic interactions were represented by coulombic potentials with a distance dependent dielectric constant and the van der Waals interactions were represented by LJ 12-6 potential. Bonded interactions were included using a structure specific torsional potential energy function. The geometric parameters were taken from available ab initio calculations on model compounds and X-ray diffraction data. The conformation of the repeat unit was described by six statistical weight matrices (one matrix for each rotatable bond including virtual bonds). The RIS model was a four-state model, which explicitly represented the symmetrically equivalent positions of the phenyl ring conformations about the carbonate group as well as about the isopropylidene group. The minimum energy conformational states in this model were taken to be equivalent for rotations about the C_α-Ph and the Ph-O bonds. The statistical weight, γ, for the *cis*, *trans* (*c*-*t*) conformation of the carbonate group was also incorporated. The calculated $\langle R^2 \rangle$ was in close agreement with the experimental values from light scattering and SANS measurements.[105,106,111,112] This model was also extended to poly (thiocarbonates), in which the methyl group at the C_α atom is replaced by the chlorophenyl group.[113]

RMMC simulations have also been employed to study the conformational statistics of BPAPC using the PCFF force-field. From the comparison of the calculated and experimentally observed intrinsic viscosities, the calculated radius of gyration was found to be closer to the experimentally derived value from measurements in either chloroform at 293 K or *p*-dioxane at 303 K.[28] Chain dimensions for BPAPC under theta conditions have also been simulated using Pseudo-Langevin dynamics and MD simulations of single chains using the PCFF force-field.[114] End-to-end vector and radius of gyration derived from simulations at different temperatures showed good agreement with experimental data. MD simulations of

BPAPC and BPCPC single chains have been performed with an aim of calculating the glass transition temperature.[115] Simulations were carried out in the temperature range from 300 K to 500 K. Time correlation functions for the various backbone vectors were plotted as a function of temperature. A regression of the vector correlation times showed an approximate change in the decay at temperatures close to T_g for these polycarbonates.

Single chain conformational characteristics of structurally modified polycarbonates have received limited attention till now except for the RIS models derived for a series of C_α substituted polycarbonates,[116] and the studies on the effect of articulated side groups at the C_α atom on the main chain flexibility.[117] In the former study,[116] conformational calculations were carried out for the following substituents: (i) H, H; (ii) H, CH_3; (iii) H, C_6H_5; (iv) CH_3, C_6H_5; (v) C_6H_5, C_6H_5; (vi) cyclohexyl and (vii) CCl_2 and described RIS models for these structural modifications of BPAPC. The force-field that was used incorporated a Lennard-Jones (LJ) 12-6 potential to describe the non-bonded interactions. The torsional contributions about the C_α-Ph bonds (connecting the isopropylidene carbon to the phenyl rings) were neglected as being small and the electrostatic interactions in the fragment compound were also not included. Conformational energy calculations were performed only for the bond pair about the C_α atom with the carbonate group being considered to be rigidly fixed in the *trans*, *trans* (*t*-*t*) conformation. Although the rotational flexibility of the backbone bonds were dependent on the nature of the substituent, the calculated characteristic ratio of these polycarbonates were insensitive to substitution of one or both of the methyl groups by either hydrogen atoms, phenyl rings or to substitution of the isopropylidene group by $C{=}Cl_2$ or cyclohexyl group. The torsional states about the C_α-Ph bonds were found to remain symmetric, with little changes in energies of the preferred regions. Attempts were also made to relate the conformational flexibility of these series of polycarbonates with different substituents at the C_α atom, to their glass transition temperatures. A linear regressed correlation between the conformational entropy and T_g was also derived.[118]

In another study,[117] conformational analysis about the C_α atom was carried out for the following substituents: (i) H, C_2H_5; (ii) CH_3, C_2H_5; (iii) C_2H_5, C_2H_5; (iv) H, CH_2Ph; (v) CH_3, CH_2Ph and (vi) CH_2Ph, CH_2Ph. Rotational states of the side groups were also varied to

determine their minimum energy positions. The force field used was the same as used for the earlier studies.[116] The main chain flexibility is found to be greatly reduced due to these substituent groups. Based on the minimum energy conformers and the conformational partition function, a steric factor was derived for making a comparison of the chain flexibilities. The results suggested that a CH_2 spacer in the articulated side chain increases the main chain rigidity as compared to that of BPAPC. The relationship between conformational entropy and T_g was found to be different for polycarbonates with and without the articulated side chains.

1.3.2. Quantum chemical calculations of polycarbonate fragments

Geometries of model compounds and chain conformations of BPAPC have been investigated by various quantum chemical methods. Previous work include MNDO type semi-empirical calculations and STO-3G level ab initio computations with fixed geometry.[119-124] Bicerano and Clark performed semi-empirical MNDO, AM1, and approximate ab initio PRDDO calculations of several small-molecule analogues of BPAPC and the poly(ester carbonate) of bisphenol A.[121,122] Sung et al. reported CNDO calculations on small molecule analogues of BPAPC and tetramethyl-bisphenol polycarbonate (TMPC).[123] The mobility of phenylene rings in TMPC was found to be very much restricted in comparison to BPAPC. The presence of methyl groups in TMPC was found to significantly reduce the rotational flexibility around the carbonate linkage.[123] Laskowski et al. performed ab initio Hartree-Fock (HF) calculations on model compounds of BPAPC and the geometrical and the conformational energy data was used to compute the unperturbed chain dimensions of BPAPC.[109] Calculations were carried out using different basis sets for phenyl formate, monophenyl carbonate and diphenyl propane. Geometries derived from 6-31G** basis set were found to be in good agreement with the crystal structure data.

Sun et al. have reported extensive quantum chemical calculations on model analogues of BPAPC using density functional theory (DFT) and HF methods.[124] Model compounds studied included carbonic acid, methyl and dimethyl carbonates, phenyl carbonate and diphenyl propane. Different basis sets were used to investigate the impact of using larger

basis sets and electron correlation on the computed geometry and energy barriers of these polycarbonate fragments. Full geometry optimizations were performed to characterize the global and local minimum energy structures and transition states of internal rotations. These calculations revealed large differences in valence coordinates especially the bond angles for the same molecule in different conformations, indicating the need for analytical functions, which must reproduce these trends if they are to accurately represent the energy surfaces of these molecules. Based on these very detailed calculations an all atom force-field for polycarbonates has been developed.[125] Ab initio calculations of DPC using HF/6-31G** basis set by Bendler showed that the stable *trans, trans* conformer can actually exist in two different conformations depending on the orientation of the phenyl rings with respect to the carbonate group.[126] The *syn* form, where the both phenyl rings are on the same side of the plane of the carbonate group has a slightly higher energy than the *anti* form where the phenyl rings are located on the opposite sides of the carbonate plane.

Jones and coworkers have applied DFT method to study organic molecules, molecular crystals and cyclic oligomers focussing on BPAPC.[127-131] Their work included the investigation of structures and vibrational frequencies of BPAPC fragments and closely related molecular crystals. DFT studies on the isolated structural unit and two crystalline analogs of BPAPC indicated that in the former the phenylene groups rotate freely, but the corresponding π-flips in the latter are hindered by neighbouring chain molecules which reflects chain packing. Isopropylidene carbon at the molecular vertex has bond distances and angles close to the ideal sp^3 bond in hydrocarbons.[127] Optimum structures derived for the two crystalline modifications of BPAPC were in fair agreement with the experimental data. DFT techniques have also been extended to study crystalline modifications of the dimer and tetramer ring oligomers of BPAPC.[128] These studies showed that when the unit cell is constrained at the experimental dimensions, DFT methods with the PBE form of the exchange-correlation energy functional reproduce the measured structures very well.

Reactions of nucleophilic molecules lithium phenoxide, sodium phenoxide and phenol with the cyclic tetramer of BPAPC were also investigated using DFT calculations.[129] Potential energy of the system was computed using a suitable reaction coordinate and

remaining degrees of freedom in the system relaxed by Car-Parrinello molecular dynamics. Simulations showed that as the reactant molecule approaches the carbonyl group, the carbonyl oxygen rotates resulting in a change in the coordination of the carbonyl carbon from sp^2 to sp^3. However, the subsequent reaction path and the change in potential energy in the case of reaction with phenol is very different from that of phenoxides. Low energy barriers were observed in the reactions involving phenoxides thus leading to ring-opening polymerization. High barriers were found for the reaction of phenol with the cyclic tetramer and this is in accordance with the low reactivity observed in the phenol-BPAPC system under experimental conditions.[129] In another study combining the DFT technique with simulated annealing, reactions of chains of BPAPC with sodium phenoxide (NaOPh), tetraphenylphosphonium phenoxide (PPh_4OPh) and DPC were performed. The energy barriers observed for reactions with PPh_4OPh were found to be larger than those involving LiOPh and NaOPh but significantly lower than those found in the case of phenol.[130] These calculations focussing on the nucleophilic attack on the carbonate group, provided a picture of the reaction paths and energy barriers that is consistent with experimental information. DFT methods were also applied to study the reactions of cyclohexene oxide and phosphites (which are polymer additive molecules) with chain segments of BPAPC to identify the possible reaction paths and energy barriers. Reactions of cylohexene oxide with OH-terminated BPAPC chain and with the carbonate group were found to be exothermic although accompanied with energy barriers higher than 10 kcal/mol. Reactions with phosphates were characterized by even higher energy barriers.[131]

Recently, ab intio and DFT calculations were performed on a series of carbonates with an aim of understanding the influence of the type of substituents on the reaction mechanism and rates of thermal elimination reactions.[132,133] The carbonates differed from each other by the groups (aliphatic and aromatic) attached to the carbonate group. The study focussed on the syn elimination of a β hydrogen of the side group. Experimental measurements of thermal degradation temperatures of the corresponding polycarbonates indicated evidence of the existence of a correlation with the reaction rates resulting from ab initio calculations. HF and DFT calculations on a dimer of BPAPC was carried out to investigate the thermal degradation behaviour of this polymer and identify energetically most

favorable route to degradation.[134] On the basis of calculated reaction enthalpies and Gibbs energies at two different temperatures, various degradation paths were ranked according to their feasibility. Data showed that the CO_2 elimination reaction and substitution reaction with water were found to be the most favourable paths in agreement with experimental data.[134] Ab initio calculations have also been applied to determine the Youngs modulus of a series of polycarbonates having different kinds of substitution at the isopropylidene carbon (C_α) as well as on the phenyl rings.[135] The model compounds studied were the dimers of the corresponding polycarbonates. The study showed that the Youngs modulus increases when the C_α is replaced by an oxygen atom and when electron donating groups (like NMe_2) are introduced on the phenyl rings.

1.3.3. Simulations of amorphous bulk state

BPAPC is one of the most widely studied polycarbonate by experimental and theoretical methods with the prime objective of understanding the local structure and molecular motions in the glassy state. Yannas and Luise developed an early model of glassy BPAPC, which included a molecular-level model that assumes hexagonal packing of quasi-lattice sites with spherical symmetry.[136] The model included intramolecular interactions represented by intrinsic torsion potentials and intermolecular contribution by Lennard-Jones type interaction between segments. Perchak, Schaefer and co-workers devised a model consisting of a two dimensional lattice of interacting phenylene rings with varying degree of lattice flexibility.[137,138] The first detailed bulk amorphous atomistic models of glassy BPAPC were by Hutnik et al. using the amorphous cell approach.[139] Force-field employed was the same as that used in the study of single chain conformations of BPAPC.[110] Static atomistic models of glassy BPAPC exhibited amorphous random coil conformations in the bulk.[139] Molecular dynamics simulations of amorphous BPAPC at two different temperatures have been reported by Shih and Chen using a modified Tripos 5.2 force-field.[141] Simulations were performed for a relatively short time of 80 ps at 300 K and 400 K. Conformational flexibility of the carbonate and phenylene groups were analyzed. With increase in temperature from 300 K to 400 K, the diffusion coefficients corresponding to the different motions investigated

were found to be tripled. Mobilities of the different structural units in the polymer were found to be dependent on the free volume of motion. Determination of glass transition temperature and thermal expansion coefficients of BPAPC via molecular dynamics simulations has also been performed with a reasonable level of accuracy.[142] In this study, NPT simulations were employed to investigate the atomistic scale dynamics of BPAPC in the vicinity of its T_g. Dreiding force-field was used which was modified to reproduce the results of quantum chemical calculations for the torsional barriers in DPC and DPP. Simulations were performed upto 1 ns. The results obtained from this study were found to disagree with the MD study of Shih and Chen with respect to the mobilities of the phenylene and carbonate group torsions at higher temperatures. The discrepancy was attributed to the force-field parameters employed in the former study. The investigation also revealed that backbone dihedrals exhibit a variety of conformational transitions, which are strongly correlated. Motion of the chain segments was found to be highly localized. The activation energy for the phenylene ring flip was estimated to be 12.6 kcal/mol and the flip frequency as 0.77 MHz at 300 K.

Computer simulations in conjunction with NMR studies have also been applied to study the local structure and conformations of BPAPC amorphous bulk system.[143,144] One of the issues relating to the structure of polycarbonates is the conformation of the carbonate group. X-ray analysis along with other experimental measurements suggests that the conformation of the carbonate group is preferably *trans*, *trans*. RIS calculations of the unperturbed chain also support this view. This view has been questioned on the basis of magnitude of the intramolecular interactions in a dense packed structure and relatively low energy barrier (16 kJ/mol) for transition from the *trans*, *trans* (*t*-*t*) to the *cis*, *trans* (*c*-*t*) state. Investigations involving NMR studies indicated that in glassy BPAPC at 135 K, carbonate group is predominantly *trans* and less than 10% of all carbonate groups are in a *cis* conformation. Probability distribution of the orientation of the phenylene rings with respect to the carbonate group is also found to be quite broad. The simulations using the amorphous cell method were usually found to predict a *cis*-*trans* content of 25-30%.

Monte Carlo and molecular dynamics simulations of crystalline, amorphous and melt polycarbonate systems have been performed using a density functional based force-field.[145]

The force-field was derived on the basis of extensive DFT studies on molecular fragments and structural analogues of BPAPC. The study focussed on the thermal properties of crystal and liquid phases, T_g and vibrational properties and surface structure of amorphous material. Satisfactory agreement with experiments was obtained for the structure factor of amorphous BPAPC. Meyer et al. have reported MD calculations on liquid DPC in the temperature range 350 K to 600 K.[146] They developed two force fields for the simulations, which differed in the torsional energy barriers and partial charges on DPC. Simulations using force field-1 (FF-1) which had a higher torsional energy barrier for the carbonate group showed that at 400 K, about 86% of the molecules are in the more favorable *t-t* conformation versus 75% of these conformers at 573 K. The second force field, FF-2 gave a fraction of *t-t* molecules of 67% at 400 K and 60% at 573 K. These results suggest that the % of the *t-t* and *c-t* conformers are very much dependent on the torsional energy barrier used in the force field. The diffusion behavior of liquid DPC, despite its larger size was found to be similar to those of usual liquids.

Modeling investigations have also used a quasi-static approach to determine the activation energy barrier of the phenyl ring flips in glassy BPAPC.[140] These glassy BPAPC ring flip simulations clearly demonstrated the effect of intermolecular environment which increases the energy that is required for the flip. The mean activation energy was found to be 43.5 kJ/mol. Witney and Yaris have developed a generalized Langevin dynamics simulation of motion for a model of pure polycarbonate and have suggested a possible mechanism for the phenyl ring flip process.[147] Brownian dynamics simulations on phenylene ring flips in glassy polycarbonates have been performed using a force-field based on the united atom CHARMM potential. The ring flip activation energy from the simulation was found to be 38.4 kJ/mol in good agreement with the experimental value of 38 kJ/mol from NMR measurements. The simulations also pointed out on the importance for each polycarbonate chain of its packing with respect to its single nearest neighbour chain. They also suggested a possible mechanism for the ring flip process. According to the Witney-Yaris model, a phenylene ring π-flip occurs when there is an increase of about 0.5 Å in the separation between the center of a ring and that of the closest ring of the nearest neighbour chain. This

separation must be accompanied by an increase in the rotational kinetic energy of the ring attempting the flip.

Molecular mechanics simulations of free volumes available to various diffusants in glassy BPAPC have been reported by Arizzi et al.[148] Delaunay tessellation was applied to determine the available space in the polymer. The total unoccupied volume, calculated as percentage of the total cube volume is found to be 0.395 ± 0.038 for BPAPC. Dynamics of small gases in amorphous glassy models of BPAPC has been investigated using transition-state theory approach.[149] The gaseous molecules were found to migrate through the polymer microstructures in a sequence of hops between local minima of potential energy. At the time scale of the simulation employed, larger molecules like Ar, O_2 and N_2 were trapped in the vicinity of the initial sites and could not reach the diffusive regime. The study indicated that the rigid-matrix approach is inadequate for studying the dynamics of light gases except for He. In a latter study, He transport in glassy BPAPC were investigated in detail by Gusev and Suter.[150] Atomistic models for BPAPC were simulated using the PCFF force-field. Favorable agreement was found for the calculated diffusive activation energy and permeability coefficients with that obtained from experiments. Fast elastic vibrations of the polymer atoms were found to affect the He transport in the polymer matrix. Water sorption in BPAPC have been investigated by Nick and Suter using a combination of thermodynamic integration approach and Widom's particle insertion method in a MD simulation of dense amorphous structures.[151] These simulations were able to reproduce the sorption behaviour for different polymers investigated.

There have also been reports on the bulk amorphous structure of a few substituted polycarbonates using atomistic as well as coarse-grained simulations.[152-162] Fully atomistic simulations of the amorphous cells of tetramethyl (TMPC) and tetrabromo (TBPC) derivatives of BPAPC and the diffusivity of various gases in these polymers have found correlation between the simulated available volume distribution and diffusion properties that is consistent with experimental results.[152] Atomistic models for polycarbonate based on 1,1'-bis(4-hydroxyphenyl)cyclohexane (BPCPC) and TMPC have been reported wherein neutron scattering curves from simulations were in reasonable agreement with experimental data.[153]

Transport of gaseous diatomic molecules in a copolymer of BPAPC with trimethylcyclohexylidene bisphenol polycarbonate (TMCPC) have been simulated using transition-state approach which gave favourable comparison with experimental results.[154,155]

Earlier investigations on BPAPC using bond fluctuation model focussed on reproducing the Vogel-Fulcher temperature of the amorphous bulk along with the static structure factor.[56,58,156,157] BPAPC and two of the structurally modified polycarbonates were studied by (i) chemically detailed simulations and (ii) simulations of coarse-grained models (iii) combination of the above two approaches by inverse mapping.[61] Bond fluctuation model when applied for the simulations of BPAPC and TMCPC showed that it was not strong enough to differentiate between the structural variants. Freezing behavior derived from these simulations were almost similar for BPAPC and TMCPC although the T_g of these polymers are very different. Coarse molecular dynamics simulations were successful in differentiating between the structural variants with respect to the freezing behaviour. Better agreement between the simulated and the experimental scattering functions of the bulk amorphous structure were observed using the inverse mapping procedure.

Recent simulations on structurally modified polycarbonates BPCPC and TMCPC have focussed on generation of well equilibrated configurations in the melt state by use of coarse-grained methods.[158-160] Tschop et al. have presented a procedure for coarse-graining atomistic models of polycarbonates into mesoscopic model which is representative of a rather simple bead spring model that allows for the fast equilibration of configurations in the melt state. This is followed by reintroduction of chemical details and further relaxation. The results from these simulations were directly compared with the neutron scattering data. Scattering experiments using spin-polarized neutrons enables one to separate the coherent and incoherent scattering and the resultant structure factors from these experiments can be directly compared with results from molecular simulations.[158,159] Experimental results on structure using these advanced scattering methods on BPAPC and substituted polycarbonates having cyclohexyl ring substituents at the C_α carbon (BPCPC and TMCPC) are available.[158,159,161,162] For BPCPC and TMPC,[153,161] where structure factors have been calculated from atomistic computer simulated models, the peak positions are in agreement

with the corresponding experimental values, but the width of the amorphous halos are quite large. The correlation lengths have been found to be less than two orders of magnitude when simulations are compared to the experimental results. In the latter study[162] employing coarse-graining procedure on polycarbonate melts, much better level of agreement has been obtained than from earlier attempts. In a recent report by Abrams and Kremer,[160] the effect of more realistically accounting for the excluded volume of phenyl units in the coarse-grained simulations has been examined. The study also showed that artifacts introduced by simplification in the coarse-grained model can be effectively nullified via straightforward MD integration at full atomistic resolution. Abrams et al. have also presented a dual-resolution coarse-graining scheme for MD simulations of BPAPC liquids in contact with a nickel surface.[163]

1.3.4. Simulations of the deformation behaviour of amorphous polycarbonate

The method developed by Theodorou and Suter[84,85] has been applied to study the small strain elastic constants and mechanisms of large-strain plastic deformation of BPAPC by atomistic simulations.[164] Three types of deformation, (1) uniform hydrostatic compression (2) pure shear and (3) pure uniaxial tension were applied to obtain the various elastic moduli with a total imposed strain of 20%. Calculated elastic moduli were higher than the experimental values and the discrepancy was explained as due to the small size of the simulation box and rigidity of the BPAPC unit. For large strain deformation averaged stress-strain response exhibited a linear region parallel to elastic loading line upto 6-7% shear strain where yielding occurs, beyond which the polymer deforms at relatively constant stress. Decrease in initial hydrostatic pressure was observed with increasing strain, indicating that the initial glassy material has a strong tendency to become denser and thus more ordered upon plastic deformation. This shear induced pressure response in BPAPC is opposite to that found in polypropylene where an initial dilatant response was found. Qian and Ludovice used constant stress molecular dynamics to calculate the bulk modulus, Youngs modulus and density of a few amorphous polymers including BPAPC.[165]

Molecular mechanics simulations of the deformation of BPAPC were performed using a modified Dreiding force-field, where the maximum strain applied was about 15%.[166]

Yield phenomenon was observed at about 10%. Calculated yield stress and Youngs modulus were higher than the experimental values. A general approach was also presented by these authors to calculate the stiffness matrix of a unit cell of any shape. In a subsequent study on the uniaxial deformation of glassy BPAPC, stretching simulations were performed by changing the cell parameters consistent with the applied strain and assumed poisson ratio of the material.[167] Maximum strain imposed was about 30%. Bisphenol and carbonate groups were found to orient parallel to the stretching direction as the deformation progresses. One should note here that experiments have shown that the deformation scheme with the constant intrinsic poisson ratio assumption is not valid at larger strain since the volume of the bulk sample and the free volume may decrease as a function of strain.[170-172]

NMR experiments in conjunction with athermal atomistic simulations have been employed by Suter and co-workers to quantify the orientational order that develops in BPAPC during plastic deformation.[168,169] Plane-strain mode of deformation was employed to study the global as well as local orientational order that develops in BPAPC and the results were compared with atomistic simulations of uniaxial compression of BPAPC. Qualitative agreement between the experiment and simulations were observed in that signs of the order parameter for the phenyl and carbonate groups being correctly predicted by the simulations but they overestimate the degree of orientational order. Limitation of this account was attributed to the finite sample cell size used in the simulations. In yet another study effects of plastic deformation on conformation and local packing in BPAPC were quantified using polarization-transfer and double-quantum NMR experiments.[169] Conformational distributions predicted by atomistic simulations agreed with those from experiments for the undeformed samples. At a deformation of $\varepsilon = -0.68$, distribution function predicted by simulations differed considerably than that experimentally observed. Simulations predict a marked sharpening of the distribution of the Ph-O angles which is not observed from NMR experiments.[169]

To the best of our knowledge there have been no reports in the literature on molecular simulation studies of deformation of substituted polycarbonates. Also, at this time there are no atomistic simulation or molecular simulation studies which describe the calculation of

birefringence of polymers in the glassy state and the optical response to deformation, in the literature. This serves as one of the key motivation for the work presented in this thesis.

1.4. References

1. Roe, R. J. *Computer Simulation of Polymers*, Prentice Hall: New York, 1991.
2. Bicerano, J. *Computational Modeling of Polymers*, Marcel Dekker: New York, 1992.
3. Monnerie, L.; Suter, U. W. *Atomistic Modeling of Physical Properties of Polymers*, *Adv. Polym. Sci*., Springer: Berlin, 1994.
4. Binder, K. *Monte Carlo and Molecular Dynamics Simulations in Polymer Science*, Oxford University Press: Oxford, 1996.
5. Baschnagel, J.; Binder, K.; Doruker, P.; Gusev, A. A.; Hahn, O.; Kremer, K.; Mattice, W. L.; Muller-Plathe, F.; Murat, M.; Paul, W.; Santos, S.; Suter, U. W.; Tries, V. *Adv. Polym. Sci*. **2000**, *152*, 41.
6. Volkenstein, M. V. *Configurational Statistics of Polymer Chains*, Interscience: New York, 1963.
7. Birshtein, T. M.; Ptitsyn, O. B. *Conformations of Macromolecules*, Science Publishing House: Moscow, 1964.
8. Flory, P. J. *Statistical Mechanics of Chain Molecules*, Interscience: New York, 1969.
9. Flory, P. J. *Macromolecules* **1974**, *7*, 381.
10. Mattice, W. L.; Suter, U. W. *Conformational Theory of Large Molecules*, John Wiley & Sons: New York, 1994.
11. Rehahn, M.; Mattice, W. L.; Suter, U. W. *Adv. Polym. Sci*. 131/132, 1995.
12. Mark, J. E.; Flory, P. J. *J. Am. Chem. Soc*. **1966**, *88*, 3702.
13. Mark, J. E. *J. Chem. Phys*. **1972**, *56*, 458.
14. Guest, J. A.; Matsuo, K.; Stockmayer, W. H.; Suter, U. W. *Macromolecules* **1980**, *13*, 560.
15. Saiz, E.; Tarazona, M. P. *Macromolecules* **1983**, *16*, 1128.
16. Kuntman, A.; Bahar, I.; Baysal, B. M. *Macromolecules* **1990**, *23*, 4959.
17. Jernigan, R. L.; Flory, P. J. *J. Chem. Phys*. **1967**, *47*, 1999.

18. Patterson, G. D.; Flory, P. J. *J. Chem. Soc., Faraday Trans. II* **1972**, 68, 1098.
19. Patterson, G. D.; Flory, P. J. *J. Chem. Soc., Faraday Trans. II* **1972**, 68, 1111.
20. Suter, U. W.; Flory, P. J. *J. Chem. Soc., Faraday Trans. II* **1977**, *73*, 1521.
21. Flory, P. J.; Saiz, E.; Erman, B.; Irvine, P. A.; Hummel, J. P. *J. Phys. Chem*. **1981**, *85*, 3215.
22. Irvine, P. A.; Erman, B.; Flory, P. J. *J. Phys. Chem*. **1983**, *87*, 2929.
23. Erman, B.; Marvin, D. C.; Irvine, P. A.; Flory, P. J. *Macromolecules* **1982**, *15*, 664
24. Erman, B.; Wu, D.; Irvine, P. A.; Marvin, D. C.; Flory, P. J. *Macromolecules* **1982**, *15*, 670.
25. Honeycutt, J. D. *Comp. Theor. Polym. Sci.* **1998,** *8*, 1.
26. Bicerano J. *Comp. Theor. Polym. Sci.* **1998**, *8*, 9.
27. Launne, T.; Neelov, I.; Sundholm, F. *Polymer* **1999**, *40*, 2313.
28. Lee, S.; Jeong, H. Y.; Lee, H. *Comp. Theor. Polym. Sci*. **2001**, *11*, 219.
29. Blomqvist, J.; Pietila, L. O.; Mannfors, B. *Polymer* **2001**, *42*, 109.
30. Blomqvist, J. *Polymer* **2001**, *42*, 3515.
31. Sulatha, M. S.; Purushotham, S.; Natarajan, U. *Polymer* **2002**, *43*, 6297.
32. Binder, K. *Monte Carlo Methods in Statistical Physics*, Springer: Berlin, 1979.
33. Burkert, U.; Allinger, N. L. *Molecular Mechanics, ACS Monograph 177*, American Chemical Society: Washington DC, 1982
34. Clark, T. A. *Handbook of Computational Chemistry*, Wiley-Interscience: Wiley, New York, 1985
35. Hirst, D. M. *A Computational Approach to Chemistry*, Blackwell Scientific: London, 1990.
36. Ciccotti, G.; Hoover, W. G. *Molecular Dynamics Simulations of Statistical Mechanical Systems*, North-Holland Amsterdam, 1986.
37. Allen, M. P.; Tildesley, D. J. *Computer Simulation of Liquids*, Clarendon Press: Oxford, 1987.
38. Binder, K.; Heermann, D. W. *Monte Carlo Simulation in Statistical Physics: Introduction*, Springer: Berlin, 1988.
39. Binder, K. In *Computational Modeling of Polymers*; Bicerano, J., Ed.: Marcel Dekker: New York, 1992, p.221.

40. Binder, K. *Monte Carlo Methods in Condensed Matter Physics*, Springer: Berlin, 1992.
41. Allen, M. P.; Tildesley D. J. *Computer Simulation in Chemical Physics*, Kluwer: Dordrecht, 1993.
42. Frenkel, D.; Smit, B. *Understanding Molecular Simulation: From Algorithms to Applications*, Academic Press, New York, 1996.
43. Leach, A.R. *Molecular Modelling: Principles and Applications*, Pearson Eduacational Ltd., Harlow, 1996.
44. Haile, J. M. *Molecular dynamics simulation: Elementary Methods*, Wiley Interscience: New York, 1992.
45. Theodorou, D. N.; Suter, U. W. *Macromolecules* **1985**, *18*, 1467.
46. Rigby, D.; Roe, R-J. *J. Chem. Phys*. **1987**, *12*, 7285.
47. Boyd, R. H.; Pant, K. In *Computer Simulation of Polymers*, Roe, R. J., Ed.: Prentice Hall: New York, 1991, p.94
48. McKehnie, J. I.; Brown, D.; Clarke, J. H. R. *Macromolecules* **1992**, 25, 1562.
49. Gusev, A. A.; Zehnder, M. M.; Suter, U. W. *Macromolecules* **1994**, 27, 615.
50. Khare, R.; Paulaitis, M. E.; Lustig, S. R. *Macromolecules* **1993**, 26, 7203.
51. Kotelyanskii, M.; Wagner, N. J.; Paulaitis, M. E. *Macromolecules* **1996**, *29*, 8497.
52. (a) Muller, M.; Nievergelt, J.; Santos, S.; Suter, U. W.; *J. Chem. Phys*. **2001**, *114*, 9764; (b) Santos, S.; Suter, U. W.; Muller, M.; Nievergelt, J. *J. Chem. Phys*. **2001**, *114*, 9772.
53. Rigby, D.; Roe, R. J. *J. Chem. Phys*. **1988**, *89*, 5280.
54. Paul, W.; Yoon, D. Y.; Smith, G. D. *J. Chem. Phys*. **1995**, *103*, 1702.
55. Smith, G. D.; Yoon, D. Y.; Jaffe, R. L. *Macromolecules* **1995**, *28*, 5397.
56. Paul, W.; Binder, K.; Kremer, K.; Heermann, D. W. *Macromolecules* **1991**, *24*, 6332.
57. Paul, W. *AIP Conf Proc* **1992**, *256*, 145.
58. Paul, W.; Binder, K.; Batoulis, I.; Pittel, B.; Sommer, K. H. *Macromol Chem. Macromol Symp.* **1993**, *65*, 1.
59. Paul, W.; Pistoor, N. *Macromolecules* **1994**, *27*, 1249.
60. Tries, V.; Paul, W.; Baschnagel, J.; Binder, K. *J. Chem. Phys*. **1997**, *106*, 738.

61. Sommer, K.; Batoulis, J.; Jilge, W.; Morbitzer, L.; Pittel, B.; Plaetschke, R.; Reuter, K.; Timmermann, R.; Binder, K.; Paul, W.; Gentile, F. T.; Heumann, D. W.; Kremer, K.; Laso, M.; Suter, U. W.; Ludovice, P. J. *Adv. Materials* **1991**, *3*, 590.
62. Rapold, R. F.; Mattice, W. L. *J. Chem. Soc. Faraday Trans* **1995**, *91*, 2435.
63. Rapold, R. F.; Mattice, W. L. *Macromolecules* **1996**, *29*, 2457.
64. Doruker, P.; Rapold, R. F.; Mattice, W. L. *J. Chem. Phys.* **1996**, *104*, 8742.
65. Doruker, P.; Mattice, W. L. *Macromolecules* **1997**, *30*, 5520.
66. Bahar, I.; Cho, J.; Doruker, P.; Erman, B.; Haliloglu, T.; Kim, E. G.; Mattice, W. L.; Monnerie, L.; Rapold, R. F. *Trends Polym. Sci.* **1997**, *5*, 155.
67. Haliloglu, T.; Mattice, W. L. *J. Chem. Phys.* **1998**, *108*, 6989.
68. Haliloglu, T.; Cho, J.; Mattice, W. L. *Macromol. Theory Simul.* **1998**, *7*, 613.
69. Haliloglu, T.; Mattice, W. L. *J. Chem. Phys.* **1999**, *111*, 4327.
70. Doruker, P.; Mattice, W. L. *Macromolecules* **1998**, *31*, 1418.
71. Doruker, P.; Mattice, W. L. *Macromol. Symp.* **1998**, *133*, 47.
72. Jang, J. H.; Mattice, W. L. *Polym. Commun.* **1998**, *40*, 1911.
73. de Gennes, P. G. *J. Chem. Phys*. **1971**, *69*, 572.
74. Bishop, M.; Ceperley, D.; Frisch, H. L.; Kalos, M. H. *J. Chem. Phys*. **1982**, *76*, 1557.
75. Boyd, R. H. *Macromolecules* **1989**, *22*, 2477.
76. Almarza, N. G.; Enciso, E.; Bermejo, F. J. *J. Chem. Phys*. **1992**, *96*, 4625.
77. Go, N.; Scheraga, H. A. *Macromolecules* **1976**, *9*, 535.
78. Dodd, L. R.; Boone, T. D.; Theodorou, D. N. *Mol. Phys.* **1993**, *78*, 961.
79. Leontidis, E.; de Pablo, J. J.; Laso, M.; Suter, U. W. In *Atomistic Modelling of Physical Properties of Polymers, Adv. Polym. Sci*., Springer: Berlin, 1994.
80 Krishna Pant, P. V.; Theodorou, D. N. *Macromolecules* **1995**, *28*, 7224.
81. Siepman, J. I. *Mol. Phys*. **1990**, *70*, 1145.
82. Frenkel, D.; Mooij, G. C. A. M.; Smit, B. *J. Phys. Condens. Matter*. **1991**, *3*, 3053.
83. Siepman, J. I.; Frenkel, D. *Mol. Phys*. **1992**, *75*, 59.
84. Theodorou, D. N.; Suter, U. W. *Macromolecules* **1986**, *19*, 139.
85. Theodorou, D. N.; Suter, U. W. *Macromolecules* **1986**, *19*, 379.

86. Mott, P. H.; Argon, A. S.; Suter, U. W. *Polym. Prepr*. **1989**, *30(2)*, 34.
87 Mott, P. H.; Argon, A. S.; Suter, U. W. *Philos. Magazine A* **1993**, *68*, 537.
88. Brown, D.; Clarke, J. H. R. *Macromolecules* **1991**, *24*, 2075.
89. McKechnie, J. I.; Haward, R. N.; Brown, D.; Clarke, J. H. R. *Macromolecules* **1993**, *26*, 198.
90. Rutledge, G. C.; Suter, U. W. *Polymer* **1991**, *32*, 2179.
91. Fan, C. F.; Hsu, S. L. *Macromolecules* **1992**, *25*, 266.
92. Cagin, T.; Karasawa, N.; Dasgupta, S.; Goddrad, W. A. *J. Phys. Chem*. **1990**, *94*, 8897.
93. Karasawa, N.; Goddard, W. A. *Macromolecules* **1992**, *25*, 7268.
94. Gestoso, P.; Brisson, J. *J. Polym. Sci. Polym. Phys*. **2002**, *40*, 1601.
95. Capaldi, F. M.; Boyce, M. C.; Rutledge, G. C. *Polymer* **2004**, *45*, 1391.
96. Roberge, M.; Prud'homme, R. E.; Brisson, J. *Polymer* **2004**, *45*, 1401.
97. Utz, M; Peng, Q.; Nandagopal, M. J. *Polym. Sci. Polym. Phys*. **2004**, *42*, 2057.
98. Weiner, J. H.; Gao, J. *Macromolecules* **1994**, *27*, 1201.
99. Kroger, M.; Luap, C.; Muller, R. *Macromolecules* **1997**, *30*, 526.
100. Picu, R. C. *Macromolecules* **2001**, *34*, 5023.
101. Mavrantzas, V. G.; Theodorou, D. N. *Comput. Theor. Polym. Sci.* **2000**, *10*, 1.
102. Mavrantzas, V. G.; Theodorou, D. N. *Macromol. Theory Simul.* **2000**, *9*, 500.
103. Le Grand, D. G.; Bendler, J. T. *Handbook of Polycarbonate Science and Technology*; Marcel Dekker, Inc.: New York, 2000.
104. Williams, A. D.; Flory, P. J. *J. Polym. Sci., Part A-2* **1968**, *6*, 1945.
105. Berry, G. C.; Nomura, H.; Mayhan, K. G. *J. Polym. Sci. A-2*. **1967**, *5*, 1.
106. de Chirico, A. *Chim. Ind*. **1960**, *42*, 248.
107. Tonelli, A. E. *Macromolecules* **1972**, *5*, 558.
108. Sundararajan, P. R. *Can. J. Chem*. **1985**, *63*, 103.
109. Laskowski, B. C.; Yoon, D. Y.; McLean, D.; Jaffe, R. L. *Macromolecules* **1988**, *21*, 1629
110. Hutnik, M.; Argon, A. S.; Suter, U. W. *Macromolecules* **1991**, *24*, 5956.
111. Gawrisch, W.; Brereton, M. G.; Fischer, E. W. *Polym. Bull.* **1981**, *4*, 687.
112. Reddy, V.; Bohdanecky, M.; Staszewska, D.; Huppenthal, L. *Polymer* **1988**, *29*,

1894

113. Saiz, E.; Abradelo, C.; Mogin, J.; Tagle, L. H.; Hernandez-Fuentes, I. *Macromolecules* **1991**, *24*, 5594.
114. Özgün, N.; Knopp, B.; Jung, B.; Wortmann, F. -J.; Höcker, H. *Macromol. Symp*. **1998**, *127*, 151.
115. Özgün, N.; Nick, B.; Jung, B.; Wortmann, F. -J.; Höcker, H. *DWI Rep.* **2000**, *123*, 521.
116. Sundararajan, P. R. *Macromolecules* **1989**, *22*, 2149.
117. Sundararajan, P. R. *Macromolecules* **1993**, *26*, 344.
118. Sundararajan, P. R. *Macromolecules* **1990**, *23*, 2600.
119. Bendler, J. T.; *Ann. N.Y. Acad. Sci*. **1981**, *371*, 299.
120. Jones, A. A.; O'Gara, J. F.; Inglefield, P. T.; Bendler, J. T.; Yee, A. F.; Ngai, K. L.; *Macromolecules* **1983**, *16*, 658.
121. Bicerano, J. H.; Clark, H. A. *Macromolecules* **1988**, *21*, 585.
122. Bicerano, J. H.; Clark, H. A. *Macromolecules* **1988**, *21*, 597.
123. (a) Sung, Y. J.; Chen, C. L.; Su, A. C. *Macromolecules* **1990**, *23*, 1941; (b) Sung, Y. J.; Chen, C. L.; Su, A. C. *Macromolecules* **1991**, *24*, 6123.
124. Sun, H.; Mumby, S. J.; Maple, J. R.; Hagler, A. T. *J. Phy. Chem*. **1995**, *99*, 5873.
125. Sun, H.; Mumby, S. J.; Maple, J. R.; Hagler, A. T. *J. Am. Chem. Soc*. **1994**, *116*, 2978.
126. Bendler, J. T. *Comput. Theor. Polym. Sci.* **1998**, *8*, 83.
127. Montanari, B.; Ballone, P.; Jones, R. O. *Macromolecules* **1998**, *31*, 7784.
128. Montanari, B.; Ballone, P.; Jones, R. O. *Macromolecules* **1999**, *32*, 3396.
129. Montanari, B.; Ballone, P.; Jones, R. O. *J. Phys. Chem. A* **2000**, *104*, 2793.
130. Ballone, P.; Jones, R. O. *J. Phys. Chem. A* **2001**, *105*, 3008.
131. Akola, J.; Ballone, P.; Jones, R. O. *Macromolecules* **2002**, *35*, 2327.
132. Van Speybroeck, V.; Martele, Y.; Waroquier, M.; Schacht, E. *J. Am. Chem. Soc*. **2001**, *123*, 10650.
133. Van Speybroeck, V.; Martele, Y.; Waroquier, M.; Schacht, E. *Int. J. Quantum Chem.* **2003**, *91*, 363.
134. Katajisto, J.; Pakkanen, T. T.; Pakkanen, T. A.; Hirva, P. J. *Theochem* **2003**, *634*,

305.

135. Katajisto, J.; Linnolahti, M.; Pakkanen, T. A. *Chem. Phys. Lett*. **2004**, *385*, 25.
136. Yannas, I. V.; Luise, R. R. *J. Macromol. Sci. Phys*. **1982**, *B21*, 443.
137. Perchak, D.; Skolnick, J.; Yaris, R. *Macromolecules* **1987**, *20*, 121.
138. Walton, J. H.; Lizak, M. J.; Conradi, M. S.; Gullion, T.; Schaefer, J. *Macromolecules* **1990**, *23*, 416.
139. Hutnik, M.; Gentile F. T.; Ludovice P. J.; Suter, U. W.; Argon, A. S. *Macromolecules* **1991**, *24*, 5962.
140. Hutnik, M.; Argon, A. S.; Suter, U. W. *Macromolecules* **1991**, *24*, 5970.
141. Shih, J. H.; Chen, C. L. *Macromolecules* **1995**, *28*, 4509.
142. Fan, C. F.; Cagin, T.; Shi, W.; Smith, K. A. *Macromol. Theory Simul*., **1997**, *6*, 83.
143. Tomaselli, M.; Zehnder, M. M.; Robyr, P.; Grob-Pisano, C.; Ernst, R. R.; Suter, U. W. *Macromolecules* **1997**, *30*, 3579.
144. Robyr, P.; Utz, A.; Gan, Z.; Scheurer, C.; Tomaselli, M.; Suter, U. W.; Ernst, R. R. *Macromolecules* **1998**, *31*, 5818.
145. Ballone, P.; Montanari, B.; Jones, R. O.; Hahn, O. *J. Phys. Chem. A* **1999**, *103*, 5387.
146. Meyer, H.; Hahn, O.; Muller-Plathe, F. *J. Phys. Chem. B* **1999**, *103*, 10591.
147. Whitney, D. R.; Yaris, R. *Macromolecules* **1997**, *30*, 1741.
148. Arizzi, S.; Mott, P. H.; Suter, U. W. *J. Polym. Sci. Polym. Phys*. **1992**, *30*, 415.
149. Gusev, A. A.; Arizzi, S.; Suter, U. W. *J. Chem. Phys*. **1993**, *99*, 2221.
150. Gusev, A. A.; Suter, U. W.; Moll, D. J. *Macromolecules*. **1995**, *28*, 2582.
151. Nick, B.; Suter, U. W. *Comput. Theor. Polym. Sci.* **2001**, *11*, 49.
152. Gentile, F. T.; Arizzi, S.; Suter, U. W.; Ludovice, P. J. *Ind. Eng. Chem. Res*. **1995**, *34*, 4193.
153. Lamers, C.; Schärpf, O.; Schweika, W.; Batoulis, J.; Sommer, K.; Richter, D. *Physica B* **1992**, *180 & 181*, 515.
154. Lopez-Gonzales, M.; Saiz, E.; Guzman, J.; Riande, E. *Macromolecules* **2001**, *34*, 4999.
155. Lopez-Gonzales, M.; Saiz, E.; Guzman, J.; Riande, E. *J. Chem. Phys*. **2001**, *115*,

6728.

156. Binder, K. *Macromol.Chem. Macromol. Symp* **1991**, *50*, 1.
157. Zimmer, K. M.; Linke, A.; Heermann, D. W. *Macromol. Theory Simul*. **1996**, *5*, 1065.
158. Tschöp, W.; Kremer, K.; Batoulis, J.; Bürger, T.; Hahn, O. *Acta Polymer* **1998**, *49*, 61.
159. Tschöp, W.; Kremer, K.; Hahn, O.; Batoulis, J.; Bürger, T. *Acta Polymer* **1998**, *49*, 75.
160. Abrams, C. F.; Kremer, K. *Macromolecules* **2003**, *36*, 260.
161. Lamers, C.; Schönfeld, C.; Shapiro, S. M.; Batoulis, J.; Timmermann, R.; Cable, W.; Richter, D. *Colloid Polym. Sci*. **1994**, *272*, 1403.
162. Eilhard, J.; Zirkel, A.; Tschöp, W.; Hahn, O.; Kremer, K.; Schärpf, O.; Richter, D.; Buchenau, U. *J. Chem. Phys*. **1999**, *110*, 1819.
163. Abrams, C. F.; Site, L. D.; Kremer, K. *Phys. Rev. E* **2003**, *67*, 021807.
164. Hutnik, M.; Argon, A. S.; Suter, U. W. *Macromolecules* **1993**, *26*, 1097.
165. Qian, C.; Ludovice, P. J. *Makromol. Chem. Macromol. Symp*. **1993**, *65*, *123*.
166. Fan, C. F.; Cagin, T.; Chen, Z. M.; Smith, K. A. *Macromolecules* **1994**, *27*, 2383.
167. Fan, C. F. *Macromolecules* **1995**, *28*, 5215.
168. Utz, M.; Atallah, A. S.; Robyr, P.; Widmann, A. H.; Ernst, R. R.; Suter, U. W *Macromolecules* **1999**, *32*, 6191.
169. Utz, M.; Robyr, P.; Suter, U. W. *Macromolecules* **2000**, *33*, 6808.
170. Xie, L.; Gidley, D. W.; Hristov, H. A.; Yee, A. F. *J. Polym. Sci. Polym. Phys. Ed*. **1995**, *33*, 77.
171. Ruan, M. Y.; Moaddel, H,; Jamieson, A. M.; Simha, R.; McGervey, J. D. *Macromolecules* **1992**, *25*, 2407.
172. Powers, J. M.; Caddell, R. M. *Polym. Eng. Sci.* **1972**, *12*, 473.

Chapter 2: Scope and Objectives of the Present Work

2.1. Introduction

Comprehension of the relation between macroscopic properties of a polymer and its chemical structure is a formidable and intricate subject in the field of polymer science. This is usually dealt with by systematic experimental studies of a class (or family) of polymers having different chemical structures and relating the effect of the structure to associated physical properties. The same goal can also be achieved in a different way i.e. by the application of various molecular modeling methods to study a series of polymers. Prime objective of the work presented in this thesis is to study the relation between the chemical structure and optical properties of a series of structurally modified polycarbonates using various molecular and atomistic simulation methods. In defining and achieving this purpose, a very detailed level of structural and geometric information is additionally brought out connecting various responses, origins and events at the molecular level and physical properties at the larger scale which provide new and fundamental understanding into the relationships that we seek. Currently there is lack of fundamental insights on the influence of different structural groups towards the conformation at the level of the repeat unit, single chain and condensed polymeric phase and its effect on polymer properties like polarizability, optical anisotropy and birefringence. Therefore molecular simulation studies, which can provide fundamental understanding of the effect of monomer structure towards these properties at various levels, constitute the prime objective of the present work.

Anisotropy in the optical polarizability of polymer chains is manifested in the birefringence of their condensed phase and is of considerable importance with potential technological applications in the area of information storage.[1-13] Optical anisotropy of polymer chains is, therefore, of considerable fundamental and practical relevance in providing an understanding of material behaviour and for the molecular design of materials with properties tailored towards specific applications. The chemical structure of the repeat unit and the conformations of the chain molecule, and the flow conditions which orient the chains during the processing of these materials, dictate their optical

properties.[4-9] An understanding of the effect of chemical structure of the polymer repeat unit or small molecular fragments, on their optical anisotropy, therefore becomes an important step towards providing qualitative as well as quantitative understanding of the optical property at the macroscopic scale. In order to design new polymeric materials that have useful optical properties, such as low optical anisotropy, $\langle\gamma^2\rangle$ and low birefringence, a thorough understanding of various structural and conformational features that control these properties is required.

Polymers are virtually indispensable as materials for a variety of optical applications. In the area of optical data storage technology bisphenol A polycarbonate (BPAPC) is widely used as a substrate material due to its combination of favourable properties such as transparency, heat resistance, toughness, stiffness, dimensional stability and economical processing. The disadvantage posed by BPAPC is its high intrinsic birefringence.[4-9] Polarizable phenylene rings along the backbone of this polycarbonate are known to provide positive birefringence. High birefringence and refractive index anisotropy renders exact focus of optical beam unsuitable for the purpose of reading and writing.[4] Birefringence in polymers occurs mainly due to the intrinsic chemical structure, which results in different polarizabilities and hence different refractive indices in different directions.[10-13] In amorphous samples in their glassy state, a part of the birefringence occurs due to the residual stresses prevailing as a result of molding conditions, which orient the chains in the direction of the stress. Although processing conditions can minimize stress and orientational birefringence, a further reduction of the intrinsic birefringence of polycarbonate is desirable. Thus, although audio compact disks (CDs) are manufactured exclusively of BPAPC, birefringence issue still precludes its use in larger form factor disks.[4-6] Increasingly stringent requirement to be met in terms of lower birefringence means that development and molecular design of suitable chemically modified or substituted polycarbonate is required. Polarizability of the monomer unit and the degree of polymer chain orientation determine the level of birefringence in the plastic substrate. Therefore polycarbonates with low anisotropy of their molecular polarizability are preferred. Researchers have attempted structural modification of the bisphenol unit to derive potential polymers having low birefringence

than BPAPC by various strategies:[7] (i) replacement of aromatic phenylene rings by less polarizable symmetric cyclic fused rings; (ii) polycarbonate variants produced by replacing the isopropylidene group by a cyclohexyl; (iii) modified polycarbonates with lateral methyl groups or with lateral groups based on *bis*-(3-phenyl-4-hydroxyphenyl)-derivatives, and by incorporation of aliphatic substituents. Although a vast amount of literature do exist on various aspects of synthesis and optical property characterization of polycarbonates, a fundamental understanding on the relationship between the chemical structure and the polarizability, optical anisotropy and birefringence and systematic theoretical studies of the polymer is currently lacking.

The main objective of the present work is to study a series of polycarbonates with different chemical structures by various molecular simulation techniques for determining polymer conformations and optical properties. The property of interest in this study is the optical properties of polycarbonates, specifically, the polarizability, optical anisotropy and birefringence. In this work, conformations of BPAPC and different substituted polycarbonates will be studied in detail, i.e., at the monomer, repeat unit, single chain and also in the amorphous condensed phase using different atomistic simulation methods. The focus is on (i) the averaged chain dimensions; (ii) polarizability and single chain optical anisotropy; (iii) packing and structure of the amorphous glassy condensed state; (iv) changes in orientation and packing in the glassy state as a result of deformation, and (v) birefringence in the glassy state. The various structural modifications to BPAPC of interest in the present work include substitutions at the C_α atom by cyclohexylidene ring, substitutions on the phenylene rings by methyl groups and both types of substitutions simultaneously. Optical properties of these substituted polycarbonates in terms of the stress-optical coefficients in the glassy and melt states have been quantified by experimental measurements in the literature.[7,14-20] Relatively, little advancement has been made in the area of molecular simulation studies of structurally modified polycarbonates and, specifically, with regard to optical properties of these polymers.

2.2. Objectives

2.2.1. Conformational analysis, RIS models and single chain properties of structurally modified polycarbonates

Conformational properties of polymer chains are of significant importance in various areas of polymer science.[21] The influence of conformational properties on the behavior of chains in solution and in the condensed bulk phase is related to and controlled to various extents by intrachain properties and local segment level structure. A fundamental understanding of conformational aspects and conformationally averaged statistical properties of polymer chains forms an intrinsic part of the overall relationship between chemical structure and macrosopic polymer properties.

Theoretical studies on the various single chain conformational aspects of BPAPC have been the subject of numerous investigations.[22-24] Except for the studies on conformations of a series of polycarbonates using a force-field that neglected a variety of interactions,[25,26] there are no theoretical studies in the literature concerning the conformational aspects and single chain properties of substituted polycarbonates. The focus of the present work is to bring out the effect of structural modifications on the conformational characteristics of small molecular segments constituting substituted polycarbonates as well as those of the single chains using a well defined force-field which satisfactorily takes into account all the interactions. The information derived from conformational analysis will be then used to formulate explicit RIS models for these structurally modified PC's and these will in turn be used to calculate the averaged chain dimensions as a function of temperature and molecular weight. Another objective in this work is to understand the local conformational behavior and properties of such fragments constituting the polycarbonate chain, and to obtain detailed information on the effect of substituent chemical structure on the chain dimensions. Another important purpose of this simulation study is to understand the role of intramolecular rigidity in a qualitative way among the various polycarbonates as dictated by their chemical structure. Theoretical study of conformational properties and chain dimensions in such polycarbonates has not been presented prior to the present work and would provide important fundamental insights into the local and long-range behaviour of polymers composed of such complicated structural repeating units.

2.2.2. Optical anisotropy of structurally modified polycarbonates having cyclohexylidene and methyl substituents using the rotational isomeric state method

Optical properties of BPAPC with respect to its polarizability, optical anisotropy and birefringence have been investigated in detail by various experimental methods.[27-35] The theoretical estimation of the mean-squared optical anisotropy ($\langle\gamma^2\rangle$) of BPAPC have been reported by Erman et al.[30,31] using the RIS/VOS approach and found to be in excellent agreement with the experimental value from scattering experiments. Polarizability tensors of the phenyl and carbonate groups have been derived from experiments on model compounds and these satisfactorily take into account the mutual inductive effects and the condensed phase. The motivation for the present work here is the lack of theoretical studies on $\langle\gamma^2\rangle$, of structurally modified polycarbonates and a lack of experimental studies with systematic structural variation concentrating on the polarizability and optical anisotropy of these polycarbonates. The present work addresses new understanding of the relationship of atomic level structure, monomer conformations, chain conformational structure, and intrinsic group polarizabilities, to the single chain optical anisotropy of BPAPC and four structurally modified polycarbonates.

One of the objectives of the present work is to derive and implement a new methodology for formulation of the polarizability tensors of polycarbonate molecular fragments, which is applicable to substituted bisphenyl fragments, diphenyl carbonates and repeat units of various structurally modified polycarbonates having cyclohexylidene group at the C_α carbon and methyl groups on backbone phenylene rings. This theoretical approach will utilize polarizability tensors of constituent groups that have been derived from DRS measurements and the geometry from conformational energy calculations. Another objective is the application of RIS/VOS for the calculation of single chain optical anisotropy of structurally modified polycarbonates. Polarizabilities and conformational averaged optical anisotropies of different bisphenyl and carbonate fragments along with the results on substituted polycarbonate chains will be presented. Another objective is to analyze in detail the contribution of the various conformers to the optical anisotropy in these polycarbonates. A comparison of the calculated single chain

optical anisotropy with the optical properties in the bulk state, for e.g. the stress optical coefficient in the glassy and melt states will be presented.

2.2.3. Ab initio calculations on small molecule fragments of structurally modified polycarbonates

Geometry and conformations of the BPAPC repeat unit have been accurately derived using different quantum chemical methods.[36-40] One of the objective of the present work is to perform ab initio calculations on bisphenyl fragments corresponding to the four structurally modified polycarbonates being studied here. Calculations will be performed using the ab initio method and the optimized geometries of various bisphenyl and carbonate fragments of various structurally modified polycarbonates having cyclohexylidene group at the C_α carbon and methyl groups on backbone phenyl rings. Another objective of the present work is to derive the polarizability tensors and calculate the optical anisotropy of the various conformers corresponding to these bisphenyl and carbonate fragments using the ab initio method. The optical anisotropies of these bisphenyl fragments will then be compared with those calculated using the experimental group polarizability tensors via the VOS scheme.

2.2.4. Detailed atomistic simulations of structurally modified polycarbonates in the glassy state

BPAPC is one of the most widely studied polycarbonate by experimental and theoretical methods with the prime objective of understanding the local structure and molecular motions in the glassy state.[41-44] There are a few reports in the literature concerning the atomistic simulation and coarse-grained molecular simulations of bulk amorphous state of substituted polycarbonates.[45-49] One of the objective of the present work is to investigate the local structure of BPAPC and four substituted polycarbonates in their amorphous glassy state using atomistic simulations with full chemical details and to understand the effect of these structural modifications on the short-range order. The results presented in this work will include amorphous models for these polycarbonates with full atomistic description, the conformational features and packing of chains in the

bulk, their torsion distributions, structure factors, radial distribution functions, the geometric packing correlation between phenylene rings and the bulk phase free volume distributions. One of the important objectives of this work is to understand the effect (influence) of chemical structure of the polycarbonate on the detailed amorphous structure of its glassy state and the cohesive energies, via the complex relationship link provided by the intermolecular energetics and packing effects. Simulation studies of this kind, through which interrelationships between the amorphous structures, bulk properties and the chemical structure of the polymer will be brought forth for a set of chemically different polymers having systematic structural differences within the same class, are important in providing valuable understanding in the area of polymer science. These types of simulation studies are scarce in the literature.

2.2.5. Atomistic simulations of the orientational birefringence of polycarbonates in the glassy state

Polycarbonates as a class of structures have been extensively investigated experimentally for their optical birefringence both in glassy as well as the melt state.[4-9,14-20,32-35] There are very few theoretical and modeling reports in literature which deal with optical birefringence of amorphous thermoplastic polymers as a function of stress or strain (deformation), and these reports have looked at very simple model alkane based polymers such as polyethylene in the melt state.[50-54] Although numerous experimental reports on birefringence of BPAPC and various structurally modified polycarbonates exists in literature, there have been no attempts till date on computer simulation studies for the estimation of this important property of polycarbonates. One of the objectives of the present work is to perform atomistic simulations of the uniaxial tensile deformation of BPAPC and two substituted polycarbonates, in the glassy state. The polycarbonate chains will be treated explicitly with full chemical description of the individual structures. An extensive analysis of the orientation behaviour of the specific chemical groups as a function of deformation will be presented. In the case of BPAPC, analysis will also be provided on the packing and orientations of phenyl rings and carbonate groups in the bulk and how it varies as a result of deformation. Another objective of this work is to calculate the birefringence of these oriented polycarbonates as a function of deformation. A

methodology will be presented for the calculation of birefringence of glassy amorphous polymers by atomistic simulations, which takes into account the individual group polarizability tensors in the repeat unit along with the chain geometry and conformation. The effect of various substitutions on the orientation and optical birefringence of polycarbonates will also be brought forth in this work. There are no reports till date on atomistic simulations of deformation of any substituted polycarbonate.

2.3. References

1. Mills, N. J. In *Encyclopedia of Polymer Science and Engineering*; Mark, H. F.; Bikales, N. M.; Overberger, C. G.; Menges, G., Eds.; John Wiley & Sons: New York, 1987; Vol. 10, p 493.
2. Jones, R. S.; Kuder, J. E In *Encyclopedia of Polymer Science and Engineering*; Mark, H. F.; Bikales, N. M.; Overberger, C. G.; Menges, G., Eds.; John Wiley & Sons: New York, 1987; In Supplement volume, p 554.
3. Erman, B.; Queslel, J-P In *Encyclopedia of Polymer Science and Engineering*; Mark, H. F.; Bikales, N. M.; Overberger, C. G.; Menges, G., Eds.; John Wiley & Sons: New York, 1987; In Supplement volume, p 18.
4. Kampf, G.; Mergel, D. In *Encyclopedia of Chemical Technology*; Howe-Grant, M., Ed.; John Wiley & Sons: New York, 1995; Vol. 14, p 277.
5. Kampf, G.; Freitag, D.; Fengler, G.; Sommer, K. *Polymers for Advanced Technologies* **1992**, 169.
6. Pisipati, R. M.; Schmid, H.; Kampf, G. In *MRS Bulletin*, *46*, 1990.
7. Le Grand, D. G. In *Handbook of Polycarbonate Science and Technology*; Le Grand, D. G.; Bendler, J. T., Ed.; Marcel Dekker, Inc.: New York, 2000.
8. Wimberger Friedl, R. *Prog. Polym. Sci*. **1995**, *20*, 369.
9. Werumeus Buning, G. H.; Wimberger Friedl, R.; Janeschitz-Kreigl, H.; Ford, T. M. In *Integration of Fundamental Polymer Science and Technology-2*; Lemstra, P. J., Kleintjens, L. A., Eds.; Elsevier: London, 1988; p 405.
10. Janeschitz-Kriegl H. *Polymer Melt Rheology and Flow Birefringence*; Springer: Berlin, 1983.

11. Ward, I. M. *Structure and Properties of Oriented Polymers*; Applied Science Publishers, Ltd.: London, 1975.
12 Riande, E.; Saiz, E. *Dipole Moments and Birefringence of Polymers*; Prentice Hall: Englewood Cliffs, 1994.
13. Read, B. E.; Duncan, J. C.; Meyer, D. E. In *Measurement Techniques of Polymeric Solids*, Brown, R. P.; Read, B. E. Eds., Elsevier Applied Science Pub., New York 1984.
14. Wimberger Friedl, R.; Schoo, H. F. M.; De Bruin, J. G. (U.S. Philips Corporation) U.S. Patent 5,424,389, June 13, 1995.
15. Toshimasa, T. I.; Kuniyuki, H. M.; Tatsumi, H. I. (Teijin Chemicals Ltd.) U.S. Patent 5,633,060, May 27, 1997.
16 Davis, G. C.; Caruso, A. J.; Wetzel, J. R.; Hariharan, R.; Wisnudel, M. B. (General Electric Company) U.S. Patent 6,001,953, December 14, 1999.
17. Shigematsu, K.; Shirouzu, S.; Sakamoto, S.; Suzuki, T. (Idemitsu Kosan Company) Eur. Patent 0312 860 A2, April 26, 1989.
18. Shirouzu, S.; Shigematsu, K.; Sakamoto, S.; Nakagawa, T.; Tagami, S. *Jpn. J. App. Phys*. **1989**, *28*, 801.
19. Shirouzu, S.; Shikuma, H.; Senda, N.; Yoshida, M.; Sakamoto, S.; Shigematsu, T.; Nakagawa, T.; Tagami, S. *Jpn. J. App. Phys*. **1990**, *29*, 898.
20. Bruder, F.; Plaetschke, R.; Schmid, H. *Jpn. J. App. Phys*. **1998**, *37*, 2120.
21. Flory, P. J. *Statistical Mechanics of Chain Molecules*; Interscience: New York, 1969.
22. Williams, A. D.; Flory, P. J. *J. Polym. Sci., Part A-2* **1968**, *6*, 1945.
23. Laskowski, B. C.; Yoon, D. Y.; McLean, D.; Jaffe, R. L. *Macromolecules* **1988**, *21*, 1629
24. Hutnik, M.; Argon, A. S.; Suter, U. W. *Macromolecules* **1991**, *24*, 5956 and references cited there in.
25. Sundararajan, P. R. *Macromolecules* **1989**, *22*, 2149.
26. Sundararajan, P. R. *Macromolecules* **1993**, *26*, 344.
27. Champion, J. V.; Desson, R. A.; Meeten, G. H. *Polymer* **1974**, *15*, 301.
28. Biangardi, M.; *Colloid. Polym. Sci*. **1981**, *259*, 111.

29. Dettenmaier, M.; Kausch, H. H. *Colloid. Polym. Sci*. **1981**, *259*, 209.
30. Erman, B.; Marvin, D. C.; Irvine, P. A.; Flory, P. J. *Macromolecules* **1982**, *15*, 664.
31. Erman, B.; Wu, D.; Irvine, P. A.; Marvin, D. C.; Flory, P. J. *Macromolecules* **1982**, *15*, 670.
32. Pietralla, M.; Schubach, H. R.; Dettenmaier, M.; Heise, B.; *Progr. Colloid. Polym. Sci*. **1985**, *71*, 125.
33. Wu, M. S. *J. App. Polym. Sci*., **1986**, *32*, 3263.
34. Peetz, L.; Krueger, J. K.; Pietralla, M. *Colloid. Polym. Sci*. **1987**, *265*, 761.
35. Vogt, H. D.; Dettenmaier, M.; Spiess, H. W.; Pietralla, M.; *Colloid. Polym. Sci*. **1990**, *268*, 22.
36. Sun, H.; Mumby, S. J.; Maple, J. R.; Hagler, A. T. *J. Phy. Chem*. **1995**, *99*, 5873.
37. Sun, H.; Mumby, S. J.; Maple, J. R.; Hagler, A. T. *J. Am. Chem. Soc*. **1994**, *116*, 2978.
38. J.T. Bendler, *Comput. Theor. Polym. Sci.* **1998**, *8*, 83.
39. Montanari, B.; Ballone, P.; Jones, R. O. *Macromolecules* **1998**, *31*, 7784.
40. Montanari, B.; Ballone, P.; Jones, R. O. *Macromolecules* **1999**, *32*, 3396.
41. Hutnik, M.; Gentile F. T.; Ludovice P. J.; Suter, U. W.; Argon, A. S. *Macromolecules* **1991**, *24*, 5962.
42. Fan, C. F.; Cagin, T.; Shi, W.; Smith, K. A. *Macromol. Theory Simul*. **1997**, *6*, 83.
43. Whitney, D. R.; Yaris, R. *Macromolecules* **1997**, *30*, 1741.
44. Ballone, P.; Montanari, B.; Jones, R. O.; Hahn, O. *J. Phys. Chem. A* **1999**, *103*, 5387.
45. Lamers, C.; Schärpf, O.; Schweika, W.; Batoulis, J.; Sommer, K.; Richter, D. *Physica B* **1992**, *180 & 181*, 515.
46. Gentile, F. T.; Arizzi, S.; Suter, U. W.; Ludovice, P. J. *Ind. Eng. Chem. Res*. **1995**, *34*, 4193.
47. Lopez-Gonzales, M.; Saiz, E.; Guzman, J.; Riande, E. *Macromolecules* **2001**, *34*, 4999.
48. Tschöp, W.; Kremer, K.; Batoulis, J.; Bürger, T.; Hahn, O. *Acta Polymer* **1998**, *49*, 61.

49. Tschöp, W.; Kremer, K.; Hahn, O.; Batoulis, J.; Bürger, T. *Acta Polymer* **1998**, *49*, 75.
50. Weiner, J. H.; Gao, J. *Macromolecules* **1994**, *27*,1 201.
51. Kroger, M.; Luap, C.; Muller, R. *Macromolecules* **1997**, *30*, 526.
52. Picu, R. C.; *Macromolecules* **2001**, *34*, 5023.
53. Mavrantzas, V. G.; Theodorou, D. N. *Comput. Theor. Polym. Sci*. **2000**, *10*, 1.
54. Mavrantzas, V. G.; Theodorou, D. N. *Macromol. Theory Simul*. **2000**, *9*, 500.

Chapter 3: Conformational Analysis, RIS models and Single Chain Properties of Structurally Modified Polycarbonates

3.1. Introduction

Rotational Isomeric State (RIS) method presents a very efficient way of providing quantification of the conformational properties of macromolecules which typically assume a large number of conformations.[1] Conformational characteristics of bisphenol A polycarbonate (BPAPC) have received considerable attention since the pioneering work by Williams and Flory who formulated the RIS model for BPAPC.[2] Various calculation methods have been utilized for investigations on the conformational characteristics of BPAPC and significant results have been summarized.[3,4] Laskowski et al. proposed a RIS model for BPAPC based on the energetic and geometrical information from ab inito calculations on model compounds.[5] Hutnik et al. formulated the RIS model for BPAPC using a force-field developed based on the results of molecular mechanics and available ab initio calculations on molecular analogues of BPAPC.[6] In this RIS model rotations about all bonds in the repeat unit were explicitly considered and the *cis*, *trans* conformation (*c*-*t*) of the carbonate group was also included which was neglected in previous studies. A variety of experimental methods have also been applied to investigate the chain conformational characteristics of BPAPC in solution and in the amorphous bulk glassy state.[7-16] The chain dimensions derived from these above mentioned RIS models were in favourable agreement with available experimental data in the case of BPAPC.

Conformational characteristics of structurally modified polycarbonates (PC's) have received little attention except for the RIS models derived for a series of C_α (isopropylidene carbon) substituted polycarbonates,[17] and also the studies on the effect of articulated side groups at the C_α atom on the main chain flexibility of PC's.[18] The existing RIS models for structurally modified PC's were derived by neglecting a variety of interactions including those based on electrostatics and short-range dispersion forces.[17] In these investigations,

conformational energy calculations were performed only for the bond pair about the C_α atom with the carbonate group considered to be rigidly fixed in the *trans*, *trans* (*t*-*t*) conformation.

In the present work in this thesis, RIS models for a series of structurally modified polycarbonates are formulated from conformational energy calculations in which all types of interactions are taken into account. The various structural modifications to BPAPC include substitutions at the C_α atom, substitutions on the phenylene rings and both types of substitutions simultaneously. In this way the effect of a single substitution and compounded substitutions on the conformational characteristics and properties were understood and compared with that of BPAPC. While some of the PC's in this work have been looked at before, there are other substituted PC's for which results are presented for the first time. Chain properties using RIS models for all substituted PC's in the present study are reported here.

Conformational energy calculations were done and RIS models derived for the following substitutions: (1) substitution at the C_α atom by cyclohexyl group (BPCPC), (2) substitution at the C_α atom by trimethylcyclohexyl group (TMCPC), (3) substitution on the phenylene rings of BPAPC by CH_3 groups (DMPC) and (4) both, cyclohexyl group at the C_α atom and methyl groups on the phenylene rings (DMBPC). The monomers used for the present study are shown in Figure 3.1.

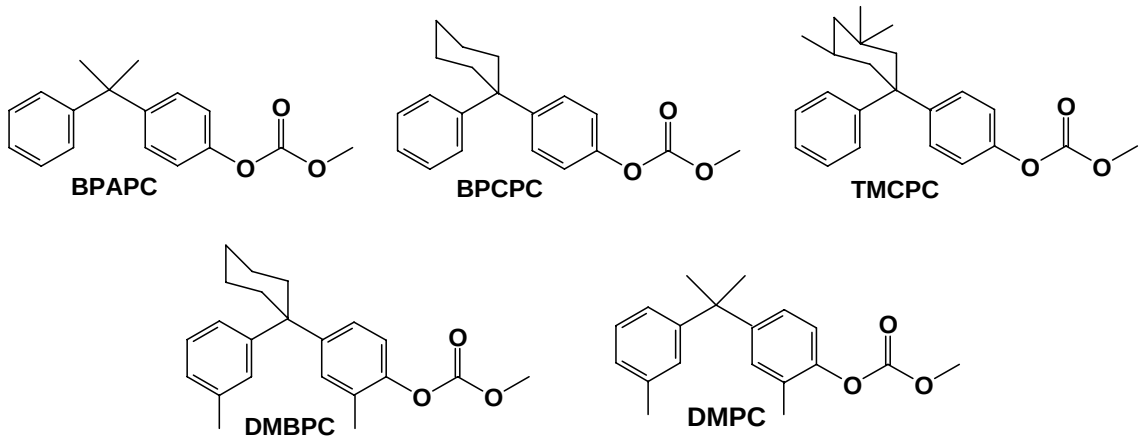

Figure 3.1. Chemical structures of the repeat units of polycarbonates studied

3.2. Simulation Methodology and Computational Details

All the calculations were performed using InsightII Polymer 4.0.0 modeling software from Molecular Simulations Inc.,[19] on Silicon Graphics O2 workstation. Conformational energies about the various bond pairs for the PC's were calculated using the PCFF force field,[20-24] which employs a quadratic polynomial for bond stretching and angle bending and a three-term Fourier expansion for torsions. Non-bonded interactions are described by Lennard-Jones 9-6 potential and the electrostatics are described using pair-wise coulombic terms. Out of plane interactions and cross terms up to third order were included. No cutoffs were used in the calculation of the dispersion and electrostatic energies with interatomic interactions being considered for all atoms in the fragments.

All model compounds were minimized until the potential energy gradient was less than 10^{-3} kcal/mol Å. Conformational analysis was done by systematic torsional variation of two consecutive bonds from -180° to 180° in 5° increments accompanied by relaxation of other degrees of freedom in the system at every specific torsion of the bond pair. The torsions were kept constant at specific values by applying a force constant of 1000 kcal/mol rad^2. The relaxation was performed using a combination of Steepest Descent and Newton-Raphson methods till the energy gradient was less than 10^{-3} kcal/mol Å for each specific conformer. From the conformational energy maps of every backbone torsional pair in the PC chain, the minima were identified and the relative energies of each minima were calculated with respect to the global minimum for the particular bond pair. Thus a set of relative energy values and corresponding minimum energy torsional values for the specific bond pairs in the polycarbonates model fragments (for eg. 6 bond pairs in BPAPC) were derived. The energy values were suitably corrected for the first order interactions. A database is created for each PC chain with these relative energy values along with the prefactor for the various torsional pairs. The prefactor is kept unity in the calculation of statistical weights because energy wells corresponding to the various rotational states of a bond pair were of similar shape and this is found to be true for all the different polycarbonates selected in this study. The energies were then used to compute the statistical weights at a particular temperature. Statistical weight matrices were thus formulated for all the rotatable bond pairs in the repeat unit. To calculate the chain properties, statistical weights were assigned sequentially to the various bonds in the

polycarbonate chain along with the required bond lengths and bond angles and the averaged conformational properties calculated.

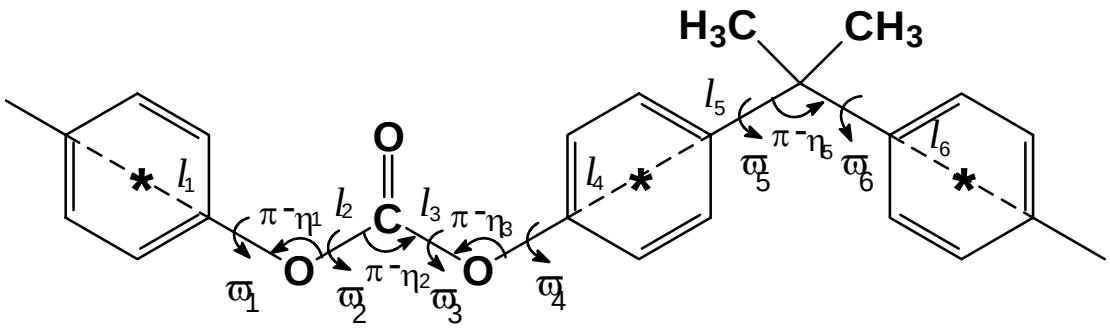

Figure 3.2. Schematic diagram of the polycarbonate chain denoting symbols for bond lengths, angles and torsions. ϕ_1 corresponds to the first bond in the repeat unit.

Figure 3.2 depicts the schematic of a BPAPC segment in a conformation where all the torsion angles are zero. Repeat units of the different structurally modified PC's used in the present study are given in Figure 3.1. For BPAPC, there are six rotatable bonds in the repeat unit (4 virtual and 2 real bonds) and statistical weight matrices were formulated for the six bond pairs from the conformational energy calculations for the respective bond pairs. In the case of BPCPC and TMCPC, conformational analysis and the derivation of statistical weight matrices were done only for three bond pairs (i) ϕ_6, ϕ_1; (ii) ϕ_4, ϕ_5; (iii) ϕ_5, ϕ_6, because it was assumed that the conformation of the carbonate group i.e. the ϕ_2, ϕ_3 torsions will not be affected by the C_α substituted cyclohexyl group due to the distance of separation between them. Our preliminary conformational calculations carried out for the torsional pairs in BPCPC repeat unit showed that this assumption is valid and the torsional values about the carbonate group (ϕ_2 and ϕ_3) are unaffected by the C_α substituent. Therefore the three statistical weight matrices describing conformation about the carbonate group, (ϕ_1, ϕ_2), (ϕ_2, ϕ_3) and (ϕ_3, ϕ_4), were taken to be the same as those for BPAPC. However, in the case of DMBPC and DMPC where there are methyl substituents on the phenylene rings, adjacent to the carbonate group, the conformational analysis was done for all the six bond pairs in the repeat unit and the different statistical weight matrices were derived. The matrices were taken to be the same for bond pairs (i) ϕ_1, ϕ_2; (ii) ϕ_2, ϕ_3; (iii) ϕ_3, ϕ_4 for DMBPC and DMPC.

Using the energy diagrams and contour plots obtained from the conformational energy calculations of the various bond pairs, the energy barriers for transition between the minima and the statistical weights for occurrence of these minima were derived. Bond lengths and bond angles for RIS chain calculations were taken from the force-field based minimization of the model compounds. The bond lengths and angles used in the present RIS calculation are given in Table 3.1.The geometrical parameters along with the statistical weights of the different bond pairs were then used to formulate the RIS models for computing chain conformational properties as function of molecular weight and temperature. Also, molecular dynamics studies for the model compounds DPC, DMDPC and chain segments in BPAPC, DMBPC and DMPC were carried out to investigate the alteration of the chain dimensions with temperature. Rationalization of the unusual behavior of chain dimensions with temperature for DMPC is done by evaluating the energetics of conformational interactions and relating these to long chain effects.

Table 3.1. Geometrical parameters of the polycarbonate chains

	l_1[a] (Å)	l_2[b] (Å)	$\theta_1=\theta_3$ (deg.)	θ_2 (deg.)	θ_4 (deg.)	θ_5 (deg.)
BPAPC	2.890	1.31	58	69	0	69
BPCPC	2.890	1.31	58	69	0	72
TMCPC	2.890	1.31	58	69	0	73
DMPC	2.885	1.31	60	68	0	69
DMBPC	2.885	1.31	60	68	0	72

[a] $l_1= l_4=l_5=l_6$; [b] $l_2= l_3$

3.3. Results and Discussion

3.3.1. Conformational analysis

Iso-energy contours for distinct bond pairs in BPAPC repeat unit are given in Figure 3.3. The iso-energy contours are at intervals of 0.5 kcal/mol. The rotation about the first bond in the repeat unit (ϕ_1) is not coupled, and it can take up all combinations of either positive or negative rotational states. The phenyl rings neighbouring the carbonate group assume a conformation of ϕ_1=50°. This agrees well with the 50° obtained from ab initio calculations by

Sun et al..[23] The energy barrier for transition between various minima is in the range of 0.1-0.5 kcal/mol.

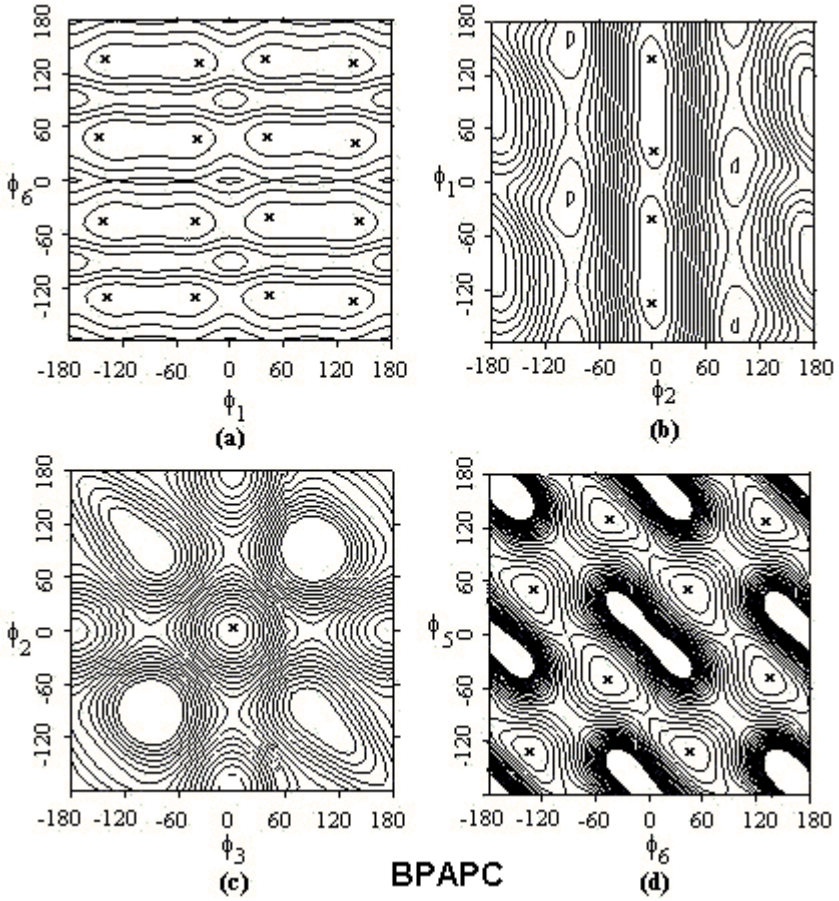

Figure 3.3. Iso-energy contours for the various dihedral pairs in BPAPC. Minima are marked as '×'. The contour lines are drawn at intervals of 0.5 kcal/mol from the minima.

Analysis of the bond pair (ϕ_2, ϕ_3) confirms the *trans*, *trans* (*t*-*t*) conformation of the carbonate group as the most stable one. But the *cis*, *trans* (*c*-*t*) conformation is also accessible with the energy difference being 1.61 kcal/mol. The energy barrier for the transition from *t*-*t* to *c*-*t* conformation is 5.4 kcal/mol. The *cis*, *cis* (*c*-*c*) conformation of the carbonate group is found to have an energy of 7.9 kcal/mol and therefore was not included in the formulation of the RIS model.[2,5,6] The energy barrier for *t*-*t* to *c*-*c* transition from the present calculations is found to be 10.9 kcal/mol.

Previous studies in literature on model compounds containing carbonate groups include ab initio calculations using a variety of basis sets such as STO-3G, HF-631G*, HF-

631G**, 6-311G** and hybrid density functional theory (B3LYP, 6-311G** basis set) calculations in the gas phase.[5,23,25-28] STO-3G calculation led to a value of 1.68 kcal/mol for the energy difference between the *t-t* and *c-t* forms of DPC. But 6-31G* calculations on MPC gave a value of 2.74 kcal/mol and this was used by Laskowski et al.[5] in the RIS model for BPAPC. Quantum chemical calculations using DFT/ B3LYP/6-311G** by Meyer et al.[26] gave a value of 1.9 kcal/mol in vacuum and 1.48 kcal/mol with an Onsager reaction field calculation. The energy barrier for transition between *t-t* and *c-t* conformations was found to be 6.2 kcal/mol. Quantum chemical calculations reported by Dybal et al.[28] showed that the high energy preference obtained from ab initio calculations at the HF/631G* level is considerably lowered when electron correlation is included using MP2 or DFT theory. From the data presented by them, gas phase calculations involving B3LYP/631G* and MP2/6-31G* gave energy differences of 2.27 and 1.89 kcal/mol for the *c-t* conformer and energy barriers of 6.62 and 7.16 kcal/mol for the *t-t* to *c-t* transition respectively. They performed calculations taking into account the various solvent effects also, and the results showed that the *c-t* conformation, which is having a higher dipole moment than the *t-t* form, is preferred in a solvent with higher permittivity. The energy values obtained using PCFF force field for the energy of the *c-t* conformer is 1.61 kcal/mol and the energy barrier for the *t-t* to *c-t* transition is 5.4 kcal/mol which are in reasonable agreement with the values reported by Meyer et al. which are 1.9 and 6.2 kcal/mol respectively.[26]

Iso-energy contours about the (ϕ_5, ϕ_6) bond pair showed one symmetrically unique minimum, where the phenyl rings are twisted out of the plane in opposite directions by 50°. Hutnik et al. reported the torsion to be (45°,45°) for this bond pair.[6] The rotations of the phenyl rings are strongly coupled due to the presence of the isopropylidene linkage, which prohibits conformations of the type (50°,130°) due to repulsive interactions between the *ortho* hydrogens on the phenyl rings. Non-zero elements in the statistical weight matrix for this bond pair correspond to conformations of the type (50°,50°). Local minima, 'morino' (0°,90°) and 'butterfly' (90°,90°), conformers are at a saddle point between two equivalent minima. The energy barriers for the transition between two equivalent minima are 1.5 kcal/mol (the intermediate conformer being 0°,90°) and 3.2 kcal/mol (intermediate

conformer 90°,90°). The planar conformation (0°,0°) occurred at 13.8 kcal/mol. DFT (ACM/DZVP) and HF/6-31G*[21] calculations reported on DPP shows that the optimized structure corresponds to a conformation in which the phenyl rings are twisted out of the plane by 50.5° which is similar to the optimized structure obtained from PCFF. The (0°,90°), (90°,90°) and (0°,0°) conformers were at an energy of 1.8, 3.5 and 17.5 kcal/mol respectively from DFT and 2.1, 3.9 and 17.2 kcal/mol from HF calculations.[21] Present calculations using the PCFF force-field gave values 1.5, 3.2 and 13.8 kcal/mol respectively.

In the case of BPCPC, TMCPC and DMBPC, the cyclohexyl group at the C_α atom can have two configurations **BPC-1** and **BPC-2** (Figure 3.4) with respect to each of the phenyl rings, axial and equatorial, and these two conformations were found to be energetically equivalent for the global minimum due to the inherent symmetry of the conformations with respect to the bisphenol unit. The disposition of the cyclohexyl group in our model compounds is as shown in the case of **BPC-1** in Figure 3.4. When the cyclohexyl group is in a particular configuration **BPC-1**, the two phenyl rings however are inequivalent. This results in a situation were one of the rings is axial (ϕ_5) and the other equatorial (ϕ_6). For **BPC-2**, the reverse holds true, i.e. equatorial (ϕ_5) and axial (ϕ_6).

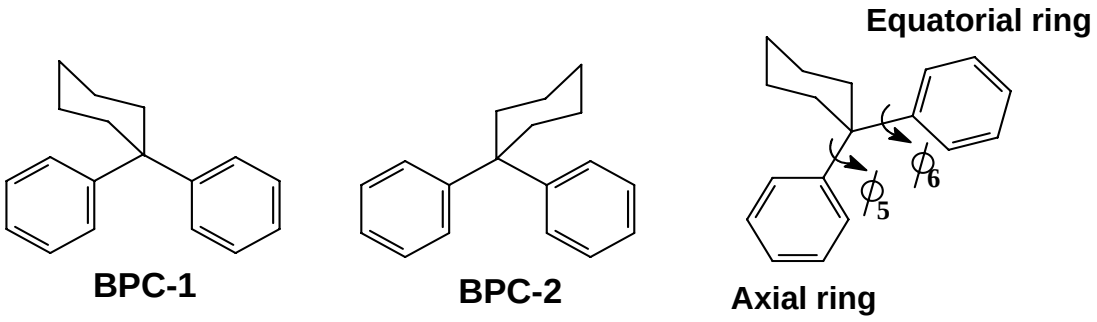

Figure 3.4. The two different dispositions BPC-1 and BPC-2 of the cyclohexyl group at the C_α carbon in BPC and the torsional definition of phenyl rings used in the study.

For BPCPC and TMCPC, the interaction between the cyclohexyl group and the carbonate group torsion is assumed to negligible due to the large distance of separation between them. Hence the energy maps were calculated for only the following pairs of dihedrals (i) ϕ_6, ϕ_1; (ii) ϕ_4, ϕ_5; (iii) ϕ_5, ϕ_6. The iso-energy contours and the 3D energy maps

for BPCPC for the situation were one of the rings is axial (ϕ_5) and the other equatorial (ϕ_6) is shown in Figure 3.5 and 3.6 respectively. Variations in steric interactions presented by the axial and equatorial substituents cause the ring rotational barriers to be different and this can be clearly seen from the energy maps.

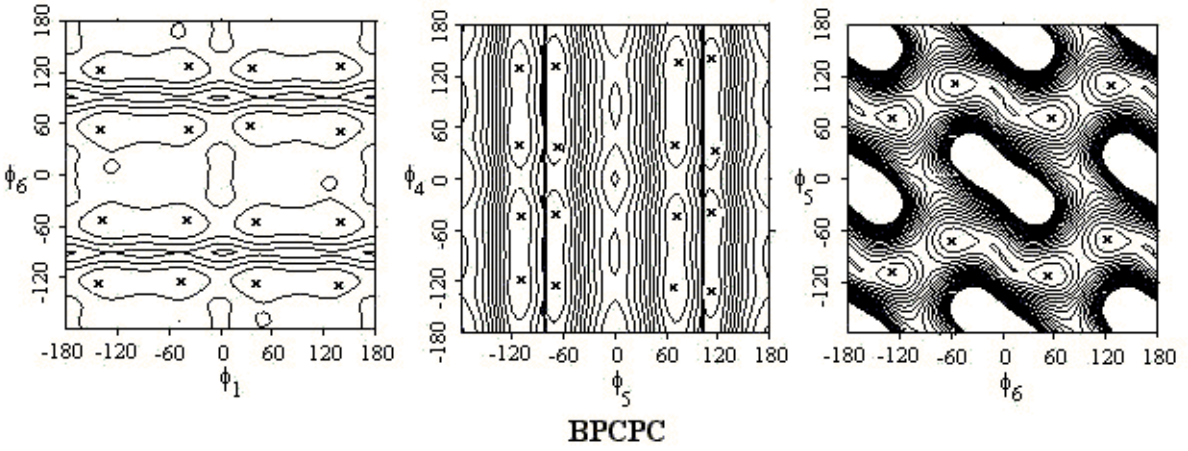

Figure 3.5. Iso-energy contours for the various dihedral pairs in BPCPC. Minima are marked as '×'. The contour lines are drawn at intervals of 0.5 kcal/mol from the minima

For the (ϕ_5, ϕ_6) bond pair, the minima correspond to the conformations in which the axial and equatorial phenyl rings are twisted out of the plane by 70° and 55° respectively. The local minima are found at (90°,0°) and (90°,90°) conformations at energies about 0.5 and 1.6 kcal/mol respectively. The conformation at (0°,90°) was found to be at a higher energy of 4.5 kcal/mol due to the interactions between the hydrogens on the axial phenyl ring (which is planar) and the cyclohexyl group. Further studies on BPC with cyclohexyl group at the alternate conformation **BPC-2**, ϕ_5 (equatorial) and ϕ_6 (axial) showed that the (0°,90°) conformers have lower energies than (90°,0°) conformers, i.e. a reversal in the energy values when compared to the former conformation of the cyclohexyl group as expected. The higher energy of the (90°,0°) conformer in this case is again due to unfavorable interactions between the hydrogens on the axial phenyl ring and those on the cyclohexyl group. The energy map for the (ϕ_5, ϕ_6) bond pair also showed that the equatorial phenyl ring could rotate from -180° to 180° with an energy barrier of 1.5 kcal/mol when the axial phenyl ring is restricted to 90°. This implies a higher intramolecular flexibility for the equatorial phenyl ring. For the axial ring, the freedom of rotation is obviously restricted due to relatively increased steric

hindrance. The energy diagrams for the ϕ_5 and ϕ_6 bonds are shown in Figure 3.6 It clearly depicts the free rotations possible for the Ph-O bond (ϕ_4) and the equatorial phenyl ring (ϕ_6), where as the axial phenyl ring is restricted to narrow regions of lower energy with associated high energy regions between the minimum locations.

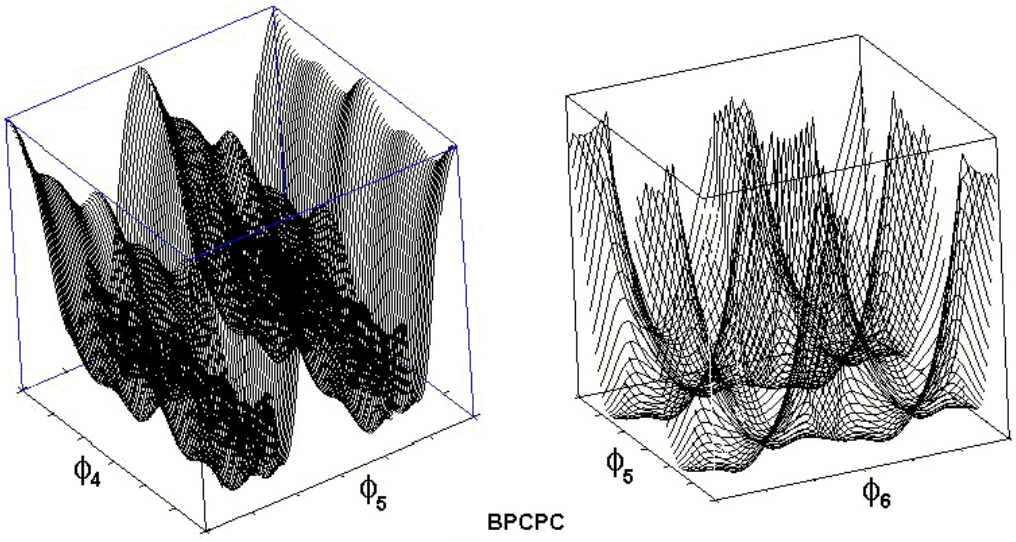

Figure 3.6. 3D energy maps for the different torsions in BPCPC

The rotations about the Ph-O bond (ϕ_1 and ϕ_4 dihedrals) in BPCPC are unhindered as in the case of BPAPC allowing for rotational states ±50° (and 50±130°). But the statistical weights calculated for these low energy states are different from that of BPAPC, indicating that the cyclohexyl group does influence the energies of these conformations although the positions of the minima are unaffected. Also, the orientation of the phenyl ring relative to the cyclohexyl group, whether axial or equatorial, influences the energies. The positions of the minima are similar to that reported by Sundararajan,[17] but the energy barriers are different considering the additional energetic interactions, which have been taken into account in the present study. The conformational aspects seen in the present work for BPCPC are in agreement with the NMR studies.[29,30]

Conformational dynamics of BPCPC in solution as well as in the bulk state have been studied using NMR,[29,30] where low activation energy barriers were observed for the conformational inversion of the cyclohexyl ring in the polycarbonate chain in comparison to unsubstituted cyclohexane ring suggesting that ground state conformation is considerably

strained relative to a pure chair form. The experimental activation energy for cyclohexyl ring inversion in BPCPC solution has been determined to be 6.7 kcal/mol.[30] This is much lower than that activation energy value for ring inversion determined for a simple substituted cyclohexane like methylcyclohexane where the energy barrier for ring inversion is found to be 10.4 kcal/mol and the corresponding value for phenylcyclohexane being 8.8 kcal/mol.[31] Dynamics and ring inversion barriers in a series of cycloalkylidene bisphenol monomers were studied using ^{13}C-NMR relaxation experiments by Lee et al.[32] Their studies yielded activation energy for ring inversion in cyclohexylidene bisphenol (BPCPC monomer) to be 11±1 kcal/mol. This suggests that in the BPCPC polycarbonate chain, the ring inversion of cyclohexyl ring is much faster than that what could be in the monomer and that the ground state conformation of the cyclohexyl in the polycarbonate chain is considerably strained relative to a pure chair form.

The differential dynamics observed for the phenylene rings in BPCPC from NMR studies[29,30] correlates well with their inequivalent conformational features, one being axial and the other equatorial. In solution, the equatorial ring in BPCPC is found to undergo internal rotations other than the segmental motion whereas the axial phenylene ring undergoes restricted rotational diffusion. The experimental value for the apparent activation energy for rotation of the equatorial ring is 4.6 kcal/mol. At temperatures close to -90°C, cyclohexyl chair-chair inversion becomes slow on the NMR time scale and the anisotropic nature of the phenylene rings becomes clearly distinct. With decrease in temperature, the axial phenylene carbons showed additional broadening relative to the equatorial carbons. This indicates the restricted motion of the axial ring relative to the equatorial. ^{13}C NMR analysis of TMCPC has also indicated different energy barriers for the phenylene rings.[33]

Figure 3.7 shows the iso-energy contours about the bond pairs in TMCPC and the associated energy diagrams are shown in Figure 3.8. In this case also, cyclohexyl substitution results in heterogeneity of the phenyl rings, as manifested in the energy maps. The map about the (ϕ_5, ϕ_6) bond pair shows only four minima at (-70°, -60°), (-70°, 120°), (110°, -60°) and (110°, 120°) as compared to eight minima observed for BPCPC. The reduction in the number of minima is caused by the proximity of the methyl groups on the cyclohexyl group and the

hydrogens on the phenyl ring for the (70°, 60°), (70°, -120°), (-110°, 60°) and (-110°, -120°) conformers. Substitution by three methyl groups in the cyclohexyl ring results in the loss of symmetry, which is otherwise present in BPCPC. This pattern of substitution on the cyclohexyl ring also leads to an increased hindrance to rotation of the phenyl rings. With the axial phenyl group at 90°, the equatorial phenyl group can undergo rotation with an energy barrier of 2.9 kcal/mol, which is approximately twice the value for BPCPC. The conformer (0°,90°) which is of higher energy (4.5 kcal/mol) for BPCPC is also found to be highly unfavorable in the case of TMCPC, with energy being 8.7 kcal/mol (for the disposition of the cyclohexyl group in the conformation indicated in Figure 3.4 i.e. phenyl ring torsions, ϕ_5 (axial) and ϕ_6 equatorial). The (90°,0°) and (90°,90°) conformers are at 1.5 and 2.1 kcal/mol from the global minimum. The conformational map about the Ph-O bond followed a pattern similar to BPCPC, although the statistical weights for the various low energy torsional states are different.

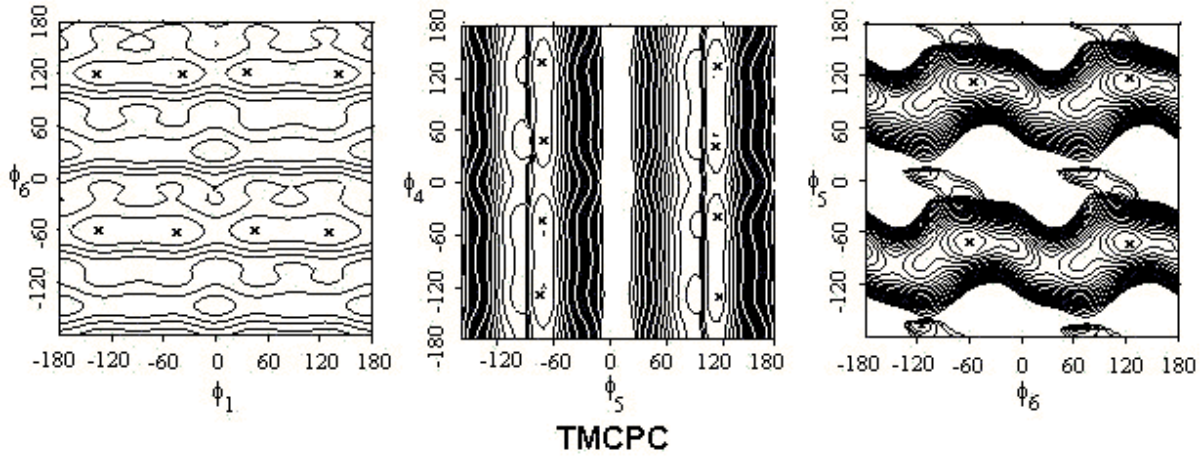

Figure 3.7. Iso-energy contours for the various dihedral pairs in TMCPC. Minima are marked as '×'. The contour lines are drawn at intervals of 0.5 kcal/mol from the minima.

3D energy map for TMCPC (Figure 3.8) shows the axial phenyl ring (ϕ_4) confined to two narrow domains of low energy in contrast to BPCPC where there are four minimum locations. The Ph-O bond shows unhindered rotation, for the bond connecting the equatorial phenyl ring the rotation is accompanied with an increased energy barrier.

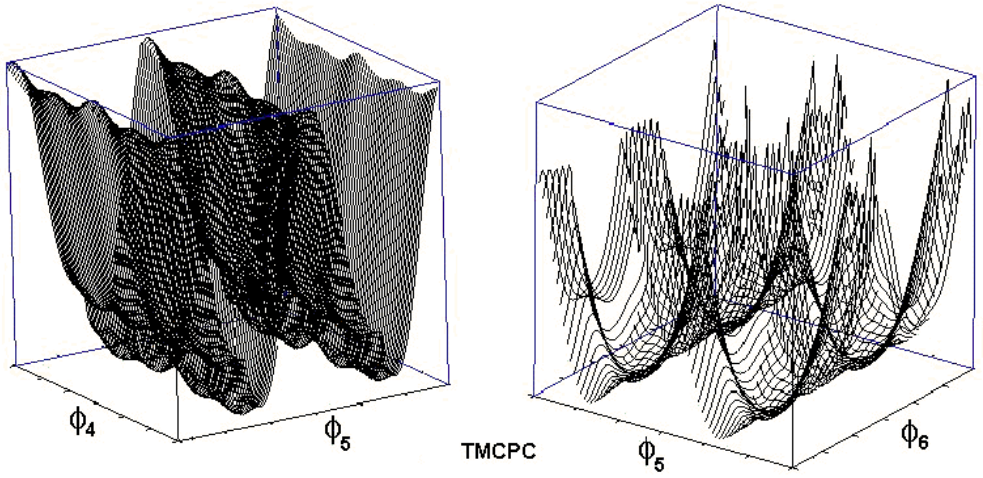

Figure 3.8. 3D energy maps for the different torsions in TMCPC

Iso-energy contours and the energy diagrams about the various bond pairs in DMBPC are given in Figure 3.9 and 3.10 and those corresponding to DMPC are shown in Figure 3.11 and 3.12 respectively. DMBPC represents a unique example in the PC's used in the present study, where in there are substitutions on the phenyl rings as well as on the C_α atom. For DMPC and DMBPC the energy maps about the (i) ϕ_1, ϕ_2; (ii) ϕ_2, ϕ_3; (iii) ϕ_3, ϕ_4 were taken to be the same because of the identical environment of these bond pairs.

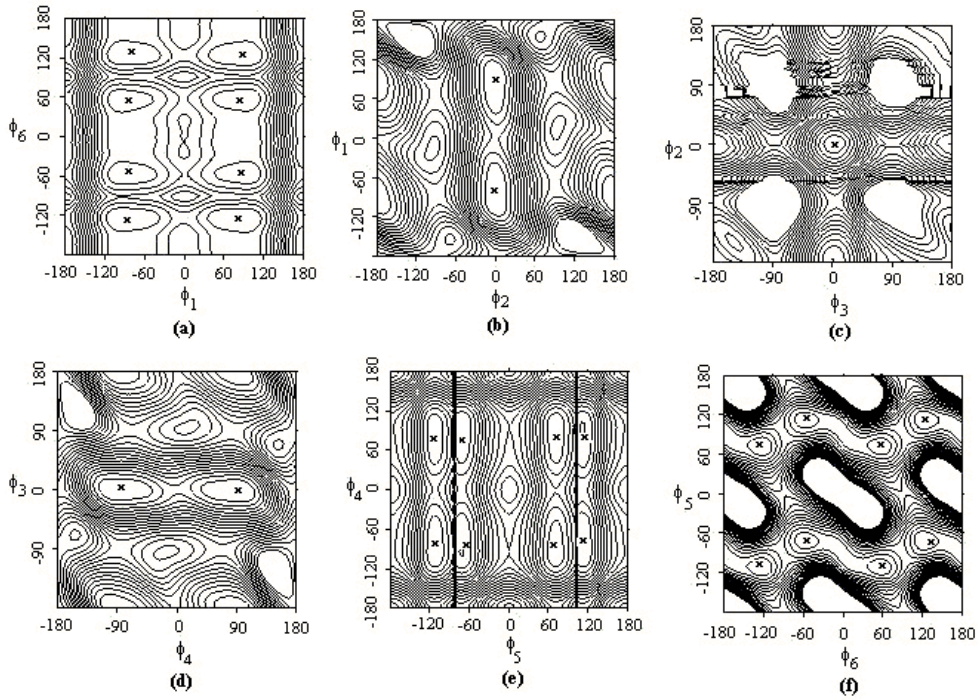

Figure 3.9. Iso-energy contours for the various dihedral pairs in DMBPC. Minima are marked as '×'. The contour lines are drawn at intervals of 0.5 kcal/mol from the minima

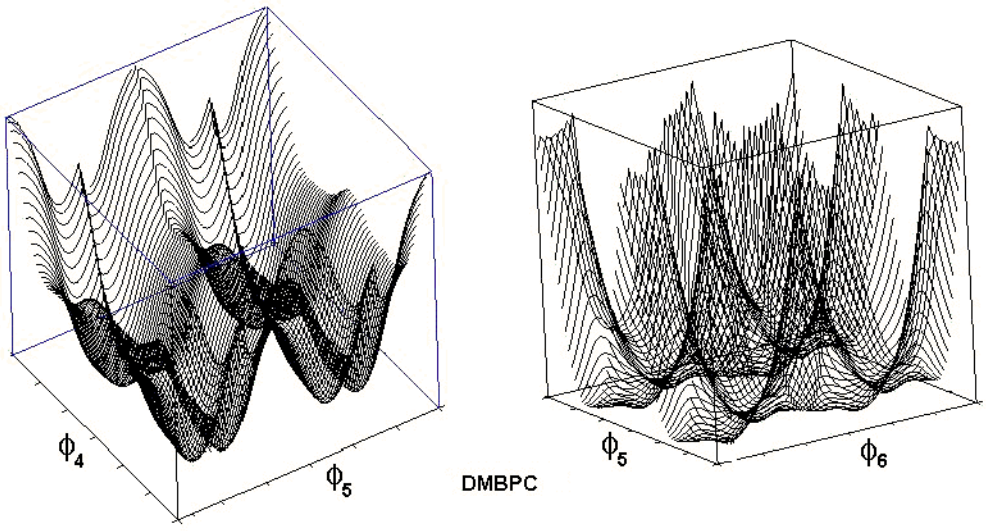

Figure 3.10. 3D energy maps for the different torsions in DMBPC

The rotational flexibility of the Ph-O bond is restricted in DMBPC and DMPC due to the presence of *ortho* methyl groups on the phenylene rings. The number of minima is reduced to two compared to BPAPC, BPCPC and TMCPC. There is a loss of symmetry of the individual phenylene rings because of the methyl group substitution. The phenylene rings prefer a conformation in which these are oriented at about 90° with respect to the carbonate group. This is due to considerable steric repulsion between the *ortho* methyl groups on the phenyl rings and the carbonate group. In BPAPC these unfavourable interactions are stronger in this case than between the *ortho* hydrogens of the phenylene rings and the carbonate group, where a compromise is made between the favourable electron delocalization energy which favours a planar conformation and the steric interaction which favours the perpendicular conformation. Hence in BPAPC, the phenyl rings ultimately prefer a conformation in between viz. 50°. In DMPC and DMBPC, steric interactions play a dominant role in deciding the conformation of the phenyl rings about the carbonate group. The energy barrier for interconversion between the two equivalent minima is 1.5 kcal/mol, which again is higher when compared to BPAPC. Preference for the *t-t* conformation of the carbonate group is retained here also, with the *c-t* conformation at 1.48 kcal/mol. The energy barrier for the *t-t* to *c-t* transition is 5.8 kcal/mol, which is slightly higher than that of BPAPC (5.4 kcal/mol). The *c-c* conformation occurs at a higher energy of 7.9 kcal/mol similar to

BPAPC and the energy barrier for the *t-t* to *c-c* transition is 12.0 kcal/mol which is higher by about 1 kcal/mol compared to BPAPC.

Iso-energy contours about the (ϕ_5, ϕ_6) bond pair in DMBPC are identical to that of BPCPC with apparent heterogeneity in the phenyl ring rotations. In the preferred conformations, the phenyl rings are twisted out of the plane by about 70° and 55° for the axial and equatorial phenyl rings respectively. The position of the minimum energy locations is thus the same as that for BPCPC. The energies of the (90°,0°), (90°,90°) and (0°,90°) conformers were found to be 0.5, 1.6 and 4.5 kcal/mol, which are similar to those noted for BPCPC (0.5, 1.6 and 4.5 kcal/mol respectively). However, there are slight differences in the energies of the eight minima from that of BPCPC. Even in the case of DMPC, the (ϕ_5, ϕ_6) iso-energy contours, as shown in Figure 3.11 is similar to that of BPAPC, with symmetrically related minima and the phenyl rings preferring out-of-plane orientations by 50°. The 'morino' (0°,90°) and 'butterfly' (90°,90°) conformers in the case of DMPC are at 1.6 and 3.2 kcal/mol above the global minima. The planar conformer (0°,0°) occurs at 19.8 kcal/mol, which is 5 kcal/mol higher than the same conformer in BPAPC.

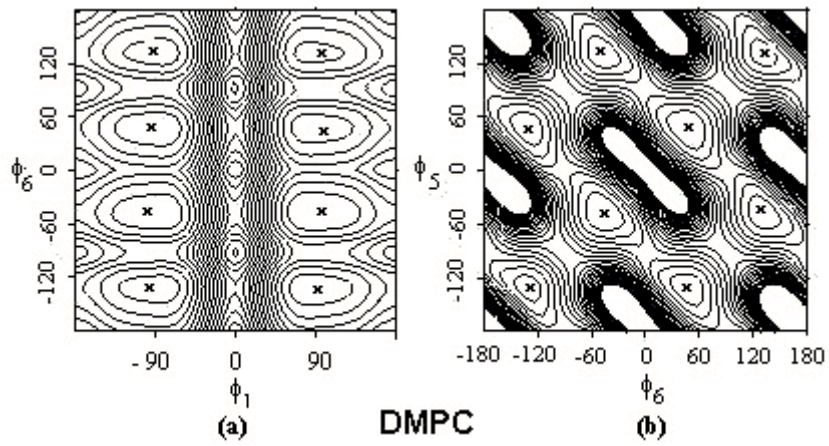

Figure 3.11. Iso-energy contours for the various dihedral pairs in DMPC

These results obtained for DMBPC and DMPC for the (ϕ_5, ϕ_6) bond pair suggest that the conformational features about the C_α atom is not altered by *ortho* methyl substitutions on the phenyl rings. The same may not hold true for longer and bulkier substituents at the C_α carbon or in the case of *meta* substitutions on the phenylene rings. The energy diagrams for

DMBPC and DMPC (Figure 3.10 and 3.12) also supports the conformational features discussed in the earlier paragraphs. DMBPC and DMPC shows two broad domains of low energy for the ϕ_4 bond centered around 90°. The ϕ_5 and ϕ_6 bonds in DMPC show four symmetrical minimum energy locations. The map for DMBPC for the ϕ_5 and ϕ_6 bonds is similar to that of BPCPC.

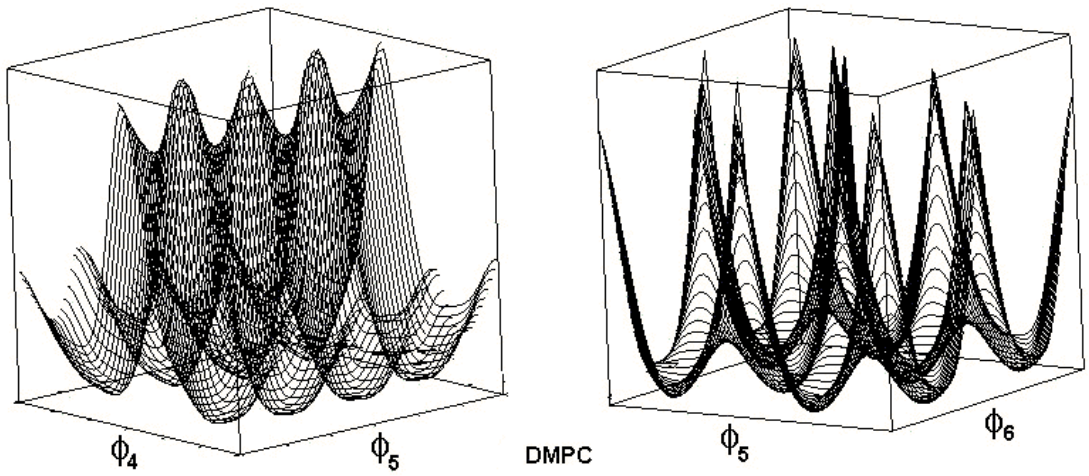

Figure 3.12. 3D energy maps for the different torsions in DMPC

It follows that substitution by the cyclohexyl group at the C_α atom restricts the conformational flexibility about the (ϕ_5, ϕ_6) torsion as indicated by the increase in energy barrier between minima and also by the maximum energy barrier, ΔE, which is the energy difference between the global minima and the highest energy conformer. ΔE values are 13.8, 19.0, 22.7, 19.0 and 19.8 kcal/mol for BPAPC, BPCPC, TMCPC, DMBPC and DMPC respectively. These values clearly indicate the increased steric hindrance to rotation by the cyclohexyl group (BPCPC) and furthermore by the trimethyl substitution (TMCPC), which results in reduction in the number of minima from eight to four. Also, the results indicate no increased rotational hindrance to the (ϕ_5, ϕ_6) bond pair in DMBPC and DMPC when compared to BPCPC and BPAPC respectively. For the Ph-O bond, the ΔE values are 2.18, 2.20, 3.40, 7.3 and 7.8 kcal/mol for BPAPC, BPCPC, TMCPC, DMBPC and DMPC respectively. The rotational flexibility of the Ph-O bond is unchanged in BPCPC but for TMCPC the barrier is higher. However, for DMBPC and DMPC the expected increase in energy barrier is due to the methyl group substitution on the phenyl rings. The carbonate

group prefers the *t-t* conformation in all PC's, but for PC's with ortho methyl substitution on the phenyl rings the preference for the *c-t* conformer is slightly higher.

3.3.2. Statistical weight matrices

Given below are the statistical weight matrices for the different distinct bond pairs in polycarbonates calculated at a temperature of 300 K.

1) BPAPC

Bond C_{ar}-O, U_1

	t^-	c^-	c^+	t^+
	−130	−50	50	130
−130	0.856	0.888	1.000	0.888
−50	0.888	0.856	0.888	1.000
50	1.000	0.888	0.856	0.888
130	0.888	1.000	0.888	0.856

Bond O-C, U_2

	t	c
	0	180
−130	1.000	0.035
−50	1.000	0.035
50	1.000	0.035
130	1.000	0.035

Bond C-O, U_3

	t	c
	0	180
0	1.000	0.067
180	1.000	0.000

Bond O-C_{ar}, U_4

	t^-	c^-	c^+	t^+
	−130	−50	50	130
0	1.000	1.000	1.000	1.000
180	0.035	0.035	0.035	0.035

Bond C_{ar}-C_α, U_5

	t^-	c^-	c^+	t^+
	−130	−50	50	130
−130	0.856	0.888	1.000	0.888
−50	0.888	0.856	0.888	1.000
50	1.000	0.888	0.856	0.888
130	0.888	1.000	0.888	0.856

Bond C_α-C_{ar}, U_6

	t^-	c^-	c^+	t^+
	−130	−50	50	130
−130	1.000	0.000	1.000	0.000
−50	0.000	1.000	0.000	1.000
50	1.000	0.000	1.000	0.000
130	0.000	1.000	0.000	1.000

2) BPCPC

Bond C_{ar}-O, U_1

	t^-	c^-	c^+	t^+
	−130	−50	50	130
−125	0.925	0.938	1.000	0.835
−55	0.938	0.925	0.835	1.000
55	1.000	0.835	0.925	0.938
125	0.835	1.000	0.938	0.925

Bond C_{ar}-C_α, U_5

	t^-	c^-	c^+	t^+
	−110	−70	70	110
−130	0.942	0.974	1.000	0.800
−50	0.974	0.942	0.800	1.000
50	1.000	0.800	0.942	0.974
130	0.800	1.000	0.974	0.942

Bond C_{α}-C_{ar}, U_6

	t^-	c^-	c^+	t^+
	−125	−55	55	125
−110	0.986	0.000	0.986	0.000
−70	0.000	1.000	0.000	1.000
70	1.000	0.000	1.000	0.000
110	0.000	0.986	0.000	0.986

3) TMCPC

Bond C_{ar}-O, U_1

	t^-	c^-	c^+	t^+
	−130	−50	50	130
−60	0.965	0.965	0.820	1.000
120	0.820	1.000	0.965	0.965

Bond C_{ar}-C_{α}, U_5

	c^-	t^+
	−70	110
−130	1.000	0.755
−50	1.000	0.910
50	0.755	0.980
130	0.940	0.965

Bond C_{α}-C_{ar}, U_6

	c^-	t^+
	−60	120
−70	1.000	1.000
110	0.968	0.968

4) DMBPC

Bond C_{ar}-O, U_1

	c^-	c^+
	−95	95
−125	1.000	0.940
−55	0.790	0.790
55	0.790	0.790
125	0.940	1.000

Bond O-C, U_2

	t	c
	0	180
−95	1.000	0.072
95	1.000	0.072

Bond C-O, U_3

	t	c
	0	180
0	1.000	0.080
180	1.000	0.000

Bond O-C_{ar}, U_4

	c^-	c^+
	−95	95
0	1.000	1.000
180	0.072	0.072

Bond C_{ar}-C_{α}, U_5

	t^-	c^-	c^+	t^+
	−110	−70	70	110
−95	0.821	0.977	0.782	0.900
95	0.753	0.940	0.800	1.000

Bond C_{α}-C_{ar}, U_6

	t^-	c^-	c^+	t^+
	−125	−55	55	125
−110	1.000	0.000	0.830	0.000
−70	0.000	0.830	0.000	1.000
70	1.000	0.000	0.830	0.000
110	0.000	0.830	0.000	1.000

5) DMPC

Bond C_{ar}-O, U_1

	c^-	c^+
	−95	95
−130	0.700	0.793
−50	0.861	1.000
50	0.838	0.712
130	0.689	0.581

Bond C_{ar}-C_{α}, U_5

	t^-	c^-	c^+	t^+
	−130	−50	50	130
−95	0.700	0.861	0.838	0.689
95	0.793	1.000	0.712	0.581

Bond C_{α}-C_{ar}, U_6

	t^-	c^-	c^+	t^+
	−130	−50	50	130
−130	0.716	0.000	0.843	0.000
−50	0.000	1.000	0.000	0.843
50	0.843	0.000	1.000	0.000
130	0.000	0.843	0.000	0.716

3.3.3. RIS models and single chain conformational properties

From the lower energy conformations evaluated from the conformational energy maps, the statistical weights for the various bond pairs were derived for BPAPC, BPCPC, TMCPC, DMBPC and DMPC. ϕ_1 refers to the first bond in the repeat unit (see Figure 3.2). The statistical weight matrices for the first and last bonds in the polymer chain were devised according to Flory's method.[1] Single chain conformational properties were calculated as a function of temperature and number of bonds in the chain and the values are listed in Tables 3.2 and 3.3. Mean squared end-to-end distance $\langle R^2 \rangle$ obtained for BPAPC from the present RIS model is 1.1 $Å^2 molg^{-1}$ at 300 K for a chain with 51 repeat units. By increasing the molecular weight corresponding to that of 1000 repeat units, the value obtained is 1.12 $Å^2 molg^{-1}$ at 300 K. These values are in close agreement with the earlier RIS models[5,6] and experimental values from dilute solution measurements on BPAPC.[7,9,12,13] The reported values are in the range 0.75-1.28 $Å^2 molg^{-1}$. The averaged chain dimensions as a function of chain length is shown in Figure 3.13.

Table 3.2. Average chain dimensions of polycarbonate chains having 1000 repeat units at 300 K

Polycarbonate	$\langle R^2 \rangle$ (nm^2)	$\langle S^2 \rangle$ (nm^2)	C_∞	a (nm)
BPAPC	2860	476	7.75	2.09
BPCPC	2810	468	7.61	2.10
TMCPC	2840	472	7.68	2.13
DMBPC	2560	425	6.94	1.97
DMPC	2420	403	6.57	1.88

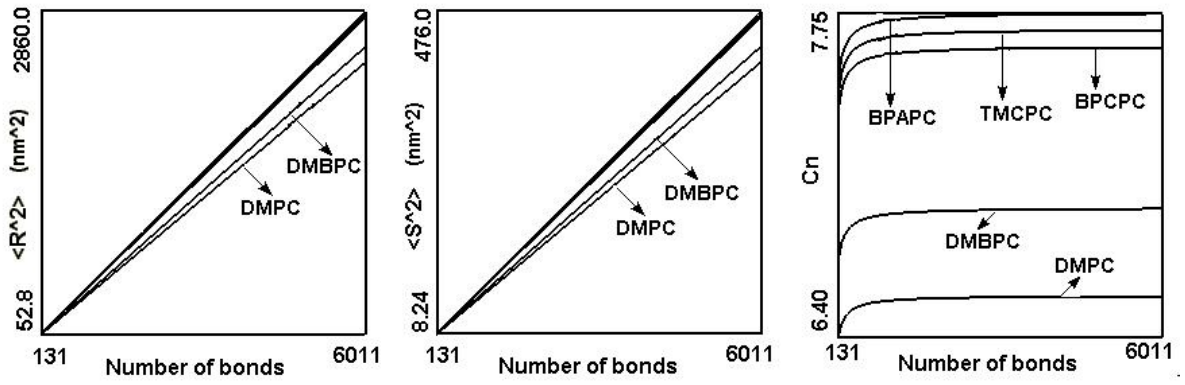

Figure 3.13. Average chain dimensions as a function of number of bonds in the polycarbonate chain at 300K. Number of repeat units in the chain varies from 20 to 1000

The $<R^2>$ values for the four structurally variant PC's suggest there is a reduction in the unperturbed dimensions of the PC chain due to structural modification. The experimental values for these PC's are not available for comparison and theoretical calculations for these PC's are reported here for the first time. The presence of cyclohexyl substitution at the C_α atom and the phenyl ring substituents each lead to more compact conformations of the PC chain. It is interesting to note that chain dimensions for TMCPC are higher than that of BPCPC with same number of repeat units in the chain. This is probably due to the steric interactions caused by the methyl groups in TMCPC, which results in a slightly more extended conformation of the polymer chain though the bisphenol fragments would have identical end-to-end distances. DMPC showed lower chain dimensions than BPAPC, due to the methyl substitutions on the phenyl rings and also possibly due to an increased preference for the compact *c-t* conformer compared to BPAPC (details are given in section 3.3.1). The chain dimensions including $<R^2>$, $<S^2>$ and C_n follow the order BPAPC > TMCPC > BPCPC > DMBPC > DMPC. Also the persistence length in the chain direction for TMCPC is the highest among the set. This behaviour reflects the relatively rigid nature of the bisphenol of TMCPC in comparison with the rest of the substituted PC's.

Table 3.3. Average chain dimensions as a function of temperature for polycarbonate chains having 51 repeat units

PC	$<R^2>$ (nm^2)		$<S^2>$ (nm^2)		C_n		a (nm)	
	300 K	500 K	300 K	500 K	300 K	500 K	300 K	500 K
BPAPC	144.8	139.1	23.33	22.42	7.64	7.33	2.92	2.03
BPCPC	142.2	133.3	22.89	21.49	7.50	7.03	2.10	2.01
TMCPC	143.6	132.4	23.08	21.35	7.57	6.98	2.13	2.01
DMBPC	129.5	121.7	20.90	19.67	6.85	6.44	1.97	1.88
DMPC	122.8	122.3	19.88	19.79	6.50	6.47	1.88	1.87

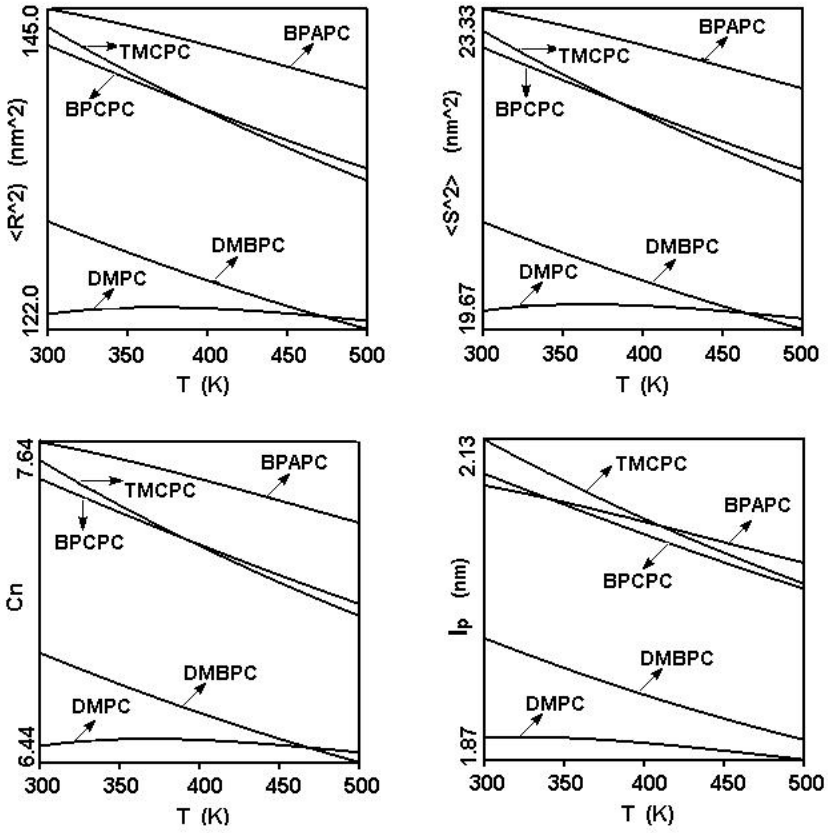

Figure 3.14. Average chain dimensions as a function of temperature for polycarbonate chains with 51 repeat units

To determine the factors responsible for the observed trend in variation of $\langle R^2 \rangle$ with structural chemistry of the bisphenols, we look at the bisphenol structural geometry, number and location of torsional minima about the bond pairs among these compounds. If the bond lengths and angles for the backbone bonds are exactly the same, then the end-to-end distance of the bisphenol will be the same for all the compounds. The states at the bond pair (ϕ_4, ϕ_5) or (ϕ_1, ϕ_6) will determine the chain dimensions, especially when the carbonate group internal torsional states are unchanged among the compounds, which is true in these structures. For BPAPC, TMCPC and BPCPC, the states –130°, 130° (having a total probability of 0.5 among the 4 states) lead to a more extended chain conformational compared to states –90°, 90°, which lead to a more compact conformation for DMBPC and DMPC. The standard deviation in repeat unit length, due to very small changes in bond angles among the various minimum energy conformations, is approximately taken to be the product of standard deviation per repeat unit and the number of repeat units (which is 50 units per chain). This value comes out to be in the range 71-74 Å depending on the bisphenol structure. Therefore the change in squared end-to-end distance is around 5112-5476 $Å^2$, and even if one takes a fraction of this value to be actually the deviation then this encompasses the net change in $\langle R^2 \rangle$ among the compounds set. Therefore, with no other factor being responsible to the differences in $\langle R^2 \rangle$ between the compounds BPAPC, TMCPC, and BPCPC, these equilibrium geometric differences can thus lead to the differences in $\langle R^2 \rangle$ that we observe among the polycarbonates. However, for DMBPC and DMPC, the relatively higher population of *c-t* conformers at the carbonate group leads a more compact chain conformational and a reduction in $\langle R^2 \rangle$ which is calculated to be of the order of the standard deviations computed due to changes in end-to-end distances arising from the compactness of the repeat unit by way of higher *c-t* conformer population.

The experimental value reported for the mean squared radius of gyration ($\langle S^2 \rangle$/M) of BPAPC is 0.208 $Å^2 molg^{-1}$.[10,16] Our RIS model predicts a value of 0.187 $Å^2 molg^{-1}$ for a chain with 1000 repeat units, which is in close agreement with the experimental value. $\langle S^2 \rangle$ values for substituted PC's as listed in Tables 3.2 and 3.3 again point towards compact conformations of the structurally modified PC's with DMPC having the lowest value of 403 nm^2 when compared to 476 nm^2 for BPAPC. The experimental value for mean squared

radius of gyration for tetramethylbisphenol polycarbonate (TMPC) is 0.14 $Å^2molg^{-1}$.[34] From the RIS model derived in the present work for DMPC, the radius of gyration is 0.143 $Å^2molg^{-1}$ for a chain with 1000 repeat units. DMPC and TMPC are expected to have similar conformational features due to the similar nature of the substituents in these PC's. DMPC has one methyl group on each phenyl ring where as TMPC has two methyl groups (symmetrically placed) on each phenyl ring. Conformations of the bisphenyl part is unaffected by ortho methyl substitutions and this would hold true for TMPC also (this has been confirmed by conformational analysis). Across the carbonate groups, methyl groups offer more steric hindrance in TMPC than in DMPC, but the minimum energy locations for the carbonate torsions are similar in these two PC's. Therefore, these are expected to have similar chain dimensions at room temperature, although the extent to which the dimensions vary with temperature will be dependent on the energy barriers and relative energy differences between the different torsional states which will be different in these two PC's. Therefore, the good comparison between the value calculated from the present work for DMPC and experimental value for TMPC indicates that the RIS models derived from force-field based conformational analysis are able to predict the chain dimensions in the experimental range even for substituted PC's. The $\langle S^2 \rangle$ value for BPCPC is 468 nm^2, which is 8 nm^2 less than BPAPC, whereas for TMCPC, the value corresponds to 472 nm^2, which is 4 nm^2 less than that for BPAPC. It is evident that a cyclohexyl or trimethyl cyclohexyl group does not drastically affect the shape of the polymer chains.

The characteristic ratio of BPAPC from the present model is 7.75. (The repeat unit was considered to be made up of six bonds, four virtual and two real). Experimental results from light scattering,[7,8] intrinsic viscosity[7] and neutron scattering[10] are in the range 8±2. For other PC's the experimental values are not available for comparison. The C_n value varies from 7.75 to 6.57, with DMPC showing the lowest value of the characteristic ratio among the five PC's. C_n for DMBPC is 6.94 and that for BPCPC is 7.61, with TMCPC showing a higher value of 7.68 when compared to BPCPC. The lowest value of C_n observed for DMPC shows a very compact conformation for the polymer chain. For the persistence length in the chain direction, TMCPC shows the highest value followed by BPCPC, BPAPC, DMBPC and DMPC. Substitution at the C_α atom by either a cyclohexyl group or a trimethylcyclohexyl

group results in reduction of the average dimensions of the single chain. The conformational properties evaluated as a function of molecular weight showed that these properties increase with increase in molecular weight. C_n do not change appreciably beyond 100 repeat units.

BPAPC shows a reduction in the unperturbed dimensions with increase in temperature. Earlier experimental studies have shown that BPAPC has a slight negative temperature coefficient for the unperturbed end-to-end distance with value in the range between zero and -0.6×10^{-3} deg^{-1}.[15] Our RIS model reproduces this experimental behavior as shown in Figure 3.14. The other PC's in the set also showed reduction in the average dimensions of the chain with increase in temperature. In the case of DMPC, the change in the dimensions with temperature is found to be insignificant. The dimensional contraction of the chains with increase in temperature is explained by the fact that the single chains prefer the more expanded *t-t* conformations of the carbonate group at low temperatures. With increase in temperature, the contracted *c-t* conformations are also accessible and this leads to reduction in the unperturbed dimensions. The statistical weights for the *c-t* and the *t-t* conformations at the carbonate group are same for BPAPC, BPCPC and TMCPC (which do not have a methyl substitution on the backbone phenyl ring), while the corresponding values for DMPC and DMBPC are the same but different from the values for BPAPC, BPCPC and TMCPC due to the methyl substitution on the phenyl rings. As seen in Figure 3.14, the decrease in chain dimensions with temperature for BPAPC, BPCPC and TMCPC occurs due to a relative increase in the population of *c-t* conformations (an increase in statistical weight) with temperature. The behavior for DMBPC is also similar to these other PC's. However, DMPC behaves differently from the rest of the polycarbonates. This is discussed in detail in the next section on the molecular dynamics of these small fragments. FT-IR measurements on solution cast films of BPAPC have shown that during sub-T_g annealing, shifts from *c-t* to the more stable *t-t* conformations occur.[35] In a previously reported study, conformational changes were monitored by the C=O stretching absorption at 1775 cm^{-1} which was identified as a doublet containing contributions at 1767 and 1785 cm^{-1} from *t-t* and *c-t* conformers.[36] In a later study, the conformationally sensitive band at 1600 cm^{-1} which is due to the in-plane stretching of the phenyl groups was used.[37] This band contains contributions from *t-t* and *c-t* conformers at 1594 and 1604 cm^{-1}. These experimental results along with WAXD and DSC

measurements[28] suggest an increase in *c-t* conformers at higher temperatures, which explains the reduction in unperturbed dimensions with temperature. This is further supported by the reported MD calculations,[26] and our MD calculations as explained in the following section.

3.3.4. Molecular dynamics simulations

The variation in the $\langle R^2 \rangle$ value with change in temperature from 300 K to 500 K in our study is 5.8 nm^2 (BPAPC), 8.9 nm^2 (BPCPC), 11.2 nm^2 (TMCPC), 7.8 nm^2 (DMBPC) and 0.5 nm^2 (DMPC). It is noted that in the case of DMPC the reduction in $\langle R^2 \rangle$ is very small, about 0.5 nm^2 when compared to other PC's. Also it is observed that $\langle R^2 \rangle$ increases by 0.5 nm^2 with temperature till 370 K and then steadily decreases although the decrease is not appreciable. This unusual behaviour prompted us to investigate the conformational features of DMPC along with BPAPC and DMBPC using molecular dynamics calculations. Since the reduction in dimensions for BPAPC was due to the percentage increase in the relative population of the *c-t* conformers, the unusual behaviour for DMPC as affected by the change in the relative population of these conformers for DMPC with increase in temperature was investigated. The MD calculations were done on the *t-t* and *c-t* forms of DPC, DMDPC and isolated chain segments of BPAPC, DMBPC and DMPC. The calculations were done at three temperatures viz. 300, 400 and 500 K. The molecules were initially equilibrated for 40 ps and simulation runs for 20 ps for sampling. The temperature control method used was Nose-Anderson. From the energies of the *t-t* and *c-t* conformers at different temperatures, the Boltzmann distribution of the two conformers was derived. The results of the MD calculations are given in Table 3.4.

For DPC, % *c-t* conformers (compact) increased from 2.9% to 34% with the raise in temperature from 300 K to 500 K. The same trend is reproduced for MD calculations done on BPAPC chain segment, where the *c-t* conformer population increases from 5.6% to 24.9% in the temperature range of 300 K to 500 K. This clearly indicates that the compact *c-t* conformers gets populated with increase in temperature and hence lead to reduction in the mean square end-to-end distances for PC's, which have no methyl substitution on the *ortho* position of the phenyl rings adjacent to the carbonate group.

Table 3.4. Population of the *c-t* conformers at different temperatures derived from molecular dynamics simulations

Model Compound	% of *c-t* conformers		
	300 K	400 K	500 K
DPC	2.9	5.8	34.0
DMDPC	14.5	13.6	9.2
BPAPC	5.6	15.0	24.9
DMBPC	4.8	44.0	80.8
DMPC	~100	~100	~100

Meyer et al. have reported MD calculations on liquid DPC in the temperature range 350 K to 600 K using two different force-fields.[26] Simulations using two different force-fields which differed in the torsional energy barriers and partial charges on DPC suggested that the % of the *t-t* and *c-t* conformers are very much dependent on the torsional energy barrier used in the force field. In their simulations using force field-1 (FF-1) which had a higher torsional energy barrier for the carbonate group showed that at 400 K, about 86% of the molecules are in the more favorable *t-t* conformation versus 75% of these conformers at 573 K. The second force field, FF-2 gave a fraction of *t-t* molecules of 67% at 400 K and 60% at 573 K. But here it is enough to reiterate the principal observation that these simulations on model compound DPC and the chain segment of BPAPC reproduce the experimental behavior in that, there is a shift from *t-t* to *c-t* conformations with increase in temperature for the polymer chain.

On the other hand, our MD calculations for DMDPC showed a slight decrease in the population of the *c-t* conformers from 14.5 to 9.2% in the temperature range 300 K to 500 K. This is in contrast to DPC where, when the temperature increased from 300 K to 500 K, there is appreciable increase (about 30%) compared to the decrease (about 5%) in population of *c-t* conformers in DMDPC.

PCFF optimized structures of the *t-t* and *c-t* conformers of the DPC and DMDPC and the chain segments of BPAPC, DMBPC and DMPC also showed that in all cases except for DMPC, the *t-t* form was the most stable conformation. The *c-t* conformer of DMDPC is

higher in energy by about 1.5 kcal/mol than the *t-t* conformer, but in the case of DMPC chain segment, the c-t conformer has lower energy, i.e. the energy of the *t-t* form is higher by about 9.7 kcal/mol than the *c-t* form, which is quite significant. This suggests that for DMPC chain segment, the carbonate groups prefer to be in the *c-t* conformation at lower temperatures while not preferring to populate the conformers at high temperatures. This is supplemented by the results from MD calculations, where in, the population is predominantly *c-t* in the temperature range 300 K to 500 K. With increase in temperature there is a slight increase in the *t-t* conformers, which does not appear to be significant. As discussed before, for DMPC, the decrease in the chain dimensions is very slight, from 122.8 to 122.3 nm^2, when compared to other PC's where there is an appreciable change in the dimension with temperature. The different behavior shown by the model compound and the chain segment suggest that long-range interactions are responsible for lowering of the energy of the *c-t* form. This behaviour is brought forth by our RIS model for DMPC. The DMPC chains are compact with predominant population of the *c-t* conformers even at low temperatures and hence there is no significant change in the chain dimensions with temperature as is predicted by the RIS model. To the best of our knowledge there have been no experimental studies on the conformational features of DMPC to verify our results. The experimental chain dimensions at room temperature for a related polymer TMPC compares well with the calculated values of DMPC here.

The MD calculations on the DMBPC chain segment also showed a similar increase in the *c-t* conformer population with increase in temperature. The population of the *c-t* conformers increased from 4.8% to 80.8% in the temperature range 300 K to 500 K. It was observed that at higher temperatures, the *c-t* conformer population in DMBPC was higher than in BPAPC. It was observed that at any temperature the *c-t* conformer population in DMBPC was higher than in BPAPC. This again is due to the increased preference for the *c-t* conformation for the case of methyl substitution on the phenylene rings as observed in the case of DMPC. The higher population of the *c-t* conformers at higher temperatures explains the reduction in chain dimensions observed for DMBPC. The higher percentage of the *c-t* conformers for ortho methyl substituted PC's (DMPC and DMBPC), compared to BPAPC and BPCPC respectively, also explains the fact that DMBPC and DMPC show relatively reduced average dimensions.

3.4. Conclusions

The conformational features of BPAPC and four structurally modified bisphenol polycarbonates were critically examined using the PCFF force field by taking into consideration all possible interactions. This study provides insights into the local structure and intramolecular flexibility of the PC's. RIS models were formulated for all the PC's from the statistical weight matrices derived from the conformational energy calculations. The average chain dimensions were also calculated and related to the structural and energetic features at the repeat unit level. The chain dimensions calculated for BPAPC compared well with the reported experimental values, while, the dimensions for the substituted PC's are reported for the first time. The modified PC's show a reduction in the chain dimensions for the same degree of polymerization as BPAPC, with DMPC having the lowest dimensions. For all the PC's, the chain dimensions decreases with increase in temperature. In the case of DMPC, the chain dimensions increased slightly till 370 K and then steadily decreased and also the reduction in the dimensions were not appreciable as compared to other PC's. This was rationalized by means of MD calculations in terms of the populations of the *t-t* and *c-t* conformers at various temperatures. For DMPC, conformational energy and MD calculations suggested a greater preference for the *c-t* conformers even at low temperatures. In summary, RIS models specifically for TMCPC, DMBPC and DMPC as well as the chain conformational properties for all the modified PC's which are presented in this study have not been reported prior to this work. Also, the relation of chain properties to properties at the bond level as well as the relationship among the various PC's due to the effect of the individual and compounded substitutions has been presented and understood in detail for the first time.

Experimental data on the chain dimensions of these polycarbonates are not available in the literature for a fruitful comparison with the theoretical calculations that are presented. The RIS methodology has been sufficiently validated over the decades for many polymers, especially, for unperturbed chain dimensions of polymers, as one can see from the huge amount of material compiled for the unperturbed chain statistics of polymers.[3,4] The effect of the force-field parameters, as has been seen, is not great for many polymers and in several cases the calculations match excellently with experimental data.[3,4] The possible errors

between the theoretical calculations and the experimentally observable properties for the unperturbed dimensions for the compounds in this work, can arise from differences in the statistical weights of the minimum energy torsional states as well as the location of the torsional states. Though the absolute values of the chain dimensions could be slightly different than the experimental values, one can ascertain the quantitative agreement/disagreement only by either quantum chemical calculations or by experiments. The qualitative results in terms of the trends among the compounds here, should however hold. The results for these substituted polycarbonates, would be a useful addition to the already existing data set for polymers and provide sufficient motivation to check, in future, the quantitative verification through some experimental data. The results presented in this work on conformational analysis and chain properties of structurally modified polycarbonates with an understanding of structural effects would serve to give useful theoretical information and new insights in this area.

3.5. References

1. Flory, P. J. *Statistical Mechanics of Chain Molecules*, Interscience: New York, 1969.
2. Williams, A. D.; Flory, P. J. *J. Polym. Sci., Part A-2* **1968**, *6*, 1945.
3. Mattice, W. L.; Suter, U. W. *Conformational Theory of Large Molecules*, John Wiley & Sons: New York 1994, p. 240.
4. Rehahn, M.; Mattice, W. L.; Suter, U. W. *Adv. Polym. Sci*. 131/132, 1995, p. 109.
5. Laskowski, B. C.; Yoon, D. Y.; McLean, D.; Jaffe, R. L. *Macromolecules* **1988**, *21*, 1629.
6. Hutnik, M.; Argon, A. S.; Suter, U. W. *Macromolecules* **1991**, *24*, 5956.
7. Berry, G. C.; Nomura, H.; Mayhan, K. G. *J. Polym. Sci. A-2.* **1967**, *5*, 1.
8. de Chirico, A. *Chim. Ind*. **1960**, *42*, 248.
9. Tsuji, T.; Norisuye, T.; Fujita, H. *Polym. J*. **1975**, *7*, 558.
10. Ballard, D. G. H.; Burgess, A. N.; Cheshire, P.; Janke, E. W.; Nevin, A.; Schelten, J.; *Polymer* **1981**, *22*, 1353.
11. Wendorff, J. H.; Fischer, E. W.; *Kolloid-Z.Z. Polym.* **1973**, *251*, 876.
12. W. Gawrisch, M.G. Brereton, E.W. Fischer, *Polym. Bull.* **1981**, *4*, 687.

13. Dettenmaier, M.; Kausch, H. H.; *Colloid Polym. Sci.* **1981**, 259, 209.
14. Cervinka, L.; Fischer, E. W.; Hahn, K.; Jiang, B.-Z; Hellman, G. P.; Kuhn, K.-J. *Polymer* **1987**, *28*, 1287.
15. Reddy, V.; Bohdanecky, M.; Staszewska, D.; Huppenthal, L. *Polymer* **1988**, *29*, 1894.
16. Maeda, N.; Norisuye, T. *Polymer* **1993**, *34*, 3475.
17. Sundararajan, P. R. *Macromolecules* **1989**, *22*, 2149.
18. Sundararajan, P. R. *Macromolecules* **1993**, *26*, 344.
19. Discover 2.9.8/96.0/4.0.0, user guide, part 1.; Polymer user 4.0.0 user guide, part 2. San Diego, CA: Molecular Simulations, 1996.
20. Sun, H. *Macromolecules* **1994**, *26*, 5924.
21. Sun, H.; Mumby, S. J.; Maple, J. R.; Hagler, A. T. *J. Am. Chem. Soc*. **1994**, *116*, 2978.
22. Sun, H. *J. Comp. Chem*. **1994**, *15*, 752.
23. Sun, H.; Mumby, S. J.; Maple, J. R.; Hagler, A. T. *J. Phy. Chem*. **1995**, *99*, 5873.
24. Sun, H. *Macromolecules* **1995**, *28*, 701.
25. Bendler, J. T. *Comput. Theor. Polym. Sci.* **1998**, *8*, 83.
26. Meyer, O. Hahn, F. Muller-Plathe, *J. Phys. Chem. B* **1999**, *103*, 10591.
27. Montanari, B.; Ballone, P.; Jones, R. O. *Macromolecules* **1999**, *32*, 3396.
28. Dybal, J.; Schmidt, P.; Baldrian, J.; Kratochvil, J. *Macromolecules* **1998**, *31*, 6611.
29. Zhao, J.; Jones, A. A.; Inglefield, P. T.; Bendler, J. T. *Polymer* **1996**, *37*, 3783.
30. Zhao, J.; Jones, A. A.; Inglefield, P. T.; Bendler, J. T. *Polymer* **1998**, *39*, 1339.
31. Squillacote, M. E.; Neth, J. M. *J. Am. Chem. Soc*. **1987**, *109*, 198.
32. Lee, Y.; Allison, B. D.; Grutzner, J. B. *J. Phys. Chem*. **1994**, *98*, 1783.
33. Hägg, M. B.; Koros, W. J.; Schmidhauser, J. C. *J. Polym. Sci. Polym. Phys*. **1994**, *32*, 1625.
34. Gentile, F. T.; Arizzi, S.; Suter, U. W.; Ludovice, P. J. *Ind. Eng. Chem. Res*. **1995**, *34*, 4193.
35. Heymans, N. *Polymer* **1997**, *38*, 3435.
36. Schmidt, P.; Dybal, J.; Turska, E.; Kulczycki, A. *Polymer* **1991**, *32*, 1862.
37. Heymans, N.; Dequenne, B. *Polymer* **2001**, *42*, 5337.

Chapter 4: Optical Anisotropy of Structurally Modified Polycarbonates Having Cyclohexylidene and Methyl Substituents Using the Rotational Isomeric State Method

4.1. Introduction

The anisotropy of the polarizability tensor of a chain molecule at optical frequencies may be manifested in the strain birefringence of an amorphous bulk polymer, in the flow birefringence of the polymer in dilute solution, in the electro-optical birefringence of solutions, or by the depolarization of light scattered (DRS) at an angle of 90°.[1] Theoretically, polarizabilities of molecules can be formulated by tensorial addition of the polarizability components of various bonds or constituent groups by the Valence Optical Scheme (VOS).[2] The tensor sum depends on the mutual orientations of these groups as dictated by the three-dimensional bonding structure and conformation. A straightforward bond additivity scheme does not satisfactorily take into account the mutual orientational and inductive effects between the groups. If larger groups are chosen instead of individual bonds, the polarizability tensors and optical anisotropies of molecules can be accurately derived using experimental data or by employing VOS or by quantum-mechanical calculations that correctly take the local environment into account. Mean-squared optical anisotropies, $\langle\gamma^2\rangle$, of polymer chains has been treated in the rotational isomeric state (RIS) approximation by proper averaging over various chain conformations with an accurate representation of the structural geometry as presented in the pioneering work of Jernigan and Flory.[3] The RIS method for the calculation of $\langle\gamma^2\rangle$ of organic molecules and oligomers in solution has shown promise and has been applied to several polymers in the past such as polyethylene,[4] poly(oxyethylene),[5] atactic polystyrene as a function of stereochemical composition,[6] aliphatic esters,[7] aromatic esters and poly(*p*-oxybenzoate),[8] and several other systems.[9]

BPAPC is the only polycarbonate for which experimental measurement of $\langle\gamma^2\rangle$ using DRS and theoretical calculation via RIS method has been performed.[10,11] DRS measurements were carried out for structural analogs dimethyl carbonate (DMC), diphenyl carbonate (DPC) and diphenyl propane (DPP) in CCl_4[10] and for BPAPC oligomer (M_n=2700

g/mol, x=10.7) in dioxane.[11] Polarizability tensors corresponding to phenyl groups in DPC and DPP, and for the carbonate group have been accurately estimated by combining information on optical anisotropy from DRS experiments in CCl_4 and the geometry of the molecule as obtained from crystal structure data (DPC) and conformational energy calculations (DPP). The calculated optical anisotropies of DPC and DPP agree well with their corresponding experimental values.[10] Using information derived from polarizabilities of constituent groups of the repeat unit (i.e. polarizability tensors of phenylene groups subjected to the effects of oxy and isopropylidene group substitution, and the tensor for the carbonate group), $\langle\gamma^2\rangle$ of BPAPC has been determined by the RIS method.[11] The calculated value 111 $Å^6$ for $\langle\gamma^2\rangle/x$, the mean-squared optical anisotropy of the repeat unit in BPAPC chain, is found to be in good agreement with the experimental value of 120 ± 5 $Å^6$.[11] Low-frequency DRS measurements by Floudas et al.[12] give results similar to those obtained from the earlier report,[11] but the actual values of $\langle\gamma^2\rangle$ slightly differ. At 25 °C, $\langle\gamma^2\rangle/x$ {8< x < 163) obtained from the measurements tends to be 117.3 $Å^6$ in solution and 115 $Å^6$ for the bulk amorphous state, indicating only slight differences in this optical property between the single chain and the amorphous states. As pointed out by Floudas et al.,[12] earlier DRS measurements of amorphous BPAPC,[13] obtained without the use of Fabry-Perot interferometer which resulted in $\langle\gamma^2\rangle/x$ = 136 $Å^6$, is an overestimation due to inclusion of collision induced anisotropy. The work by Navard and Flory in which $\langle\gamma^2\rangle$ of cyanocyclohexane, bicyclohexyl and *trans*-4-cyano-*trans*-4-n-alkyl bicyclohexyls were determined from DRS experiments, is of particular relevance to the present study here.[14] The formulation of the polarizability tensors of substituted cyclohexanes based on group tensor additivity, leads to calculation results for cyclohexanes and related compounds in agreement with the experimental and calculated values based on correct bond polarizability additivity as given by Le Fevre et al. for these small cycloaliphatic organic molecules.[15-17]

In the present work, the effects of modification of BPAPC chain by various chemical groups on the optical anisotropy of the polycarbonate chain are studied: (i) cyclohexylidene group at the C_α carbon (BPCPC); (ii) additional methyl substituents on the cyclohexylidene group (TMCPC); (iii) methyl substituents on the phenyl rings (DMPC); and (iv)

cyclohexylidene group at the C_α carbon as well as methyl groups on the phenyl rings (DMBPC). The input information required for the calculations includes the geometry derived from force-field based conformational energy calculations and the polarizability tensors of constituent groups which are derived from DRS experiments reported in the literature. Formulation of the polarizability tensors of repeat units of polycarbonates having cyclohexylidene group at the C_α carbon and methyl substituents on the phenylene rings is presented. The polarizability tensors are incorporated fruitfully into a RIS scheme for the estimation of $\langle\gamma^2\rangle$. The conformational characteristics, RIS models and single chain properties of the structurally different polycarbonates in this work have been discussed earlier in Chapter 3, where the statistical weights for the probable rotational states of various bond pairs are given. The structures of bisphenyls, carbonates and repeat units corresponding to these polycarbonates are shown in Figure 4.1. These polycarbonates correspond to a set where a systematic change of the chemical structure is made to see the effect on optical anisotropy at the level of the monomer and the chain.

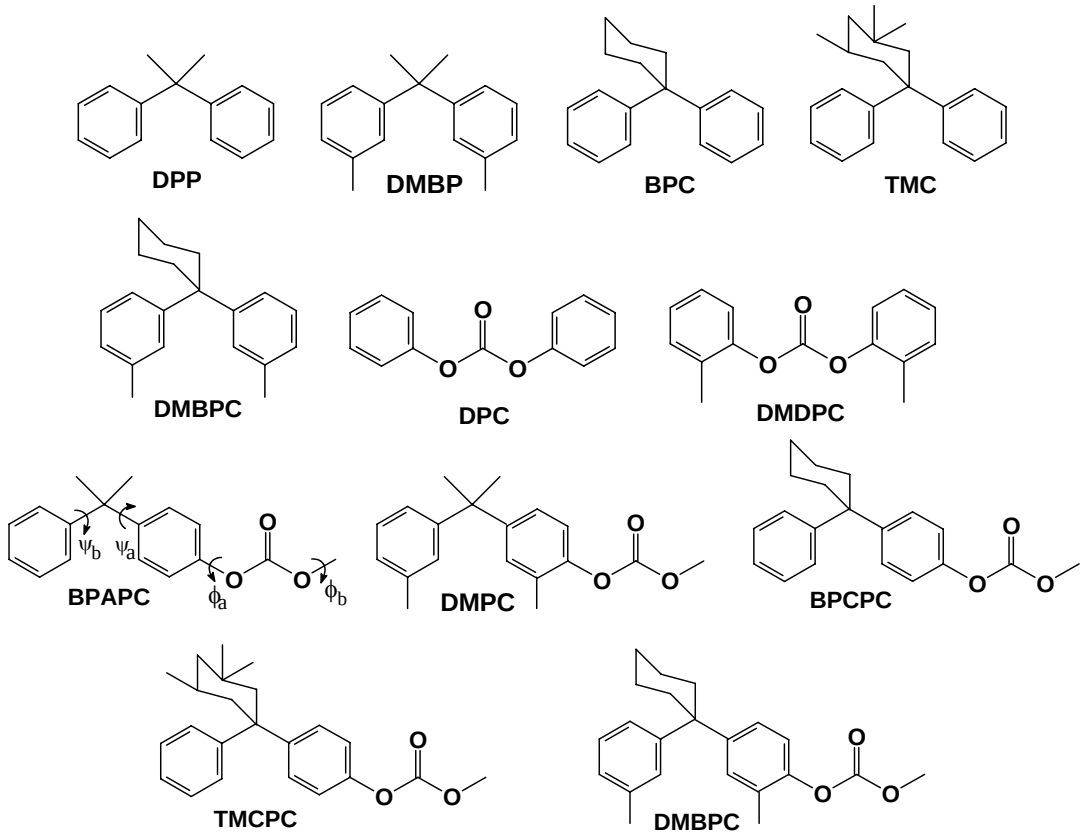

Figure 4.1. Structures of the bisphenyls, carbonate fragments and repeat units of structurally modified polycarbonates studied

4.2. Theoretical Framework and RIS Formalism

4.2.1. Optical anisotropy of bisphenyl DMBP, carbonate DMDPC and polycarbonate DMPC.

In this section, a new formalism for calculating the polarizability tensor and optical anisotropy of polycarbonates having substituents on the phenylene rings is described. The formalism employed by Erman et al.[10,11] for BPAPC, is used here with modifications for the case of DMPC by suitable group polarizabilities and geometrical parameters. The cartesian coordinate reference frames employed to express individual group polarizability tensors for substituted structures is the same as that which was earlier used for DPP and DPC.[10] The reference frames for DMBP and DMDPC are given in Figure 4.2.

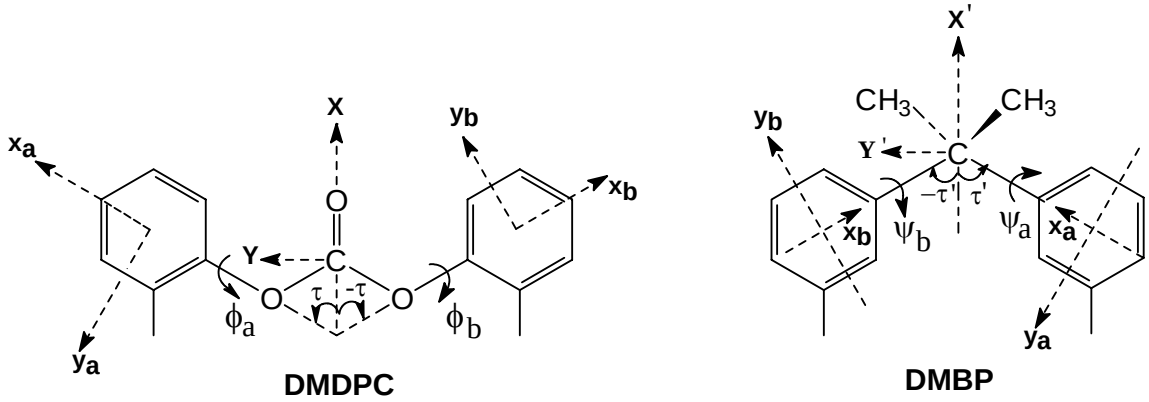

Figure 4.2. Coordinate reference frames of the various groups in DMDPC and DMBP

According to the method by Erman et al.,[10] the polarizability tensor of DPP is formulated by adding up contributions of two phenyl rings which are subject to the effect of isopropylidene group. Following a similar approach, DMBP is considered to be formed from neopentane and two molecules of toluene according to the hypothetical process

$$CH_3\text{-}C_6H_4\text{-}H + C(CH_3)_4 + H\text{-}C_6H_4\text{-}CH_3 \rightarrow (CH_3\text{-}C_6H_4)_2C(CH_3)_2 + 2CH_4 \quad (1)$$

involving no net changes in the numbers of C-C and C-H bonds. Neopentane and methane being symmetric, the polarizability tensor for DMBP is constructed from two phenyl ring tensors subjected simultaneously to the presence of isopropylidene group between the rings as well as methyl groups on the rings, such as

$$\hat{\alpha}_{DMBP} = \hat{\alpha}_{ph,a} + \hat{\alpha}_{ph,b} \quad (2)$$

The polarizability tensor for the phenyl group in DPP in the *xyz* frame can be derived as *diag* [3.46, -0.23, -3.23] and that for an unsubstituted phenyl group in the same reference frame is *diag* [1.21, 1.21, -2.42].[10] From these values the polarizability tensor corresponding to the effect of isopropylidene substitution is *diag* [2.25, -1.44, -0.81]. The tensor for a phenyl group with methyl substitution can be equated to that of toluene and is given by *diag* [2.32, 0.34, -2.66] in a reference frame (*x*"*y*"z") where the *x*"*y*" plane is the plane of the molecule with *x*" axis in the direction of the C-C bond.[6] This tensor is then transformed to the reference frames $x_b y_b z_b$ and $x_a y_a z_a$ on the phenyl rings by the equations

$$(\hat{\alpha}_{ph,b})_{x_b y_b z_b} = R_z(-\theta)\,(\hat{\alpha}_{ph,b})_{x"y"z"}\,R_z^{-1}(-\theta)$$
$$(\hat{\alpha}_{ph,a})_{x_a y_a z_a} = R_z(\theta)\,(\hat{\alpha}_{ph,a})_{x"y"z"}\,R_z^{-1}(\theta) \qquad (3)$$

where $\theta = 120°$. Subsequently, the components of the tensor are summed up along with the contribution from the isopropylidene group. The tensors in the *xyz* reference frames for the phenyl groups in DMBP are

$$(\hat{\alpha}_{ph,b,DMBP})_{xyz} = \begin{bmatrix} 3.085 & 0.857 & 0 \\ & 0.385 & 0 \\ & & -3.47 \end{bmatrix}$$
$$(\hat{\alpha}_{ph,a,DMBP})_{xyz} = \begin{bmatrix} 3.085 & -0.857 & 0 \\ & 0.385 & 0 \\ & & -3.47 \end{bmatrix} \qquad (4)$$

The tensor for DMBP is formulated by adding the contributions from the two phenyl groups expressed in the same reference frame. The ring tensors which are now in their own corresponding *xyz* frames are then transformed to the X'Y'Z' frame by using the same equations of transformation as given earlier,[10]

$$(\hat{\alpha}_{ph,b})_{X'Y'Z'} = R_z(-\tau')\, R_x(\psi_b)\, (\hat{\alpha}_{ph,b})_{xyz}\, R_x^{-1}(\psi_b)\, R_z^{-1}(-\tau')$$
$$(\hat{\alpha}_{ph,a})_{X'Y'Z'} = R_z(\tau')\, R_x(\psi_a)\, (\hat{\alpha}_{ph,a})_{xyz}\, R_x^{-1}(\psi_a)\, R_z^{-1}(\tau') \qquad (5)$$

The tensor of DPC is constructed from those of two phenyl groups with the influence of *oxy* substitution and the carbonate moiety.[10] The tensor of the phenyl groups in DPC (with effects of *oxy* substitution) in the *xyz* frame is *diag* [2.67, 0.17, -2.84] and from this the tensor corresponding to *oxy* substitution is obtained as *diag* [1.46, -1.04, -0.42]. The tensor for the carbonate group in the XYZ frame is *diag* [0.17, 1.04, -1.21] which is identified with the same as that for dimethyl carbonate.[10] Tensor for DMDPC can be formulated from sum of contributions from two phenyl groups (with effects of *oxy* as well as *methyl* substitution) and from carbonate group when all of these tensors are in the same reference frame. To get the former tensor, the tensors of toluene and that corresponding to oxy substitution are added up after transformation to the common frame, XYZ, which is located at the carbonate group as shown in Figure 4.2. The tensors corresponding to the phenyl groups 'a' and 'b' in DMDPC are obtained as

$$(\hat{\alpha}_{ph,b,DMDPC})_{xyz} = \begin{bmatrix} 2.295 & 0.857 & 0 \\ & 0.785 & 0 \\ & & -3.08 \end{bmatrix}$$
$$(\hat{\alpha}_{ph,a,DMDPC})_{xyz} = \begin{bmatrix} 2.295 & -0.857 & 0 \\ & 0.785 & 0 \\ & & -3.08 \end{bmatrix} \qquad (6)$$

The transformation equations which are similar to that used by Erman et al. are employed to transform the tensors of the phenyl groups in DMDPC to the XYZ frame.[10] These are

$$(\hat{\alpha}_{ph,a})_{XYZ} = R_z(\tau)\, R_x(\phi)\, (\hat{\alpha}_{ph,a})_{xyz}\, R_x^{-1}(\phi)\, R_z^{-1}(\tau)$$
$$(\hat{\alpha}_{ph,b})_{XYZ} = R_z(-\tau)\, R_x(\phi)\, (\hat{\alpha}_{ph,b})_{xyz}\, R_x^{-1}(\phi)\, R_z^{-1}(-\tau) \qquad (7)$$

In order o calculate the polymer chain optical anisotropy of DMPC, its repeat unit is treated in a manner similar to that of BPAPC.[11] The polarizability tensor is constructed by adding contributions from two phenylene groups which are subjected to effects of isopropylidene group, oxy and methyl group substitution (groups-1 and 3) and the carbonate group (group-2). Thus, for the constituting groups in DMPC

$$(\hat{\alpha}_1)_{xyz} = \begin{bmatrix} 4.545 & 0.857 & 0 \\ & -0.655 & 0 \\ & & -3.89 \end{bmatrix}$$

$$(\hat{\alpha}_2)_{XYZ} = diag\begin{bmatrix} 0.17 & 1.04 & -1.21 \end{bmatrix} \quad (8)$$

$$(\hat{\alpha}_3)_{xyz} = \begin{bmatrix} 4.545 & -0.857 & 0 \\ & -0.655 & 0 \\ & & -3.89 \end{bmatrix}$$

$\hat{\alpha}_1 = \hat{\alpha}_{ph,b}$; $\hat{\alpha}_2 = \hat{\alpha}_C$; $\hat{\alpha}_3 = \hat{\alpha}_{ph,a}$ with indices *i* = 1, 2, 3 corresponding to those in eq 8. The equations of transformation, T_1, T_2 and T_3 are identical to that used for BPAPC[11] which are as follows.

$$T_1 = R_x(-\psi_b)R_Z(2\tau')R_x(\psi_a)$$
$$T_2 = R_Z(-\tau)R_x(\phi_b) \quad (9)$$
$$T_3 = R_x(-\phi_a)R_z(-\tau)$$

4.2.2. Optical anisotropy of cyclohexylidene bisphenyl fragments

The formulation of polarizability tensors for bisphenyls BPC, TMC and DMBPC having cyclohexyl substitution at C_α atom, is as follows. Consider the fragment BPC, which is hypothesized to be formed from two molecules of benzene and one molecule of 1,1-dimethylcyclohexane (DMCYX) as shown structurally in Figure 4.3 and through the following process as depicted in eq. (10) which involves no net changes in the number of C-C and C-H bonds.

$$C_6H_5\text{-}H + C_6H_{10}(CH_3)_2 + H\text{-}C_6H_5 \rightarrow (C_6H_5)_2C_6H_{10} + 2CH_4 \quad (10)$$

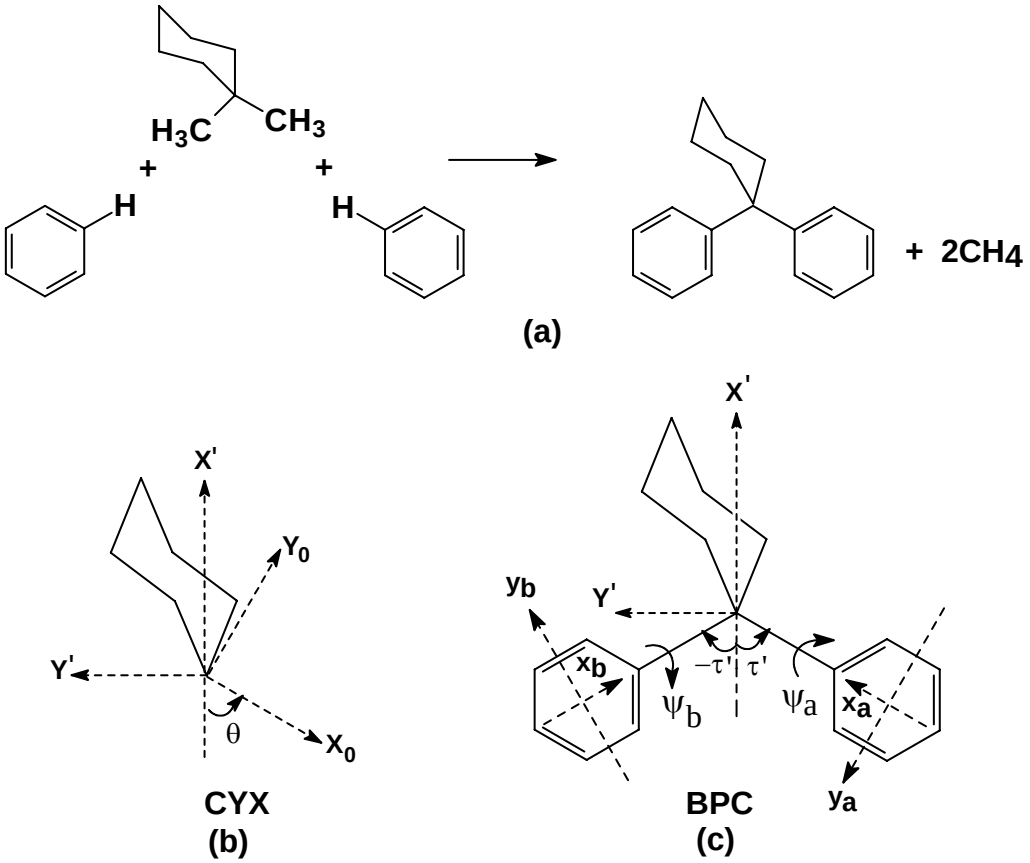

Figure 4.3. (a) Hypothetical process for the formation of BPC from phenyl groups and dimethylcyclohexane. Coordinate reference frames of (b) cyclohexane and (c) phenyl groups in BPC

Since the polarizability tensor for methane is considered to be zero and the polarizability tensor for BPC can be formulated from sums of contributions from two phenyl groups and DMCYX (where all tensors are expressed in a common reference frame), this gives

$$\hat{\alpha}_{BPC} = \hat{\alpha}_{ph,a} + \hat{\alpha}_{DMCYX} + \hat{\alpha}_{ph,b} \tag{11}$$

The tensor of DMCYX can be obtained from that of cyclohexane by taking into account the replacement of two hydrogen atoms by two methyl groups, one axial and the other equatorial. The method described by Navard and Flory is conveniently adopted here for the formulation of tensors of substituted cyclohexanes.[14] For methylcyclohexane the tensor construction is obtained by replacing a hydrogen atom of cyclohexane by a methyl group, either in the equatorial or axial orientation, which corresponds to the formation of a C-C bond with the

contribution equal to Γ_{cc}. Here Γ_{cc} is taken to be 0.53 Å^3.[3] For the equatorial orientation of the methyl group

$$\left(\hat{\alpha}_{CYX-Me,e}\right)_{X_0Y_0Z_0} = \left(\hat{\alpha}_{CYX}\right)_{X_0Y_0Z_0} + \hat{\alpha}_e$$
$$\hat{\alpha}_e = \Gamma_{cc} \ \text{diag}\left[\frac{2}{3} \quad -\frac{1}{3} \quad -\frac{1}{3}\right] \tag{12}$$

while when the methyl group is oriented axially (ξ=cos^{-1}(-1/3)),

$$\left(\hat{\alpha}_{CYX-Me,a}\right)_{X_0Y_0Z_0} = \left(\hat{\alpha}_{CYX}\right)_{X_0Y_0Z_0} + R_Z(\xi)\ \hat{\alpha}_e\ R_Z^{-1}(\xi) \tag{13}$$

The tensor for DMCYX in the $X_0Y_0Z_0$ frame is therefore

$$\left(\hat{\alpha}_{DMCYX}\right)_{X_0Y_0Z_0} = \left(\hat{\alpha}_{CYX}\right)_{X_0Y_0Z_0} + \hat{\alpha}_e + R_Z(\xi)\ \hat{\alpha}_e\ R_Z^{-1}(\xi) \tag{14}$$

The transformation from $X_0Y_0Z_0$ frame to X'Y'Z' frame is performed by the following equation, where θ = 54.75° and is one-half of the tetrahedral bond angle.

$$\left(\hat{\alpha}_{DMCYX}\right)_{X'Y'Z'} = R_Z(\theta)\ \left(\hat{\alpha}_{DMCYX}\right)_{X_0Y_0Z_0} R_Z^{-1}(\theta) \tag{15}$$

The tensors of the phenyl groups in the *xyz* frame, which is diag [1.21, 1.21, -2.42], are then transformed to the X'Y'Z' frame by using eq. 5. The contributions of the phenyl rings are then added to the tensor components for DMCYX in the same reference frame. For the formulation of DMBPC, instead of the tensor for the phenyl group (eq. 11), the tensor corresponding to that for toluene in the appropriate reference frame (*xyz*) is employed.

Bisphenyl molecule TMC is considered to result from two molecules of benzene and one molecule of 1,1,3,3,5-pentamethylcyclohexane (PMCYX). The tensor for TMC is formulated as the sum of contributions from two phenyl groups and PMCYX, all expressed in a common reference frame.

$$\hat{\alpha}_{TMC} = \hat{\alpha}_{ph,a} + \hat{\alpha}_{PMCYX} + \hat{\alpha}_{ph,b} \tag{16}$$

The methyl group at the 5 position of PMCYX can be oriented either as equatorial or axial. Depending on the orientation of this methyl group two tensors can be derived which are given as

$$\left(\hat{\alpha}_{PMCYX,e}\right)_{X_0Y_0Z_0} = \left(\frac{\Gamma_{CC}}{9}\right)\begin{bmatrix} 18 & 0 & 0 \\ & -9 & 0 \\ & & -9 \end{bmatrix}$$
$$\left(\hat{\alpha}_{PMCYX,a}\right)_{X_0Y_0Z_0} = \left(\frac{\Gamma_{CC}}{9}\right)\begin{bmatrix} 10 & -2\sqrt{2} & 0 \\ & -1 & 0 \\ & & -9 \end{bmatrix} \qquad (17)$$

These are then transformed to the X'Y'Z' frame using eq. 15 where the components corresponding to PMCYX are used instead of those corresponding to DMCYX. This tensor corresponding to PMCYX, when added to those of the phenyl groups in the X'Y'Z' frame, provides the final polarizability tensor for bisphenyl TMC.

The optical anisotropy γ^2, which is the quadratic tensor invariant, is calculated as

$$\gamma^2 = \frac{3}{2} tr\left(\hat{\alpha}\hat{\alpha}\right) \qquad (18)$$

4.2.3. Optical anisotropy of cyclohexylidene substituted polycarbonate chains

A segment of the polycarbonate BPCPC depicting the reference frames of various groups is shown in Figure 4.4.

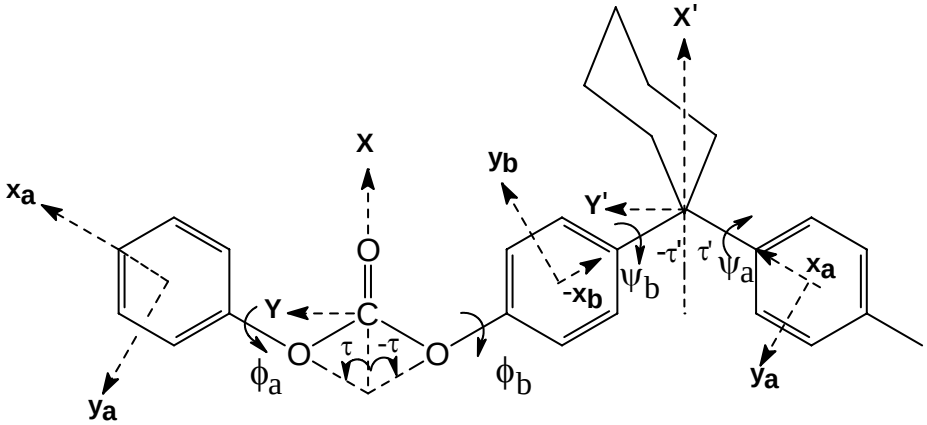

Figure 4.4. Coordinate reference frames of the various groups in BPCPC chain segment

The polarizability tensor of the repeat unit of BPCPC comprises of contributions from four groups: 2 phenylenes (group-1 and group-3) subject to the effects of oxy substitution, DMCYX (group-4) and carbonate group (group-2). The tensors for these groups in their respective reference frames are

$$
\begin{aligned}
(\hat{\alpha}_1)_{xyz} &= (\hat{\alpha}_3)_{xyz} = diag\begin{bmatrix} 2.67 & 0.17 & -2.84 \end{bmatrix} \\
(\hat{\alpha}_2)_{XYZ} &= diag\begin{bmatrix} 0.17 & 1.04 & -1.21 \end{bmatrix} \\
(\hat{\alpha}_4)_{X'Y'Z'} &= \begin{bmatrix} -0.3142 & 0.3884 & 0 \\ & 0.3142 & 0 \\ & & 0 \end{bmatrix}
\end{aligned}
\tag{19}
$$

For TMCPC the corresponding groups comprising the repeat unit are (a) two phenylenes (group-1 and group-3) subject to the effects of oxy substitution, (b) PMCYX (group-4) and (c) carbonate group (group-2). The tensor for PMCYX in the X'Y'Z' frame is

$$
\begin{aligned}
(\hat{\alpha}_4, e)_{X'Y'Z'} &= \begin{bmatrix} 0 & 0.7493 & 0 \\ & 0.5303 & 0 \\ & & -0.5303 \end{bmatrix} \\
(\hat{\alpha}_4, a)_{X'Y'Z'} &= \begin{bmatrix} 0.3137 & 0.3608 & 0 \\ & 0.2163 & 0 \\ & & -0.53 \end{bmatrix}
\end{aligned}
\tag{20}
$$

Similarly, the repeat unit tensor of DMBPC is formulated from the sum of contributions from (a) two phenylene groups subject to the effects of oxy as well as methyl substitution, (b) DMCYX and (c) carbonate group. The tensor for the phenylene groups in DMBPC is similar to those in DMDPC as given in eq. 6. The transformation matrices for the calculation of the optical anisotropy of cyclohexylidene substituted polycarbonates are

$$
\begin{aligned}
T_1 &= R_x(-\psi_b) R_Z(\tau') \\
T_2 &= R_Z(-\tau) R_x(\phi_b) \\
T_3 &= R_x(-\phi_a) R_z(-\tau) \\
T_4 &= R_Z(\tau') R_x(\psi_a)
\end{aligned}
\tag{21}
$$

4.2.4. Optical anisotropy of isolated repeat units

Separate calculations were performed for $\langle\gamma^2\rangle$ of each type of polycarbonate single repeat unit, with a consideration of all most probable rotational states. In the case of BPAPC, the tensor for the repeat unit is expressed in the frame of the phenyl group 'b' ($x_b y_b z_b$) and the tensors for the phenyl group ('a') and carbonate group are transformed to $x_b y_b z_b$ frame.

$$\left(\hat{\alpha}_{RU}\right)^C = \hat{\alpha}_1^C + \left(T_1 \otimes T_1\right)\hat{\alpha}_3^C + \left(T_1 \otimes T_1\right)\left(T_3 \otimes T_3\right)\hat{\alpha}_2^C \tag{22}$$

where transformation matrices T_1 and T_3 are the same as given in the earlier work for BPAPC[11] and are provided in eq. 9. For cyclohexylidene substituted polycarbonates, repeat unit optical anisotropies are calculated following a similar procedure using the expression

$$\left(\hat{\alpha}_{RU}\right)^C = \hat{\alpha}_1^C + \left(T_1 \otimes T_1\right)\hat{\alpha}_4^C + \left(T_1 \otimes T_1\right)\left(T_4 \otimes T_4\right)\hat{\alpha}_3^C + \left(T_1 \otimes T_1\right)\left(T_4 \otimes T_4\right)\left(T_3 \otimes T_3\right)\hat{\alpha}_2^C \tag{23}$$

where matrices T_1, T_3 and T_4 are those which are given by eq 21. The $\langle\gamma^2\rangle$ values provided in Table 4.2 are obtained by averaging over all conformations of the repeat unit for each polycarbonate structure.

4.2.5. Conformationally averaged optical anisotropy of substituted polycarbonate chains

The mean-squared optical anisotropy $\langle\gamma^2\rangle$ which is averaged over the probable conformations of the chain having x repeat units is obtained by incorporating the statistical weight matrices into the respective P matrices as[1,3,9]

$$\left\langle P_i \right\rangle = \left(U_i \otimes I_P\right)\|P_i\| \;\; ; \;\; \text{where} \;\; P_i = \begin{bmatrix} 1 & 2\hat{\alpha}_i^R (T_i \otimes T_i) & \hat{\alpha}_i^2 \\ 0 & T_i \otimes T_i & \hat{\alpha}_i^C \\ 0 & 0 & 1 \end{bmatrix} \tag{24}$$

$$\langle\gamma^2\rangle = \frac{3}{2} \times Z^{-1} J^* \langle P_1\rangle \langle P\rangle^{x-1} \langle P_3\rangle J \qquad \text{for BPAPC and DMPC}$$

$$\text{where} \;\; \langle P\rangle = \langle P_3\rangle\langle P_2\rangle\langle P_1\rangle$$

$$\langle\gamma^2\rangle = \frac{3}{2} \times Z^{-1} J^* \langle P_1\rangle \langle P\rangle^{x-1} \langle P_4\rangle\langle P_3\rangle J \qquad \text{for BPCPC, TMCPC and DMBPC} \tag{25}$$

$$\text{where} \;\; \langle P\rangle = \langle P_4\rangle\langle P_3\rangle\langle P_2\rangle\langle P_1\rangle$$

where Z is the partition function. The contributions of the end groups are taken into account

by $J^*\langle\mathcal{P}_1\rangle$ and $\langle\mathcal{P}_3\rangle J$ (for BPAPC and DMPC) and $J^*\langle\mathcal{P}_1\rangle$ and $\langle\mathcal{P}_4\rangle\langle\mathcal{P}_3\rangle J$ for cyclohexylidene substituted polycarbonates.

The statistical weights for energetically favorable conformers and their corresponding torsional states and bond angles, which are derived using conformational analysis with bonded and interatomic non-bonded potentials described by the PCFF force-field (Chapter 3) are used here for the calculation of $\langle\gamma^2\rangle$. The minimum energy torsions and bond angles for these polycarbonates are given in Table 4.1. Calculations of optical anisotropy are also performed here for these polycarbonates by assigning equivalent weights for all the energetically favorable conformational rotational isomeric states which were obtained from previous conformational energy calculations (Chapter 3). In the case of BPAPC, the calculation was performed using torsions and bond angles as provided by Erman et al.,[10,11] and also independently by using the values derived from our PCFF based simulations. It should be noted that in the calculation method of $\langle\gamma^2\rangle$ of polycarbonate chains outlined here, only the *trans-trans* (*t-t*) conformations of the carbonate groups are considered. Calculations of the mean-squared optical anisotropy $\langle\gamma^2\rangle$ of the polycarbonate chains were performed using a FORTRAN code by incorporating the matrix multiplication scheme in the RIS formalism as provided by Flory.[1,3] The polycarbonate chains consisted of 11 repeat units in accordance with the earlier reports on BPAPC in that $\langle\gamma^2\rangle/x$ reaches an asymptotic value for $x \approx 10$.[11,12] $\langle\gamma^2\rangle/x$ is calculated as a function of x as well, and our results for all five polycarbonates show the same asymptotic behavior. The detailed analysis is provided specifically by comparing tabulated values of $\langle\gamma^2\rangle/x$ calculated for $x = 11$. The chemical constitution of the polycarbonate chain, for example for BPCPC, for the purpose of chain optical anisotropy calculation via RIS, is given as **R**–(O–CO–O–C_6H_4–C_6H_{10}–C_6H_4)$_{x-2}$–O–CO–O–**R** where **R** = HO–C_6H_4–C_6H_{10}–C_6H_4 and these are the same end groups on either side of the chain.

Table 4.1. Geometrical parameters of the repeat units of polycarbonates

PC	ϕ_a	ϕ_b	ψ_b	ψ_a	2τ'	τ
BPAPC	-130, -50, 50, 130	-130, -50, 50, 130	-130, -50, 50, 130	-130, -50, 50, 130	110.7	67
DMPC	-95, 95	-95, 95	-130, -50, 50, 130	-130, -50, 50, 130	110.7	65
BPCPC	-130, -50, 50, 130	-130, -50, 50, 130	-110, -70, 70, 110	-125, -55, 55, 125	107.7	67
TMCPC	-130, -50, 50, 130	-130, -50, 50, 130	-70, 110	-60, 120	106.7	67
DMBPC	-95, 95	-95, 95	-110, -70, 70, 110	-125, -55, 55, 125	107.7	65

4.3. Results and Discussion

4.3.1. Mean squared optical anisotropy of bisphenyls, carbonates and repeat units

Mean-squared optical anisotropy,$\langle\gamma^2\rangle$, of bisphenyls, carbonate segments and the repeat units for the five polycarbonates are given in Table 4.2.

Table 4.2. Mean-squared optical anisotropies of bisphenyls, carbonates and single repeat units

PC fragments	$\langle\gamma^2\rangle$ (Å^6)		
	monomer fragments	repeat unit	
		equal weights	PCFF weights
DPP	39.08	89.38	89.63
DMBP	40.71	74.38	75.20
BPC	14.74	26.05	26.30
TMC	13.58 (*e*)	29.14 (*e*)	29.44 (*e*)
	10.55 (*a*)	18.17 (*a*)	
DMBPC	28.00	23.38	24.51
DPC	73.18		
DMDPC	52.92		

The use of PCFF based torsions and bond angles for DPP leads to a $\langle\gamma^2\rangle$ value 39.1 $Å^6$ resulting from our calculation. Using the geometry reported by Erman et al.[10] leads to a value of 43.6 $Å^6$ for $\langle\gamma^2\rangle$. Experimental value reported for DPP from depolarized Rayleigh scattering is 40±2 $Å^6$.[10] The values provided in Table 4.2 were averaged over the energetically accessible most probable rotational isomeric conformations of these bisphenyl fragments. In cases where methyl substitution is absent on the phenyl rings (DPP, BPC and TMC) the energetically accessible conformers in each of these fragments are symmetric and have a unique value of γ^2. In the case of fragments with methyl substitution on the phenyl rings (DMBP, DMBPC), the rotational isomeric conformers are not structurally and optically symmetric and these have different optical anisotropies and energy statistical weights. In order to see the influence of statistical weights on optical anisotropy, for DMBP and DMBPC, $\langle\gamma^2\rangle$ was also calculated based on equal probability of the conformers. Compared to DPP, it is observed that the cyclohexyl group at the C_α atom leads to significant reduction in $\langle\gamma^2\rangle$, whereas presence of methyl substituents on the phenyl rings *slightly enhances* optical anisotropy such as in case of DMBP and *significantly enhances* optical anisotropy when one compares DMBPC with BPC. The effect of structural modification on the optical anisotropy of bisphenyls can be explained on the basis of two factors: (1) substituent structural effects and (2) conformational effects. It is important to understand the separate influences of these effects as follows.

Cyclohexylidene group at C_α lowers $\langle\gamma^2\rangle$ by approximately a factor of 2 (comparing DPP and BPC). The aliphatic cyclohexyl group and its low intrinsic anisotropy make these fragments more optically isotropic. The conformational effects are manifested through torsions (ψ) and the bond angle ($2\tau'$). The phenyl rings are inequivalent due to the presence of cyclohexylidene group and in order to minimize the steric repulsions that arise from 1,3-diaxial interactions the axial phenyl ring (ψ_b) prefers an orientation which is twisted by about 70° out-of-the-plane while the torsion about the equatorial phenyl ring (ψ_a) is 55°. The axial phenyl ring prefers more of a perpendicular orientation and this leads consequently to a reduction in $\langle\gamma^2\rangle$. The same explanation holds true for TMC as well, where the bisphenyl conformers having either axial or equatorial orientation of the methyl group at the 5 position

on cyclohexane ring give lower value of $\langle\gamma^2\rangle$ than for BPC. Calculation of $\langle\gamma^2\rangle$ of DPP was also performed using the same geometrical parameters as BPC, in order to get a quantitative understanding of the effect of only the torsions on the $\langle\gamma^2\rangle$ of DPP. For DPP, $\langle\gamma^2\rangle$ for a geometry derived from BPC (70º, 55º for ψ and 2τ' of 107.7º) is 23.86 Å^6, which is about 15 Å^6 lower than $\langle\gamma^2\rangle$ for the minimum energy DPP (50º, 50º) conformation. This reduction of 15 Å^6 resulting from torsional differences between BPC and DPP is the dominating effect than the effect of intrinsic group polarizability differences, in facilitating a lower optical anisotropy for BPC as compared to DPP. The higher value of $\langle\gamma^2\rangle$ for TMC-*e* (having equatorially oriented methyl substituent at 5 position of cyclohexyl ring) than for TMC-*a* (having axially oriented methyl substitution at 5 position on cyclohexyl ring) is due to a higher polarizability arising from the equatorially oriented methyl group. Equatorial substituents tend to enhance the anisotropy in substituted cyclohexanes.[17] The preferred torsions about the C_α carbon are (-70º,-60º) and (-80º,-65º) for TMC-*e* and TMC-*a* respectively, where the phenyl rings are closer to a perpendicular orientation in the latter, and this feature also contributes to the lower anisotropy. For TMC, the axial conformer has energy of about 6 kcal/mol greater than the equatorial conformer, hence the population of the former can be considered to be negligible at 300 K. Thus, the conformationally averaged anisotropy of TMC will be predominantly contributed by the equatorial conformers.

The optical anisotropies of a series of other substituted cyclohexanes and the corresponding cyclohexylidene bisphenyl molecules have also been calculated by Sulatha et al., the details of which can be found elsewhere.[18] The important conclusions from that study are as follows. Cyclohexanes with phenyl group substitution show higher anisotropy than those with methyl substituents. For the same substitution, a higher optical anisotropy is observed for equatorial orientation than axial. The optical anisotropy for the cyclohexanes is dependent on the orientation of the substituent group than its position, while for the bisphenyl fragments the anisotropy is dependent on both these factors along with the conformation of the whole molecule. All of these cyclohexyl substituted bisphenyl fragments studied show lower optical anisotropy than DPP indicating the effectiveness of the cyclohexyl group for lowering the optical anisotropy.

DMBP has eight energetically favorable conformers, which we categorize into three sets with different γ^2 values, with conformers in each set having the same γ^2 value. Among these, conformers at (50º, 50º) and (-50º,-50º) states, have the lowest anisotropy (18.17 Å^6), where the methyl groups are pointing in the same direction with respect to the backbone and away from the isopropylidene group. For conformers with (ψ_b, ψ_a) values of (50º, -130º), (-50º, 130º), (130º, -50º) and (-130º, 50º), γ^2 is obtained as 38.44 Å^6, where the methyl groups on the two phenyl rings are pointing in opposite directions. When both methyl groups are oriented in the same direction and towards the isopropylidene group this leads to a relative increase in the optical anisotropy of the bisphenyl. This is seen by the value of γ^2 which is 67.8 Å^6 for conformers (130º, 130º) and (-130º, -130º). By weighting all eight conformers equally, $\langle\gamma^2\rangle$ is obtained as 40.71 Å^6. In comparison, energetic averaging done using statistical weights derived using PCFF leads to a slightly lower value of 38.66 Å^6. From the statistical weight matrices it is found that the weights corresponding to the conformers that have higher optical anisotropy are lower than that of the conformers having lower optical anisotropy (1, 0.843 and 0.716 for the three sets respectively). Importantly, it should be noted that the geometry (in terms of ψ and 2τ') is identical for DPP and DMBP. Hence the slight differences in $\langle\gamma^2\rangle$ for DPP and DMBP are due to the asymmetric conformers for the latter resulting from methyl substituents on the phenyl rings.

BPC and DMBPC are also conformationally identical, each having the same torsional and bond angle values about the C_α carbon (Table 4.1). DMBPC by virtue of the methyl substituents on the phenyl rings has conformers which do not have a unique γ^2 value. These can be divided into four sets of two optically identical conformers which are (i) (70º, 55º), (-70º, -55º); (ii) (70º, -125º), (-70º, 125º); (iii) (110º, -55º), (-110º, 55º); and (iv) (110º, 125), (-110º, -125º). For these sets, γ^2 values are 9.42 Å^6, 23.66 Å^6, 28.87 Å^6 and 50.05 Å^6 respectively. Since the phenyl rings are inequivalent, conformers (ii) and (iii) do not possess the same optical anisotropy. Comparing fragments DPP versus DMBP and BPC versus DMBPC, it turns out that the effect of methyl substituents on the optical anisotropy is not uniform for these fragments. In fact one would expect that methyl substitution on the phenyl rings should increase the polarizability in the *xy* plane and thus enhance the optical anisotropy, in a manner similar to a $\langle\gamma^2\rangle$ comparison between benzene and toluene. But we

find that this behaviour does not apply uniformly for bisphenyls, which no longer remain symmetric due to methyl substituents on the phenyl rings. For BPC and DMBPC, presence of methyl substituents have a pronounced effect by which $\langle\gamma^2\rangle$ is higher for the latter by almost a factor of 2. The results show that the reason for this behaviour is that six out of eight conformers of DMBPC have higher γ^2 than that which the conformers for BPC have (8 conformers of BPC which have a unique value of γ^2). Therefore the conformationally averaged $\langle\gamma^2\rangle$ of the bisphenyl fragments decreases in the order DPP > DMBP > DMBPC > BPC > TMC.

In the case of carbonate fragments, for DPC, the calculated $\langle\gamma^2\rangle$ as reported previously by Erman et al. is 77.2 Å^6 ($\phi_a=\phi_b$=46°, τ=67°) and the experimentally determined value is 72±4 Å^6.[10] From the present calculations, the $\langle\gamma^2\rangle$ value for DPC for its twisted conformation as obtained using PCFF based geometry ($\phi_a=\phi_b$=50°, τ=67°) by considering only the *trans-trans* conformation, is 73.18 Å^6, which is in good agreement with the experimental value.[10] For DMDPC, conformational analysis has shown that the torsion about the Ph-O bond is 95° and that here also the *trans-trans* conformation is the most stable one (section 3.3.1 in Chapter 3). Calculated $\langle\gamma^2\rangle$ for DMDPC (*trans-trans*) is 52.92 Å^6 which is significantly lower (by 20 Å^6) than that for DPC. The predominant effect leading to the reduction of $\langle\gamma^2\rangle$ of DMDPC relative to $\langle\gamma^2\rangle$ of DPC arises from the preferred conformation for DMDPC where phenyl rings are oriented perpendicular to the plane of the carbonate group. A reduction by 17 Å^6 is observed when the relative orientation of the phenyl rings in DPC changes from twisted conformation to being perpendicular ($\langle\gamma^2\rangle$ = 56.22 Å^6 when $\phi_a=\phi_b$=90°). Reduction in conformationally averaged anisotropy due to polarizability contribution from methyl groups is only ~ 3 Å^6 while the major effect comes from the torsional differences between DPC and DMDPC.

For isolated polycarbonate repeat units, the calculations were performed considering a single repeat unit (for eg. having the formula $\{(C_6H_5)_2C(CH_3)_2COO\}$ such as for BPAPC) which can take different permitted variations of torsions ψ and ϕ, over which the averages were taken. The number of permissible conformers is 128 each for BPAPC and BPCPC, 64 for TMCPC, 32 each for DMBPC and DMPC. The number of unique conformers having

different values of γ^2 were 4 each for BPAPC, BPCPC, TMCPC, DMPC and 8 for DMBPC. $\langle\gamma^2\rangle$ of these repeat units are provided in Table 4.2. Methyl groups on the phenylene rings lead to a lowering of $\langle\gamma^2\rangle$ of the repeat units (see DMPC versus BPAPC), while this is in contrast to the trend in case of the bisphenyl fragments. Similar to the behaviour observed in the case of bisphenyls, $\langle\gamma^2\rangle$ of the three different cyclohexylidene substituted polycarbonate repeat units are considerably lower than the value seen for BPAPC. Since the geometry of the carbonate group is similar in BPAPC, BPCPC and TMCPC, their relatively lower $\langle\gamma^2\rangle$ values are due to structural as well as conformational effects that are brought about by the presence of the cyclohexyl group. For TMCPC, the orientation of the methyl group determines whether $\langle\gamma^2\rangle$ should be higher or lower relative to BPCPC. This trend is in contrast to the observation for the bisphenyl fragments, where irrespective of the orientation of the methyl group (at 5 position), $\langle\gamma^2\rangle$ of TMCPC is lower than that of BPCPC. All the four unique conformers of TMCPC-*e* (equatorial) have higher optical anisotropy than their corresponding counterparts of BPCPC. Polycarbonate repeat units possessing methyl groups on the phenyl rings have lower mean-squared optical anisotropy than their unsubstituted counterparts which comes from the conformational rigidity of the Ph-O torsion. Resulting conformation is one in which the phenyl rings orient perpendicular to the carbonate group and this is the major factor quantitatively contributing to the optical anisotropy. Methyl groups lower the optical anisotropy to different extents in DMPC and DMBPC in comparison to their respective unsubstituted counterpart polycarbonates. For DMPC the reduction amounts to 15 $Å^6$, while for DMBPC it is only 2.67 $Å^6$, which is due to a significant lowering of optical anisotropy already affected by presence of a cyclohexylidene ring in the case of DMBPC. An examination of the calculated $\langle\gamma^2\rangle$ for the various types of repeat units reveals that cyclohexylidene group is far more effective in lowering the anisotropy as compared to methyl groups which are on the phenyl rings. In a case where both types of substitution are present, such as for DMBPC, the reduction in optical anisotropy is 66 $Å^6$ which denotes the non-additivity of polarizability changes due to different contributing groups.

4.3.2. Single chain optical anisotropy of polycarbonate chains

The calculations were performed for polycarbonates as a function of chain length. However, as seen from previous reports on BPAPC,[11,12] 11 repeat units are sufficient to obtain

constancy of $\langle\gamma^2\rangle/x$. The variation of $\langle\gamma^2\rangle/x$ with x for all polycarbonates provided in Figure 4.5 is also in agreement with the above observation. Results are provided in Table 4.3.

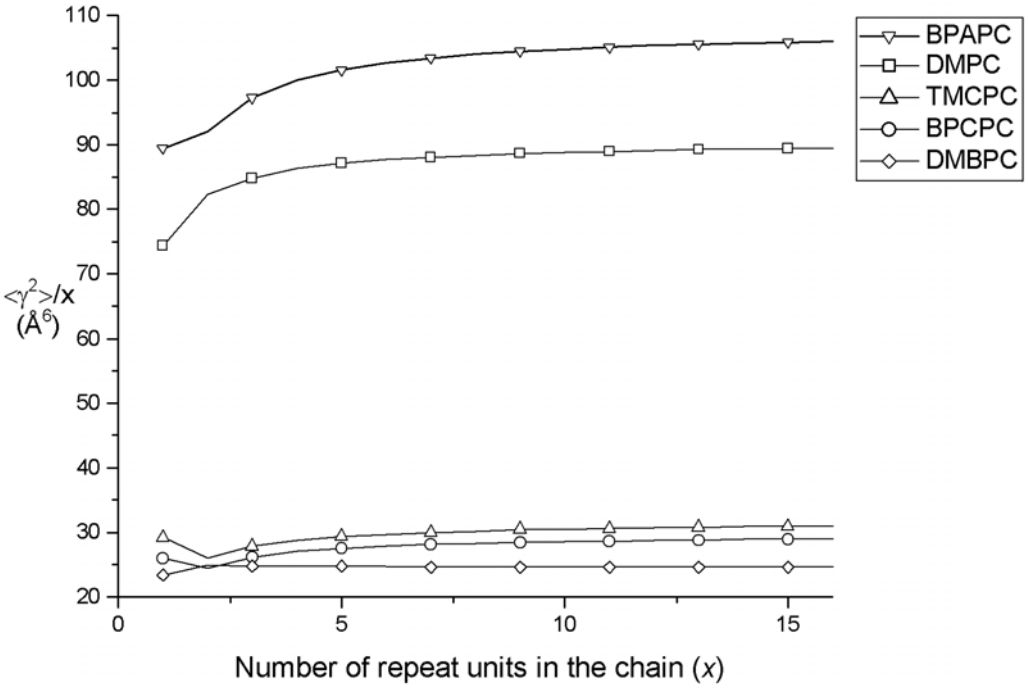

Figure 4.5. Conformational averaged optical anisotropy per repeat unit in polycarbonate chain, $\langle\gamma^2\rangle/x$, as a function of the number of repeat units, x

Table 4.3. Mean-squared optical anisotropy per repeat unit in polycarbonate chains (x=11) from RIS calculations

PC	$\langle\gamma^2\rangle/x$ (Å^6)	
	equal weights	PCFF weights
BPAPC[a]	105.20	105.10
	109.00	
	111.00	
DMPC	89.00	80.40
BPCPC	28.67	29.16
TMCPC	30.61 (*e*)	33.10 (*e*)
	20.03 (*a*)	20.45 (*a*)
DMBPC	24.63	26.37

[a] The three different $\langle\gamma^2\rangle/x$ given here for BPAPC correspond to the three different values used for the torsional pair (ψ_b, ψ_a) which are (50°,50°), (48°,48°) and (47°,47°) respectively. The values of (ψ_b, ψ_a) used for other polycarbonates correspond to the minimum energy states from 5° conformational search from results given in Chapter 3.

The relative trend in $\langle\gamma^2\rangle/x$ among these polycarbonates is the same as that for their isolated single repeat units, but the absolute values differ due to the influence of the neighboring repeat units in the case of the chains. Calculation of $\langle\gamma^2\rangle/x$ for BPAPC using the bond angle geometry and conformations used by Erman et al.[11] (with equal probability for all the energetically favorable conformers) using the matrix multiplication code developed here gives a value of 111.3 Å^6 which is in perfect agreement with their reported value 111 Å^6. Torsional values of ϕ and ψ in our work were obtained from conformational analysis of the bond pairs using PCFF and a grid size of 5°. Using these torsions and bond angles obtained from PCFF conformational analysis and by assigning equal probability for all the conformers, we obtain an anisotropy value of 105.2 Å^6 for BPAPC. Incorporation of PCFF derived conformational energy statistical weights does not alter the anisotropy value for BPAPC ($\langle\gamma^2\rangle/x$= 105.1 Å^6), but for the methyl substituted polycarbonates there are considerable differences between the optical anisotropy values. For BPAPC, a superior level agreement between calculations and experiment is met if (ψ_b, ψ_a) = (47°, 47°) is used, which are the minimum energy conformational states obtained from a 1° incremental search, as shown in Table 4.3. Nonetheless, the relative trends and accuracy of results are not substantially different. The optical anisotropy calculations presented here for substituted polycarbonates and those reported earlier for BPAPC[11] deal with a single chain having an *all trans* carbonate linkage. For the carbonate group, *cis*-*trans* conformers are not included in the formalism employed. NMR experiments in the glassy state of BPAPC at 135 K have shown that the carbonate group is predominantly in the planar *tran*s form and less than 10% of all carbonate groups are in the *cis* conformation.[19] Additionally, a parametric sensitivity analysis was performed for BPAPC, using different values of torsions ϕ and ψ, where only one of the torsions was changed (reflecting a change in the torsional state at the rotational energy minima) and the optical anisotropy was accordingly calculated. Performing the conformer searches for ϕ and ψ with a step size of 1° from 45° to 55° shows that for the pair (ψ_b, ψ_a) the torsional states (49º, 49º), (48º, 48º) and (47º, 47º) have similar energies as the state (50º, 50º). For (ϕ_a, ϕ_b) the lowest energy conformations are found to correspond to the (50º, 50º) state from the conformational analysis performed with 5° increments. $\langle\gamma^2\rangle/x$ calculated for a geometry of the BPAPC chain is 109 Å^6 when the set of parameters {ψ = 48º, ϕ =50º, τ=67º,

$2\tau'=110.7^{o}\}$ is used, while the value comes out to be 111 $Å^6$ when $\psi = 47^{o}$ is used (keeping other parameters the same). $\langle\gamma^2\rangle/x$ is critically dependent on the value of ψ rather than ϕ, where a 5° change in ψ torsion results in 5.3 % change in $\langle\gamma^2\rangle/x$, whereas a similar variation of the ϕ torsion results in only 0.8% change. For substituted polycarbonates, as seen for BPCPC, the lowering of $\langle\gamma^2\rangle/x$ is appreciable and this is true for TMCPC and DMBPC as well. Axially oriented TMCPC-*a* gives the lowest optical anisotropy. The reduction in $\langle\gamma^2\rangle/x$ in going from BPCPC to DMBPC, due to the methyl groups, is 4 $Å^6$, which is not insignificant. Significant differences in the optical anisotropy come about due to the presence of the methyl group (comparing DMPC with BPAPC).

In order to obtain a thorough understanding of the influence of the various conformers, calculations were performed which were conformationally biased (details given in Appendix II). For BPAPC, when ϕ and ψ have similar absolute torsion values for eg. (ϕ,ψ) of (50^{o}, 50^{o}), (130^{o}, 130^{o}) and so forth (and all positive and negative combinations of the dihedrals), the value of $\langle\gamma^2\rangle/x$ is 168.2 $Å^6$. When torsions ϕ and ψ are (50^{o}, 130^{o}) or (130^{o}, 50^{o}) and for all positive and negative combinations, $\langle\gamma^2\rangle/x$ is 68.1 $Å^6$. There are two sets of conformers which act in opposite directions in determining the final averaged optical anisotropy. Similar results are obtained for BPCPC and TMCPC-*e* as well. For DMPC and DMBPC, the higher anisotropy conformers are those for which the methyl groups are oriented on the same side of the backbone and towards the backbone-to-side-group directional vector at the C_α carbon; whereby these are extended conformations of the repeat unit. For the conformers having lower optical anisotropy, the methyl groups are oriented away from the backbone-to-side-group directional vector at C_α, and the overall conformation is less extended. In general extended conformations lead to higher optical anisotropy. Therefore, the difference in the optical anisotropy of various conformers (sets with different torsional values) is greater with respect to the cumulative conformationally averaged values in the case of DMPC and DMBPC. These polycarbonates contain bisphenyls which have optically non-symmetric minimum energy rotational isomers leading to relatively large differences in their optical anisotropy values. Calculations were also performed, by averaging over each set of repeat unit conformations which are optically symmetric and the information is provided in Appendix III. Some representative conformers of the polycarbonate chain

segments, which have different γ^2 values are given in Figure 4.6 in order to highlight how conformational structure dictates optical anisotropy.

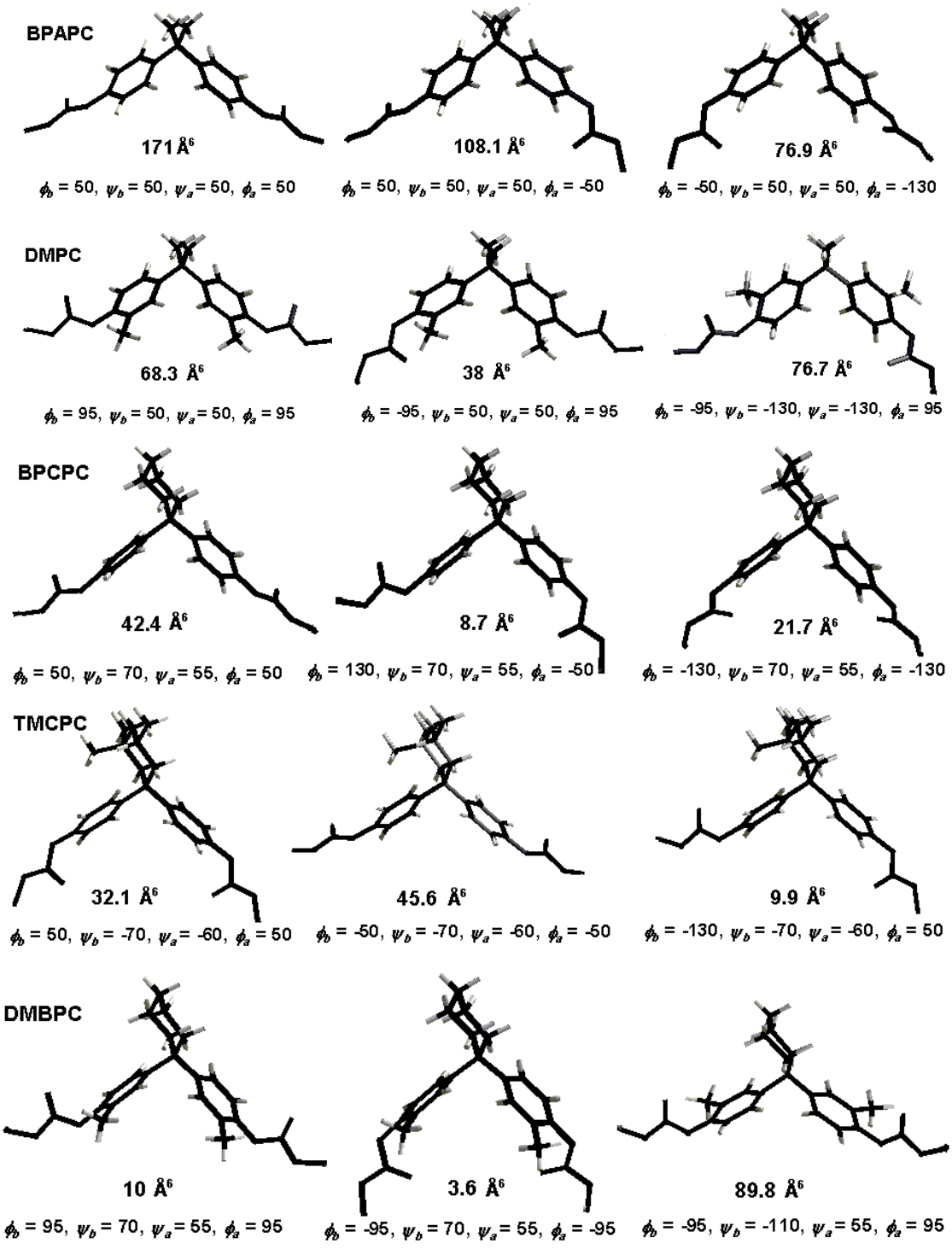

Figure 4.6. Conformations of repeat units of polycarbonates having different values of optical anisotropy. The conformers are depicted as segments of the chain and torsional specifications follow the order ϕ_b, ψ_b, ψ_a, ϕ_a as given in Figure 4.1 for BPAPC repeat unit.

Calculations show that the repeat unit γ^2 in each polycarbonate varies over a significant range of values depending on the energetically accessible conformation. In a conformation where the angle between the planes defined by the carbonate group and the phenyl ring is large, γ^2 is lower as compared to when they are closer to a parallel orientation.

For BPCPC, TMCPC and DMBPC, the values of $\langle\gamma^2\rangle/x$ are higher, but not significantly, by the use of PCFF statistical energy weights. For DMPC there is considerable reduction (by 8.6 $Å^6$) when more realistic PCFF weights are used. For DMPC, the results reveal that conformers with higher optical anisotropies {(ϕ, ψ) of (±95º, ±130º)} have lower statistical weight (σ=0.717) than those with lower anisotropies (ϕ, ψ) = (±95º, ±50º) (σ=1.0). About the (ψ_b, ψ_a) bond pair it is found that states (130º, 130º) and (-130º, -130º) give higher $\langle\gamma^2\rangle/x$ than that shown by states (50º, 50º) and (-50º, -50º). In contrast, for DMBPC, the statistical weights corresponding to higher anisotropy conformers {(ϕ , ψ) = (±95º, ±125º), σ=1.0} are higher than those for the lower anisotropy {(ϕ , ψ) = (±95º, ±55º), σ=0.79}. DMBPC bisphenyl fragment, for states at the (ψ_b, ψ_a) pair, the (110º, 125º) and (-110º, -125º) conformers have higher γ^2 than (70º, 55º) and (-70º, -55º) conformers. Statistical weight of the former set of conformational states is higher than that of the latter (1 versus 0.83) and this effect also contributes to higher $\langle\gamma^2\rangle/x$ values by using the PCFF statistical weights.

4.3.3. Relationship between chain optical anisotropy and bulk optical properties

The mean-squared optical anisotropy of polycarbonates estimated in this study were compared to the optical properties of the bulk polymer as manifested through the birefringence and stress optical coefficients in the glassy and melt states. Two measures of the suitability of a material as optical data storage disk are its stress optical coefficient in the melt (C_m) and its stress optical coefficient in the glassy state (C_g). C_m is directly proportional to the polarizability anisotropy of the polymer chains. These coefficients represent the degree of orientation of the segments and the optical anisotropy inherent in the polymer chains. BPAPC has positive values of C_m and C_g, which are 5600 and 82 Brewsters respectively (for samples with M_w=20,000).[20] C_m and C_g values of the polycarbonate of spirobisindane

(6,6'-dihydroxy-3,3,3',3'-tetramethy-1,1'-spirobisindan, SBIPC) are –650 and 20 Brewsters respectively.[21] It is found that the copolymer of SBIPC (86.3 mol%) and BPAPC (13.7 mol%) has C_m close to zero and is an intrinsically isotropic polymer (M_w=59,000, C_m measured at Tg+15°C).[21] C_g for DMPC[22] and DMBPC (M_w=35,200 gmol^{-1})[23] are found to be 51 and 47 Brewsters and the values for C_m are 4500 and 2350 Brewsters respectively, and are lower than those corresponding to BPAPC. C_g and C_m for BPAPC:DMBPC copolymers are available for a range of compositions (molar composition $\rightarrow$ C_g , C_m in the order: {20:80 $\rightarrow$ 54.3, 2910}; {40:60 $\rightarrow$ 59.7, 3480}; {60:40 $\rightarrow$ 68.4, 3940}) and this data indicates that both C_g and C_m increase linearly with BPA content (mol%) in the copolymer.[23] Similar behavior is also reported for TMCPC:BPMPC copolymer (copolymer of TMCPC and polycarbonate of 4,4'-(m-phenylenediisopropylidene) diphenol) in which case C_g increases linearly with the BPM content.[24] From a regression analysis of the copolymer data, we extrapolated C_g for TMCPC homopolymer to a value of 33.4 Brewsters. C_m for TMCPC is reported to be around 2500 Brewsters (high M_w, measurement temperature is Tg+10K).[25] C_m for BPCPC homopolymer is 2300 Brewsters while that for a copolymer with BPAPC (50:50) is 3400 Brewsters (viscosity average molecular weight of 16,200 and 15,700 gmol^{-1} respectively).[26]

The experimental values of C_m reported for the homopolycarbonates were plotted against the mean-squared optical anisotropy obtained from RIS calculations in this work for isolated repeat units as well as for repeat units in a chain. The results are given in Figure 4.7. C_m for these polycarbonates increases linearly with $\langle\gamma^2\rangle/x$ of the repeat unit in the chain and with $\langle\gamma^2\rangle$ of isolated single repeat unit. Same linear trend is also observed between C_m and $\alpha_{\parallel}$-$\alpha_{\perp}$ (which is $\{\langle\gamma^2\rangle/x\}^{1/2}$) of the repeat unit in a chain. The same linear behavior of C_m with the polarizability anisotropy of a Kuhn statistical segment, when comparing different polymer structures having little variation in their refractive index, is experimentally known and also specifically brought forth for polycarbonate melts.[27] Use of $\langle\gamma^2\rangle/x$ as the molecular scale optical property (parameter) based on the smallest exactly definable structure as shown here, instead of the polarizability anisotropy of a Kuhn statistical segment[27] which is typically used in describing the effect of structure on melt stress-optical coefficient, would

provide a more accurate way of scaling of the macroscopic optical property of polymers as a function of chemical structure.

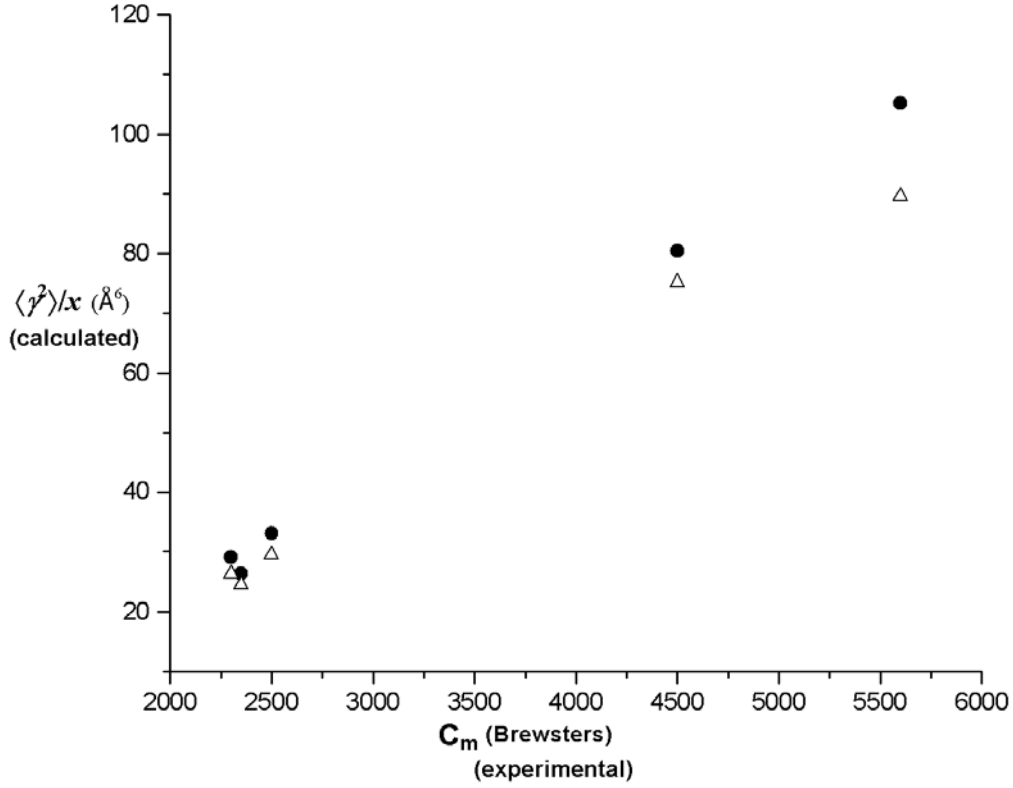

Figure 4.7. Plot of the calculated optical anisotropy per repeat unit, $\langle\gamma^2\rangle/x$, versus experimental values of C_m; (●) repeat unit in a chain and (Δ) isolated repeat unit

Molecular dynamics and Monte Carlo simulations of stress relaxation and stress-optical coefficient of polyethylene chain melts[28,29] have shown that the use of a monomer polarizability anisotropy for CH_2 groups, as derived from anisotropic components of the C-C and C-H bond polarizabilities, into the relationship between the stress-optical coefficient and monomer level polarizability anisotropy shows good comparison with the experimental data. However, for polymer chains which are more complicated than polyethylene in their chemical structure, an exact definition of the monomer level optical anisotropy parameter, that can be used to either confirm theoretical calculations or to make predictions for new systems, has not been yet specifically presented in the literature. Experimental C_g data were available only for three polycarbonates (BPAPC, DMPC and DMBPC) and the plot of C_g vs $\langle\gamma^2\rangle/x$ (for repeat unit in the chain) did not show a linear trend even though C_g increases with $\langle\gamma^2\rangle/x$. C_g for TMCPC (extrapolated from the copolymer data) is lower than that for DMBPC,

even though optical anisotropy follows the opposite trend. This behaviour may be attributed to the predominant conformational effects as manifested through bond angle distortion occurring in the glassy state under stress and/or packing effects in the condensed phase which can occur during sample stretching. Orientation of the bulky trimethylcyclohexylidene group in TMCPC also would lead to stringent interchain correlation, packing effects and residual stresses.

4.4. Conclusions

A general extension of the Flory method for formulation of the polarizability tensors of bisphenol A polycarbonate molecular fragments, applicable to substituted bisphenyl fragments, diphenyl carbonates and repeat units of various structurally modified polycarbonates is presented in this study. The methodology utilizes polarizability tensors of constituent groups that have been derived from DRS measurements in solvents like CCl_4 and the geometry (bond angles and torsions) from conformational energy calculations. The contribution of the various conformers towards the optical anisotropy is analyzed in detail here.

For bisphenyl fragments, a significant reduction in optical anisotropy is observed due to the presence of a cyclohexylidene group substitution at the C_α carbon in comparison to fragments of BPAPC. Methyl substitutions on phenyl rings tend to increase the optical anisotropy of the bisphenyls. Due to the preferred mutually perpendicular orientation of the phenyl rings arising from interactions of *ortho* methyl groups, the optical anisotropy of carbonate fragment DMDPC is lower than that of DPC. The presence of cyclohexylidene group at C_α results in a change in the conformations of the bisphenyl fragment and this is the predominant effect responsible for lowering of the optical anisotropy in cyclohexylidene substituted polycarbonates. Calculated optical anisotropy of the repeat units were compared with the experimental bulk optical properties reported in literature. The substituted polycarbonates have lower values of stress optical coefficients C_g and C_m in comparison to those for BPAPC, in accordance with the calculated optical anisotropy values of these repeat units. It is also found that experimentally observed C_m of the polycarbonates studied here increase linearly with the calculated value of the repeat unit optical anisotropy from the RIS

approach, which provide validity to the calculations since C_m is known to be a linear function of monomer level polarizability anisotropy. The polycarbonates studied here are some of the most complicated polymer chain structures for which RIS method with group polarizability has been applied in order to calculate optical anisotropy. The scheme presented here for calculation of optical properties of cyclohexylidene substituted polycarbonates can be applied to bisphenols and their polycarbonates with any kind of substitution on the cyclohexylidene ring provided accurate group polarizability tensors corresponding to the substituents are known apriori.

The results presented in this work would aid in a better understanding of the effect of structural and conformational features of the monomer units comprising such moieties, on the optical anisotropy of polymer chains. With the fundamentally attractive set of insights provided by the present study on the molecular structure-optical property behavior of small but complicated fragments and the polymer chains along with the specific information on the overall conformational behavior of polymer chains, one would be able to structurally construct particular chain molecules with desired optical properties. The results presented here have implications and potential applications in the design of molecules as well as polymers for optical media and for molecular design of new polycarbonates towards lowering the chain optical anisotropy.

4.5. References

1. Flory, P. J. *Statistical Mechanics of Chain Molecules*; Interscience: New York, 1969.
2. Volkenstein, M. V. *Configurational Statistics of Polymer Chains*; Interscience: New York, 1963.
3. Jernigan, R. L.; Flory, P. J. *J. Chem. Phys*. **1967**, *47*, 1999.
4. Patterson, G. D.; Flory, P. J. *J. Chem. Soc., Faraday Trans. II* **1972**, 68, 1098.
5. Patterson, G. D.; Flory, P. J. *J. Chem. Soc., Faraday Trans. II* **1972**, 68, 1111.
6. Suter, U. W.; Flory, P. J. *J. Chem. Soc., Faraday Trans. II* **1977**, *73*, 1521.
7. Flory, P. J.; Saiz, E.; Erman, B.; Irvine, P. A.; Hummel, J. P. *J. Phys. Chem*. **1981**, *85*, 3215.

8. Irvine, P. A.; Erman, B.; Flory, P. J. *J. Phys. Chem.* **1983**, *87*, 2929.
9. Mattice, W. L.; Suter, U. W. *Conformational Theory of Large Molecules*; Wiley Interscience: New York, 1994, p 364.
10. Erman, B.; Marvin, D. C.; Irvine, P. A.; Flory, P. J. *Macromolecules* **1982**, *15*, 664.
11. Erman, B.; Wu, D.; Irvine, P. A.; Marvin, D. C.; Flory, P. J. *Macromolecules* **1982**, *15*, 670.
12. Floudas, G.; Lappas, A.; Fytas, G.; Meier, G. *Macromolecules* **1990**, *23*, 1747.
13. Dettenmaier, M.; Kausch, H. H. *Colloid. Polym. Sci*. **1981**, *259*, 209.
14. Navard, P.; Flory, P. J. *J. Chem. Soc. Faraday Trans. I* **1986**, *82*, 3367.
15. Le Fevre, C. G.; Le Fevre, R. J. W. *Rev. Pure Appl. Chem*. 1955, *5*, 261.
16. Le Fevre, C. G.; Le Fevre, R. J. W. *J. Chem. Soc*. **1956**, 3549.
17. Le Fevre, C. G.; Le Fevre, R. J. W.; Roper, R.; Pierens, R. K. *Proc. Chem. Soc*., **1960**, 117.
18. Sulatha, M. S.; Sivaram, S.; Natarajan, U. *J. Phys. Chem. A* **2003**, *107*, 97.
19. Tomaselli, M.; Zehnder, M. M.; Robyr, P.; Grob-Pisano, C.; Ernst, R. R.; Suter, U. W. *Macromolecules* **1997**, *30*, 3579.
20. Shyu, G. D.; Isayev, A. I.; Li, C. T. *J. Polym. Sci. Polym. Phys*., **2001**, *39*, 2252.
21. Wimberger Friedl, R.; Schoo, H. F. M.; De Bruin, J. G. (U.S. Philips Corporation) U.S. Patent 5,424,389, June 13, 1995.
22. Shirouzu, S.; Shigematsu, K.; Sakamoto, S.; Nakagawa, T.; Tagami, S. *Jpn. J. Appl Phys*., **1989**, *28*, 801.
23. Davis, G. C.; Caruso, A. J.; Wetzel, J. R.; Hariharan, R.; Wisnudel, M. B. (General Electric Company) U.S. Patent 6,001,953, December 14, 1999.
24. Toshimasa, T. I.; Kuniyuki, H. M.; Tatsumi, H. I. (Teijin Chemicals Ltd.) U.S. Patent 5,633,060, May 27, 1997.
25. Bruder, F.; Plaetschke, R.; Schmid, H. *Jpn. J. App. Phys*., **1998**, *37*, 2120-2124.
26. Shigematsu, K.; Shirouzu, S.; Sakamoto, S.; Suzuki, T. (Idemitsu Kosan Company) Eur. Patent 0312 860 A2, April 26, 1989.
27. Werumeus Buning, G. H.; Wimberger Friedl, R.; Janeschitz-Kreigl, H.; Ford, T. M. In *Integration of Fundamental Polymer Science and Technology-2*; Lemstra, P. J., Kleintjens, L. A., Eds.; Elsevier: London, 1988; p 405.

28. Gao, J.; Weiner, J. H. *Macromolecules* **1994**, *27*, 1201.
29. Mavrantzas, V. G.; Theodorou, D. N. *Comput. Theor. Polym. Sci.* **2000**, *10*, 1.

Chapter 5: Ab initio Calculations on Small Molecule Fragments of Structurally Modified Polycarbonates

5.1. Introduction

Ab initio quantum chemical calculations are widely used for the determination of equilibrium geometries, conformations, torsion barriers and electronic excitation energy of small sized molecules. Improvements in computer hardware and algorithms have permitted the application of these techniques to somewhat larger molecules including oligomeric models of polymers with reasonable confidence. Chain conformations of BPAPC model analogues have been investigated previously by different quantum chemical methods, such as MNDO and CNDO type semi-empirical calculations and by the STO-3G level and approximate PRDDO ab initio computations.[1-6] Laskowski et al. presented results of ab initio HF calculations on model compounds of BPAPC using different basis sets and these were used to compute the chain dimensions.[7] Extensive quantum chemical calculations on model analogues of BPAPC using HF and DFT techniques were reported by Sun et al.[8,9] Different basis sets were used in order to investigate the influence of using larger basis sets and electron correlation on the computed molecular geometry and dihedral rotational energy barriers. Agreement of the computed geometry with crystal structure data was observed in these calculations. The rotational energy barriers and the energy difference between the various conformers have been deduced from these calculations. Based on these very detailed calculations an all atom force-field for polycarbonates has been developed.[8] Also HF calculations using a split valence basis set have been reported for DPC by Bendler.[10]

Jones and co-workers applied DFT methods on small organic molecules focussing on BPAPC.[11-15] Their work included the investigation of structures and vibrational frequencies of BPAPC fragments and closely related molecular crystals. The geometries compared favourably well with those from earlier theoretical studies and also experimental crystal structure data. Studies were also performed on reactions of nucleophilic molecules with the cyclic tetramer and chain segments of BPAPC to identify the possible reaction paths and energy barriers. Ab initio and DFT calculations were performed on a series of carbonates with an aim of understanding the influence of the type of substituents (aliphatic vs aromatic

side groups) on the different reaction mechanisms leading to thermal elimination reactions. Comparison has been made with experimentally measured thermal degradation temperature.[16-18] Ab initio calculations have also been reported for dimers of polycarbonates, to determine the Youngs moduli and the results compared favourably well with the experimental values.[19] Optimized geometrical parameters of the polycarbonates studied were not provided in this report.

Estimation of polarizability tensors and polarizability anisotropies of organic molecules from first principles is a field of ever growing interest. In the area of polymer science, the need for reliable computation of these properties is of great significance since in recent years demand on new organic materials with useful linear and non-linear optical properties has increased. Molecular polarizability is a measure of the ease with which the electrons in a molecule can be displaced when the molecule is placed in a uniform electric field. Measurement of molecular polarizability, especially polarizability anisotropy has long been known to be a sensitive probe of molecular conformation. Polarizabilities calculated by ab initio quantum chemical methods are usually found to be in good agreement with gas phase experimental observations. But discrepancies are often found while comparing these values with those measured in solutions and in the condensed phase.

There are many reports in literature concerning the application of quantum mechanical methods on the determination of polarizabilities of small organic molecules.[20-27] One report, which is of relevance to the present work is by Sun and Mumby.[28] The study showed that calculated polarizability anisotropies for molecules in solution are highly dependent on the near-molecule local field correction. The authors used a direct approach to calculate the local-field correction based on the solute molecular structure, liquid structure of the solvent incorporated in the DFT formalism, to determine the apparent polarizability anisotropies of molecules in dilute solution in nonpolar solvents. But even with the local field correction the computed polarizability anisotropies for compounds like diphenyl carbonate (DPC) (31.3 $Å^6$)[28] were far below the experimental value (72±4 $Å^6$)[29] which was measured by DRS experiments in solution.

Ab initio calculations on the geometry and conformation of substituted polycarbonates of interest in the present work have not been reported in literature prior to this study. In this work accurate geometries and conformations of the bisphenyl fragments and diphenyl carbonate moieties which represent model analogues of the substituted polycarbonates are derived using HF calculations using two different basis sets, 6-31G and 6-31G**. The derived geometries are then used for the computation of polarizabilities and subsequently optical anisotropies of these molecules.

5.2. Details of Computational Methodology

All ab initio calculations reported in this thesis were performed on Silicon Graphics Octane workstation. Equilibrium geometry and conformations of the model compounds of polycarbonates, viz., the bisphenyl fragments and carbonates, were determined by the Hartree-Fock method (HF) with 6-31G and 6-31G** basis sets. The chemical structures of these molecules for which ab initio calculations were performed are given in Figure 5.1. Full geometry optimizations of the model compounds were performed separately using HF/6-31G and HF/6-31G** calculations. Optimizations were performed without any constraint in that all atomic coordinates were allowed to relax. Starting structures for these geometry optimizations were those derived from the force-field minimized structures derived from the conformational analysis of these compounds (the results of which are presented in Chapter 3). Calculations using 6-31G basis set were done using GAMESS[30] (General Atomic and Molecular Electronic Structure System) and those with 6-31G**, using Spartan.[31] Single point calculations were performed on these geometry optimized structures in order to determine the optical polarizability tensors. Time dependent Hartree-Fock method (TDHF)[32] in the HF approximation is employed here to calculate the polarizability components. Only static polarizabilities were determined using this method although TDHF method allows the calculation of frequency dependent polarizabilities. The polarizability calculations were performed using the TDHF method implemented in GAMESS. The model compounds selected to explore the conformational characteristics of various polycarbonates are given in Figure 5.1. These compounds include the important molecular structures or fragments comprising the polycarbonates of interest in the present work. The illustration of the

structures of these molecules and the numbering of atoms are also provided in Figure 5.1. Geometry optimization and polarizability calculations using HF/6-31G basis set were performed for different conformers of the bisphenyl fragments, for eg. 8 conformers in the case of DPP. The starting conformations of these molecules were taken from those derived from PCFF force-field based conformational energy calculations, the results of which are presented earlier in Chapter-3 of this thesis. Geometry optimization and polarizability calculation with the 6-31G** basis set is performed for only one particular minimum energy conformer corresponding to each bisphenyl fragment. For the diphenyl carbonates calculations were performed on *trans, trans* (*t-t*) and *cis, trans* (*c-t*) conformers using the two different basis sets. For comparison full geometry optimizations were performed for DPP and DPC using the DFT method (BP approximation)[33,34] incorporated in Spartan.[31]

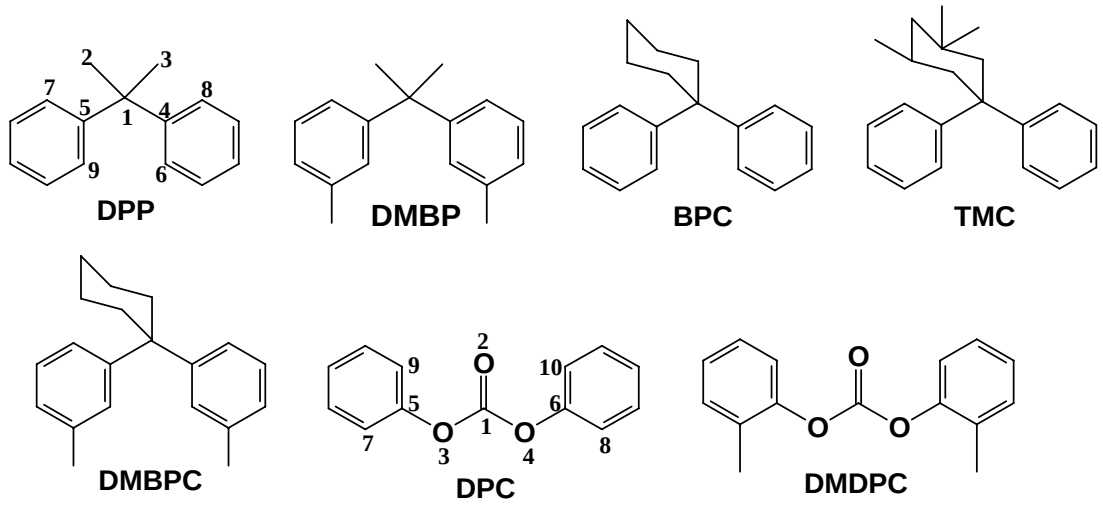

Figure 5.1. Chemical structures of the model compounds of polycarbonates with numbering of atoms shown in the case of DPP and DPC

5.3. Results and Discussion

5.3.1. Geometry optimization and structure parameters for BPAPC model compounds

Information on the geometry and conformation of the BPAPC polymer model compounds DPP and DPC is already available from previous ab initio studies[9,10] and crystal structure data.[35,36] The consequence of using different basis sets is evaluated in the case of DPP and DPC, by comparing the present results here by using two different basis sets (6-31G and 6-

31G**) with the literature reported values. A comparison of the geometrical parameters for diphenyl propane (DPP) calculated at different levels of theory is provided in Table 5.1.

The geometry of DPP predicted by the various quantum chemical methods with different basis sets are fairly similar. The HF/6-31G** calculations lead to slightly smaller values of bond lengths. The parameters derived using the HF method independently using 3 different basis sets, 6-31G, 6-31G* and 6-31G**, are almost identical which suggests that HF/6-31G optimization gives reasonably accurate estimation of the geometry of DPP and that the inclusion of polarization functions on the heavy atoms and hydrogens does not appreciably change the geometrical parameters of the bisphenyl fragment.

Table 5.1. Comparison of the geometry of DPP calculated using different levels of theory

DPP	Present study		HF/6-31G*[9]	Present study	DFT[11]
	HF/6-31G	HF/6-31G**		DFT(PB)	
C1-C2	1.5470	1.5428	1.543	1.5491	1.541
C1-C4	1.5421	1.5406	1.541	1.5409	1.536
C3-C1-C2	107.1	107.1	107.3	108.3	107.7
C4-C1-C5	109.9	109.9	109.6	108.6	109.4
C1-C4-C6	119.2	119.3	119.3	119.1	119.3
C1-C4-C8	123.0	123.0	123.1	122.9	122.9
C4-C1-C5-C9	53.3	52.2	50.5	54.0	50.8
C5-C1-C4-C6	53.3	52.2		54.0	

Bond lengths are in units of Å, bond angles and torsions in units of degrees

In the case of DPC, calculations using 6-31G basis set always led to 'planar' and 'perpendicular' structures which correspond to the local minima. The planar and perpendicular structures of DPC correspond to situations whereby in the former case phenyl groups are in the same plane as the carbonate group and in the latter case phenyl groups are perpendicular to the carbonate group. Global minimum energy structure of DPC could not be obtained using 6-31G basis set, while optimizations based on 6-31G** basis set lead to global energy minima and geometric structures which compare favorably well with the reported geometries for DPC.[10] This observation emphasizes the importance of the basis set in calculations involving carbonate group wherein the inclusion of polarization functions on

heavy atoms as well as hydrogens in estimating the accurate geometries and conformations is significantly important. Calculations using the 6-31G** basis set leads to three different energy minima states in the case of DPC which are designated here as I, II and III. The geometrical information corresponding to the structure of lowest energy conformation (I) using 6-31G** basis set obtained from the calculations is compared with the reported geometries from other studies in literature in Table 5.2. The geometry obtained using 6-31G** here is similar to that reported by Bendler[10] for DPC using the same basis set. Bond lengths obtained from HF methods are smaller than those obtained using DFT calculations, but agree better with data from crystal structure determination.[35,36] Valence parameters predicted for DPC by the two different DFT calculations are also in agreement with each other. In general there is agreement between the geometries derived using the different methods although they do somewhat differ in specific details. Also shown in Table 5.2 is the geometry obtained from optimization by DFT in the case of DPC.

Table 5.2. Comparison of the geometry corresponding to the global minima of DPC with the reported data in literature

DPC	HF/6-31G**		DFT		Crystal structure data (BPA dimer)[35-36]
	present study	Bendler[10]	(present study) (PB)	(PBE)[11]	
C1-O2	1.1804	1.1804	1.2085	1.2100	1.172
C1-O3	1.3228	1.3227	1.3633	1.3640	1.333
C1-O4	1.3228	1.3227	1.3633	1.3640	1.326
C5-O3	1.3851	1.3848	1.4086	1.4100	1.407
C6-O4	1.3852	1.3849	1.4086	1.4100	1.413
C1-O3-C5	119.5	119.6	119.0	119.2	119.3
O3-C1-O4	107.1	107.0	104.6	105.1	106.5
C1-O4-C6	119.3	119.5	119.0	119.2	115.4
O2-C1-O4	126.4	126.4	127.7	126.1	126.1
C1-O3-C5-C7	-114.5	115.8	-137.2	69.3	135.5, -96.5
C1-O3-C5-C9	69.3	-68.0	47.0	-	-48.0, 89.0
C5-O3-C1-O2	-1.9	1.7	-0.3	0.00	6.3, 7.7
O3-C1-O4-C6	178.1	178.6	-179.6	-	-178.9, 177.5
C1-O4-C6-C10	-113.1	69.5	-47.0	44.8	89.2, -102.4
O2-C1-O4-C6	-1.9	-1.5	0.3	0.50	1.2, -1.2

Geometrical information corresponding to conformers I, II and III of DPC, while in the *t-t* conformation of the carbonate group, is given in Table 5.3. The optimized geometry of the *c-t* conformation is also provided. As expected, C1-O3 and C1-O4 bonds which are characterized by an increased π bonding nature are shorter compared to C5-O3 and C6-O4 bonds and this result is a good validation of the calculations here. The orientation of the phenyl rings, with respect to the carbonate group, is twisted in the lowest energy conformer (I). Such a conformation is adopted in order to relieve the steric repulsion between the carbonyl oxygen and the phenyl ring hydrogens (*ortho* to the carbonate group). The steric strain is lowest in magnitude in the perpendicular conformation (III), but the additional energy stabilization due to electron delocalization is completely lost in adopting such a conformation. Therefore the phenyl rings adopt a twisted conformation with respect to the carbonate group. The difference in the geometry, especially with respect to the valence coordinates, can be seen from the relevant bond angles (C_{Ph}-C_{Ph}-O) which adjust accordingly to such changes in the conformation of the phenyl rings. In the perpendicular conformer (III), the steric factor due to repulsion between the hydrogens and carbonyl oxygen is not present. Also, the 4 bond angles corresponding to C_{Ph}-C_{Ph}-O, formed by the phenyl carbon and carbonate oxygen (O3-C5-C7, O3-C5-C9, O4-C6-C8, O4-C6-C10) have values 119° and 119.2° which are very close to the usual value 120° (sp^2 hybridization). In case of I, the C_{Ph}-C_{Ph}-O bond angles are distorted from 120° taking up values 120.7° and 117.5° to reduce the amount of steric repulsion. The differences in the valence coordinates between I and III conformers can also be seen in the values of C1-O3-C5 and C1-O4-C6 bond angles. In III, these are considerably distorted and have the value 118.6° which is considerably distorted from the equilibrium value of 120°, owing to the complete loss in electron delocalization due to perpendicular orientation of phenyl rings with respect to the carbonate group. Thus, differences in the bond angle geometry are seen clearly between the different conformers of DPC. Energy difference between the 3 conformers of *t-t* form of DPC is not very appreciable and this indicates the flexibility of the Ph-O bond and a relatively free rotation ability of the phenyl rings accompanying a low energy barrier.

The carbonyl double bond in the *c-t* form is found to be slightly shorter than that in the *t-t* form. Other bond lengths are almost similar in DPC (*t-t*) and DPC (*c-t*). In the *t-t* form

the bond angle at the tetrahedral carbonyl carbon (O3-C1-O4) is smaller (107.1) than the usual tetrahedral value of 109.9°. In the *c-t* conformer this angle is opened up and takes a value of 111.8°. This is accompanied by a decrease in the O2-C1-O4 bond angle. Orientation of phenyl rings with respect to plane of carbonate group is 79.7° when the conformation is *trans* and almost perpendicular in case of *cis* conformer. We obtain the result that the *c-t* conformer of DPC is 2.8 kcal/mol higher in energy than the *t-t* conformer and this value is in agreement with the reported values from other quantum chemical calculation methods.[11]

Table 5.3. Comparison of the geometries of different conformers of DPC obtained from HF/6-31G** calculations in the present work

HF/6-31G**	DPC (*trans, trans*)			DPC
	I	II	III	(*cis, trans*)
C1-O2	1.1804	1.1801	1.1800	1.1773
C1-O3	1.3228	1.3232	1.3234	1.3272
C1-O4	1.3228	1.3232	1.3234	1.3244
C5-O3	1.3851	1.3854	1.3856	1.3864
C6-O4	1.3852	1.3854	1.3856	1.3842
O2-C1-O3	126.5	126.4	126.4	126.0
C1-O3-C5	119.4	118.9	118.6	118.9
O3-C1-O4	107.1	107.2	107.2	111.8
O2-C1-O4	126.4	126.4	126.4	122.2
C1-O4-C6	119.3	118.9	118.6	123.1
O3-C5-C7	117.5	118.2	119.2	118.3
O3-C5-C9	120.7	120.0	119.0	119.8
O4-C6-C8	120.6	118.2	119.2	119.0
O4-C6-C10	117.6	120.0	119.0	119.2
C1-O3-C5-C7	-114.5	-105.2	-90.5	-103.7
C1-O3-C5-C9	69.3	78.4	93.0	79.7
C5-O3-C1-O2	-1.9	-0.8	0.03	-0.7
O3-C1-O4-C6	178.1	-179.3	180.0	-0.
C1-O4-C6-C10	-113.0	-78.4	-93.0	91.0
C1-O4-C6-C8	70.7	105.2	90.5	-93.2
O2-C1-O4-C6	-1.9	0.8	-0.03	179.7
E (kcal/mol)	0.0	0.1024	0.1294	2.797

5.3.2. Geometry optimization and structure parameters for substituted bisphenyl and carbonate fragments

Full geometry optimizations were performed for various bisphenyl fragments which are model compounds for different substituted polycarbonates. Calculations were performed independently using 6-31G as well as 6-31G** basis sets. The geometrical information including the bond lengths, angles and torsional parameters derived using 6-31G and 6-31G** basis sets are provided in Table 5.4 and Table 5.5 respectively. In Table 5.4, geometries corresponding to only one conformer for the model compounds of each of a particular polycarbonate is given, although geometry optimizations were carried out for more number of conformers for each bisphenyl fragment. Similar to what is observed earlier in the case of DPP, the geometries of various bisphenyl fragments are insensitive to the basis set used here as well. The calculated geometries are found to be similar using 6-31G and 6-31G** basis set for each fragment. The bond angle at the C_α carbon is at its equilibrium value corresponding to a tetrahedral carbon in the case of DPP and DMBP. For cyclohexylidene bisphenyl fragments, this particular bond angle is considerably distorted, with the maximum distortion seen in the case of TMC fragment. This distortion from the tetrahedral geometry is due to the presence of the cyclohexylidene group. Considerable steric repulsion caused due to the hydrogens lying above the axial phenyl ring could be one reason for the reduction in the bond angle which forces the phenyl rings to be away from the hydrogens of the cyclohexyl group. The inequivalent nature of the phenyl groups in cyclohexyl substituted bisphenyls is seen from the present results of the derived geometries for these compounds. Additional methyl groups on the cyclohexyl group as in TMC leads to further contraction of this angle. In contrast, geometry of the bisphenyl fragment is unaffected if the only substituting groups are methyls on phenyl rings. The various valence parameters and the torsions are similar for DPP and DMBP. Similarly this is as well found to be true in the case of BPC and DMBPC.

Table 5.4. Geometry of bisphenyl fragments derived from HF/6-31G optimization

HF/6-31G	DPP	DMBP	BPC	TMC	DMBPC
C1-C2	1.5470	1.5472			
C1-C3	1.5470	1.5472			
C1-C4	1.5420	1.5422	1.5484	1.5541	1.5486
C1-C5	1.5421	1.5422	1.5470	1.5474	1.5474
C3-C1-C2	107.1	107.1			
C4-C1-C5	109.9	110.0	107.4	106.2	107.6
C4-C1-C2	107.4	107.4			
C5-C1-C2	112.5	112.5			
C1-C4-C6	119.2	119.1	119.2	118.9	119.0
C1-C4-C8	123.0	122.9	123.3	123.7	123.3
C1-C5-C7	119.2	119.1	119.3	119.2	119.0
C1-C5-C9	123.0	122.9	123.4	123.4	123.5
C4-C1-C5-C9	53.3	52.9	68.7	-67.3	67.8
C5-C1-C4-C8	53.3	52.9	57.7	-61.0	58.1

Table 5.5. Geometry of bisphenyl fragments derived from HF/6-31G** optimization

HF/6-31G**	DPP	DMBP	BPC	TMC	DMBPC
C1-C2	1.5428	1.5428			
C1-C3	1.5428	1.5428			
C1-C4	1.5406	1.5405	1.5467	1.5517	1.5468
C1-C5	1.5406	1.5405	1.5463	1.5464	1.5461
C3-C1-C2	107.1	107.1			
C4-C1-C5	109.9	110.0	107.2	106.2	107.4
C4-C1-C2	107.4	107.4			
C5-C1-C2	112.5	112.5			
C1-C4-C6	119.3	119.1	119.1	118.9	119.0
C1-C4-C8	123.0	123.0	123.5	123.9	123.5
C1-C5-C7	119.3	119.1	119.3	119.2	119.0
C1-C5-C9	123.0	123.0	123.5	123.5	123.6
C4-C1-C5-C9	52.2	52.2	68.1	-66.5	67.5
C5-C1-C4-C8	52.2	52.3	57.5	-60.7	57.7

Table 5.6. Geometry of DMDPC derived using HF/6-31G and HF/6-31G** optimizations

DMDPC	HF/6-31G		HF/6-31G**	
	t-t	*c-t*	*t-t*	*c-t*
C1-O2	1.2083	1.2020	1.1813	1.1783
C1-O3	1.3370	1.3451	1.3224	1.3265
C1-O4	1.3370	1.3394	1.3224	1.3238
C5-O3	1.4120	1.4104	1.3888	1.3900
C6-O4	1.4121	1.4100	1.3888	1.3874
O2-C1-O3	125.7	125.9	126.3	125.8
C1-O3-C5	122.3	125.6	118.8	118.9
O3-C1-O4	108.5	111.6	107.4	112.0
O2-C1-O4	125.7	122.6	126.3	122.1
C1-O4-C6	122.3	125.9	118.8	123.2
O3-C5-C7	119.7	115.2	119.5	119.3
O3-C5-C9	117.2	121.6	117.8	117.9
O4-C6-C8	119.7	119.3	119.5	118.9
O4-C6-C10	117.2	117.5	117.8	118.4
C7-C5-O3-C1	-81.7	-141.7	-87.6	-85.4
C9-C5-O3-C1	101.8	41.5	96.1	98.3
C5-O3-C1-O2	3.4	-0.8	3.2	0.2
O3-C1-O4-C6	177.1	-3.6	177.1	-2.4
C1-O4-C6-C10	-101.8	-97.4	-96.1	-90.7
C1-O4-C6-C8	81.7	87.1	87.6	93.9
O2-C1-O4-C6	-3.4	176.9	-3.2	177.6
E (au)	-800.4596637	-800.4578180	-800.8197834	-800.815508
Kcal/mol	0.0	1.16	0.0	2.682

Parameters derived from HF/6-31G and HF/6-31G** geometry optimization of *t-t* as well as *c-t* form of DMDPC are provided in Table 5.6. As was noted earlier for DPC, the geometry obtained using the two basis sets differ appreciably from each other. In the following section, the data from 6-31G** optimizations will be discussed. The carbonyl double bond is shorter in the *c-t* form when compared to the *t-t* conformer as is observed in DPC. The difference between the two conformers is evident from the three bond angles on

the same side as the phenyl ring, which is now in a *cis* orientation with respect to the carbonyl group. The angles O3-C1-O4 and C1-O4-C6 are at higher values in the *c-t* form when compared to *t-t* conformer. This is accompanied by a decrease in the bond angle O2-C1-O4 in the *c-t* conformer when compared to *t-t*. This change in geometry occurs to minimize the steric crowding and strain between the *ortho* hydrogens/methyl group on the phenyl ring (which is in a *cis* conformation) with the carbonate oxygen. This is also seen in the geometry of *t-t* and *c-t* forms of DPC. The energy difference between the *t-t* and *c-t* conformers of DMDPC is 2.68 kcal/mol which is slightly lower than the value found in the case of DPC.

5.3.3. Polarizability

Polarizabilities were calculated for the optimized conformers by a single point calculation. In the case of bisphenyl fragments geometry optimization using HF/6-31G basis set were performed for the discrete rotational states, ie., 8 minimum energy conformers in the case of DPP, 8 for BPC, 4 for TMC, 8 for DMBPC and 8 for DMBP. Polarizabilities were calculated for all these different conformers for each bisphenyl monomer fragment using the HF-TDHF method with 6-31G basis set. Optimizations using 6-31G** basis set were performed only for one conformer corresponding to each monomer fragment and the corresponding polarizabilities were also calculated with 6-31G** basis set. Polarizabilities calculated are in arbitrary reference frames and these are then transformed using a coordinate tensor transformation scheme. The reference frames to which the polarizabilities are transformed for the carbonates and bisphenyls are shown in Figure 5.2.

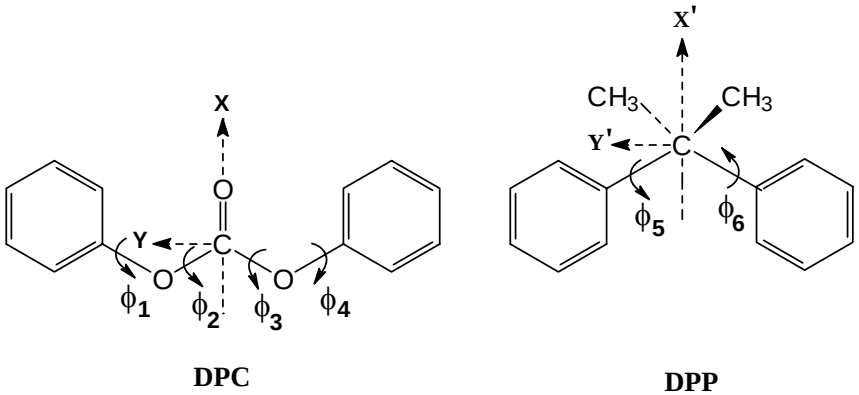

DPC **DPP**

Figure 5.2. Schematic representation of the reference frames in DPC and DPP in which the polarizabilities are calculated

Calculated polarizabilities for the different bisphenyls are given in Tables 5.7 to 5.11. One characteristic feature that emerges from these calculations is that bisphenyl fragments which do not have methyl substituents on the phenyl rings (DPP, BPC and TMC) have the same components of total polarizability and average polarizability for all the distinct conformers in each case. In the case of monomer fragments with methyl substitution on the phenyl rings (DMBP and DMBPC), polarizabilities are different which is decided by the conformation of the bisphenyl as well as the orientation of the methyl groups. This feature is also brought forth from the polarizability calculations presented in Chapter 4 using the VOS.

Table 5.7. Polarizabilities (Å^3) for various conformers of DPP using HF/6-31G method

	I	II	III	IV	V	VI	VII	VIII
ϕ_5(°)	53.3	-53.3	53.3	-53.3	128.9	-128.9	128.9	-128.9
ϕ_6(°)	53.3	-53.3	-128.9	128.9	-53.3	53.3	128.9	-128.9
α_{xx}	18.003	18.007	18.002	18.002	18.002	18.002	18.002	18.002
α_{yy}	25.422	25.423	25.422	25.422	25.422	25.422	25.423	25.423
α_{zz}	17.027	17.023	17.024	17.022	17.024	17.020	17.023	17.023
α_{xy}	0.000	0.000	0.000	0.000	0.000	0.000	0.000	0.000
α_{xz}	0.000	0.000	0.000	0.000	0.000	0.000	0.000	0.000
α_{yz}	-2.719	2.717	-2.719	-2.718	-2.719	-2.723	2.719	2.718
$\bar{\alpha}$	20.150	20.150	20.149	20.148	20.149	20.150	20.149	20.149

Table 5.8. Polarizabilities (Å^3) for various conformers of BPC using HF/6-31G method

	I	II	III	IV	V	VI	VII	VIII
ϕ_5(°)	68.7	-68.7	68.7	-68.7	108.4	-108.4	108.3	-108.4
ϕ_6(°)	57.7	-57.6	-123.0	123.0	-57.6	57.6	123.0	-123.0
α_{xx}	22.907	22.903	22.906	22.905	22.905	22.907	22.901	22.905
α_{yy}	27.202	27.200	27.195	27.195	27.201	27.202	27.197	27.199
α_{zz}	22.429	22.413	22.437	22.437	22.433	22.429	22.439	22.431
α_{xy}	0.137	0.152	0.138	0.136	0.145	0.137	0.137	0.144
α_{xz}	0.629	-0.640	0.639	-0.639	-0.633	0.629	-0.642	0.634
α_{yz}	-2.445	2.431	-2.438	2.438	2.443	-2.445	2.441	-2.443
$\bar{\alpha}$	24.179	24.172	24.179	24.179	24.179	24.179	24.179	24.178

Table 5.9. Polarizabilities (Å^3) for various conformers of TMC using HF/6-31G method

HF/ 6-31G	I	II	III	IV
ϕ_5(°)	-67.3	-67.3	109.5	109.5
ϕ_6(°)	-60.9	118.6	-60.9	118.7
α_{xx}	27.910	27.899	27.913	27.907
α_{yy}	30.576	30.579	30.586	30.576
α_{zz}	27.257	27.265	27.253	27.257
α_{xy}	0.696	0.698	0.695	0.696
α_{xz}	-0.624	-0.622	-0.624	-0.624
α_{yz}	2.110	2.108	2.109	2.110
$\bar{\alpha}$	27.257	28.581	28.584	28.580

Table 5.10. Polarizabilities for (Å^3) various conformers of DMBPC using HF/6-31G method

HF/ 6-31G	I	II	III	IV	V	VI	VII	VIII
ϕ_5(°)	67.8	-73.0	68.1	-68.5	108.9	-108.9	108.5	-108.4
ϕ_6(°)	58.1	-58.6	-123.3	123.3	-58.1	58.1	122.7	-122.6
α_{xx}	26.460	26.459	25.743	25.895	26.176	26.170	25.346	25.291
α_{yy}	29.792	29.804	30.743	30.818	30.224	30.225	31.204	31.153
α_{zz}	26.105	26.155	26.121	25.936	26.074	26.067	26.198	26.305
α_{xy}	0.145	0.122	-0.131	-0.189	0.384	0.383	0.037	0.092
α_{xz}	0.621	-0.6215	-0.148	0.162	-1.464	1.489	-0.797	0.746
α_{yz}	-1.453	1.419	-2.649	2.727	2.931	-2.831	4.037	-4.013
$\bar{\alpha}$	27.452	27.473	27.535	27.549	27.491	27.487	27.582	27.583

Table 5.11. Polarizabilities (Å^3) for various conformers of DMBP using HF/6-31G method

HF/ 6-31G	I	II	III	IV	V	VI	VII	VIII
ϕ_5 (°)	52.9	-53.4	52.9	-52.6	128.4	-128.2	128.4	-128.1
ϕ_6 (°)	52.9	-53.0	-128.2	128.3	53.4	53.0	128.4	-128.1
α_{xx}	21.697	21.791	20.983	21.074	21.092	20.983	20.533	20.251
α_{yy}	27.610	27.586	28.519	28.650	28.509	28.519	29.750	29.430
α_{zz}	20.966	20.846	21.012	20.824	20.885	21.012	20.591	21.135
α_{xy}	0.000	-0.027	-0.395	-0.471	0.372	0.395	-0.074	0.000
α_{xz}	0.000	-0.015	-0.640	0.617	-0.649	0.640	-0.038	0.000
α_{yz}	-2.201	2.253	-3.394	3.392	3.450	-3.394	4.569	-4.602
$\bar{\alpha}$	23.425	23.408	23.505	23.516	23.496	23.505	23.624	23.605

Table 5.12. Polarizabilities (Å^3) determined using HF/6-31G** method for bisphenyl monomers

(HF/6-31G**)	DPP	BPC	TMC	DMBPC	DMBP
ϕ_5 (°)	52.2	68.1	-66.5	67.4	53.0
ϕ_6 (°)	52.2	57.5	-60.7	57.7	53.0
α_{xx}	26.007	27.499	30.370	29.781	22.695
α_{yx}	-2.736	1.162	-0.973	-0.355	0.002
α_{zx}	0.0000	-2.017	1.327	-1.780	0.003
α_{yy}	17.368	24.077	27.768	27.408	27.619
α_{zy}	0.0000	-1.238	-1.976	1.004	2.973
α_{zz}	18.738	22.656	29.529	27.272	21.891
$\bar{\alpha}$	20.704	24.744	29.222	28.154	24.068

In Table 5.12, polarizabilities calculated for one conformer each of the bisphenyl fragment using the 6-31G** basis set is presented. TMC exhibits the highest average polarizability among these bisphenyl fragments followed by DMBPC, BPC, DMBP and DPP. Table 5.13 provides a comparison of the mean polarizabilities and squared optical anisotropy of the bisphenyl fragments calculated using 6-31G and 6-31G** basis sets. The comparison is provided for conformers having almost similar geometry in the case of each bisphenyl fragment. There are some subtle differences in the torsions and angles between the

geometries derived using 6-31G and 6-31G** basis set for each fragment. The differences in the mean polarizability and optical anisotropy thus seen in the case of bisphenyl fragments calculated with two different basis sets is predominantly due to this difference in the geometrical parameters and not due to the basis sets. Thus similar to what is observed for the geometry, polarizabilities are also insensitive to the basis sets used in the case of bisphenyl fragments.

Table 5.13. Comparison of polarizability and optical anisotropy derived from HF/TDHF method using 6-31G and 6-31G** basis sets

Bisphenyl fragments	QC-HF			
	Mean polarizability, $\bar{\alpha}$ (Å^3)		Optical anisotropy, γ^2 (Å^6)	
	6-31G	6-31G**	6-31G	6-31G**
DPP	20.15	20.70	85.47	87.10
DMBP	23.42	24.07	54.34	55.33
BPC	24.18	24.74	39.90	39.45
TMC	27.26	29.22	25.25	25.60
DMBPC	27.45	28.15	19.96	18.87

Squared optical anisotropy of the bisphenyl fragments can be calculated using the valence optical scheme (VOS) as is described earlier in Chapter 4 where the group polarizability tensors derived from DRS experiments were made use of in conjunction with the relevant torsions and bond angles representing the geometry of the concerned molecule. Here, squared optical anisotropies of the bisphenyl fragments can also be calculated using VOS method by employing the experimentally derived group polarizability tensors, but by using the geometry (torsions and bond angles) derived from the quantum chemical optimizations (Tables 5.4 and 5.5) for the purpose of comparison. The optical anisotropy calculated using the VOS method is given in Table 5.14 along with those derived from the polarizabilities obtained from the QC/HF-TDHF method. Thus a comparison is provided for bisphenyls having the same geometry, but the molecular polarizabilities calculated using two different methods (i) VOS employing the experimental group polarizability tensors and (ii) polarizabilities estimated from the QC method. The optical anisotropies calculated from polarizabilities obtained from the QC method are higher than those determined using the

VOS method as is seen from Table 5.14. It has been shown in Chapter 4 that, VOS scheme employing the experimentally derived group polarizability tensors give excellent comparison with experimentally determined optical anisotropies for the model compounds DPP, DPC as well as for BPAPC. For eg, optical anisotropy calculated via the VOS method is 39.1 $Å^6$ for a conformation ($\phi_5=\phi_6=50°$, $2\tau'=110.7°$) and the experimental value is 40±2 $Å^6$.[29]

The QC calculations for determination of polarizabilities are performed for isolated molecules in vacuum and hence the solvent medium and the consequent interaction of the solvent molecules with the solute is not taken into account. This could be the major reason for the discrepancy in the optical anisotropy values calculated from QC method with those derived from experiments and the VOS scheme. This has been noted previously by researchers who found good comparison with polarizabilities and anisotropies calculated by QC methods with experimental gas phase measurements, but agreement with those calculated from condensed phase/solution measurements were always far from satisfactory.[28] Sun and Mumby has emphasized the importance of solute-solute and solute-solvent interactions in comparing the QC derived polarizabilities of molecules in vacuum with the condensed phase measurements.[28] From their report, even by incorporating a local field correction the calculated polarizabilities and optical anisotropies were far from being in agreement with the experimental values for MPC and DPC model compounds. The calculated optical anisotropy of DPC after incorporating the local field effect was found to be 31.3 $Å^6$ and the experimental value[29] in CCl_4 solution is reported to be 72 $Å^6$.

The general trend in the optical anisotropy of the bisphenyl fragments from QC calculations is similar to that obtained from the VOS method. This suggests that the effect of different substituent groups towards the polarizability and optical anisotropy is predicted correctly by the QC method. The averaged optical anisotropies estimated by averaging the values over all the accessible conformers are given in Table 5.14 where again the trend among the different bisphenyls is retained as that obtained from the VOS method. In Table 5.15, a comparison is provided for the optical anisotropies of the various conformers in the case of DMBP and DMBPC. Optical anisotropy is different for the different conformers in

the case of each of bisphenyl fragment and the trend in the anisotropy values obtained from the QC method is the same as that calculated using the VOS method.

Table 5.14. Comparison of averaged optical anisotropy of bisphenyl fragments derived from quantum chemical calculations and VOS

Bisphenyl fragments	Mean-squared optical anisotropy, $\langle\gamma^2\rangle$(Å^6)	
	HF/6-31G	VOS
DPP	85.43	34.38
DMBP	96.53	37.50
BPC	39.90	14.99
TMC	25.25	13.90
DMBPC	48.53	29.00

Table 5.15. Comparison of optical anisotropy, γ^2, (Å^6) derived from quantum chemical methods and VOS for the various conformers in DMBP and DMBPC

	DMBP		DMBPC	
	HF/6-31G	VOS	HF/6-31G	VOS
I	54.34	14.22	19.96	10.02
II	55.18	13.92	19.54	12.32
III	92.82	35.06	44.44	24.40
IV	95.67	35.29	46.54	24.40
V	93.94	34.89	49.46	30.07
VI	92.82	34.94	48.00	30.10
VII	147.0	67.16	80.84	50.37
VIII	140.5	64.59	79.45	50.35

The polarizabilities and optical anisotropies of the carbonate fragments, DPC and DMDPC calculated using the 6-31G** basis set are given in Table 5.16. As can be seen these values obtained from QC/TDHF/6-31G** calculations are considerably higher than that calculated via the VOS. In Chapter 4, it has been shown that the anisotropy calculated using the VOS for the equilibrium geometry of DPC is in good agreement with the value estimated from DRS experiments (73.2 A^{o6} from VOS vs 72±4 A^{o6} from experiments). From DFT

calculations Sun and Mumby[28] derived a value of 291.32 A^{o6} for DPC in vacuum and by including the solvent effects the value obtained was 31.3 A^{o6}. None of these agree with the experimental value of 72±4 A^{o6}.[29] Reports by Sun and Mumby and the present ab initio calculation results outlined here thus underline the importance of taking into account the solute-solvent interactions when comparing the QC chemically derived values with those determined in solution. Also in the case of carbonates, the basis set employed in the calculation plays a decisive role. Calculations for the same geometry of DPC using 6-31G basis set led to a much higher value than that calculated using the 6-31G** basis set.

The perpendicular orientation of the phenyl rings lead to a reduction by about 20 A^{o6} in the case of DPC (I vs III). A similar reduction by about 17 A^{o6} is also noted in the results from VOS calculations presented in Chapter 4. Optical anisotropy of the *c-t* conformer of DPC is lower than that of the *trans, trans* conformer. The same is true for DMDPC also. For the same geometry and conformation, DMDPC has a higher value of optical anisotropy than DPC (II of DPC (*t-t*) vs DMDPC (*t-t*)).

Table 5.16. Polarizabilities of DPC and DMDPC determined using HF/6-31G** method

	DPC			DMDPC	
	t-t		*c-t*	*t-t*	*c-t*
	I	III			
α_{xx}	17.6287	24.9543	21.6710	24.2421	24.8202
α_{yx}	-1.720	0.0000	1.2046	0.000	1.4904
α_{zx}	1.7817	0.0000	-1.7652	-0.5954	1.2631
α_{yy}	25.5821	20.1166	19.9018	28.1200	19.5632
α_{zy}	-0.5593	-0.0922	0.7134	0.0000	-4.2547
α_{zz}	12.0125	9.8682	13.0625	12.2842	19.8870
$\bar{\alpha}$ (A^{o3})	18.4078	18.3130	18.2118	21.5488	21.4234
γ^2 (A^{o6})	158.80	178.10	77.23	205.60	91.80

5.4. Conclusions

Ab initio geometry optimization of model compounds corresponding to BPAPC and four structurally modified polycarbonates have been performed. HF calculations were carried out using two different basis sets, 6-31G and 6-31G**. Geometry and conformation of the bisphenyl fragments were almost similar from calculations using the two basis sets. This was not found to be true in the case of carbonate fragments, where inclusion of polarization functions on heavy atoms as well as hydrogens was necessary to derive accurate geometry and conformation of DPC and DMDPC. Calculations for the bisphenyl fragments were also performed for all the accessible conformers of the different bisphenyl moieties using the HF/6-31G calculations.

Furthermore TDHF calculations for determination of polarizability were performed on these fully geometry optimized fragments. The mean-squared optical anisotropies calculated from the computed polarizabilities were higher when compared to the experimental values in solution. The present calculation results thus emphasizes the importance of taking into account the solute-solvent interactions in the calculation procedure for polarizability to make any possible comparison with the experimental values which have been derived in either condensed phase or in solution.

Although the absolute comparison of the optical anisotropy with the experimental value is not satisfactory, the QC method employed here is able to predict the differences in the anisotropy among the different bisphenyl fragments. The trend in the optical anisotropy observed in these bisphenyl fragments from the experimental group poalrizability/VOS approach is reproduced also from the QC calculations. This indicates that the contributions to the polarizability and optical anisotropy due to the different structural groups are correctly predicted by the QC calculation data presented here. Rigorous methods which take into account the various interactions between the solute and the solvent would provide a better platform for performing these kinds of calculations which will enable researchers to predict the polarizability and optical anisotropy of organic molecules in an accurate way and even before they are synthesized. This indeed will be a significant step towards the design of organic molecules and more importantly polymers with desired structures tailored towards specific applications with respect to their optical properties.

5.5. References

1. Bendler, J. T. *Ann. N.Y. Acad. Sci*. **1981**, *371*, 299.
2. Jones, A. A.; O'Gara, J. F.; Inglefield, P. T.; Bendler, J. T.; Yee, A. F.; Ngai, K. L. *Macromolecules* **1983**, *16*, 658.
3. Sung, Y. J.; Chen, C. L.; Su, A. C. *Macromolecules* **1990**, *23*, 1941.
4 Sung, Y. J.; Chen, C. L.; Su, A. C. *Macromolecules* **1991**, *24*, 6123.
5. Bicerano, J. H.; Clark, H. A. *Macromolecules* **1988**, *21*, 585.
6. Bicerano, J. H.; Clark, H. A. *Macromolecules* **1988**, *21*, 597.
7. Laskowski, B. C.; Yoon, D. Y.; McLean, D.; Jaffe, R. L. *Macromolecules* **1988**, *21*, 1629.
8. Sun, H.; Mumby, S. J.; Maple, J. R.; Hagler, A. T. *J. Am. Chem. Soc*. **1994**, *116*, 2978.
9. Sun, H.; Mumby, S. J.; Maple, J. R.; Hagler, A. T. *J. Phy. Chem*.**1995**, *99*, 5873.
10. Bendler, J. T. *Comput. Theor. Polym. Sci.* **1998**, *8*, 83.
11. Montanari, B.; Ballone, P.; Jones, R. O. *Macromolecules* **1998**, *31*, 7784.
12. Montanari, B.; Ballone, P.; Jones, R. O. *Macromolecules* **1999**, *32*, 3396.
13. Montanari, B.; Ballone, P.; Jones, R. O. *J. Phys. Chem. A* **2000**, *104*, 2793.
14. Ballone, P.; Jones, R. O. *J. Phys. Chem. A* **2001**, *105*, 3008.
15. Akola, J.; Ballone, P.; Jones, R. O. *Macromolecules* **2002**, *35*, 2327.
16. Van Speybroeck, V.; Martele, Y.; Waroquier, M.; Schacht, E. *J. Am. Chem. Soc*. **2001**, *123*, 10650.
17. Van Speybroeck, V.; Martele, Y.; Waroquier, M.; Schacht, E. *Int. J. Quantum Chem.* **2003**, *91*, 363.
18. Katajisto, J.; Pakkanen, T. T.; Pakkanen, T. A.; Hirva, P. J. *Theochem* **2003**, *634*, 305.
19. Katajisto, J.; Linnolahti, M.; Pakkanen, T. A. *Chem. Phys. Lett*. **2004**, *385*, 25.
20. Voisin, C.; Cartier, A.; Rivail, J-L. *J. Phys. Chem. A* **1992**, *96*, 7966.
21. Guan, J.; Duffy, P.; Carter, J. T.; Chong, D. P.; Casida, K. C.; Casida, M. E. *J. Chem. Phys.* **1993**, *98*, 4753 and references cited therein
22. Dykstra, C. E. *Chem. Rev.* **1993**, *99*, 2339.
23. Gough, K. M.; Srivastava, H. K.; Belohorcova, K. *J. Phys. Chem.* **1994**, *98*, 771.

24. Stout, J. M.; Dykstra, C. E. *J. Am. Chem. Soc.* **1995**, *117*, 5127.
25. Sherman, B. J.; Sen, S.; Galiatsatos, V. G. *Polymer* **1996**, *10*, 1759.
26. Lukes, V.; Breza, M.; Palszegi, T.; Laurinc, V.; Vrabel, I. *Macromol. Theory Simul.* **2001**, *10*, 592.
27. Ewig, C. S.; Waldman, M.; Maple, J. R. *J. Phys. Chem. A* **2002**, *106*, 326.
28. Sun, H.; Mumby, S. J. *J. Chem. Phys* **1996**, *104*, 1018.
29. Erman, B.; Marvin, D. C.; Irvine, P. A.; Flory, P. J. *Macromolecules* **1982**, *15*, 664.
30. Schmidt, M. W.; Baldridge, K. K.; Boatz, J. A.; Elbert, S. T.; Gordon, M. S.; Jensen, J. H.; Kosiki, S.; Matsunaga, N.; Nguyen, K. A.; Su, S. J.; Wundus, T. L.; Dupuis, M.; Montgomery, J. H.; *J. Comput. Chem.*, **1993**, *14*, 1347.
31. Spartan, Wavefunction Inc. USA
32. Karna, S. P.; Dupuis, M. *J. Comput. Chem.*, **1991**, *12*, 487.
33. Becke, A. D.; *Phys. Rev. A.* **1988**, *38*, 3098.
34. Perdew, J. P. *Phys. Rev. B.* **1986**, *33*, 8822.
35. Perez, S.; Scaringe, R. P. *Macromolecules* **1987**, *20*, 68.
36. Henrichs, P. M.; Luss, H. R.; Scaringe, R. P. *Macromolecules* **1989**, *22*, 2731.

Chapter 6: Detailed Atomistic Simulations of Structurally Modified Polycarbonates in the Glassy State

6.1. Introduction

The structure of amorphous polymers in their glassy state has been known to be dominated by intrachain conformations as well as contributions arising from interchain packing interactions. This leads to the so called "short-range" order. Local structure in amorphous bulk state of polymers has been probed over the years by a variety of experimental techniques such as solid-state NMR spectroscopy, neutron scattering, wide-angle X-ray scattering, Infrared and Raman spectroscopy. Molecular simulation techniques have also been in practice in order to investigate structure and conformations of amorphous polymers in their glassy state.[1-4]

BPAPC is one of the most widely studied polycarbonate, both, theoretically and experimentally with the prime objectives to characterize the structure and dynamics at the molecular level. Atomistic simulations of glassy amorphous BPAPC have been reported by Hutnik et al.[5,6] The structure factor and mechanical properties as well as the local chain dynamics near the glass transition temperature were studied by Fan et al.[7-9] MD simulations of amorphous BPAPC have also been performed by Shih and Chen.[10] Whitney and Yaris have performed Langevin dynamics simulations to simulate ring flips in glassy polycarbonate.[11] MD and Monte Carlo simulations of crystalline, amorphous and melt polycarbonates using a DFT based force-field have also been reported.[12]

Molecular simulation studies of bulk amorphous structurally modified polycarbonates with full chemical details have been very limited to date. Atomistic simulations to investigate the transport of gaseous molecules have been performed for amorphous tetramethyl (TMPC) and tetrabromo (TBPC) derivatives of BPAPC[13] and for a copolymer of BPAPC and TMCPC.[14] Atomistic simulations in conjunction with neutron scattering experiments were reported for cyclohexylidene-bisphenol polycarbonate (BPCPC) and TMPC.[15] More recently coarse-grained attempts on structurally modified polycarbonates BPCPC, and TMCPC have

focussed on generation of well equilibrated configurations in the melt state, the results of which compared satisfactorily with the experimental neutron scattering data.[16-18]

In this chapter, amorphous glassy models of BPAPC and four structurally modified polycarbonates are derived from detailed atomistic simulations with full structural and chemical details. These are analyzed with respect to the local conformational properties and interchain packing in the bulk state. The substituted polycarbonates studied in the present work are those with the following chemical modifications (i) cyclohexyidene group at C_α carbon, BPCPC; (ii) trimethylcyclohexylidene group at C_α, TMCPC; (iii) methyl groups at ortho position of the backbone phenyl rings, DMPC; (iv) cyclohexylidene group at C_α and methyl groups on phenyl rings, DMBPC. The structures of the repeat units are shown in Figure 6.1.

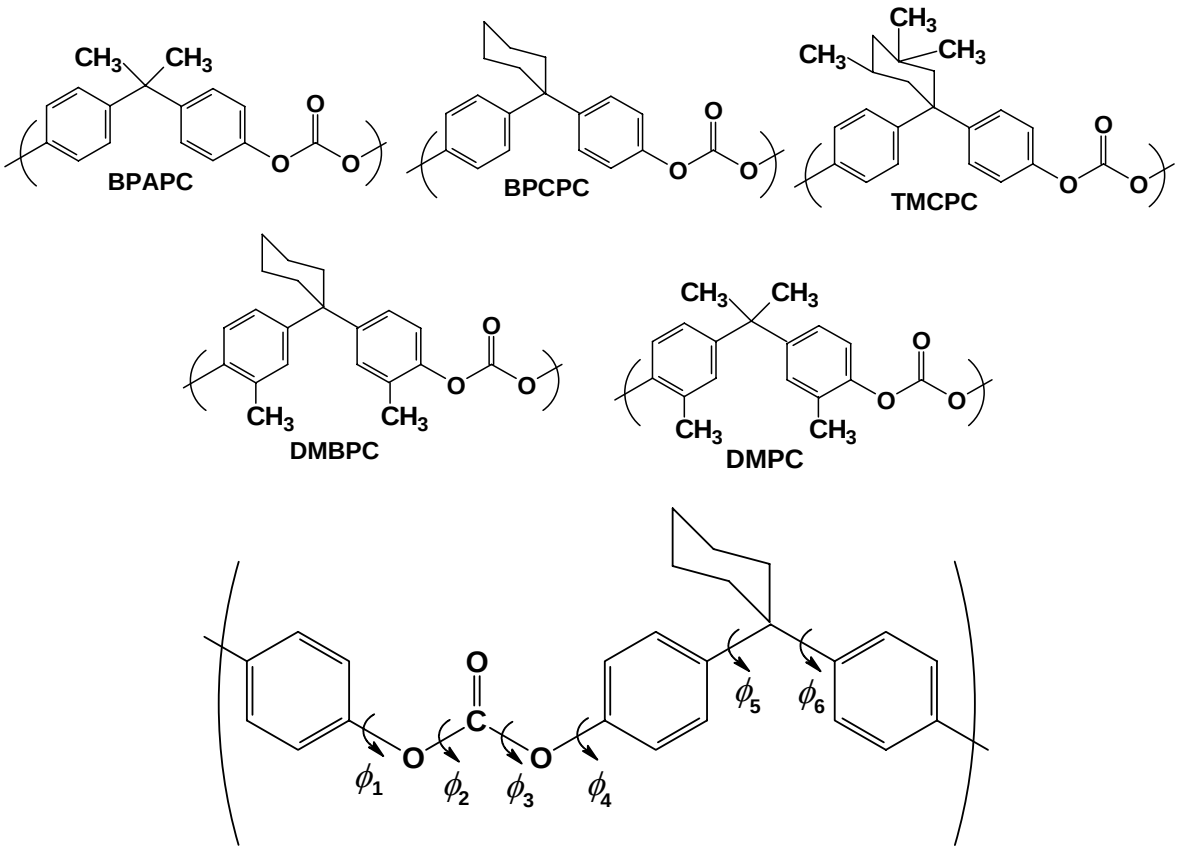

Figure 6.1. (a) Chemical structures of the repeat units of polycarbonates. (b) Schematic representation of the definition of torsion angles with respect to a BPCPC chain segment

6.2. Computational Details

6.2.1. Force-field

PCFF force-field[19-23] which is well parameterized for polycarbonate structures is used to describe the atom-atom interactions at the fully atomistic level. The force field uses a quadratic polynomial for bond stretching and angle bending and a three-term Fourier expansion for torsions. Lennard-Jones 9-6 potential is used for describing van der Waals (*vdw*) interactions and the electrostatics are described using pair-wise Coulombic terms. Out of plane interactions and cross terms up to third order were included in the simulations. The *vdw* and electrostatic parameters for the various relevant atom types in the studied polycarbonates as defined in the PCFF force-field are given in Tables 6.1 and 6.2. A dielectric constant of 3.17 that corresponds to the static value for BPAPC was used for all the polycarbonates in this study since the different substituents in the studied polymers here were simple aliphatic hydrocarbon groups whose concentrations in the chains are not expected to dramatically change the dielectric constant. Computations were carried out using Cerius^2 molecular modeling software[24] on Silicon Graphics Octane SE workstation.

Table 6.1. Definition of the atom types for relevant atoms in the polycarbonates studied

Atom type	Definition
c	Carbon attached to four other carbons
cp	Aromatic carbon in phenyl ring
c1	Carbon attached to one hydrogen and three heavy atoms (substituted cyclohexyl ring carbon)
c2	Aliphatic carbon attached to two hydrogens (cyclohexyl ring carbon)
c3	Methyl carbon attached to three hydrogens
cz	Carbonyl carbon of the carbonate group
oo	Carbonyl oxygen of the carbonate group
oz	Backbone oxygen of the carbonate group
hc	Hydrogen

Table 6.2. Non-bonded interatomic potential energy parameters for various atom types in polycarbonates as defined in the PCFF force-field

Atom type	r	ε	Charge[a]
c	4.01	0.054	0.000
cp	4.01	0.064	-0.127 (cp) 0.170 (oz) 0.000 (c,c3)
c1	4.01	0.054	-0.053
c2	4.01	0.054	-0.106
c3	4.01	0.054	-0.159
cz	3.900	0.064	0.700
oo	3.200	0.257	-0.500
oz	3.320	0.240	-0.270 (cp) -0.550 (cz)
hc	1.098	0.013	0.053 (c2,c3) 0.127 (cp)

[a] The atom bonded to the particular atom type is in parenthesis

6.2.2. Generation of chains and amorphous samples

Initially isolated polycarbonate chains were generated by assigning random values to the backbone torsions and these chains were relaxed using steepest descent and conjugate gradient methods based potential energy minimization and short canonical molecular dynamics (NVT) runs at 300 K. From the sample set of energy minimized single chains, one chain corresponding to the lowest energy was used for the construction of the amorphous bulk structures. Details of the number of repeat units in the chains, amorphous periodic box (cell) parameters, cell volumes and specified experimental densities for the five polycarbonates are given in Table 6.3. The number of repeat units in each polycarbonate chain was chosen such that the edge length of the periodic bulk cells is around 32 Å for specified mass density. The procedure of Theodorou and Suter[1,24] was used for the construction of the amorphous bulk structures. More than 100 initial guess structures were generated for each polycarbonate by packing a single polymer chain into a cubic box having periodic boundary conditions and a box edge length of about 32 Å. The density of the amorphous cells during structure generation was set at the respective experimental bulk

amorphous densities of these polycarbonates.[25,26] During the generation of the amorphous structures the use of different *vdw* scale factors were attempted. This is a scale factor for atomic *vdw* radius and is used to determine the allowable center-of-mass approach distance factor between two atoms during the building procedure. It was found that for BPAPC, three scale factors viz., 0.3, 0.4 and 0.5 resulted in successful generation of amorphous cells during the Markov process of generation, but the initial energies of the structures generated using a scale factor of 0.3 were significantly higher than those generated using 0.4 and 0.5. For DMPC and DMBPC, the amorphous cells were constructed with a *vdw* scale factor of 0.3 and 0.4, while a scale factor of 0.5 failed to generate even a single amorphous cell in several attempts due to packing inefficiencies.

Table 6.3. Simulation parameters for bulk periodic cells of polycarbonates

PC	No. of repeat units	Mol. weight (g/mol)	Density (g/cm^3)	Cell volume ($Å^3$)	Cell edge length (Å)
BPAPC	94	23904.78	1.200	33079.812	32.10
BPCPC	81	23844.31	1.200	32996.117	32.07
TMCPC	74	23888.53	1.107	35834.443	32.96
DMBPC	74	23859.83	1.184	33463.757	32.22
DMPC	84	23718.44	1.167	33750.049	32.31

The potential energies of the initial guess structures were minimized using steepest descent and conjugate gradient methods. From 100 initial structures corresponding to each of the five polycarbonates, 20 structures were chosen for each chemically different polycarbonate with regard to their minimum potential energy and the chain dimensions, which were within the range as obtained from their respective RIS models (section 3.3 in Chapter 3). The potential energies of the 20 structures corresponding to each polycarbonate were further minimized and subjected to a short molecular dynamics run of 5 ps at 300 K. The structures corresponding to the final snapshot of the MD trajectory were further subjected to energy minimization using conjugate gradient method till the gradient of energy with respect to atom coordinate variations was less than 0.1 kcal/mol Å. Finally, a set of 10 independently generated amorphous structures out of the 20 short-listed samples were chosen corresponding to each of BPAPC, TMCPC, DMPC and DMBPC, and 9 amorphous

structures in the case of BPCPC, for performing further equilibration and sampling using molecular dynamics simulations in the NVT ensemble.

6.2.3. Relaxation and structural sampling

Three-dimensional periodic boundary conditions were used to simulate the amorphous structures. All molecular dynamics simulations employed constant NVT conditions. The MD simulations were performed at a temperature of 300 K using Nose thermostat.[27] Verlet velocity algorithm[28] was used for integration of the equations of motion with a time step of 0.001 ps. Non-bonded interactions defined by the *vdw* and coulombic terms were truncated at 15.5 Å using a fifth order spline switching function from 12.5 to 15.5 Å. All atoms in the polycarbonate chain were treated explicitly during the simulations and all degrees of freedom involving atoms were allowed to vary without any constraints. Initially MD simulations of 100 ps were performed on each bulk sample. It was found that for TMCPC and DMBPC, the structures were not properly equilibrated and required further MD runs to relax them fully. In the case of BPAPC and BPCPC, after 110-160 ps of MD simulations, the structures were well equilibrated. Equilibration was achieved for TMCPC, DMBPC and DMPC after 120-200 ps depending on the structure. This was followed by 40 ps sampling runs on all of the equilibrated amorphous cells at 300 K. The trajectories were recorded every 0.5 ps for further analysis. The final snapshot of the sampling run was energy minimized and used for calculating the mean potential energies, cohesive energy densities, chain dimensions and torsion distributions. Radial distribution functions and scattering curves over the sample set were obtained from the 40 ps trajectories corresponding to the sampling runs. The potential energies, chain dimensions and cohesive energies of all the minimized structures after the sampling simulations used for the analysis presented here are given in Appendix-IV. The relaxed structures of the structurally modified polycarbonates subsequent to sampling runs are given in Figure 6.2.

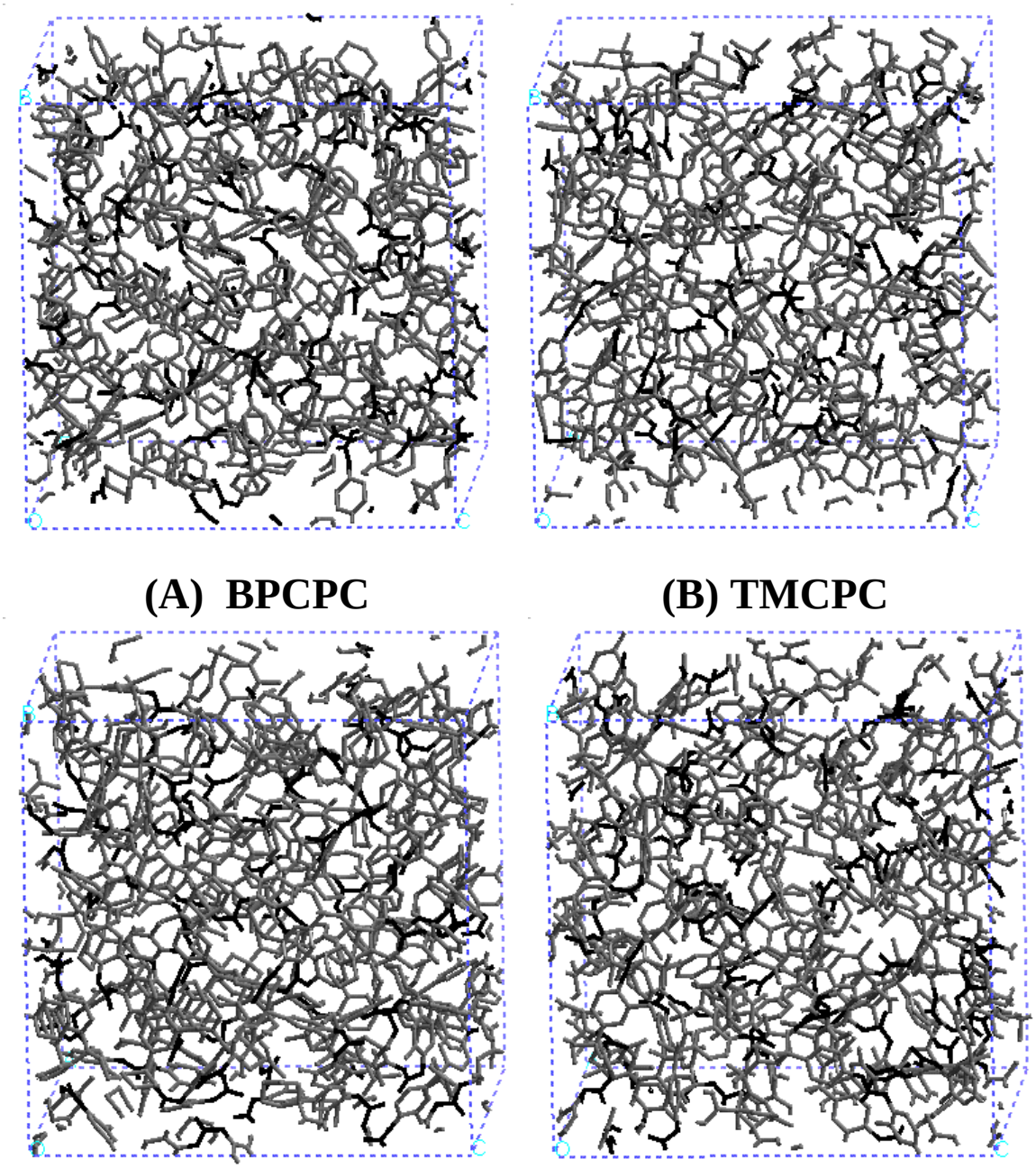

Figure 6.2. Amorphous bulk structures of polycarbonates obtained from the simulations. Hydrogens are not shown for clarity. Phenyl rings and the substituent groups like cyclohexyl and methyl (grey) and carbonate groups (black) are shown

6.3. Results and Discussion

6.3.1. Energetics

The final snapshot of the sampling trajectories were energy optimized and the averaged energies were calculated for the ensemble of structures for each of the five polycarbonates. The component contribution to mean potential energy of minimized structures subsequent to the sampling stage is given along with the standard deviation in Table 6.4. The potential and total (potential and kinetic) energies of the samples as a function of the simulation time are shown in Figure 6.3. In all five polycarbonates the non-bonded energy differences stabilize the bulk phase. The *vdw* interaction energy per atom is higher for TMCPC and DMBPC due to increased steric interactions due to multiple substitutions**.** The difference in the *vdw* and coulomb energy between the single chain and the bulk structure of the polycarbonates are given in Table 6.5. The difference between the bulk and single chain *vdw* energies is lowest for TMCPC followed by DMBPC, due to highest level of repulsive unfavourable energies in these two polycarbonates. For the coulomb energy difference as well, TMCPC and DMBPC show relatively lesser amount of favourable electrostatic cohesion because of the larger level of electrostatic attraction energy in BPAPC, DMPC and BPCPC. Among the five polycarbonates in this study, the increased steric interactions are found to be in TMCPC. From Table 6.5, it can be seen that ΔE_{vdw} and $\Delta E_{coulomb}$ are more positive for substituted polycarbonates compared to BPAPC. Repulsive interaction is greatest especially in TMCPC and DMBPC.

Table 6.4. Contributions to mean potential energies (kcal/mol) of amorphous structures of polycarbonates from simulations

PC	Bonds	Angles	Torsions	Inversion	Cross terms	vdw	Coulomb
BPAPC	449.6±1.6	755.2±11.2	-2686.9±21.1	16.3±0.7	-728.8±5.7	-416.9±12.9	-1206.2±8.6
BPCPC	460.9±2.3	797.1±21.7	-2913.7±24.9	16.7±1.7	-679.1±7.4	-348.7±14.3	-936.9±9.1
TMCPC	452.2±1.8	878.3±17.3	-3093.8±21.2	16.0±1.0	-620.5±6.5	-60.5±13.8	-1204.5±11
DMBPC	485.9±2.0	720.4±19.7	-2900.8±16.9	17.4±1.0	-796.0±4.0	-253.3±14.5	-609.9±10
DMPC	473.7±2.2	653.1±17.6	-2703.5±18.2	16.4±1.4	-847.7±6.4	-295.2±17.0	-798.1±7.7

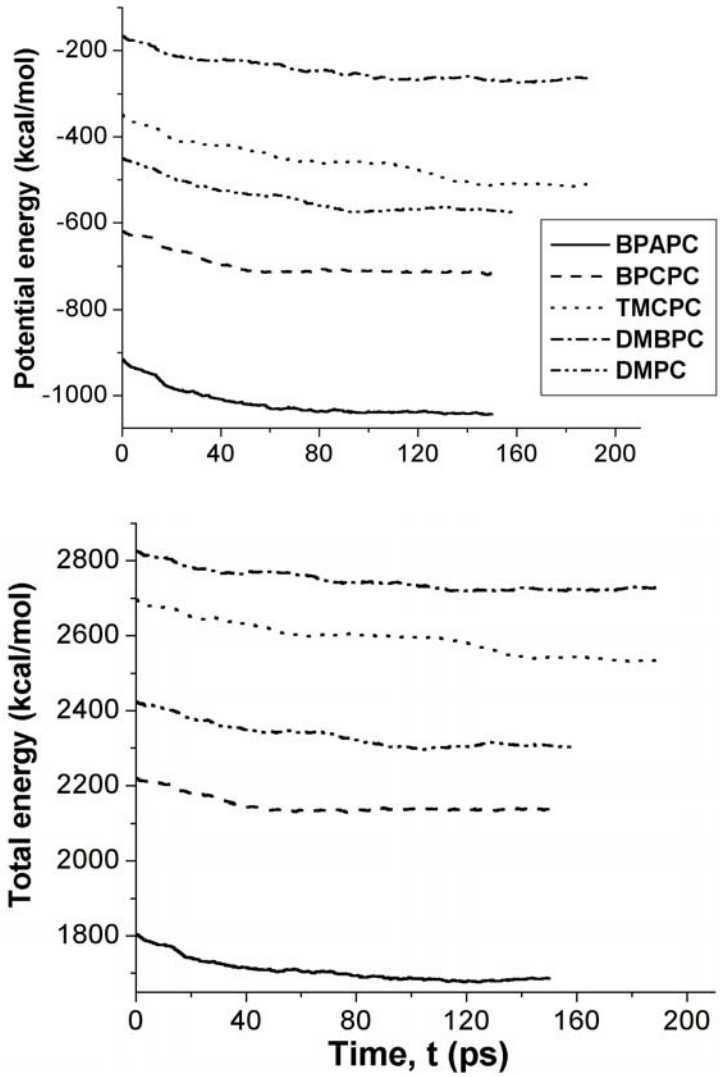

Figure 6.3. Evolution of potential energy and total energy of the bulk amorphous polycarbonates during the molecular dynamics simulations

Table 6.5. Difference in potential energies (kcal/mol) of amorphous bulk and single chain of polycarbonates from simulations

PC	ΔE_{vdw}	$\Delta E_{coulomb}$	Total Potential Energy	
	(E_{bulk} - E_{chain})	(E_{bulk}- E_{chain})	Bulk	Parent chain
BPAPC	-1827.82	-149.15	-3817.62±17.1	-1840.65±37.6
BPCPC	-1715.05	-119.63	-3603.68±32.7	-1768.98±49.6
TMCPC	-1534.85	-95.30	-3632.97±25.4	-2002.84±60.6
DMBPC	-1619.65	-82.83	-3336.33±32.6	-1636.86±47.1
DMPC	-1705.92	-99.33	-3501.33±23.1	-1692.46±39.7

6.3.2. Chain conformations in the bulk

Mean squared end-to-end distance, $\langle r^2 \rangle / M$ of relaxed structures of the polycarbonates is given in Table 6.6. The initial guess structures were chosen so that they are in the range as derived from RIS calculations of these polycarbonates (results presented in Chapter 3). These were the structures that also had relatively lower potential energies. It is found that the chain dimensions of these structures did not change much during further stages of minimization and molecular dynamics simulations similar to what has been reported earlier.[1,5] The averaged dimensions of substituted polycarbonates are lower than that of BPAPC.

6.3.3. Cohesive energy density and solubility parameter

Cohesive energy density (CED) gives a quantitative account of the intermolecular interactions in these amorphous polycarbonates. CED and solubility parameter (δ) averaged over the ensemble of microstructures for each polycarbonate are given in Table 6.6. The experimental values reported for the solubility parameter of BPAPC are 9.92 and 9.82 $(cal/cm^3)^{1/2}$.[29-31] The averaged value 9.96 $(cal/cm^3)^{1/2}$ for amorphous BPAPC obtained from our simulations is in excellent agreement with the reported experimental values. For other polycarbonates studied here, no estimate of the solubility parameters from experiments are available for direct comparison with the simulation results.

Table 6.6. Chain statistics and solubility parameters of amorphous bulk polycarbonates obtained from atomistic simulations

PC	$<r^2>/M$ ($Å^2 mol.g^{-1}$)	Cohesive energy density (CED) (cal/cm^3)			Solubility parameter $(cal/cm^3)^{1/2}$
		vdw	coulomb	Total	
BPAPC	1.06±0.22 (1.12)	91.74	7.48	99.23±2.1	9.96±0.11
BPCPC	0.95±0.12 (0.96)	86.30	6.02	92.33±2.8	9.60±0.14
TMCPC	0.79±0.12 (0.84)	71.11	4.41	75.54±2.3	8.69±0.13
DMBPC	0.85±0.21 (0.80)	80.36	4.11	84.48±3.3	9.19±0.18
DMPC	0.94±0.17 (0.86)	83.92	4.88	88.98±2.0	9.43±0.11

The values in brackets given for $<r^2>/M$ correspond to the limiting values of polycarbonates as obtained from RIS models (Chapter 3)**,** T=300K

The substituted bisphenol polycarbonates show lower CED and δ values when compared to BPAPC. Lower values of CED exemplify reduced intermolecular forces in the bulk state and lower levels of energy stabilization of these polycarbonates. *vdw* dispersive non-bonded interactions are found to play a dominant role in determining the CED of these polycarbonates in their bulk state. The relative order of difference in the *vdw* energy between the single chain and the bulk, among these polycarbonates, follow the same pattern as the CED and δ. A cyclohexylidene group at the C_α carbon (BPCPC) lowers the CED of a polycarbonate to a greater extent than what methyl groups present on the backbone phenyl rings (DMPC) would effect. Our simulations yield lowest values of CED and solubility parameter for TMCPC. Additional methyl groups on the substituent cyclohexylidene group on this polycarbonate is responsible for significant repulsive *vdw* interactions and relatively lower levels of attractive packing energies in the bulk amorphous state thus leading to lower intermolecular interaction energies. δ value estimated for TMPC (tetramethyl bisphenol polycarbonate) from experimental measurements[31] is 9.2 $(cal/cm^3)^{1/2}$ which is lower than BPAPC. The lower values of solubility parameters obtained for the polycarbonates studied in this work are therefore consistent with those for polycarbonate with methyl substitution. δ values higher than that for BPAPC have been reported for chloral polycarbonate (10.1)[31] TBPC (10.2)[32] and dicyano bisphenol carbonate (10.9).[31] Experimental results on the δ values suggest that the CED is enhanced in the bulk due to the presence of polar substituents (like chlorine, bromine and cyano), where as aliphatic groups (for eg. methyl) lower the CED. Hence the lower values of CED and δ values for substituted polycarbonates (that are devoid of any polar substituents and where the substituents are purely aliphatic in nature) when compared to BPAPC are in accordance with the experimental observations.

6.3.4. Torsion distributions

The definition of the various torsions as depicted with respect to a BPCPC chain segment in Figure 6.1 conforms to the earlier definition for RIS models of these polycarbonates (Chapter 3). The torsion distributions averaged over the ensemble of optimized structures of the amorphous polycarbonates are given in Figures 6.4 and 6.5. For the simulated polycarbonates in the bulk, the probability for *trans* conformations of the carbonate group is found to be

higher when compared to the *cis* conformations. NMR experiments of bulk amorphous BPAPC suggest that less than 10% of all carbonate groups are in the *cis* conformation so that *trans-trans* conformation is predominant compared to the *cis-trans* conformation.[33,34] Results in literature from IR and Raman scattering studies[35] on amorphous BPAPC indicate a high preference for the *cis-trans* conformation at room temperature. This data imply relatively higher *cis-trans* content in amorphous BPAPC than what is observed from NMR experiments. Earlier atomistic models[5] of amorphous BPAPC also showed a higher *cis*, *trans* content in the bulk than derived from NMR experimental data. Torsions of the phenyl rings with respect to the carbonate group in BPAPC (ϕ_1 and ϕ_4) are distributed in the entire conformational range with peak maxima at their respective RIS states. 2D-separation field NMR experiments also suggest a disordered distribution for this dihedral with population maxima at 55°.[33] The torsions representing highly interdependent conformations about the isopropylidene group ϕ_5 (ϕ_6) are restricted within the range 50°-150° with maximum probability at 54°. The discrete rotational states derived from the conformational energy calculations on small segments of BPAPC are 50° for ϕ_1 (ϕ_4), 0° for ϕ_2 (ϕ_3) and 50° for ϕ_5 (ϕ_6) and the torsional distribution for the amorphous samples have peak maxima at these values although scattered.

For BPCPC and TMCPC polycarbonates containing the substituting cyclohexylidene group, torsions ϕ_5 (axial) and ϕ_6 (equatorial) are not equivalent and hence their distributions are plotted separately in Figure 6.4. Torsions ϕ_1 and ϕ_4 for BPCPC and TMCPC show the same distribution as that for BPAPC for the entire range of conformational map with peak maxima probabilities at the respective rotational isomeric states of their unperturbed single chain conformational statistics. This illustrates that the cyclohexylidene group as positioned in the polycarbonate does not influence the conformational properties of the carbonate group in the bulk amorphous structures of these polycarbonates and is similar and in agreement with the unperturbed single chain results (Chapter 3). Restricted rotations about these phenyl-oxy bonds is brought about solely due to substituents in the *ortho* position of the backbone phenylene rings as seen in the case of DMPC and DMBPC where maximum probability occurs at around 100° as shown in Figure 6.5.

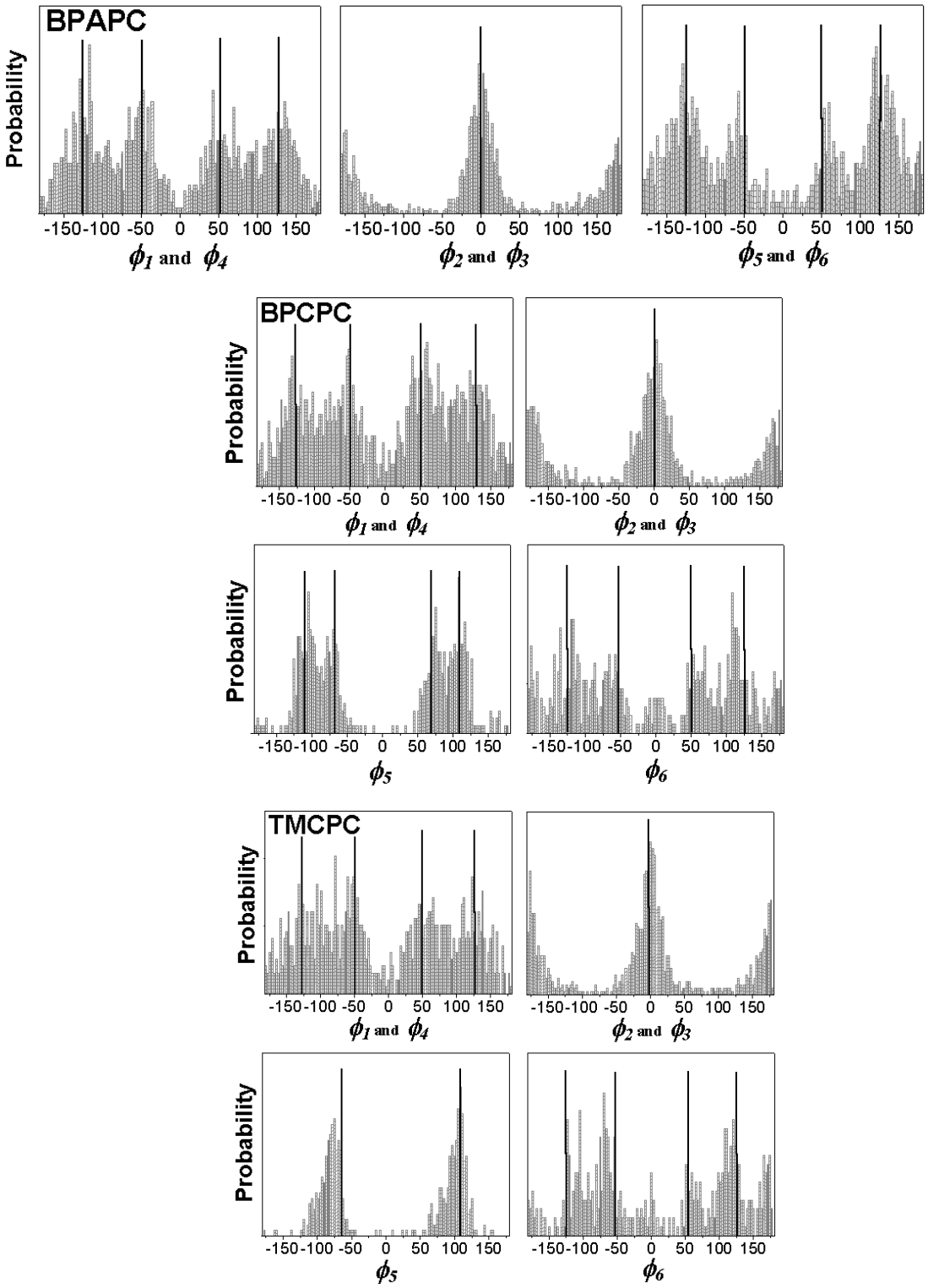

Figure 6.4. Averaged torsional distributions in polycarbonate bulk amorphous structures corresponding to BPAPC, BPCPC and TMCPC from atomistic simulations. The thick dark lines indicate the minimum energy rotational states for the dihedrals obtained from conformational analysis of bisphenyl and carbonate fragments which represent the single chain statistics of these polycarbonates (data given in Chapter 3)

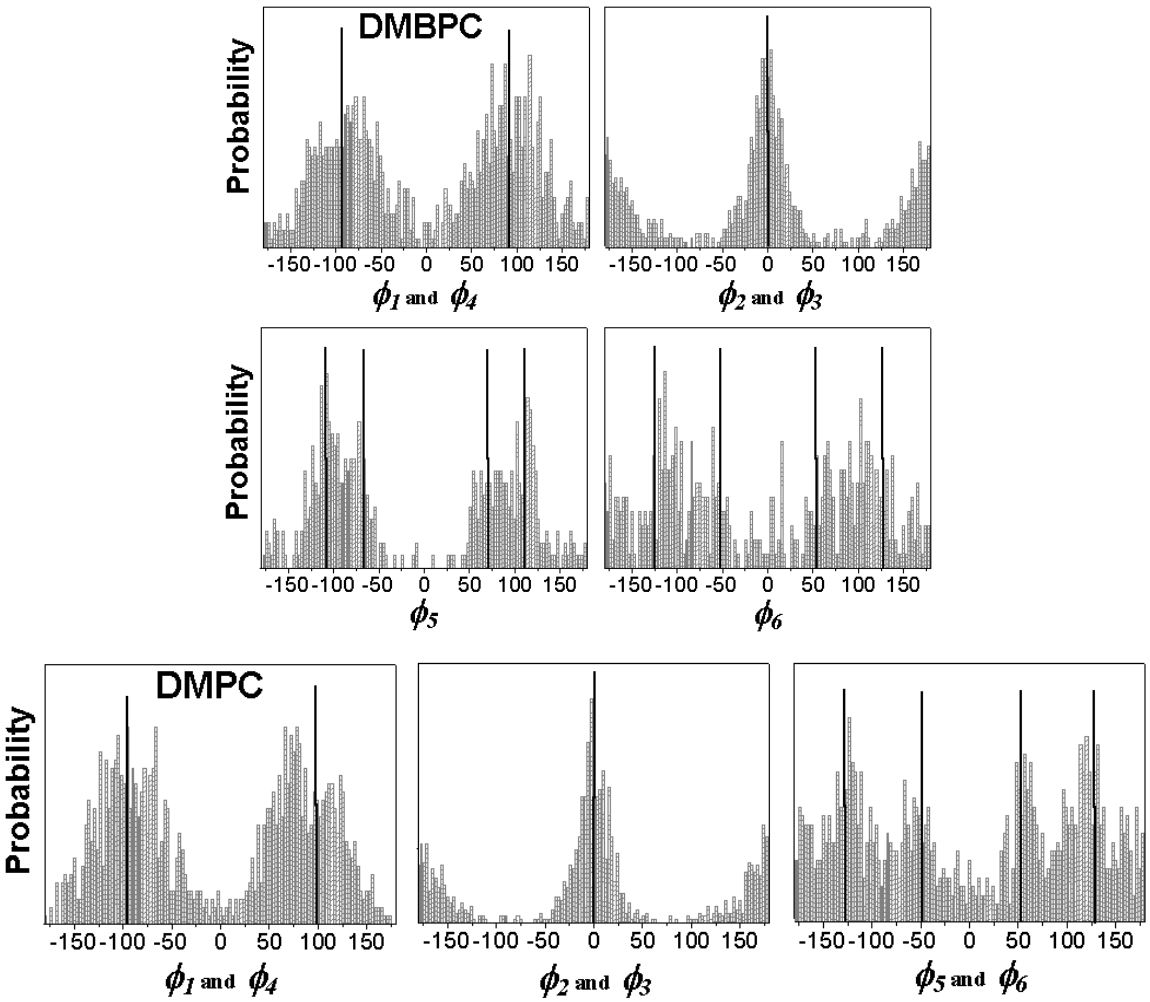

Figure 6.5. Averaged torsional distributions in polycarbonate bulk amorphous structures corresponding to DMBPC and DMPC from atomistic simulations. The thick dark lines indicate the minimum energy rotational states for the dihedrals obtained from conformational analysis of bisphenyl and carbonate fragments which represent the single chain statistics of these polycarbonates (data given in from Chapter 3)

The equatorial and axial backbone phenylene rings in cyclohexylidene substituted polycarbonates show distinctly different conformational probability distributions in the bulk state. Distributions of the axial phenylene rings are restricted to the range 70°-125° in BPCPC and in DMBPC, whereas the equatorial phenylene rings exhibit a broad distribution in the entire possible range from –180° to 180°, with maximum probability in the range 50°-150°. For TMCPC, the torsion distribution for the axial phenyl ring is much narrower because of 1,4-diaxial interactions due to the methyl groups on the cyclohexyl ring in comparison to BPCPC and DMBPC. These results are consistent with conformational energy

calculations on bisphenyl fragments of these polycarbonates and the conformational features which indicate greater hindrance for the axial phenyl rings in comparison to the equatorial rings in the bulk portray the influence provided by intrachain effects rather than interchain packing effects. The probability of the torsions ϕ_1 (ϕ_4) for DMPC is centered around 100° due to steric overlap from the methyl groups on backbone phenyl rings and for the ϕ_5 (ϕ_6) torsions the distribution follows the same pattern as BPAPC.

As seen from the distribution plots, relatively dense population of the dihedrals near the corresponding rotational states in each of these polycarbonate structures occur although accompanied by a large fluctuation. A large number of conformations, which although would be energetically unfavourable for the unperturbed chain in the absence of interchain effects are observed to exist in the bulk structure. Although a large scatter is found in the distributions, the maximum probabilities for the various torsions are clustered around their respective intramolecular RIS states. As seen from these results, intramolecular interactions determine the position of the minimum energy states and the deviation from this value is dictated by the intermolecular chain packing interactions in the bulk

6.3.5. Radial distribution functions

The radial distribution function, g(r), for a pair of atoms with a separation of r, are shown in Figure 6.6 and Figure 6.7 of various atom pairs of the polycarbonates, as obtained from the final set of samples. The distributions for those atom pairs that present relevant information with respect to the local structure in the bulk are discussed here. Some of the features of the RDF's of a few atom pairs are common to all five polycarbonates: (i) Weak intermolecular correlations are observed between the C_α carbons in the range 6-6.5 Å; (ii) Similar intermolecular correlations are observed between carbonyl carbons (cz-cz) within a distance range 4-4.5 Å; (iii) Weaker correlations are also observed between the carbonyl oxygens (oo-oo) at ~ 3–3.5 Å; (iv) Relatively longer ranged interactions between the carbonyl carbons and also between the carbonyl oxygens, in the range of 10-11 Å are also seen; (v) For dissimilar carbon atom pairs and between carbon and oxygen, stronger local order is clearly seen; (vi) Prominent peaks having relatively higher intensities are observed in the range 6-7 Å between the pair of atoms carbonyl carbon-C_α carbon along with a shoulder around 5.5 Å, and similar

features are observed for the carbonate oxygen-C_α carbon atom pairs, where a prominent peak at 5.8 Å is seen. A peak of lower intensity at 7.9 Å in this pair arises solely due to intermolecular interactions. These observations suggest that some weak intermolecular ordering is observed in the polycarbonate bulk amorphous structures studied here, although beyond a separation distance of 12 Å the bulk structures appear completely random for all atom pairs. RDF's calculated between all hydrogens and the atoms in the carbonate group also show some correlations upto distances ~ 9 Å. Atoms constituting the carbonate group (cz, oo, oz) show longer range correlations in BPAPC as well as other polycarbonates than those shown by other atoms such as of the phenylene rings in the repeat units.

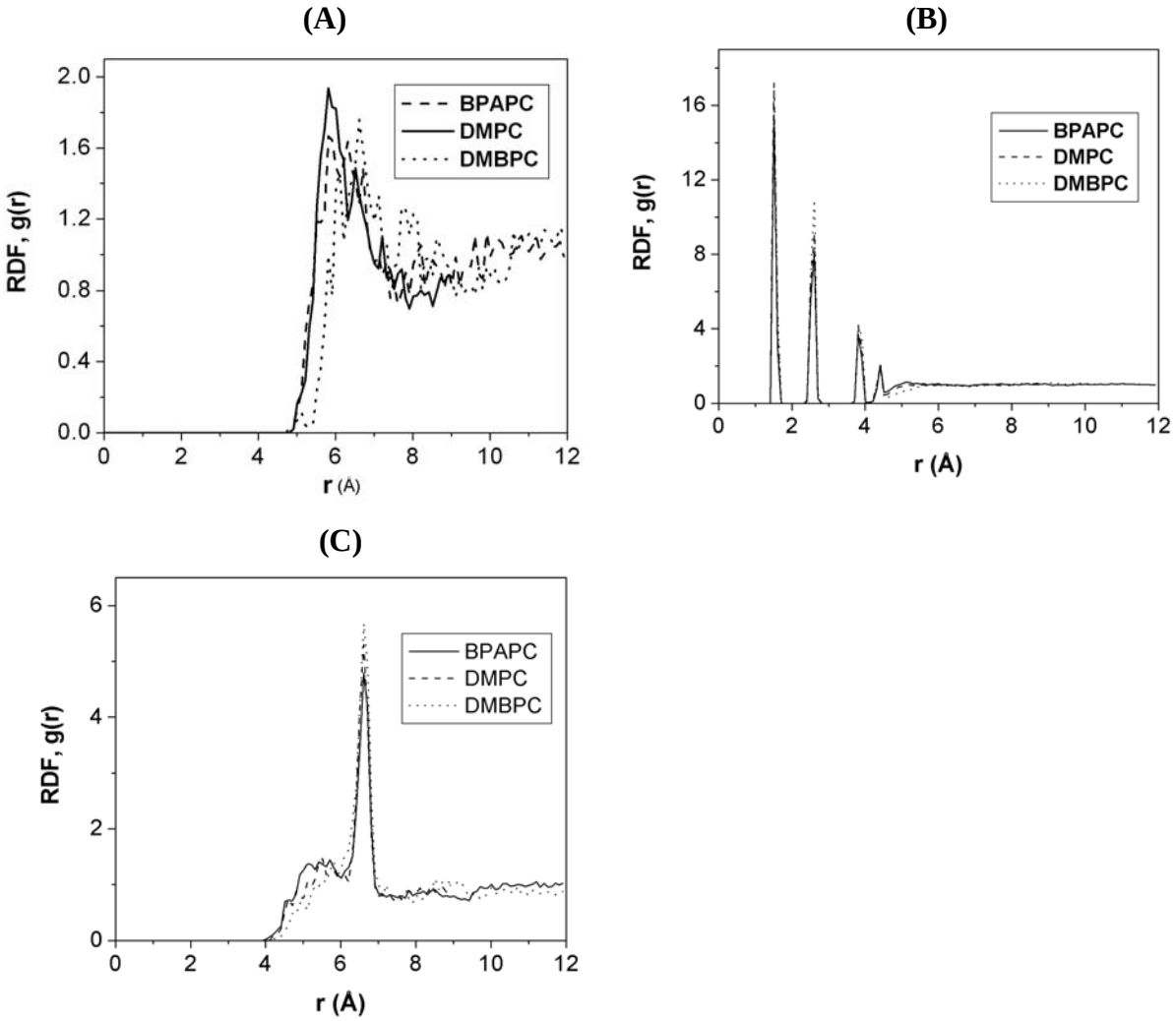

Figure 6.6. Comparison of total radial distribution functions of the atom pairs (**A**) **c-c**; (**B**) **cp-c**; (**C**) **cz-c** in bulk structures of polycarbonates, BPAPC, DMPC and DMBPC. The definition of various atom types used in calculating the RDF's are given in Table 6.1

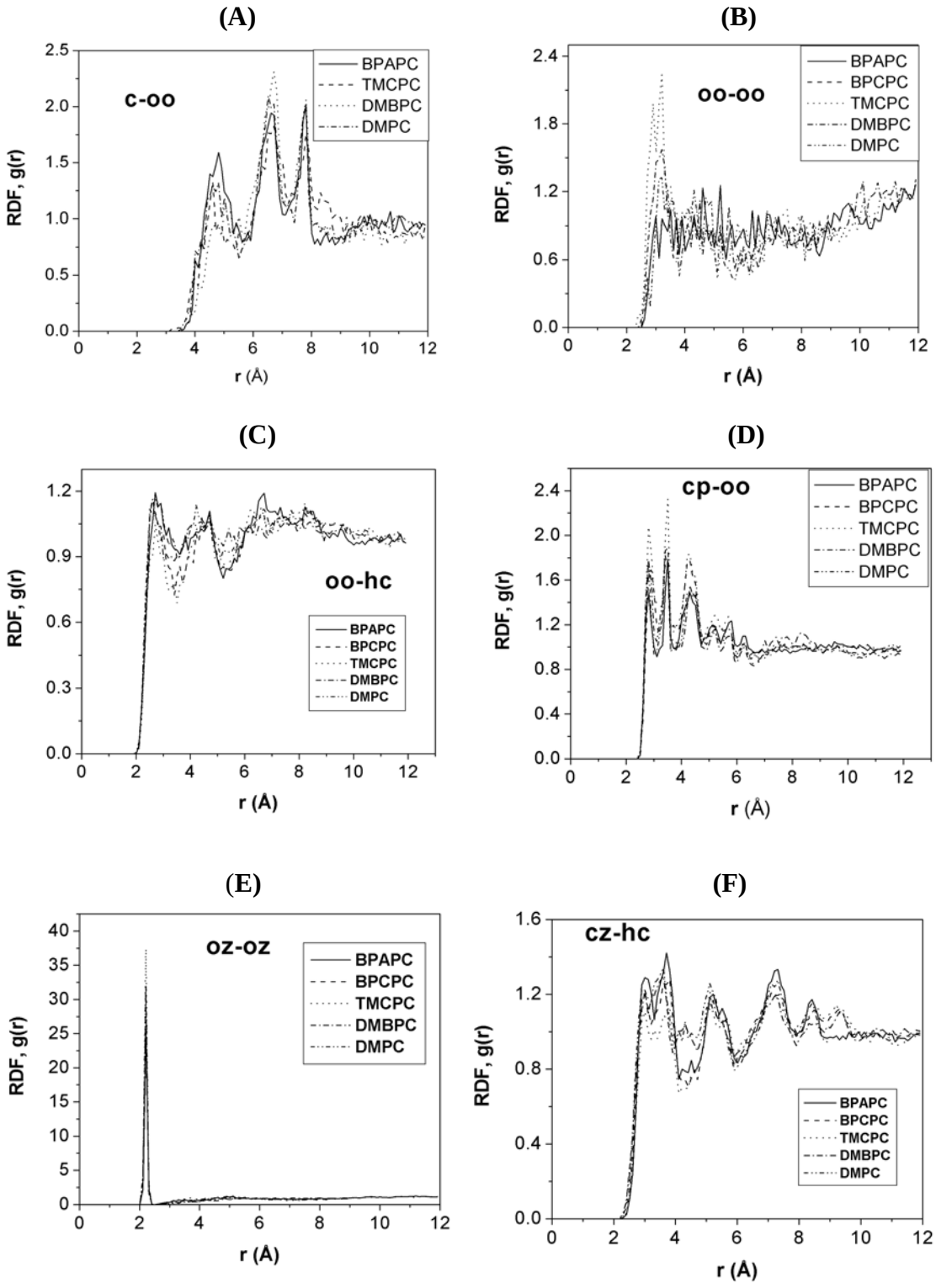

Figure 6.7. Comparison of total radial distribution functions of the atom pairs (**A**) c-oo; (**B**) oo-oo; (**C**) oo-hc; (**D**) cp-oo; (**E**) oz-oz; (**F**) cz-hc in bulk structures of the five polycarbonates studied here. The definition of various atom types is given in Table 6.1

For cyclohexylidene substituted polycarbonates, no long-range correlations between the cyclohexyl groups (c2-c2) are observed in the bulk. Nearest neighbour cyclohexyl-cyclohexyl ring correlations are not found to exist. In order to have intermolecular correlations between cyclohexyl rings, the bisphenyl fragments need to arrange in some manner which seems energetically infeasible. For BPCPC and DMBPC, in addition to the peak observed at 6-6.5 Å there exist some weak interactions between the C_α carbons in the range 11 Å. Correlations (separation ~ 4.8 Å) between the side group cyclohexyl ring methyl carbons and the phenyl ring carbons in TMCPC are due to short-range interactions. In DMPC and DMBPC, the carbonyl oxygen-methyl carbon atom pair shows correlation peaks at 3.4, 4.6 and 7.3 Å. All these information suggest that in polycarbonate bulk amorphous structures, there are no strong correlation peaks that are longer (>10 Å) ranged in nature.

Schaefer and co-workers have used rotational-echo double resonance (REDOR) to determine the local packing in glassy deuterated BPAPC and have reported various intermolecular distances.[36-40] Very short distances, for e.g. phenylene ring carbon to phenylene ring deuterium distance of 2.6 Å, ring carbon to methyl deuterium distance of 3.2 Å,[38] average intermolecular distance of 3.8 Å between carbonyl carbon and nearest neighbour methyl deuterons,[37] were obtained from these experiments. Using DRAMA and CEDRA dephasing spins in the ^{13}C-^{13}C dipolar coupling NMR experiments in BPAPC it has been found that 90% of the quaternary-carbonyl intermolecular distances are within ±20% of an average 5.6 Å.[40] The data suggest that local orientational order may not be fully random in the glassy state of BPAPC. Parallel alignment of short sequences of chains has been postulated to be existing in bulk amorphous BPAPC based on evidence from NMR, DSC and DMS experiments of samples prepared with varying thermal history.[39] The RDF data for BPAPC in the present work indicates that there exist a correlation between the carbonyl carbons in the bulk as seen from a peak at about 4.5 Å followed by a shoulder peak at 5.6-5.8 Å in qualitative agreement with the NMR measurements in the literature. The average distance between the neighbouring carbonyl carbons along the chain backbone (intramolecular distance) is approximately 10-11 Å. This data indicates that in the simulated bulk BPAPC in the present work, the intermolecular distance between the carbonyl carbons

is roughly in the same range (±20% of 5.6 Å) as has been reported from NMR experiments.[40] The RDF for the carbonyl carbon (cz) and methyl carbon (c3) in BPAPC shows two peaks, one at 3.9 Å of lower intensity and at 7.4 Å which is of a higher intensity. The intramolecular distance for this pair in BPAPC is in the range 6.5-7.5 Å. Hence the higher intensity peak seen in the RDF is due to this intramolecular correlation and the peak at 3.9 Å arises exclusively due to the intermolecular correlation and is in agreement with the intermolecular distance of 3.8 Å reported for carbonyl carbon to methyl deuterons from NMR experiments.[37]

6.3.6. Neutron scattering functions

The static structure factors of the different polycarbonates from the simulations are given in Figure 6.8. These are related by a Fourier transform of the radial distribution functions and is given by

$$S(k) = \sum_{ij} \frac{\langle b_i \rangle \langle b_j \rangle (Sinkr_{ij})}{kr_{ij}} \qquad (1)$$

where *b* corresponds to the scattering lengths of atoms, *k* is the magnitude of the scattering vector and indices *i* and *j* run over all atoms in the chain. The observed experimental maxima for BPAPC appear at *k* values of 1.3, 3.1 and 5.3 $Å^{-1}$ and shoulders near 0.7 and 1.8 $Å^{-1}$. Structure factor calculated from radial distribution function excluding hydrogens are in better agreement with the experimental peak positions than using the total radial distribution function, and has been noted previously by Fan et al[7] as well for BPAPC. Our results for BPAPC show peak positions at k values 1.23, 3.1 and 5.4 $Å^{-1}$ and is in agreement with the data from neutron scattering experiments.[41-43] Neutron scattering experiments using spin-polarized neutrons enables one to separate the coherent and incoherent scattering and the resultant structure factors from these experiments can be directly compared with results from molecular simulations. Experimental results on structure using these advanced scattering methods on BPAPC and substituted polycarbonates having cyclohexyl ring substituents at the C_α carbon (BPCPC and TMCPC) are available in the low *k* range ($k \leq 2.2$ $Å^{-1}$).[15,44,45] The peak positions obtained from scattering experiments are compared with the present simulation results as well as with the earlier atomistic simulation results in Table 6.7.

Table 6.7. Comparison of neutron scattering data from atomistic simulations and experimental values

PC	k (Å^{-1})		d (Å)	
	Present atomistic simulations[a]	Exptl[b]	Present atomistic simulations[a]	Exptl[b]
BPAPC	1.23	1.27 (1.21)[b]	5.10	4.93 (5.19)
BPCPC	1.22	1.26	5.15	4.98
TMCPC	1.09	1.23 (1.20)	5.76	5.12 (5.23)
DMBPC	1.17	-	5.37	-
DMPC	1.15	-	5.46	-

[a] as obtained from simulations in the present study
[b] The experimental values are from refs. 15 and 45
[c] The values given in brackets are those obtained from coarse-grained simulations of polymer melts as given in ref. 45

A brief discussion of the results of the scattering curves presented in previous reports for polycarbonates is provided here for clarity and comparison.[15,44,45] The amorphous halo observed for BPAPC at 1.27 Å^{-1} has been ascribed to correlation between neighboring chains and the shoulder peak at 0.5 Å^{-1} to intramolecular correlations along the chain. For BPCPC, the amorphous halo is in a similar position as in case of BPAPC, but is slightly lower (1.26 Å^{-1}) and comparatively broader. The calculated scattering curve reported for TMCPC from coarse-grained simulation of melts,[45] shows two small peaks in the region 1-1.5 Å^{-1} (one peak at 1.2 and the other at 1.1 Å^{-1}) wherein the peak at 0.5 Å^{-1} which is of a lower intensity has been ascribed to the cyclohexyl group. Distance between neighboring chains (d) is higher for TMPC (5.96 Å) and TMCPC (5.12 Å), due to the methyl groups in the former and methyl substituted cyclohexylidene rings in the latter.[15,45] The previous simulations were able to reproduce the general features of the peak positions from experimental scattering although the intensities and the width of the peaks were not in satisfactory agreement.

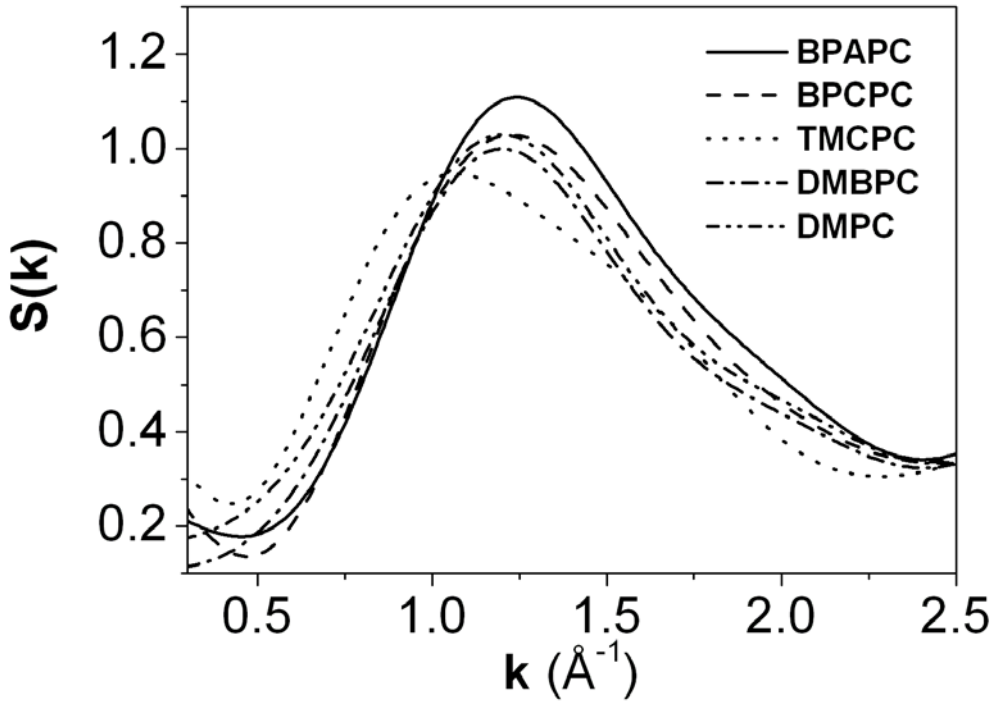

Figure 6.8. Neutron scattering structure factors of bulk polycarbonates obtained from atomistic simulations

The neutron scattering curves calculated for polycarbonates studied in the present work are given in Figure 6.8. These were calculated from the radial distribution functions by excluding the hydrogen atoms. The shoulder peak at *k* value in the range 0.4-0.6 $Å^{-1}$ of low intensity, experimentally observed for BPAPC, is absent in the calculated scattering curves. This peak is generally ascribed to intramolecular correlations along the chain. As can be seen from Table 6.7 there is fair agreement between calculated scattering data from our work here and those obtained from experiments and previous simulation studies in literature. The relative trend in the distance between the neighbouring chains among the different polycarbonates is found to be in agreement with the reported neutron scattering measurements carried out on some of the polycarbonates studied here, although the present simulations seem to overestimate the difference in the interchain distance between BPAPC and TMCPC. Only a slight increase in the interchain distance is observed due to a cyclohexyl substituent as in BPCPC. But additional methyl groups on the cyclohexyl ring as in TMCPC, leads to the largest distance between neighbouring chains among these polycarbonates from the present simulations. This is reasonable in view of the bulky and rigid

trimethylcyclohexylidene group that hinders the packing and prevents the chains from being in close proximity.

Methyl groups on the backbone phenyl rings as in DMPC tend to increase the interchain distance in the bulk as is seen from our results and this aspect has been experimentally observed previously in the case of TMPC.[15,45] Considering the effect of one kind of substitution, the methyl group on the phenyl rings (DMPC) in comparison to a cyclohexylidene group at the C_α carbon (BPCPC), it appears that the latter case does not result in appreciable changes in the interchain distances, which is not true with the former case. The *d* value for DMBPC, which has both these types of substitutions, is higher than that for BPCPC, but lower when compared to DMPC. Interchain distance for DMBPC is lower than that of TMCPC, which show that presence of methyl groups on the cyclohexyl rings result in a larger separation of the neighbouring chains in the bulk when compared to methyl groups on the phenylene ring. The *d* values obtained from our simulation studies seem reasonable when we compare these to the experimental bulk amorphous densities of these polycarbonates given in Table 6.3. BPAPC and BPCPC have similar densities and the interchain distances for these polymers are also fairly close. TMCPC has the lowest density among these polycarbonates and the larger distance between neighboring chains as observed from our simulations is in accordance with its lower density. DMBPC, which has a higher bulk density than DMPC, is expected to show a lower interchain distance and our simulations yield the same results thus providing consistency between simulations and experiment.

The approximate correlation lengths (ξ) of the polymer chains can be calculated from the width of the amorphous halos of the scattering curves. Experimental data suggest that the chains in bulk TMCPC are less densely packed than in BPAPC and are also less correlated with each other. In the case of BPCPC as well, chains seem to be less correlated than in BPAPC, although their interchain distances are similar. The correlation lengths calculated from previously reported experimental data are in better agreement with those available from coarse graining of melt configurations.[45] The correlation lengths calculated for BPCPC and TMPC from atomistic simulations reported earlier[15] were underestimated because the amorphous halos calculated were much broader than those derived from experiments. The

simulations also show very broad amorphous halos in the case of polycarbonates in this study and hence the calculation of correlation lengths is not provided. The discrepancy observed in the width of the amorphous halos could be due to the finite size of the amorphous cell used in simulations as reported earlier,[15] which is about 32 Å and the experimental correlation lengths for some of these polycarbonates are in the range 19-27 Å. Nonetheless, the atomistic simulations presented here are able to capture the distinct features of the scattering curves in these polycarbonates brought about by the various structural modifications and there is reasonable agreement between the peak positions observed experimentally and those obtained from the present simulations for BPAPC, BPCPC and TMCPC.

6.3.7. Intermolecular phenylene ring and carbonate plane orientations

To get further insight into the packing of chains in the bulk structures, orientational correlations of the nearest neighbour phenyl rings were determined using the same procedure as reported for the phenyl rings in polystyrene. Angles (β) between the nearest neighbour phenyl ring planes were calculated for different intervals of distances. The correlation of the phenyl groups in amorphous atactic polystyrene (a-PS) has been studied using radio-frequency driven ^{13}C NMR polarization transfer experiments and the results were compared with those from atomistic simulations.[46] There was favorable agreement in that both experiments and simulations yielded similar weighted distributions of the angle between the phenyl ring planes and local ordering between the phenyl rings were found at distances within 4-5 Å. Beyond 5 Å the distribution suggested random orientation of the phenyl rings in a-PS. In the case of BPAPC, distance factor spectra were determined for the phenyl and carbonate groups from ^{13}C polarization transfer NMR experiments by Robyr et al.[47] These distance factors were calculated by contributions from pairs of carbon whose distance is less than 7 Å. These neighboring carbons can belong either to different chains or to monomer units of the same chain which folds back on itself. The phenyl rings are found to have a preference for parallel orientations or for smaller angles between their longitudinal axes, while the relative orientations between their radical directions (or between their planes) is random. The carbonate groups were shown to have equal preference and probability for both parallel and perpendicular orientations from their distance factor spectra. In the same study,

atomistically simulated structures showed a preference for parallel alignment of phenyl ring planes which is in contrast to what was derived from NMR, but the carbonate groups showed both parallel and perpendicular alignment as was found experimentally. The disagreement between the simulated phenyl ring packing and the NMR results were attributed to the finite size of the simulation box.

In this section the orientation of the phenyl ring planes in the bulk is compared for BPAPC and the substituted polycarbonates. The plots showing the distributions corresponding to ($P(\beta)$) are shown in Figure 6.9. From the distribution plots, within a distance of 3.5-6 Å, for BPAPC, the probability for the neighboring phenyl ring planes to have parallel as well as perpendicular orientations is almost identical. When the intermolecular distances between the phenyl rings is greater than 6 Å (6-10 Å), the angular distribution clearly show a higher probability for perpendicular alignment of phenyl ring planes. The probability for phenyl ring planes to have smaller angles between their planes (parallel alignment) is higher in the case of neighbouring rings (3.5-6 Å) than when the distance between them is in the range 6-10 Å. In the case of substituted polycarbonates, the pattern is almost identical to that seen in the case of BPAPC. The neighbouring phenyl ring planes do not show any preference for any particular kind of orientation, although they exhibit a higher probability for parallel alignment of the planes than when they are separated by more than 6 Å. On the other hand, as the distance between them increases, perpendicular orientations are strongly preferred.

The intermolecular orientation of the nearest neighbour carbonate planes were also determined within a distance of 4-6 Å and 6-10 Å and is shown in Figure 6.10. In the case of BPAPC, the distributions suggest higher probabilities for near perpendicular orientations of carbonate planes. For substituted polycarbonates, carbonate planes have higher probabilities for perpendicular orientations for neighbouring groups as well as groups separated by more than 6 Å in a manner similar to BPAPC. The only difference being the probabilities for near perpendicular orientations of carbonate planes within 4-6 Å is greater for substituted polycarbonates than when compared to BPAPC. The distributions presented in this section were obtained from the minimized structures of the polycarbonate cells after MD and were averaged over two such structures in the case of each polycarbonate.

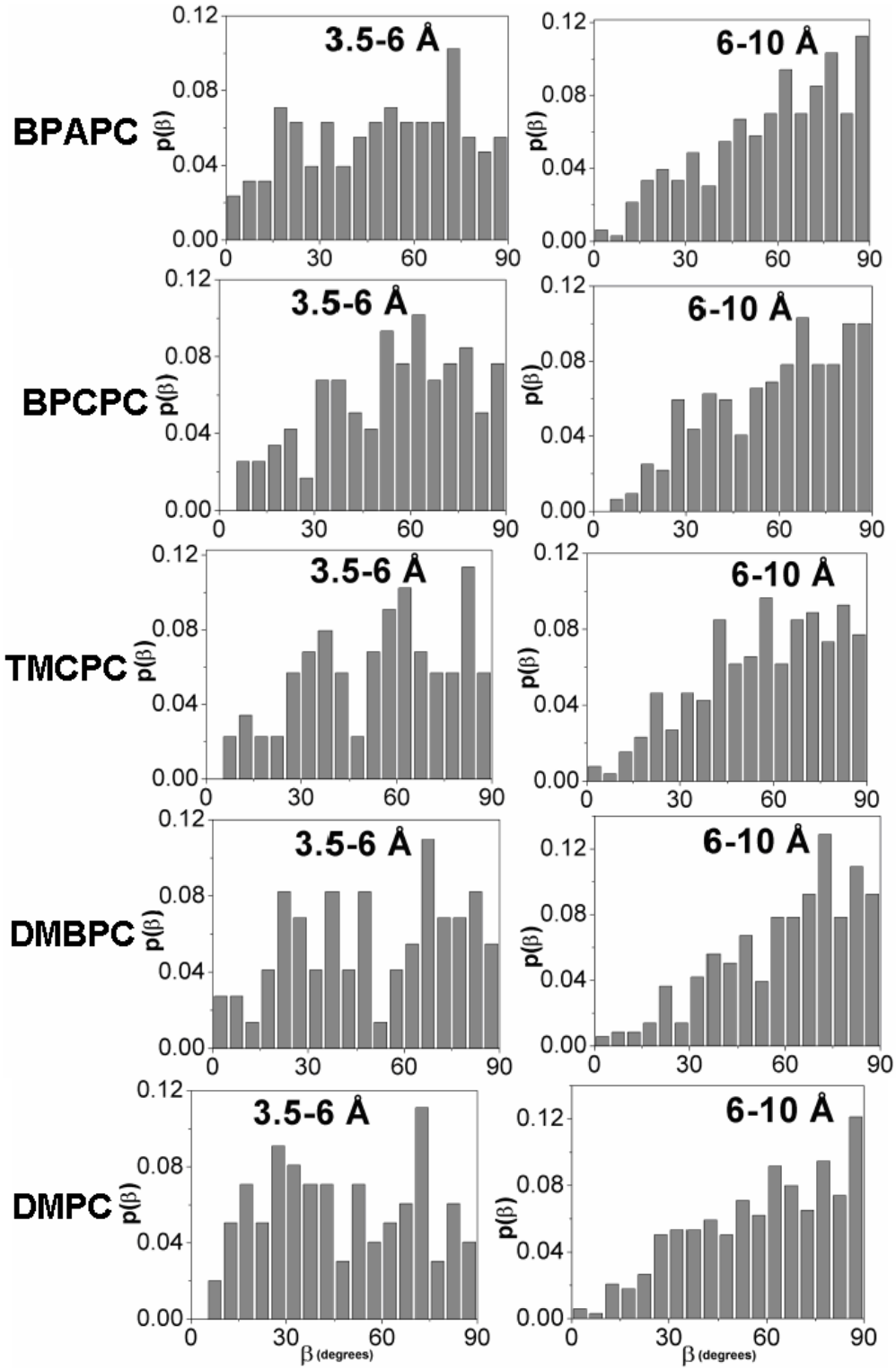

Figure 6.9. Orientational distributions of the probabilities of angles between the phenylene ring planes in bulk polycarbonates. The fractional contributions of ring pairs from which the distributions were plotted for the distance intervals 3.5-6 and 6-10 Å in the order for various polycarbonates are (a) BPAPC, 0.256, 0.664 (b) BPCPC, 0.251, 0.682 (c) TMCPC, 0.185, 0.546 (d) DMBPC, 0.14, 0.684 and (e) DMPC, 0.20, 0.686

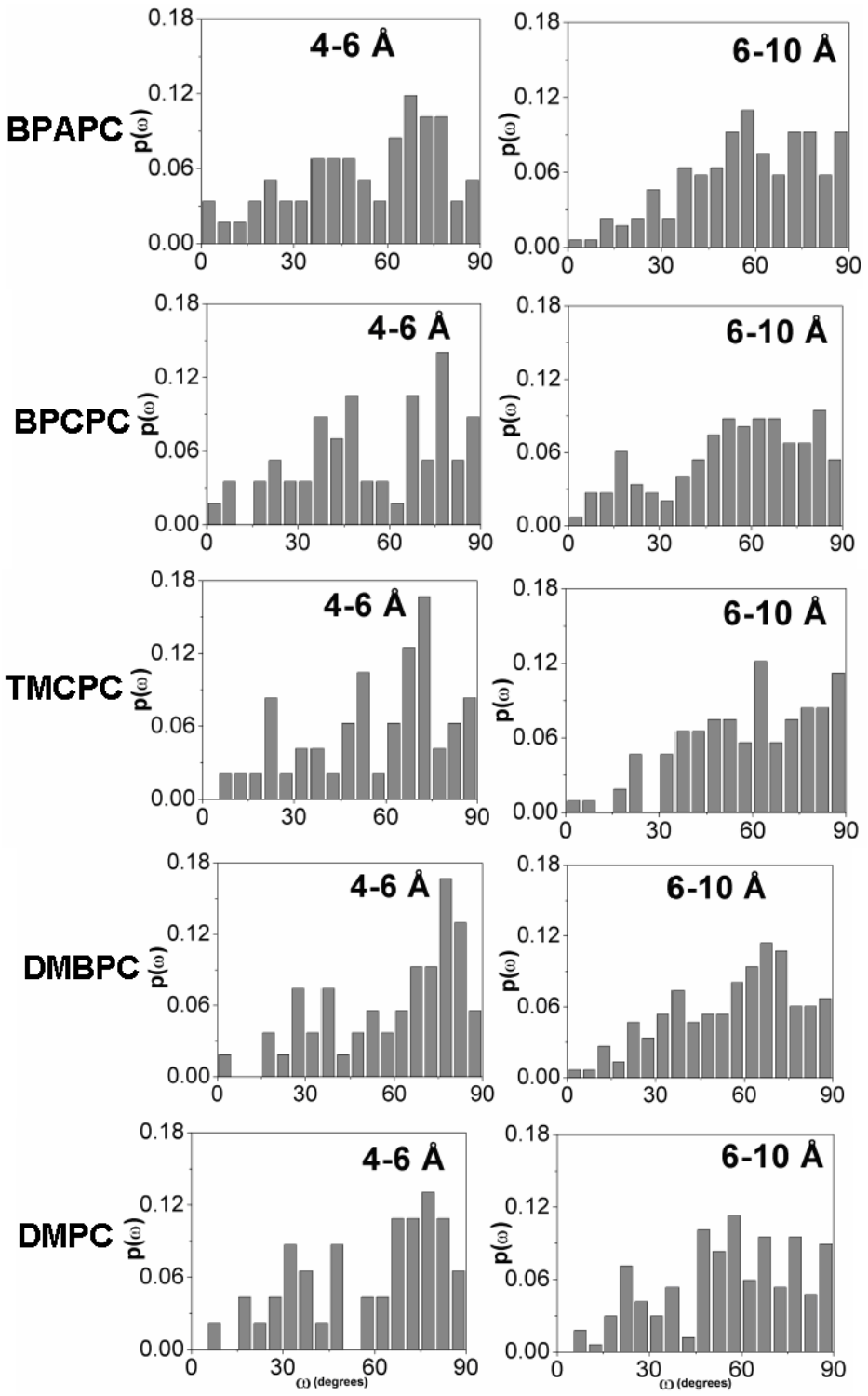

Figure 6.10. Orientational distributions of the probabilities of angles between the carbonate planes in bulk polycarbonates. The fractional contributions of carbonate pairs from which the distributions were plotted for the distance intervals 4-6 and 6-10 Å in the order for various polycarbonates are (a) BPAPC: 0.254, 0.746 (b) BPCPC: 0.278, 0.722 (c) TMCPC: 0.31, 0.69 (d) DMBPC: 0.266, 0.734 and (e) DMPC: 0.215, 0.785

6.3.8. Free volume distributions

The polycarbonate amorphous structures were analyzed for their free volume distributions using the Voronoi tessellation statistics and also with respect to available free volume in the bulk. The volume distributions obtained using Voronoi polyhedrons are given in Figure 6.11. and Figure 6.12. The probability distributions of the voronoi volume represent the probability of the volume in a tetrahedron of a particular size that is not occupied by the van der Waals volumes of the atoms. There is a greater probability for tetrahedrons having volume of the order of 7-10 $Å^3$ for all structures. BPAPC and DMPC show the same pattern of volume distribution having equal probability distributions for free volume within tetrahedra of size of about 7-10 $Å^3$ and 15-30 $Å^3$. BPCPC and DMBPC show a similar pattern with respect to tetrahedrons of smaller size (7-10 $Å^3$), but the volume available in larger tetrahedra is lower in the case of DMBPC.

Gas permeability and selectivity in a series of structurally different polycarbonates have been performed over the past few years and researchers have tried to find a correlation between the gas permeability and polymer structure.[14,25,26,48-52] Polycarbonates with structural features that inhibit inter chain packing and hence a higher fractional free volume along with a restricted intra chain rotational mobility have been found to exhibit higher permeability than BPAPC. A flexible cyclohexyl substituent as in BPCPC[48] is found to facilitate better packing and hence lower permeabilities when compared to a bulky trimethylcyclohexyl group as in TMCPC[14,26] which lowers the packing efficiency and result in higher gas permeability than BPAPC. Reports on positron annihilation lifetime spectroscopic studies on BPAPC and a few substituted polycarbonates suggest that average hole volume shows an inverse correlation with bulk density.[53,54] Predictive methods in which the gas diffusion and permeability of polymers is proposed to be controlled by the polymer structure and polymer specific volume has been put forward.[55-58] Further refinements of these empirical correlations have been suggested by Thran et al.[58] wherein the gas diffusivity has been found to strongly depend on chain stiffness and cohesive energy density in addition to the fractional free volume of the polymer.

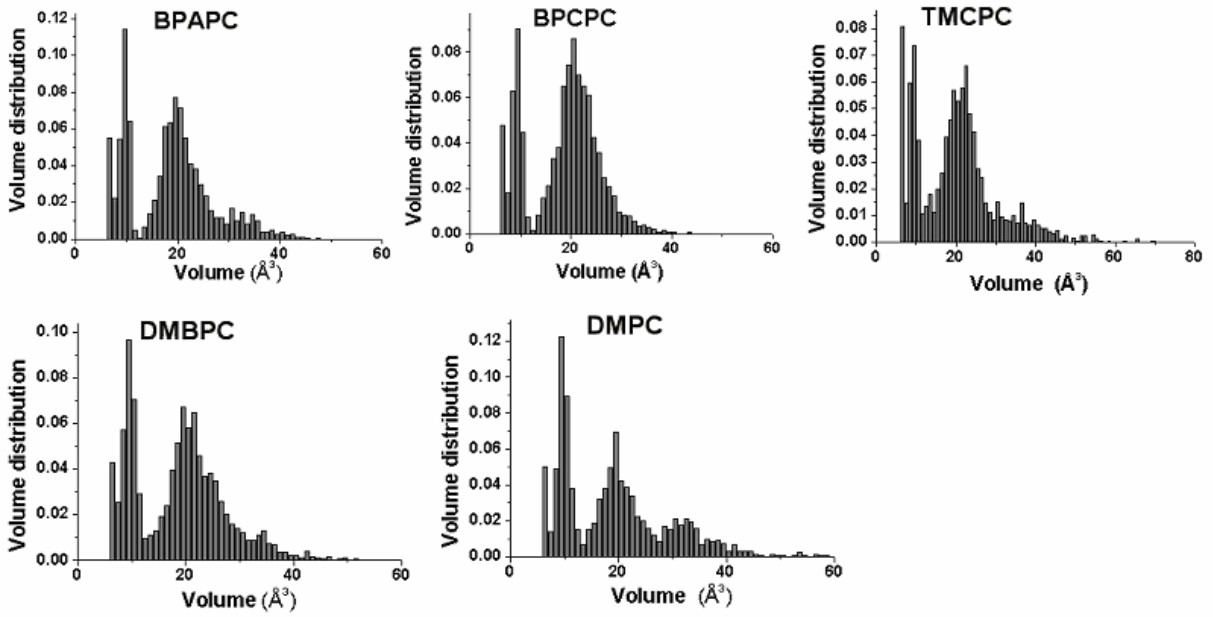

Figure 6.11. Voronoi tessellation statistics in bulk amorphous polycarbonates from atomistic simulations

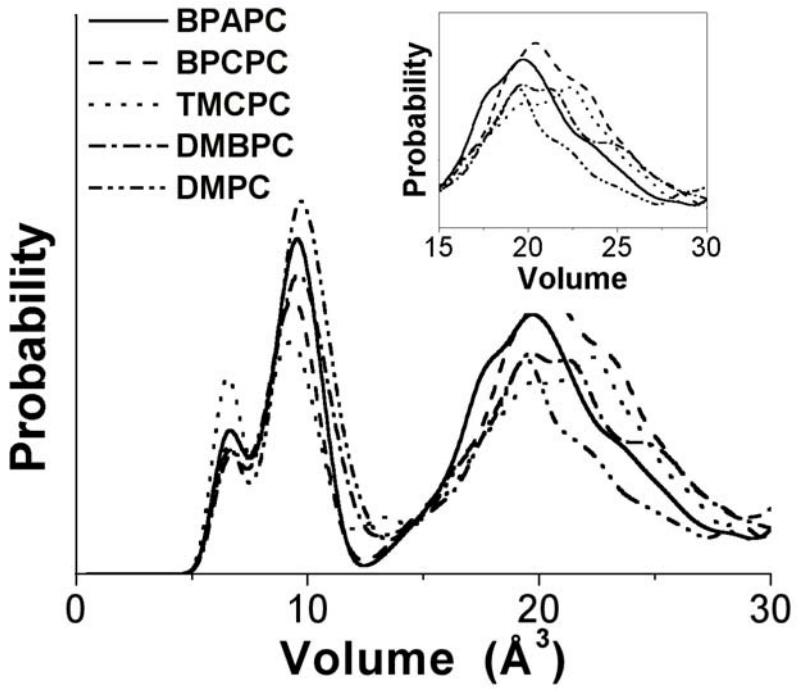

Figure 6.12. Voronoi volume distributions in bulk amorphous polycarbonates from atomistic simulations

Table 6.8. Free volume distributions in polycarbonate bulk structures

PC	Voronoi free volume [a] (peak maximum) ($Å^3$)	Available volume/Cell volume (Ratio)	FFV[b]
BPAPC	9.5 (0.11) 19.5 (0.08)	0.308	0.164
BPCPC	9.5 (0.09) 20.5 (0.09)	0.301	0.156
TMCPC	6.5 (0.08) 22.5 (0.07)	0.329	0.190
DMBPC	9.5 (0.10) 19.5 (0.07)	0.293	0.113
DMPC	9.5 (0.12) 19.5 (0.07)	0.306	0.149

[a] Probability of occurrence of the peak is given in paranthesis

[b] Fractional free volumes reported in refs 25,26 and 48**.** For DMBPC and DMPC, FFV is calculated from the specific free volume given in ref. 25

The free volume of the simulated bulk structures is calculated as ratio of the available volume to the cell volume, averaged over ensemble of all structures in each type of polycarbonate. The values are 0.308 (BPAPC), 0.301 (BPCPC), 0.329 (TMCPC), 0.293 (DMBPC) and 0.306 (DMPC). Except for TMCPC, other substituted polycarbonates have lower fractional free volume than BPAPC and DMBPC has the lowest free volume among this set of polycarbonates. The values obtained here follow the same trend as the fractional free volumes reported earlier for some of these polycarbonates,[25,26,48] where the gas permeabilities of a series of polycarbonates have been correlated with the fractional free volumes. FFV for correlating with experimental gas permeabilities is calculated as $(V\text{-}V_o)/V$ where V_o is the polymer occupied specific volume and V is the measured polymer specific volume (inverse of the experimental density). The calculated free volume from the present amorphous cell simulations and the FFV reported are given in Table 6.8. It should be noted that the absolute values of the FFV calculated from the two different approaches are not expected to be identical, we are interested only in the relative trend among these polycarbonates. It is known that polycarbonates having methyl substituents at the 3,3' positions on the backbone phenylene rings (DMPC)[25] as well as those having cyclohexyl group at the C_α carbon (BPCPC)[48] show lower gas permeabilities than BPAPC. This has

been explained on the basis of closer interatomic packing of the structures and lower free volume available to the gas diffusants. For BPCPC the lower free volume is explained on the basis of a better packing in the bulk brought about due to the flexible cyclohexyl substituent.[48] On the other hand, TMCPC with additional methyl groups on the cyclohexyl ring has a higher free volume which inhibits the chain packing and result in higher gas permeabilities.[26] The higher free volume observed for TMCPC points towards a relatively loosely packed open structure which was also shown to be the case by the scattering structure factor and the RDF's earlier in section 6.3.5 and 6.3.6 respectively. Oxygen permeability for DMBPC was found to be the lowest among a series of 24 structurally different polycarbonates which were studied by Schmidhauser et al.[25] The free volume calculated from the simulation for DMBPC was found to be the lowest and gas permeability data[25] also support this result.

It is interesting to compare the structure, packing and the implications thereof for TMCPC and DMBPC that is brought forth from the amorphous simulations reported here. TMCPC shows random distribution of the phenyl rings and carbonate groups in the range studied ie. upto 10 Å. Interchain distance as calculated from the scattering structure factor is the largest for TMCPC among these polycarbonates. Also supporting this is the higher fractional free volumes calculated for this simulated bulk amorphous polymer. Interchain distance for DMBPC is found to be lower than TMCPC. More strikingly the free volume is the lowest for DMBPC among this set of polycarbonates. The information that emerges from the different types of analysis performed on these bulk structures is that methyl groups on the cyclohexyl rings as in TMCPC inhibits the packing of chains in the bulk, whereas an unsubstituted cyclohexyl group at the C_α carbon along with the methyl groups at the aromatic 3, 3' position (DMBPC) may not have drastic effect on chain packing in the bulk. These packing differences in the bulk between these two polycarbonates result in higher gas permeability for TMCPC while that for DMBPC is found to be lower.

6.4. Conclusions

Molecular dynamics simulations of bulk amorphous BPAPC and four structurally modified polycarbonates with full atomistic description are reported here. The distance between the

neighboring chains calculated from the scattering curves indicate a rather open structure for TMCPC due to the bulky trimethylcyclohexylidene substituent. It is found that structural modification of the BPAPC repeat unit by aliphatic groups like in the polycarbonates studied here lowers the CED and solubility parameter. Population maxima of the various torsional distributions are located at the various discrete rotational states as derived from conformational intramolecular energy calculations, but in the bulk structure large deviations results from the interchain packing constraints. Short distances for some of the atom pairs derived from RDF of BPAPC is found to be in agreement with reported NMR measurements. The peak positions of the calculated neutron scattering curves are in agreement with the experimental reports leading to a correct trend in the neighboring chain distances for the various polycarbonates studied here. Fractional free volume analysis along with the neutron scattering curves indicates higher spatial distance between the neighbouring chains in TMCPC and higher free volume. DMBPC on the other hand seems to have a better packed structure with a lower free volume when compared to TMCPC. The effect of structural modification on the macroscopic properties clearly emerges from this study of substituted polycarbonates.

6.5. References

1. Theodorou, D. N.; Suter, U. W. *Macromolecules* **1985**, *18*, 1467.
2. Smith, G. D.; Boyd, R. H. *Macromolecules* **1991**, *24*, 2731.
3. Monnerie, L.; Suter, U. W. *Atomistic Modeling of Physical Properties of Polymers*, *Adv. Polym. Sci*., Springer 1994.
4. Roe, R. J. *Computer Simulation of Polymers*, Prentice Hall: New York, 1991.
5. Hutnik, M.; Gentile F. T.; Ludovice P. J.; Suter, U. W.; Argon, A. S. *Macromolecules* **1991**, *24*, 5962.
6. Hutnik, M.; Argon, A. S.; Suter, U. W. *Macromolecules* **1991**, *24*, 5970.
7. Fan, C. F.; Cagin, T.; Chen, Z. M.; Smith, K. A. *Macromolecules* **1994**, *27*, 2383.
8. Fan, C. F. *Macromolecules* **1995**, *28*, 5215.
9. Fan, C. F.; Cagin, T.; Shi, W.; Smith, K. A. *Macromol. Theory Simul*., **1997**, *6*, 83.
10. Shih, J. H.; Chen, C. L. *Macromolecules* **1995**, *28*, 4509.

11. Whitney, D. R.; Yaris, R. *Macromolecules* **1997**, *30*, 1741.
12. Ballone, P.; Montanari, B.; Jones, R. O.; Hahn, O. *J. Phys. Chem. A* **1999**, *103*, 5387.
13. Gentile, F. T.; Arizzi, S.; Suter, U. W.; Ludovice, P. J. *Ind. Eng. Chem. Res*. **1995**, *34*, 4193.
14. Lopez-Gonzales, M.; Saiz, E.; Guzman, J.; Riande, E. *Macromolecules* **2001**, *34*, 4999.
15. Lamers, C.; Schärpf, O.; Schweika, W.; Batoulis, J.; Sommer, K.; Richter, D. *Physica B* **1992**, *180 & 181*, 515.
16. Tschöp, W.; Kremer, K.; Batoulis, J.; Bürger, T.; Hahn, O. *Acta Polymer* **1998**, *49*, 61.
17. Tschöp, W.; Kremer, K.; Hahn, O.; Batoulis, J.; Bürger, T. *Acta Polymer* **1998**, *49*, 75.
18. Abrams, C. F.; Kremer, K. *Macromolecules* **2003**, *36*, 260.
19. Sun, H. *Macromolecules* **1994,** *26*, 5924.
20. Sun, H.; Mumby, S. J.; Maple, J. R.; Hagler, A. T. *J. Am. Chem. Soc*. **1994**, *116*, 2978.
21. Sun, H. *J. Comp. Chem*. **1994**, *15*, 752.
22. Sun, H.; Mumby, S. J.; Maple, J. R.; Hagler, A. T. *J. Phy. Chem*.**1995**, *99*, 5873.
23. Sun, H. *Macromolecules* **1995**, *28*, 701.
24. Cerius^2, San Diego, CA: Molecular Simulations 1996.
25. Schmidhauser, J. C.; Longley, K. L. *J. App. Polym. Sci*. **1990**, *39*, 2083.
26. Hägg, M. B.; Koros, W. J.; Schmidhauser, J. C. *J. Polym. Sci. Polym. Phys*. **1994**, *32*, 1625.
27. Nose, S. *Prog. Theoret. Phys. Supplement* **1991**, *103*, 1.
28. Verlet, L. *Phys. Rev*. **1967**, *159*, 98.
29. Kambour, R. P.; Gruner, C. L.; Romagosa, E. E. *Macromolecules* **1974**, *7*, 248.
30. Kambour, R. P.; Gruner, C. L. *J. Polym. Sci. Polym. Phys*. **1978**, *16*, 703.
31. Kambour R. P. *Polymer Commun*. **1983**, *24*, 292.
32. Beck, N. H. *Ind. Eng. Chem. Res*. **1992**, *31*, 2628.
33. Tomaselli, M.; Zehnder, M. M.; Robyr, P.; Grob-Pisano, C.; Ernst, R. R.; Suter, U.

W. *Macromolecules* **1997**, *30*, 3579.

34. Robyr, P.; Utz, M.; Gan, Z.; Scheurer, C.; Tomaselli, M.; Suter, U. W.; Ernst, R. R. *Macromolecules* **1998**, *31*, 5818 and references cited therein
35. Dybal, J.; Schmidt, P.; Baldrian, J.; Kratochvil, J. *Macromolecules* **1998**, *31*, 6611.
36. Lee, P. L.; Schaefer, J. *Macromolecules* **1992**, *25*, 5559.
37. Schmidt, A.; Kowalewski, T.; Schaefer, J. *Macromolecules* **1993**, *26*, 1729.
38. Lee, P. L.; Schaefer, J. *Macromolecules* **1995**, *28*, 1921.
39. Lee, P.L.; Kowalewski, T.; Poliks, M. D.; Schaefer, J. *Macromolecules* **1995**, *28*, 2476.
40. Klug, C. A.; Shu, W.; Tasaki, K.; Schaefer, J. *Macromolecules* **1997**, *30*, 1734.
41. Neki, K.; Geil, P. H. J. *Macromol. Sci*. **1973**, B8, 295.
42. Saffell, J. R.; Windle, A. H. *Colloid. Polym. Sci*. **1985**, *263*, 280.
43. Cervinka, L.; Fischer, E. W.; Hahn, K.; Jiang, B.-Z.; Hellmann, G. P.; Kuhn, K. –J. *Polymer* **1987**, *28*, 1287.
44. Lamers, C.; Schönfeld, C.; Shapiro, S. M.; Batoulis, J.; Timmermann, R.; Cable, J. W.; Richter, D. *Colloid Polym. Sci*. **1994**, *272*, 1403.
45. Eilhard, J.; Zirkel, A.; Tschöp, W.; Hahn, O.; Kremer, K.; Schärpf, O.; Richter, D.; Buchenau, U. *J. Chem. Phys*. **1999**, *110*, 1819.
46. Robyr, P.; Tomaselli, M.; Grob-Pisano, C.; Meier, B, H.; Ernst, R. R.; Suter, U. W. *Macromolecules* **1995**, *28*, 5320.
47. Robyr, P.; Gan, Z.; Suter, U. W. *Macromolecules* **1998**, *31*, 6199.
48. Mchattie, J. S.; Koros, W. J.; Paul, D. R. *J. Polym. Sci. Polym. Phys*. **1991**, *29*, 731.
49. Hellums, M. W.; Koros, W. J.; Paul, D. R. *J. App. Polym. Sci*. **1991**, *43*, 1977.
50. Muruganandam, N.; Koros, W. J.; Paul, D. R. *J. Polym. Sci. Polym. Phys*. **1987**, *25*, 1999.
51. Hellums, M. W.; Koros, W. J.; Husk, G. R.; Paul, D. R. *J. Membr. Sci*. **1989**, *46*, 93
52. Chiou, J. S.; Paul, D. R. *J. App. Polym. Sci*. **1987**, *33*, 2935.
53. Kluin, J.-E.; Yu, S.; Vleeshouwers, S.; McGervey, J. D.; Jamieson, A. M.; Simha, R.; Sommer, K. *Macromolecules* **1993**, *26*, 1853
54. Bartoš, J.; Krištiaková, K.; Šauša, O.; Krištiak, J. *Polymer* **1996**, *37*, 3397.
55. Lee, W. M. Polym. Eng. Sci. **1980**, *20*, 65.

56. Kirchheim, R. *Macromolecules* **1992**, *25*, 6952.
57. Gruger, A.; Gotthardt, P.; Ponitsch, M.; Brion, H. G.; Kirchheim, R. *J. Polym. Sci. Polym. Phys*. **1998**, *36*, 483.
58. Thran, A.; Kroll, G.; F. Faupel. *J. Polym. Sci. Polym. Phys*. **1999**, *37*, 334.

Chapter 7: Atomistic Simulations of the Orientational Birefringence of Polycarbonates in the Glassy State

7.1. Introduction

Atomistic simulation studies on deformation of bisphenol A polycarbonate reported till date in the literature have focussed on deriving mechanical response properties including small strain elastic constants and structural events during plastic deformation.[1-4] Utz et al. have applied NMR experiments in conjunction with atomistic simulations to study in detail the effect of compressive strain on the orientation, conformation and packing of chain segments in BPAPC.[5-7] There have been no atomistic simulation studies on deformational behaviour of substituted polycarbonates till date. There have been very few reports on the simulation of the optical properties of polymers, be it amorphous or semi-crystalline, which have dealt with very simple model polymers (polyethylene-like) in the melt state. [8-12] Currently no reports are available for the strain-optical or stress-optical behaviour in the glassy state of amorphous polymers.

For polymers birefringence is commonly observed by applying an anisotropic macroscopic deformation, usually uniaxial tension, and measuring the differences between the refractive indices of the sample along two perpendicular directions.[13-18] Polymer chains respond to this tensile strain by orientation of chain segments towards the stretching direction by rearrangements in the chain backbone. In considering the stress-induced birefringence of amorphous polymers a distinction must be made between rubbery and glassy materials due to the basic differences in the deformation mechanism in the respective states.[15,18,19] In the glassy state short-range processes such as valence bond twisting, twisting about single bonds and change in intermolecular distances occurs in addition to chain orientation. In the glass-to-rubber transition region the entropic nature of deformation of polymers is activated resulting in a time dependent relation for the stress-optical coefficient.[19] Inoue and coworkers have done extensive work on birefringence of amorphous polymers in the glass transition zone and have made use of a modified stress-optical rule to explain the behaviour of the complex part

of the Youngs modulus and the complex part of the strain optical coefficient in going from the rubbery plateau zone to the glassy zone.[20-23]

Birefringence and stress-optical properties of BPAPC have been investigated using various experimental measurement techniques.[24-39] The birefringence and stress-optical properties of BPAPC were first reported by Ito[25] and later by LeGrand.[26] Champion et al. studied flow and magnetic birefringence of BPAPC.[27] Many experimental investigations later on in the literature were focussed on the determination of intrinsic birefringence of BPAPC and studies were carried out on both cold and hot-drawn polycarbonate. Orientation and optical birefringence of heat stretched samples of BPAPC were determined using IR dichroism, WAXS and birefringence measurements by Biangardi.[28] Intrinsic birefringence of BPAPC was determined to be 0.236±0.004 from a least squares fit of birefringence as a function of orientation.[28-30]

Birefringence, anisotropic heat conduction and WAXS studies were performed on uniaxially drawn samples of BPAPC which were oriented above and below T_g. Good correlation was found between the orientation parameters from WAXS and heat conduction. Intrinsic birefringence derived from heat conduction falls in the range 0.1-0.13. WAXS showed that orientation of BPAPC does not change the short- range order up to 15 Å.[31,32] IR dichroism have been used to obtain direct experimental observations of chain orientation under the application of an external stress.[36-39] In one such study by Wu,[37] birefringence of uniaxially oriented BPAPC stretched over a wide range of temperatures were measured. Measured birefringence yielded a linear relationship within each series (one above T_g and the other below T_g) which allowed for the determination of intrinsic birefringence of amorphous BPAPC to be 0.192. A regression analysis indicated that the glassy state birefringence exceeds the melt birefringence by 26% at a given orientation.

2D-MAS NMR studies to measure the orientation parameter of the diphenyl propane unit in BPAPC oriented by stretching to various extension ratios at 295 K and 403 K have been reported.[34] Experimental data for BPAPC stretched to various extension ratios fall close

to a straight line yielding a maximum birefringence, $\Delta n^{\circ}=0.189$, which is in agreement with the value derived by Wu.[37]

Rheo-optical properties and dynamic birefringence of BPAPC have been the subject of various investigations.[40-47] There have been numerous studies on the stress-strain and the orientation behaviour of BPAPC and researchers have proposed different phenomenological models to explain the behaviour during the plastic deformation of BPAPC.[48-53] Studies on the residual birefringence in quenched and injection-molded specimens of BPAPC have also been reported.[54-57] In literature a range of values exist for the intrinsic birefringence of BPAPC and there is considerable disagreement between the various reported values. Pietralla and Pieper discussed the problems of determining the intrinsic birefringence of BPAPC.[35] Biangardi estimated theoretical value of the intrinsic birefringence of BPAPC to be 0.207 from the information on bond polarizabilities and geometry of the chain, but the reference frame in which the polarizability tensor of the polycarbonate single chain is calculated is not mentioned in that report.[29] Pietralla and Pieper have attempted the calculation of polarizability tensor and subsequently the intrinsic birefringence of some hypothetical conformations of BPAPC.[35] The generated conformations in that study suffered from the uncertainty whether those indeed were energetically possible.

Barring these attempts which were mainly based on the polarizability tensor of an unperturbed BPAPC single chain which was then eventually used to estimate the intrinsic birefringence, there have been no other reports on the theoretical estimation of this macroscopic property for BPAPC or other substituted polycarbonate in the literature. Birefringence represents an important property for polycarbonates specifically with respect to its application in optical data storage technology. An understanding of the contributions to birefringence from the different structural groups in substituted polycarbonates, would present valuable fundamental information and understanding and aid in design of new monomers for optical applications. In this work, atomistic simulation methods are employed to study the deformation of BPAPC and two substituted polycarbonates. The orientational as well as conformational differences due to the different chemical substitutions and the calculation of birefringence through a new method formulated here are presented for the first

time. The deformation behaviour of substituted polycarbonates using atomistic simulations is being reported here for the first time.

7.2. Modeling Methodology and Simulation Details

PCFF force-field[58-62] which is well parameterized for polycarbonate structures is used to describe the atom-atom interactions at the fully atomistic level. Atomistic simulations of uniaxial tensile deformation were performed using Cerius^2 molecular modeling software[63] on Silicon Graphics Octane SE workstation. In the present work atomistic simulations are performed on three polycarbonates BPAPC, DMPC and DMBPC, structures of which are given in Figure 7.1.

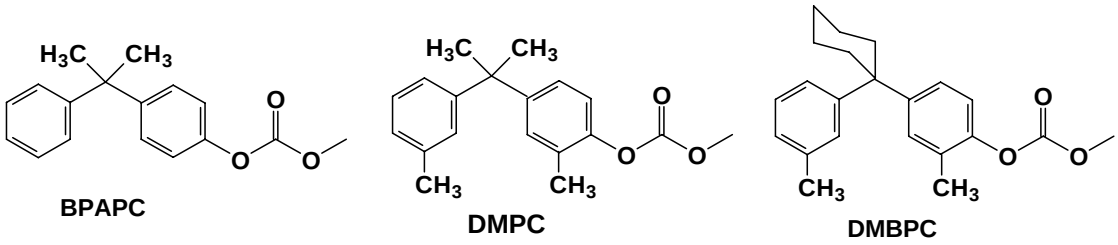

Figure 7.1. Chemical structures of repeat units of polycarbonates studied in the present work

Amorphous polycarbonate structures representing dense random packing at their respective experimental densities were taken from the work described in section 6.2 in Chapter 6. Three independently generated and relaxed samples corresponding to each type of polycarbonate were subjected to molecular dynamics simulations for duration of about 150 ps at 300 K with a new spline-switching cut off. Non-bonded interactions defined by the *vdw* and coulombic terms were truncated at 11 Å using a fifth order spline switching function from 9 to 11 Å. (In the MD simulations described in the previous chapter, the cut offs used were 12.5–15 Å). Structures at the end of the MD simulation were minimized using the conjugate gradient method. These structures can be described as static models (0 K models) at a density corresponding to room temperature. Thermal effects are included in these structures in an average fashion by the use of correct density appropriate to room temperature. Mode of deformation applied in this work is uniaxial tension. Starting with a structure that is at its potential energy minimum, a small extension strain step is imposed on the periodic box, by extending one of the cell edge length. The other two edge lengths are

compressed correspondingly to conform to a constant volume deformation procedure. The deformation with constant intrinsic poisson ratio assumption will not be valid here as the total strain and deformation imposed is well past the elastic regime and actually represents plastically deformed sample. Experimental data indicate that deformation scheme with constant intrinsic poisson ratio assumption will not be valid at large strain, since the volume of the bulk sample and the free volume actually may decrease as a function of strain.[64] Energy of the system increases as the strain is imposed and the system is then re-minimized. This procedure ensures that the system is maintained at the bottom of a potential energy well. To simulate large strain deformations, this process is done in a step-wise manner where at each step only a very small strain increment of the order of 0.003 (this corresponds to extending the cell edge length in the stretching direction by 0.1 Å) is applied to the system to avoid convergence difficulties in the energy optimization. The application of the very small strain increment will ensure that the system trajectory will follow the lowest potential energy path compatible with the prescribed strain. This procedure is repeated as many times until the desired total strain is attained. Total strain imposed on the polycarbonate systems in the present work is 100%, which corresponds to a draw ratio of 2. Since time does not enter and there is no thermal activation, the rate of deformation is undefined in this simulation procedure. In the case of DMBPC, since the repeat unit structure itself is rigid with two kinds of substitutions when compared to BPAPC, the strain increment applied in each step is 0.0015 (0.05 Å extension).

For each polycarbonate three statistically different dense amorphous samples were chosen as the starting structures. For each sample deformation simulations were performed in all the three, viz., X, Y and Z directions. Thus for the three samples in the case of each polycarbonate there are a total of nine stretching simulations. The oriented structures thus derived from the stretching simulations are then analyzed in terms of the orientation functions of the specific groups in the polycarbonate chain, torsional distribution in these polycarbonates, intermolecular packing of the phenyl and carbonate groups in the case of BPAPC and finally the calculation of birefringence of these structures as a function of strain. The results presented in the following sections are averaged over all the nine simulations in each polycarbonate.

7.2.1. Calculation of birefringence for the atomistic structures

7.2.1.1. Direct calculation of birefringence using polarizability tensors

The first new methodology adopted in the present work for the calculation of birefringence of oriented polycarbonate structures is described here.

We define the optical birefringence as known in the literature as

$$\Delta n = \Delta n^{\circ} \langle P_2 \rangle \tag{1}$$

where $\langle P_2 \rangle$ is the orientation function and Δn° is the maximum birefringence for a perfectly oriented sample which is expressed as,

$$\Delta n^{0} = \frac{2\pi}{9} \frac{\left(n^2 + 2\right)^2}{n} \frac{\rho N_A}{M} \Delta\alpha \tag{2}$$

where n is the average refractive index, ρ is the density of the polymer, N_A is the Avagadro number, M is the molar mass of the monomer repeat unit and $\Delta\alpha$ is the polarizability anisotropy of the repeat unit.

In order to calculate birefringence of the atomistically derived oriented structures, we need to determine the polarizability anisotropy ($\Delta\alpha$) of the oriented polycarbonate chain. Polarizability tensor for the polycarbonate chain is calculated using the valence optical scheme, which involves the addition of group polarizability tensors of the constituent groups when expressed in the same coordinate reference frame. Polarizability tensors of the phenyl and carbonate groups in DMPC and DMBPC in their respective molecular reference frames have been derived earlier in Chapter 4. The polarizability tensors for the phenyl and carbonate groups in BPAPC were derived by Erman et al.[65,66] from DRS studies on model compounds for this polymer (DMC, DPC and DPP) and have been found to give the mean-squared optical anisotropy of BPAPC chains in good agreement with experimental values.[66,67] The group polarizability tensors for the phenyl groups in the case of DMPC and DMBPC were also derived taking into account the contribution due to substitutions and mutual inductive effects and were also used to calculate the optical anisotropy of these chains (section 4.2 in Chapter 4). Figure 7.2 shows a DMBPC chain segment with definition of the reference frames of the various groups in the repeat unit. The polarizability tensors of the

various groups in their own molecular reference frames for BPAPC, DMPC and DMBPC are given below.

BPAPC

$$(\hat{\alpha}_{Ph,b})_{xyz} = diag\begin{bmatrix}4.9 & -1 & -3.9\end{bmatrix}$$

$$(\hat{\alpha}_{Carb})_{XYZ} = diag\begin{bmatrix}0.17 & 1.04 & -1.21\end{bmatrix}$$

$$(\hat{\alpha}_{Ph,a})_{xyz} = diag\begin{bmatrix}4.9 & -1 & -3.9\end{bmatrix}$$

DMPC

$$(\hat{\alpha}_{Ph,b})_{xyz} = \begin{bmatrix}4.545 & 0.857 & 0\\ & -0.655 & 0\\ & & -3.89\end{bmatrix}$$

$$(\hat{\alpha}_{Carb})_{XYZ} = diag\begin{bmatrix}0.17 & 1.04 & -1.21\end{bmatrix}$$

$$(\hat{\alpha}_{Ph,a})_{xyz} = \begin{bmatrix}4.545 & -0.857 & 0\\ & -0.655 & 0\\ & & -3.89\end{bmatrix}$$

DMBPC

$$(\hat{\alpha}_{ph,b,DMDPC})_{xyz} = \begin{bmatrix}2.295 & 0.857 & 0\\ & 0.785 & 0\\ & & -3.08\end{bmatrix}$$

$$(\hat{\alpha}_{Carb})_{XYZ} = diag\begin{bmatrix}0.17 & 1.04 & -1.21\end{bmatrix}$$

$$(\hat{\alpha}_{ph,a,DMDPC})_{xyz} = \begin{bmatrix}2.295 & -0.857 & 0\\ & 0.785 & 0\\ & & -3.08\end{bmatrix}$$

$$(\hat{\alpha}_{CYX})_{X'Y'Z'} = \begin{bmatrix}-0.3142 & 0.3884 & 0\\ & 0.3142 & 0\\ & & 0\end{bmatrix}$$

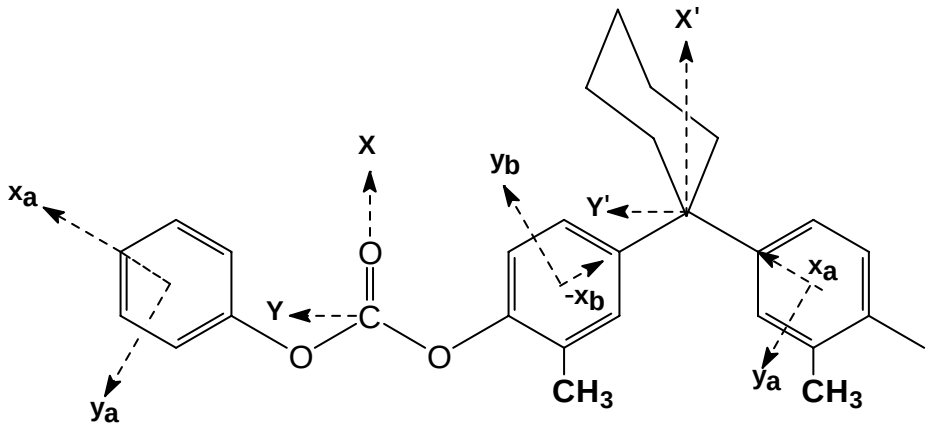

Figure 7.2. Coordinate reference frames of the various groups in DMBPC chain segment

Consider an oriented structure at a particular strain (for example 10%) corresponding to one BPAPC sample, stretched along the X direction. Each of the phenyl and carbonate groups (which are in their molecular reference frames) in the oriented polycarbonate chain are then successively transformed to the box reference frame (laboratory reference frame) by using the coordinate tensor transformation procedure. Thus, all of the phenyl and carbonate groups in the chain in the bulk sample are transformed to a common reference frame, which in this case is the box reference frame. These polarizability tensors are then added up to get the final polarizability tensor for the BPAPC chain in the box reference frame at a specific value of strain (for the atomistic sample stretched to the particular strain value). From the diagonal polarizability components of the final polarizability tensor, the polarizability anisotropy of the chain is then calculated as

$$\Delta\alpha = \alpha_{xx} - (\alpha_{yy} + \alpha_{zz})/2 \text{ (in this case stretching is performed along the X direction)} \quad (3)$$

This procedure is repeated for oriented structures of the same sample obtained by stretching along the Y and Z direction also. The respective polarizability anisotropies are calculated as

$$\Delta\alpha = \alpha_{yy} - (\alpha_{xx} + \alpha_{zz})/2 \text{ (stretching performed along the Y direction)} \quad (4)$$

$$\Delta\alpha = \alpha_{zz} - (\alpha_{xx} + \alpha_{yy})/2 \text{ (stretching performed along the Z direction)} \quad (5)$$

Thus for one specific sample, the polarizability anisotropy for the chain is averaged over the anisotropies calculated along the three stretching directions at a specific value of strain. This procedure is repeated for the other two samples (totally 3 samples were used for

the statistical purpose). And therefore, the average polarizability anisotropy at a particular strain is thus averaged over three samples and each along three stretching directions. The polarizability anisotropy per repeat unit is used to calculate the birefringence at a particular value of strain using eqs 1 and 2. Birefringence is then calculated for oriented samples corresponding to 10%, 20%, 30% till 100% strain. In short, the procedure can be described as follows. Polarizability anisotropy is calculated for the polycarbonate chain with respect to the direction along which the uniaxial strain is applied and then averaged over three stretching direction for one model to get the anisotropy value at a particular strain from which the birefringence is calculated. This is then averaged over all models and the procedure is repeated for oriented samples corresponding to other values of strain.

It should be noted that the density (experimental density corresponding to the amorphous sample) remains constant irrespective of the amount of deformation imposed on the sample. A constant volume approach is used in the present atomistic simulations, where the density remains constant during the deformation. In the present work, amount of total strain applied is 100%, which represents plastic deformation for polycarbonates. The simulation approach using an assumed poisson ratio will be valid only at lower values of strain[3,4] and hence cannot be used in the present simulations. Previous simulation studies on plastic deformation of BPAPC also have employed a constant volume approach.[6,7] This approach is followed in the present work for substituted polycarbonates as well. The various molecular parameters (constants) used in the calculation of birefringence are given in Table 7.1.

Table 7.1. Constant parameters used in the calculation of birefringence

Polycarbonate	Refractive index, n	M_o (g/mol)	ρ (g/cm^3)
BPAPC	1.5850	254	1.200
DMPC	1.5783	282	1.167
DMBPC	1.5833[a]	322	1.184

[a] Difference in the experimental refractive index value between BPAPC and DMPC is 0.0067. It is assumed that refractive index for DMPC is lowered by 0.0067 due to the presence of methyl groups on phenyl rings. Experimental refractive index for BPCPC is 1.59. From this refractive index for DMBPC can be calculated by subtracting the methyl group contribution (0.0067) from the value for BPCPC (1.59). The difference between the chemical structures of BPCPC and DMBPC is the same as that between BPAPC and DMPC.

Orientation function used in eq. 1 for the calculation of birefringence is determined by considering the average orientation of all the backbone vectors of the repeat unit across the polymer chain in each polycarbonate and the values at different % strain along with the calculated birefringence are provided in Table 7.2.

7.2.1.2. Indirect calculation of birefringence using atomistic samples

In a second method for the calculation of birefringence, experimental intrinsic birefringence of BPAPC is made use of in eq. 1 along with the orientation function from the atomistically strained samples (given in Table 7.2). For DMPC and DMBPC, polarizability anisotropy of the repeat unit calculated using the VOS-RIS method (data in Chapter 4) is employed to obtain an estimate of the intrinsic birefringence using eq. 2 and used along with the corresponding orientation functions from atomistically strained samples to calculate birefringence.

7.3. Results and Discussion

7.3.1. Deformation behaviour of bisphenol A polycarbonate

7.3.1.1. Energetics

Change in potential energy of the bulk samples as a function of strain is shown in Figure 7.3. Energy curves corresponding to 9 stretching simulations of BPAPC roughly follows the same pattern. As the cell is deformed, the potential energy linearly increases with strain in the elastic regime as has been found in previous simulation studies. In the present simulations, yielding of BPAPC is not clearly seen possibly due to the constant volume approach employed here. Large variability in energy is seen in the individual sample energy curves which is apparent beyond 15% strain. Jaggedness in energy at high strain values is due to plastic relaxations and movements. This kind of behaviour has been reported from earlier simulation studies in the literature.[1,7]

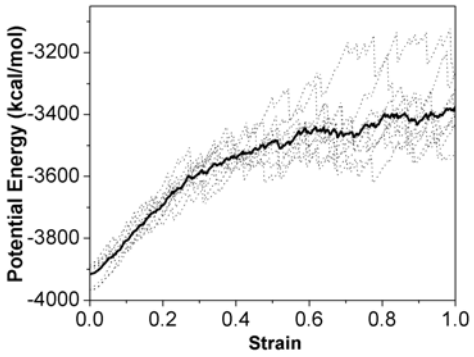

Figure 7.3. Variation of potential energy with uniaxial strain for BPAPC. Solid curve is averaged behaviour over three independent microstructures each stretched along X, Y and Z directions. Dotted curves correspond to individual sample stretching simulations

7.3.1.2. Orientation

The orientation of the specific groups (as defined by specific vectors) in the deformed system can be characterized by the second moment of the orientation distribution function, which is usually called the Hermans orientation function,[18]

$$\left\langle P_2 \right\rangle = \frac{\left(3\left\langle \cos^2\theta \right\rangle - 1\right)}{2} \qquad (6)$$

where θ is the angle between a vector and the stretching direction. Figure 7.4 shows a repeat unit of BPAPC where the orientation of the different vectors studied in the present work are defined. There are three vectors, out of which two are defined to be main chain vectors (Ph and Oz-Oz) and the Cz-OO vector, which is in a direction perpendicular to the main chain. The detailed analysis presented here is first time report study being carried out on BPAPC and substituted polycarbonates.

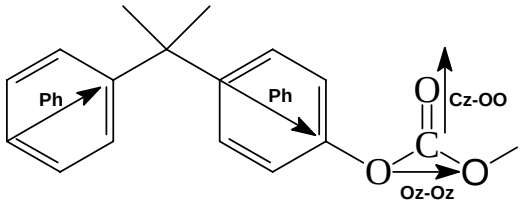

Figure 7.4. Structure of BPAPC repeat unit with the definition of various vectors used for calculating the respective group orientation functions.

The orientation behavior of the different vectors in the BPAPC chain as a function of strain is shown in Figure 7.5. $\langle P_2 \rangle$ is zero for the initial starting structure before deformation. This indicates random orientation of the initial amorphous bulk structures and is achieved

because all three axes (X, Y and Z) were independently chosen as the stretching direction for each sample cell. Thus the deformation protocol used here eliminates any anisotropy of the model structure with respect to a particular stretching direction. Average orientation function is determined for each representative vector in the chain with respect to the direction along which the extension is applied and then averaged over three extension directions for one sample and then averaged over all three samples.

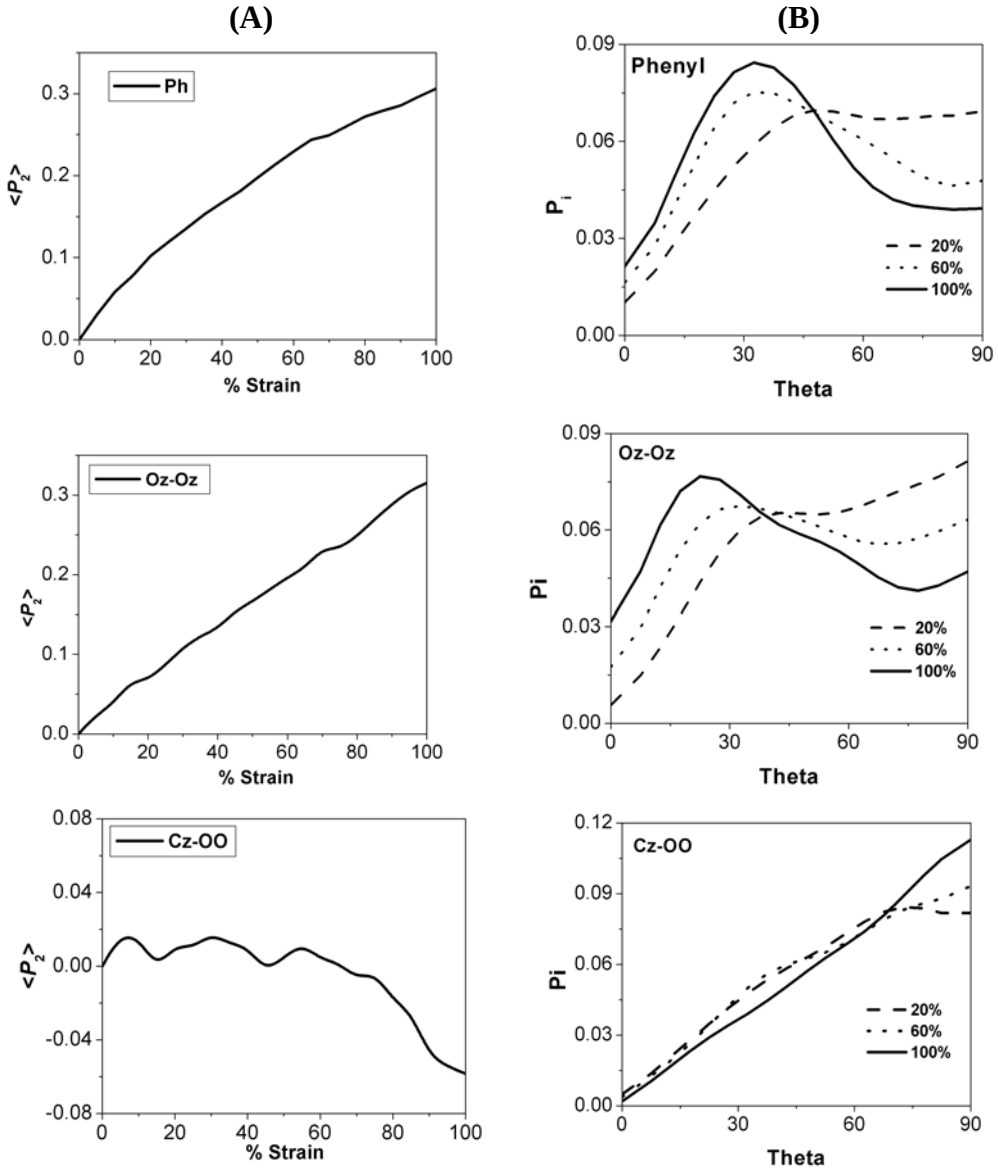

Figure 7.5. **(A)** Orientation functions of individual group vectors in BPAPC as a function of strain. Vectors are defined in Figure 7.4. **(B)** Probability distribution of the angle between the specified vectors and the stretching direction at different % strain.

Orientation functions of the phenyl and the carbonate group vectors linearly increase with strain. These represent vectors along the chain backbone and hence are increasingly

getting aligned parallel with respect to the stretching direction as the deformation progresses. The orientation function for the carbonyl double bond vector on the other hand is found to oscillate near to a value zero till about 60% strain beyond which it becomes negative. This transition to negative values indicates a relative perpendicular alignment of this vector with respect to stretching direction. When compared to the main chain vectors the change in orientation of this vector is small and not dominant. The phenyl and the carbonate group vectors reorient by about 14° and 15° respectively towards the stretching direction at about 100% strain. The carbonyl double bond reorientation is only 3°. The analysis shows that the polycarbonate chain is preferentially getting aligned in a direction parallel to the stretching direction.

Probability distribution of the angle between the specified vector and the stretching direction is also shown in Figure 7.5. The results conform to that obtained from the respective orientation functions for individual chemical groups in the chain. Vectors along the main chain, phenylene ring axis and carbonate (Oz-Oz) tend to orient parallel with respect to the stretching direction. The location of the distribution peak maximum for these main chain vectors shifts more towards lower angles (increasingly getting aligned parallel with respect to the stretching direction) with increase in strain. For the carbonyl double bond vector (Cz-OO), the shift in the population maximum is not appreciable although there is a clear indication of the increase in probability for perpendicular arrangement of vectors with respect to the stretching direction (angles near to 90°) at higher strain. From NMR experiments on uniaxially compressed BPAPC samples, the angles between the compression direction and the principal axes of the chemical shift tensor were calculated from the orientational distribution functions.[5] Vectors along the main chain tend to orient perpendicular to the axis of compression as expected from an affine deformation of the random coil under homogeneous compressive strain. The C=O bond vector and the vector normal to the plane of the phenylene rings tend to orient themselves parallel with respect to the macroscopic axis of compression. In the present work here from the simulations of tensile strain (extension) performed on BPAPC, results should be in opposite to that observed in compression. For the main chain phenylene and carbonate (Oz-Oz) vectors there is a marked increase in their population and a preference for lower angles with respect to the stretching direction. Literature results from NMR investigations of global and local orientational

aspects of BPAPC during uniaxial compressive deformation showed that atomistic simulations overestimate the order parameters (orientational) of the phenyl and carbonate groups.[6] The order parameter determined from NMR measurements for the phenylene rings is –0.077 (negative sign because the mode of deformation employed is compression) and that derived from atomistic simulations was higher by a factor of 3 at a total compressive strain of 61%. Order parameter determined from our simulations (0.229 at 60% strain) is similar to that derived from the previous atomistic simulations[4,6] all of which show higher values than those from NMR measurements.

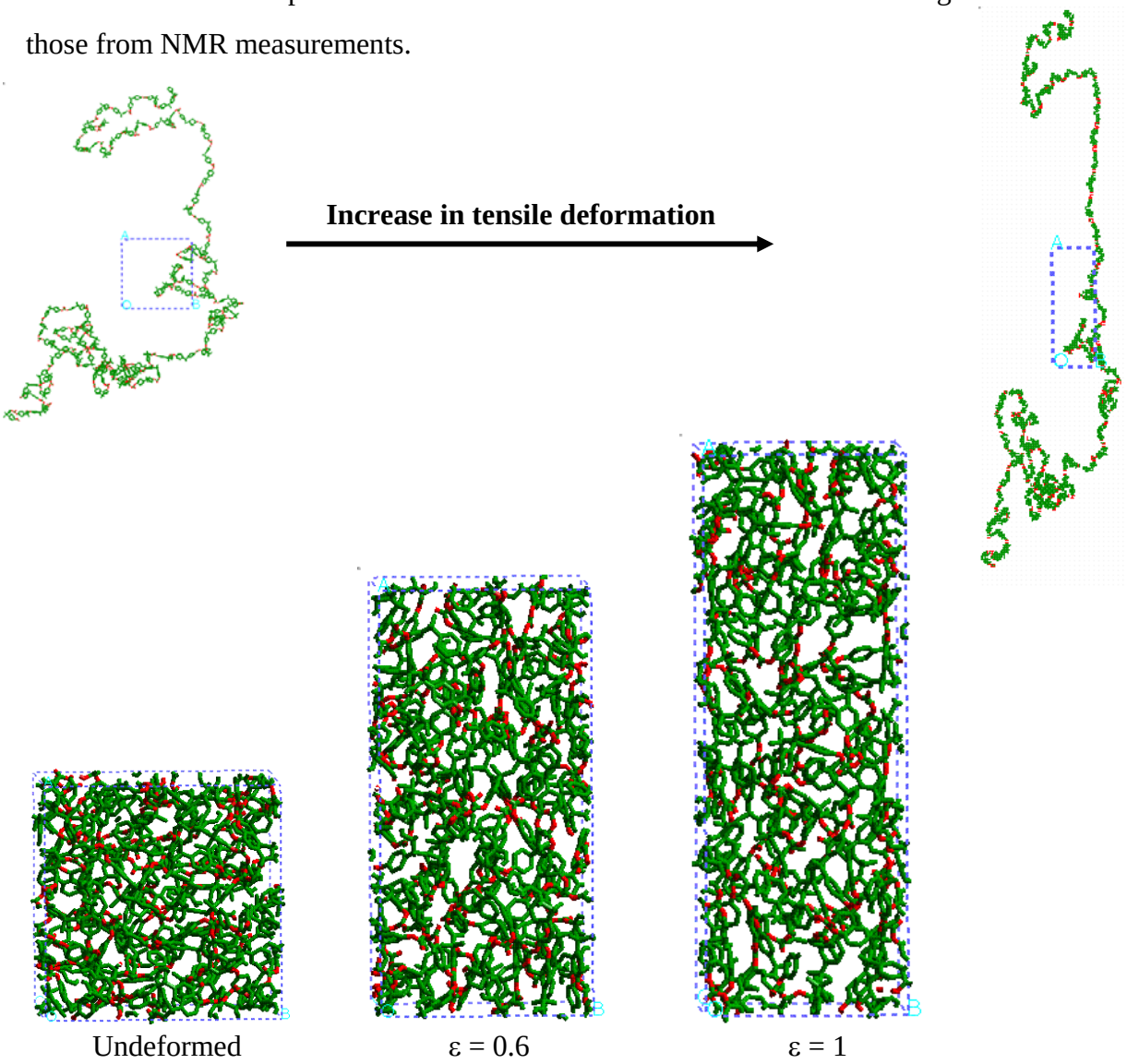

Figure 7.6. Structure evolution during uniaxial tensile deformation of BPAPC in the glassy state for one particular atomistic sample.

The structure evolution during uniaxial tensile deformation in BPAPC is schematically represented using actual sample coordinates at specified strains in Figure 7.6. The bulk amorphous initial undeformed sample is shown along with the oriented structures at higher strains. The chain extension of the polycarbonate due to uniaxial tension can be seen from the snapshot in Figure 7.6 as the chain becomes increasingly aligned parallel with respect to the stretching direction.

7.3.1.3. Changes in intermolecular packing in BPAPC due to uniaxial deformation

7.3.1.3.1. Packing of phenylene rings

To get further insight into the packing of chains in the bulk structures, orientational correlations of the nearest neighbour phenylene rings are determined using the same procedure as given for the phenyl rings in bulk amorphous polycarbonates (section 6.3.7 in Chapter 6). Angles (β) between the nearest neighbour phenylene ring planes were calculated for different intervals of distances between the rings in the oriented structures as well as the initial bulk amorphous structures. Probability distribution of the angle between nearest neighbour phenylene ring planes is then plotted as a function of strain at different distance intervals. The analysis is performed for phenylene rings separated by a distance falling within 4-6 Å, 6-8 Å and 8-10 Å. The probability is calculated as $P(\beta)$, where β is the angle between the phenylene ring planes and $P(\beta)$ is the probability of occurrence of the particular angle. The results are averaged over two samples each stretched along three directions. The plots for the initial amorphous undeformed sample along with oriented samples corresponding to 20%, 40%, 60%, 80% and 100% strain are given in Figure 7.7. The distribution curves representing the probability of the angles, $P(\beta)$, between spatially proximate phenylene ring planes reveal a better picture of the differences in the orientation and packing of the phenylene rings due to uniaxial deformation in BPAPC. The distribution pattern within a distance of 4-6 Å is markedly different from that within 6-8 and 8-10 Å range. Comparing the probability distribution of the angle between phenylene ring planes at different percentage extension shows a shift in the population maximum towards angles close to 30° within a distance of 4-6 Å. For the initial amorphous sample and for the oriented structures, at different stages of deformation, the probability of occurrence of nearly parallel phenylene ring planes is higher within 4-6 Å when compared to 6-8 Å and 8-10 Å. The reverse holds

true for angles close to 90° that represents nearly perpendicular orientation of phenylene ring planes in which case the distribution within 4-6 Å shows the lowest probability. For undeformed sample, the distribution at 4-6 Å shows two peak maxima around 40° and 60° having equal probabilities. As deformation progresses, this peak shifts more to lower angles with increasing probability. At 100% strain, still there are two peaks, one at around 30° with a higher probability than the second peak which is concentrated around 50°. There is an increase in the probability for nearly parallel packing of phenylene ring planes in the 4-6 Å range with increasing strain. The distribution also shows that within 4-6 Å, the probability for perpendicular alignment of phenylene ring planes is lower.

In the distance intervals 6-8 Å and 8-10 Å, the probabilities for perpendicular orientation of phenylene ring planes, intermolecular, is higher for the starting undeformed sample as well as for the oriented structures. This is the case even for the sample corresponding to 100% strain. Nonetheless, the distribution plots reveal a clear tendency for the neighboring phenylene ring planes to orient parallel to each other (or in other words to adopt lower angles between their planes with increase in strain). At 100% strain, within 6-8 Å and 8-10 Å, the plots show peaks emerging, which are centered around lower values of the angles between the phenylene ring planes, (30°-40°), and these are absent in the undeformed samples. Therefore, the applied strain on the BPAPC samples leads to orientation of the chains parallel to the stretching direction. Neighbouring interchain phenylene ring planes tend to align parallel to each other as the applied strain in the sample increases. This tendency for nearly parallel orientation of phenylene ring planes can occur not only within 4-6 Å (where the probability of nearly parallel orientation of phenylene ring planes is maximum) but also in the case of phenylene rings which are farther apart (distances between the phenyl rings any where between 4 to 10 Å). Even when the distance between the phenylene rings is between 6-10 Å, there is a clear tendency for the phenylene ring planes to orient in such a way that their orientation moves more and more towards a parallel arrangement with strain. The probability for parallel packing is lower at farther inter-ring distances than when the rings are much closer. Probability distributions corresponding to that of only the undeformed sample and the maximum oriented sample (i.e. at 100% strain) are

shown in Figure 7.8. These distributions clearly show preferences for the parallel orientation of phenylene ring planes as a result of uniaxial stretching.

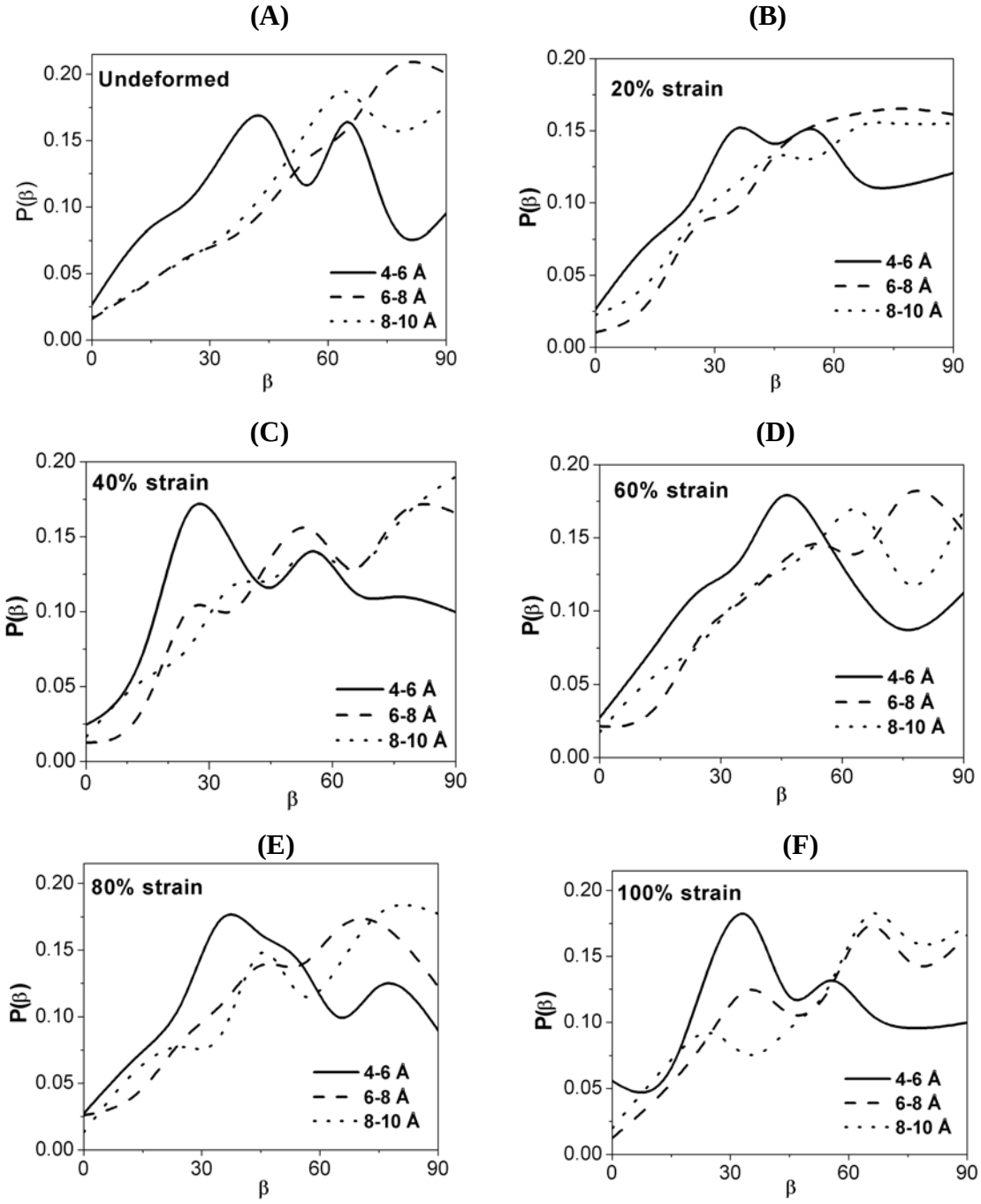

Figure 7.7. Probability distribution of the intermolecular packing of phenylene ring planes in BPAPC oriented samples as a function of deformation. The fractional contributions of phenylene rings from which the distributions were plotted for the distance intervals 4-6 Å, 6-8 Å and 8-10 Å respectively are (**A**) 0.28, 0.46, 0.26 (undeformed); (**B**) 0.27, 0.43, 0.30 (20% strain); (**C**) 0.27, 0.43, 0.30 (40% strain); (**D**) 0.26, 0.45, 0.29 (60% strain); (**E**) 0.25, 0.44, 0.20 (80% strain); (**F**) 0.26, 0.46, 0.29 (100% strain)

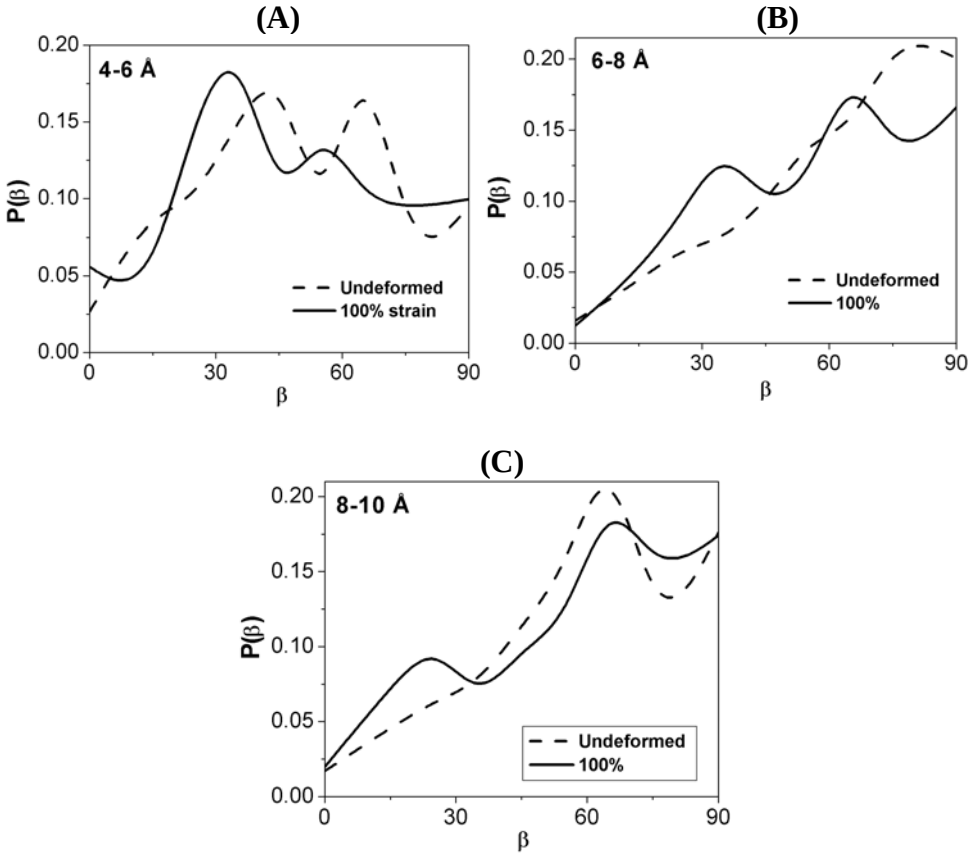

Figure 7.8. Probability distribution of the angle between nearest neighbour phenylene ring planes in BPAPC oriented samples at different distance intervals as a function of deformation. Results are shown for the undeformed sample and sample at 100% strain

Distance factor spectra of phenylene rings (contributed by rings which are separated by less than 7 Å) in amorphous BPAPC have been determined from ^{13}C polarization transfer NMR experiments in literature.[69] Although atomistic simulations[69] revealed a preference for parallel alignment of neighbouring phenylene ring planes in the amorphous bulk, no such preference for packing was detected from the NMR measurements. Utz et al. have pointed out that overestimation of the orientational order in BPAPC by atomistic simulations might be due to the limited cell size used.[6] The reason for the local ordering of phenyl ring planes found in atomistic simulations within distances less than 7 Å was also attributed to the limited periodic cell size.[69] To our knowledge, no analysis on the packing of phenylene ring and carbonate planes have been performed on atomistically derived uniaxially stretched samples for polycarbonates as is presented here. Robyr et al. have performed this analysis only for the undeformed bulk BPAPC atomistic sample and compared with NMR results.[69]

The distribution plots shown in Figure 7.8 for the starting undeformed and the oriented sample corresponding to 100% strain are clearly indicative of the shift in the orientation and packing of phenylene ring planes as a result of uniaxial extension. Although the behaviour is markedly diverse, for different inter-ring distances, the common observation is a better packing and nearly parallel orientation of the ring planes accompanying deformation, which means ring planes tend to align parallel to each other as a result of deformation irrespective of whether they are spatially proximate or not (based on analysis for distances between 4-10 Å). These results are in good agreement with NMR studies on plastically deformed BPAPC samples performed by Utz et al. where they have detected a distinct tendency of the ring planes to orient parallel to one another upon deformation.[7] NMR data indicated that mean distance between the groups with parallel phenylene planes becomes 5% shorter after deformation.[7]

7.3.1.3.2. Packing of carbonate planes

Orientational correlations of the neighbouring carbonate planes were determined using the same procedure that was applied in the case of phenylene ring planes. Angles (ω) between the carbonate planes were calculated for different intervals of distances. Probability distribution of the angle between carbonate groups is plotted as a function of strain at different distance intervals 4-6 Å, 6-8 Å and 8-10 Å (distance between the carbonate planes that fall in these ranges) are given in Figure 7. 9. Distributions are calculated as probability $P(\omega)$ where ω is the angle between interchain carbonate planes.

In the 4-6 Å range, for the undeformed sample the peak maxima are seen at around 50° and 70° with a shoulder close to 30°. The shift in the peak maximum towards lower angles does not follow a consistent pattern, but with increasing strain in the sample there is an enhancement in the probability for peaks towards lower values of ω. At 100% strain (large strain) there are two peaks, one at around 45° and the other at 30°, both at higher probabilities than those observed in the undeformed sample. The probability for perpendicular orientation of carbonate planes is found to be higher in the undeformed sample in all the three different distance intervals. Also in the 6-8 Å and 8-10 Å range this probability for perpendicular orientation of carbonate planes is higher than that within a distance of 4-6 Å.

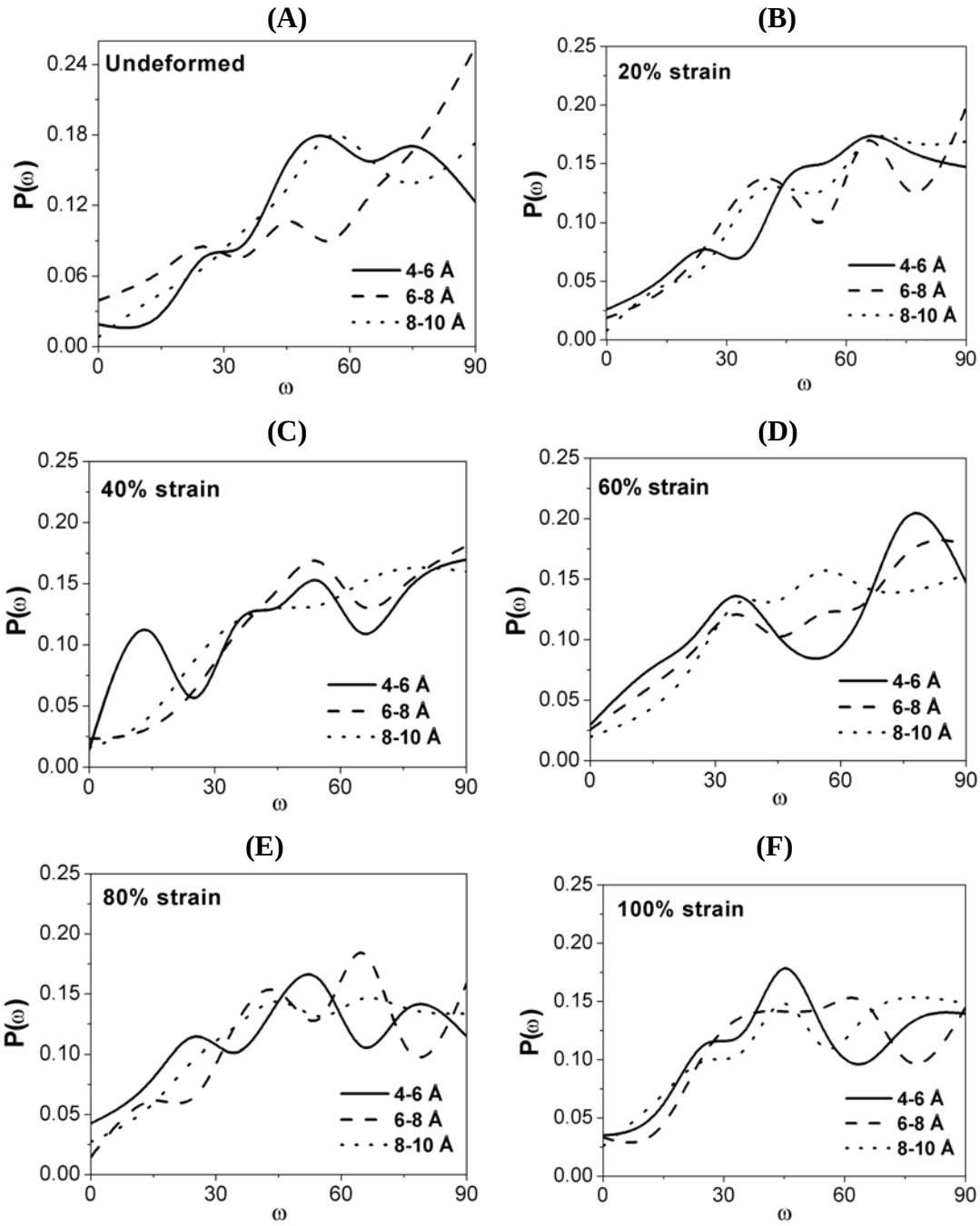

Figure 7.9. Probability distribution of the intermolecular packing of carbonate groups in BPAPC oriented samples as a function of deformation. The fractional contributions of carbonate pairs from which the distributions were plotted for the distance intervals 4-6 Å, 6-8 Å and 8-10 Å respectively are (**A**) 0.32, 0.30, 0.38 (undeformed); (**B**) 0.29, 0.29, 0.43 (20% strain); (**C**) 0.28, 0.30, 0.43 (40% strain); (**D**) 0.29, 0.29, 0.43 (60% strain); (**E**) 0.26, 0.30, 0.44 (80% strain); (**F**) 0.27, 0.28, 0.45 (100% strain)

The plots shown in Figure 7.10 reveal a better picture of the change in the orientation of the carbonate planes with stretching. Thus just by comparing the undeformed structure and

the oriented structures at 100% strain, it follows that the carbonate planes also exhibit a tendency for nearly parallel orientation due to deformation. This is seen in all the three different distance intervals analyzed here, with a tendency for better packing. Changes in the population probability maximum going towards lower values of carbonate plane angles is prominent in the 4-6 Å distance range. Even when the distances between the carbonate groups are in the range 6-10 Å, there is an increase in the population of carbonate planes aligned parallel to each other. The number density of such nearly parallel carbonate planes is however found to be higher when the distances are within 4-6 Å than when the distances are within 6-10 Å.

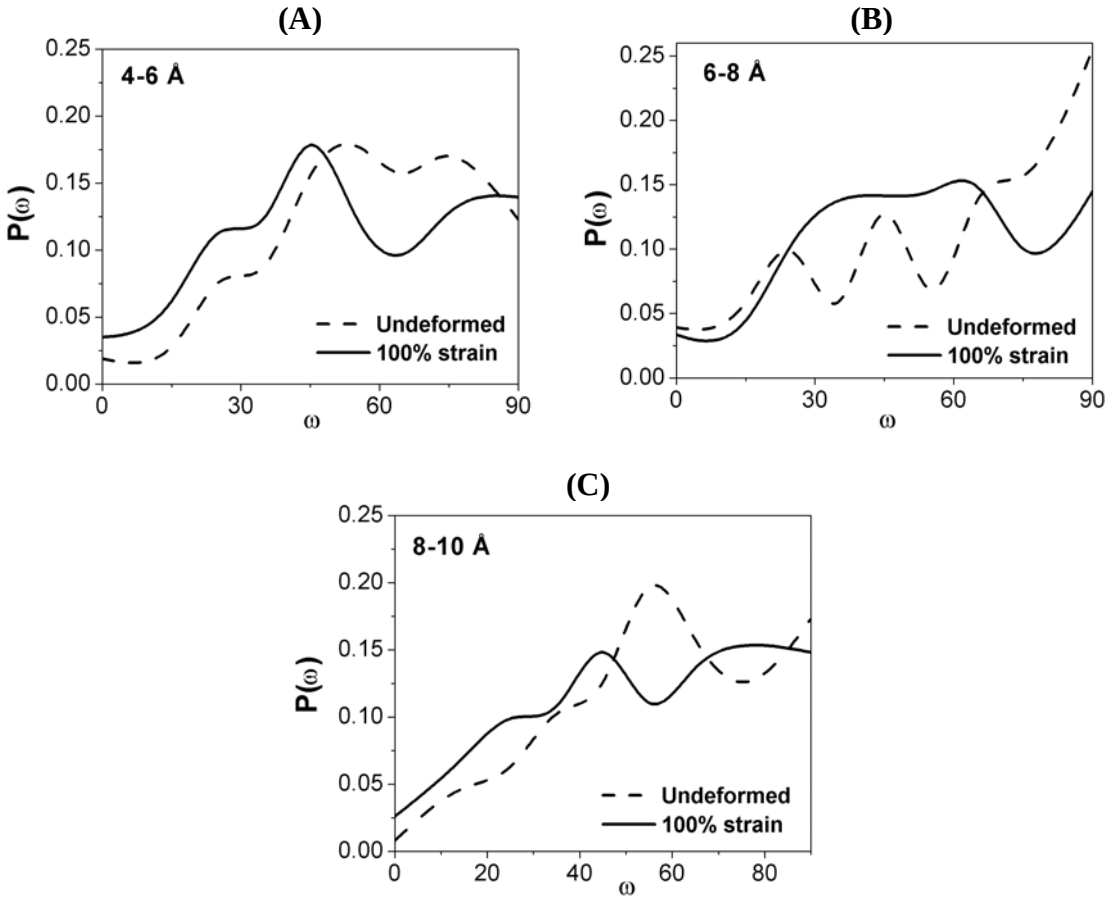

Figure 7.10. Probability distribution of the angle between nearest neighbour carbonate planes in BPAPC oriented samples at different distance intervals as a function of deformation. Results are shown for the undeformed sample and100% strained sample where the distances between the carbonate groups are between (A) 4-6 Å, (B) 6-8 Å, (C) 8-10 Å

NMR studies on plastically deformed BPAPC samples by Utz et al. up to a total compressive strain 68%, showed that there is very little change in the local packing of the

carbonate groups during the deformation process.[7] Distance factors of the carbonate carbons after deformation were found to resemble very similar to that before deformation. The distribution curves curves ($P(\omega)$) shown in Figure 7.10 suggest a clear tendency towards parallel orientation of carbonate planes due to deformation.

Analysis of the packing of inter carbonate planes and inter phenylene ring planes here clearly indicates a better orientation to stretching direction and a parallel packing upon deformation. NMR studies indicate a tendency for phenyl ring planes to orient parallel to one another upon deformation. For the carbonate groups, NMR shows no appreciable differences in the packing of carbonate groups in BPAPC deformed by applying a compressive strain of about 68%. But at the same time the values of the distance factors for the carbonate groups were almost higher by about 6% after deformation over the entire spectral range. This increase in the distance factor values was also observed in the distance factor spectra for the phenyl groups. According to Utz et al., if the density increase of BPAPC upon deformation is responsible for the increase in distance factor values, a 10 fold increase in density is required to explain the higher distance factor values whereas experiments have shown that the increase in density for BPAPC due to deformation is only 0.2-0.3%.[37,70] Hence the increase in distance factor value observed was attributed to the changes in the pair correlation functions between the labeled segments in BPAPC. Reorientation of the carbonate planes is not as prominent as in the case of phenyl rings (which are clearly orienting parallel to each other due to deformation as confirmed by NMR measurements). Present results on the intermolecular packing of carbonate planes suggest that at lower strains the distribution pattern is similar to that of the undeformed sample. But, appreciable differences in the packing of carbonate groups and tendency for parallel alignment is seen for samples oriented at 100% strain as shown in Figure 7.10.

7.3.1.4. Torsion distributions during deformation

In this section, discussion is provided on the changes in the population and distributions of the various dihedral angle torsional states for the BPAPC chain as a result of uniaxial tensile deformation. For the undeformed sample, plots correspond to the three initial starting amorphous structures. For oriented structures at different values of strain, the plots contain

contributions from the 9 simulated structures (at a particular strain, 3 cells deformed along 3 stretching directions). Hence it should be kept in mind that the number of data points in the plots corresponding to oriented structures is three times more than that in the undeformed structure. The definition of the various dihedral angles in the BPAPC repeat unit is given in Figure 7.11 and this is in accordance with the RIS model definition provided in chapter 3.

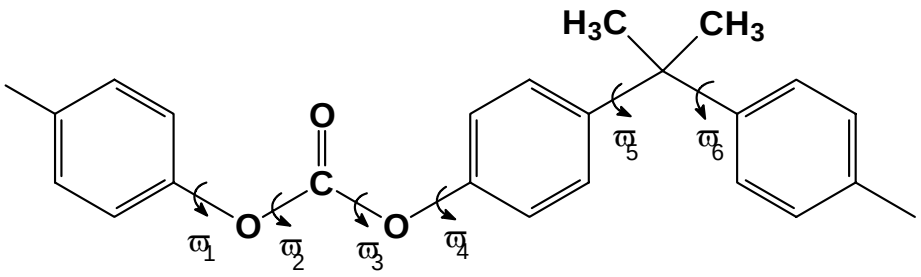

Figure 7.11. Schematic of BPAPC chain segment with the definition of various torsions

For all the torsional distributions shown here for the undeformed BPAPC sample, one finds a striking similarity to the contour plots obtained from conformational analysis on the polycarbonate model compounds (data presented earlier in section 3.3.1 in Chapter-3). The population density of the different torsions is found to be higher at their respective RIS torsional states, although there is a scatter of values around this region. NMR experiments on BPAPC bulk amorphous structures have shown that the torsional distribution in the bulk state are very similar to the RIS states.[71,72] NMR studies have also revealed that the overall conformational distribution is not affected appreciably due to deformation.[7] Conformational characteristics of the carbonate group are affected slightly upon deformation as revealed by NMR study.[7] The distribution for the (ϕ_3, ϕ_4) pair is shown in Figure 7.12 for the undeformed sample as well those for the oriented structures. The ϕ_3 torsion (carbonate group) is well defined with maximum population at states close to 0° followed by torsional states around 180°. The ϕ_4 torsion (Ph-O) is highly disordered with the entire range from –180° to 180° being equally populated in the undeformed sample as well as in the oriented samples. In the initial stages of deformation, (ϕ_3, ϕ_4) distribution shows some population density at (±180°, ±90°). As the deformation progresses, ϕ_4 in this area gets distributed over the entire range with ϕ_3 still around 180°. At 100% strain it is seen that, the ϕ_3 torsions move towards a value

of zero from either ±180°, i.e. the carbonate group tends to move towards the *trans* conformation, which is more extended compared to the *cis* state. From the studies of Utz et al. conformational distributions predicted by atomistic simulations agreed with those from experiments for the undeformed samples. At a deformation of ε = -0.68, distribution function predicted by simulations differed considerably from those experimentally observed. Simulations predicted a marked sharpening of the distribution of the Ph-O angles. Conformational distribution for the (ϕ_3, ϕ_4) from NMR data shows a probability density concentrated at ϕ_3 = 0 with ϕ_4 highly disordered. This is found to the case before and after deformation. Upon deformation, orientation of the phenyl planes is better defined, ϕ_4 exhibiting a pronounced peak at a value of 0°. Present simulation studies showed an increase in probability density at $\phi_4 \sim 0$ at 100% strain, the distribution still remains broad from results in the present study.

In the bulk state the carbonate group is found to be predominantly in the *trans* conformation (~90% of groups).[71,72] In the atomistically simulated structures reported in the literature, there is always an enhanced population of the *cis* conformers in the bulk which has been noted previously.[71] For the (ϕ_2, ϕ_3) torsional pair (Figure 7.13), which represents the conformation of the carbonate group, it is seen that for the undeformed sample the population density is maximum at (0°, 0°) which is the *trans*, *trans* conformation followed by (±180°, 0°) which is the *cis*, *trans* conformation. Upon deformation, there is a clear indication for the ϕ_2 and ϕ_3 torsions to move towards a value of 0° and thus attain the *trans* conformation. Analysis indicates that there is 8% increase in the population of *trans* conformation of the carbonate group in BPAPC when the sample is deformed to a draw ratio of 2 (ie 100% strain in the sample). Thus the strain in the sample leads to an increase in the *trans* (extended) conformation of the carbonate group and this aids in the extension of the polycarbonate chain and its alignment parallel to the stretching direction with imposed strain.

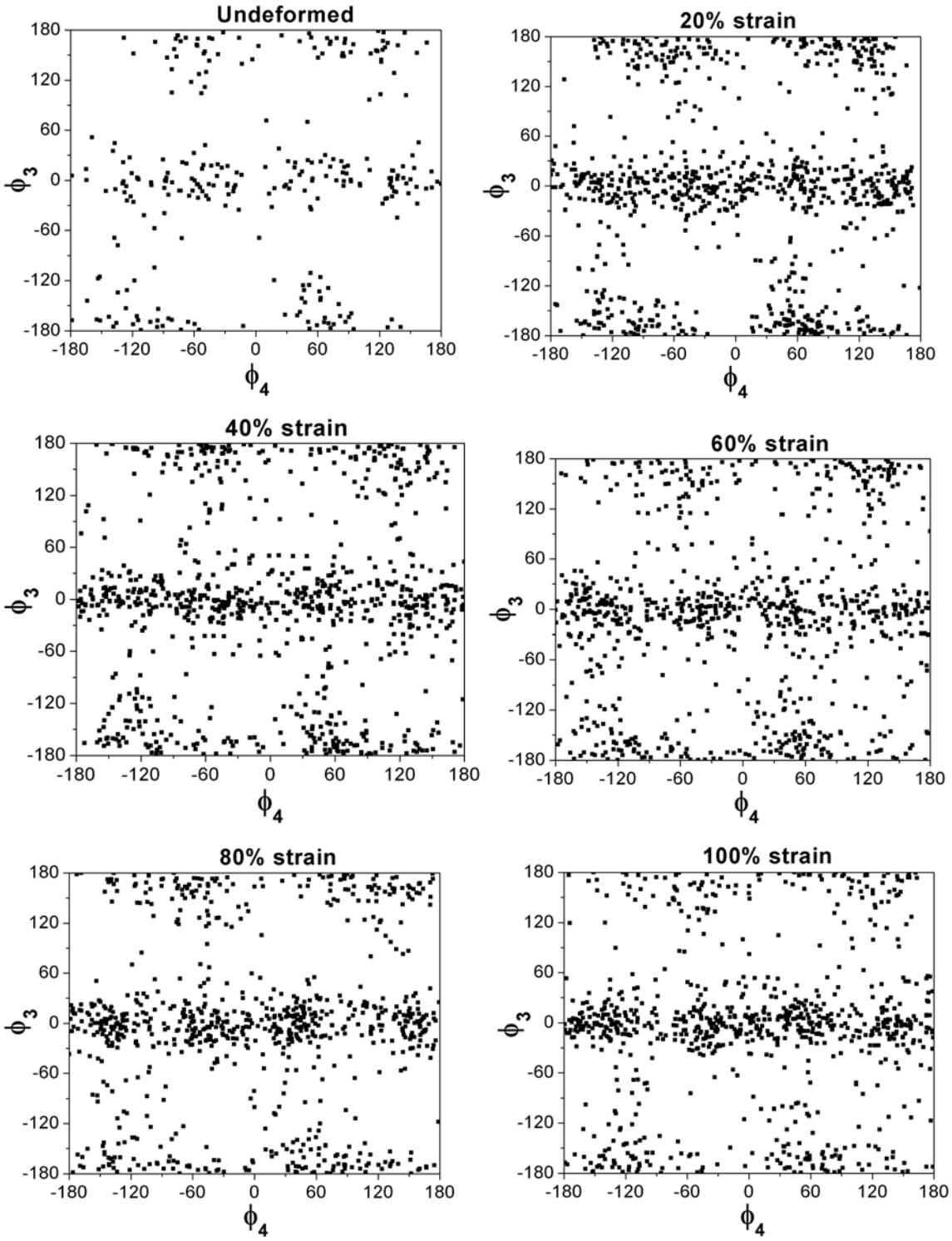

Figure 7.12. Torsional distributions ϕ_3 and ϕ_4 for BPAPC samples as a function of deformation

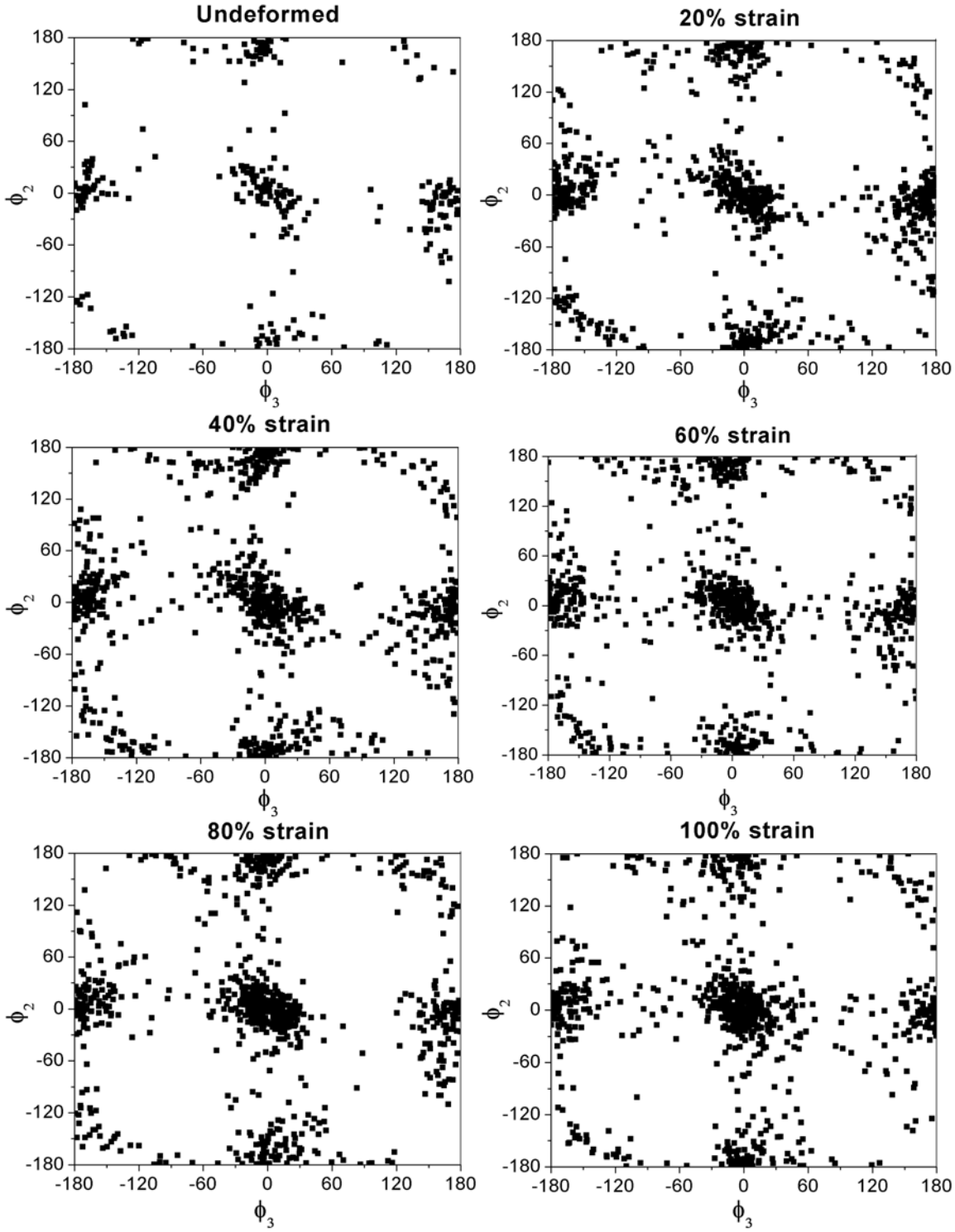

Figure 7.13. Torsional distributions ϕ_2 and ϕ_3 for the BPAPC samples as a function of deformation

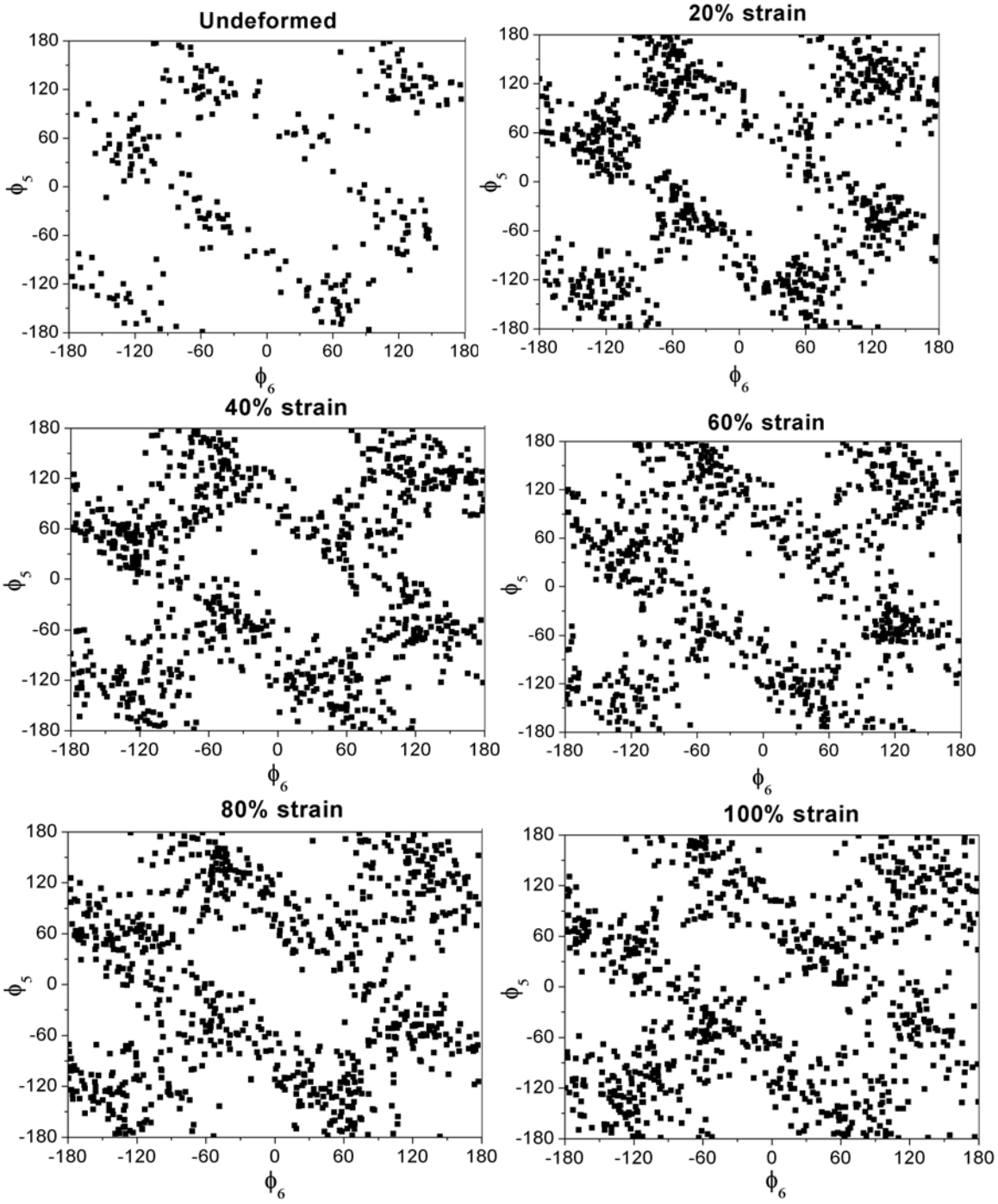

Figure 7.14. Torsional distributions ϕ_5 and ϕ_6 for the BPAPC samples as a function of deformation

The population distribution for pair (ϕ_5, ϕ_6) in case of undeformed sample of BPAPC (Figure 7.14) essentially resembles the contour plot obtained from conformational analysis of small chain segment, DPP that was presented earlier in section 3.3.1 in Chapter 3 of this thesis. This torsional distribution pattern is retained even during deformation and no

appreciable changes are observed due to the imposed strain. Only at about 100% strain, there is a slight increase in the population of angles at (0°, 0°) which represents nearly planar intrachain nearest phenylene rings. But this population is negligible and the distribution can be looked upon as being rather unaffected upon plastic deformation. This conforms to the results derived from NMR measurements by Utz et al.,[7] wherein the effect of deformation on the local conformations was found to be small compared to the overall substantial change imposed on the sample shape.[7] It appears that local rearrangements in the polymer chain due to the imposed deformation do not bring about appreciable changes in the conformational distribution in the oriented samples as compared to the undeformed sample. These local rearrangements are found to be sufficient to provide the longer-ranged and larger scale effect of chain orientations.

7.3.1.5. Chain conformational properties

The response of the polymer chains to deformation also occurs by the change in the chain dimensions and this is clearly seen from the simulations here. The chain conformational properties viz., end-to-end distance (R), radius of gyration (S) and characteristic ratio (C_n) for BPAPC due to deformation are given in Figure 7.15. As can be seen the chain dimensions show an increase with increase in strain in the sample. BPAPC chain gets extended by 31.6 Å as a result of 100% strain in the sample. One of the ways by which the polymer chains respond to imposed uniaxial deformation is by chain extension and this is clearly seen in the case of oriented BPAPC samples. The stretching of the polymer chains is brought about by the conformational rearrangements and also by the tendency of the chain segments to orient parallel to the stretching axis.

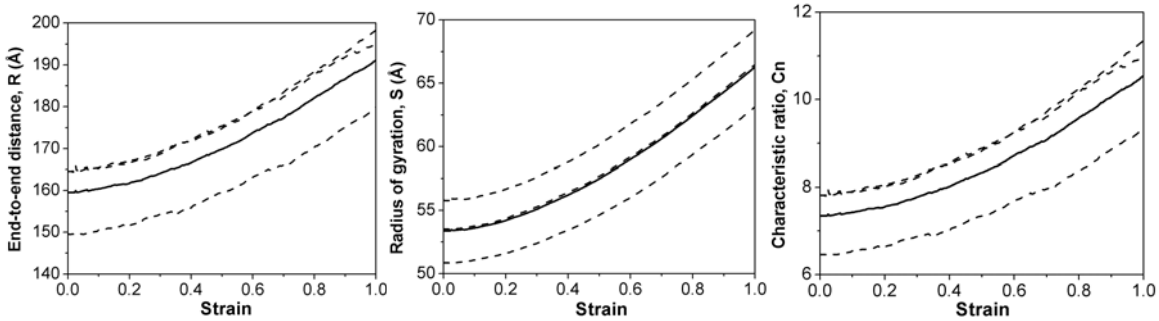

Figure 7.15. Chain dimensions of oriented BPAPC samples due to deformation. The dotted curves represent the three samples each averaged over three simulations along X, Y and Z directions. The solid curve is averaged over all the three samples

7.3.2. Uniaxial Deformation of Substituted Polycarbonates: DMPC and DMBPC

7.3.2.1. Energetics

The averaged potential energy curves derived from the uniaxial deformation of DMPC and DMBPC simulations are given in Figure 7.16. It is seen that the energy increases linearly with strain at lower values of strain. At higher strain values, the increase in energy proceeds in a non-linear fashion for the different samples corresponding to each polycarbonate. Jaggedness in energy is seen in these polymers also as in the case of BPAPC.

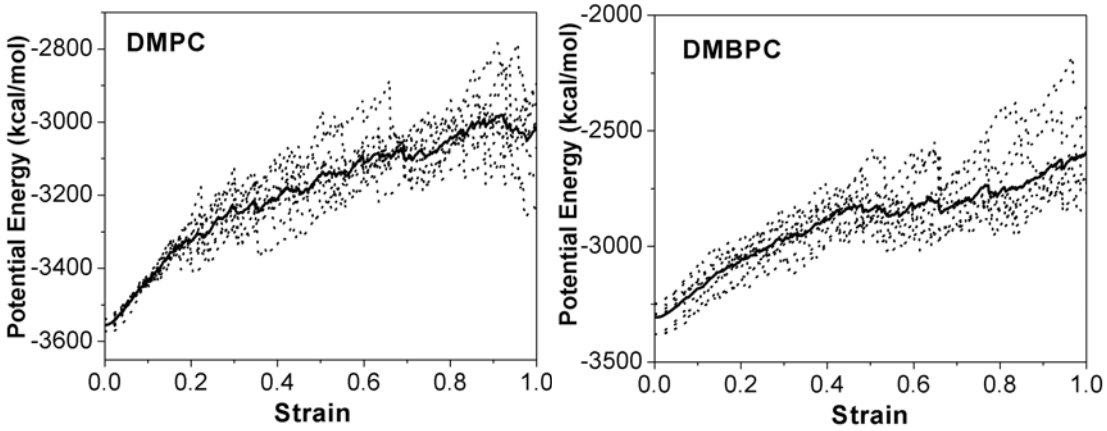

Figure 7.16. Variation of potential energy with uniaxial strain for DMPC and DMBPC. Solid curve is averaged behavior over three independent microstructures and three different stretching directions. Dotted curves correspond to individual sample stretching simulations

7.3.2.2. Orientation

The orientation of the different vectors in DMPC and DMBPC (definition given in Fgure 7.4 for BPAPC) during uniaxial deformation simulations are provided in Figures 7.17 and 7.18 respectively. The changes in orientations of the phenyl and carbonate vectors during deformation follow qualitatively similar behaviour as seen for BPAPC. In substituted polycarbonates as well, main chain vectors, viz., phenyl and carbonate (Oz-Oz) vectors show clear tendency to preferentially orient along the chain backbone which gets aligned increasingly parallel to the stretching direction in response to the deformation. At 100% strain the orientation function for Oz-Oz vector has a slightly higher value than that seen for the phenylene 1-4 axis vector in both DMPC and DMBPC (this was found to be the case for BPAPC also). The phenylene and the carbonate group vectors reorient by about 14.4° and 16.4° respectively towards the stretching direction at about 100% strain in the case of DMPC. For DMBPC, the reorientation of the phenyl and carbonate vectors is by 14.4° and

16.5° degrees. The carbonyl bond vector similarly orients perpendicular to the main chain as the stretching progresses. The reorientation behavior of the carbonyl bond vector in DMPC and DMBPC is different from that observed for BPAPC. In BPAPC, the reorientation of this vector is not appreciable (by applying 100% strain in the BPAPC sample the reorientation of the carbonyl bond vector is only by 3°). In DMPC and DMBPC, it is observed that the vector continuously reorients perpendicular to the stretching direction in a smoother fashion as the stretching progresses. The total reorientation of the carbonyl bond vector towards the stretching direction at about 100% is by about 6.3° (DMPC) and 6.2° (DMBPC).

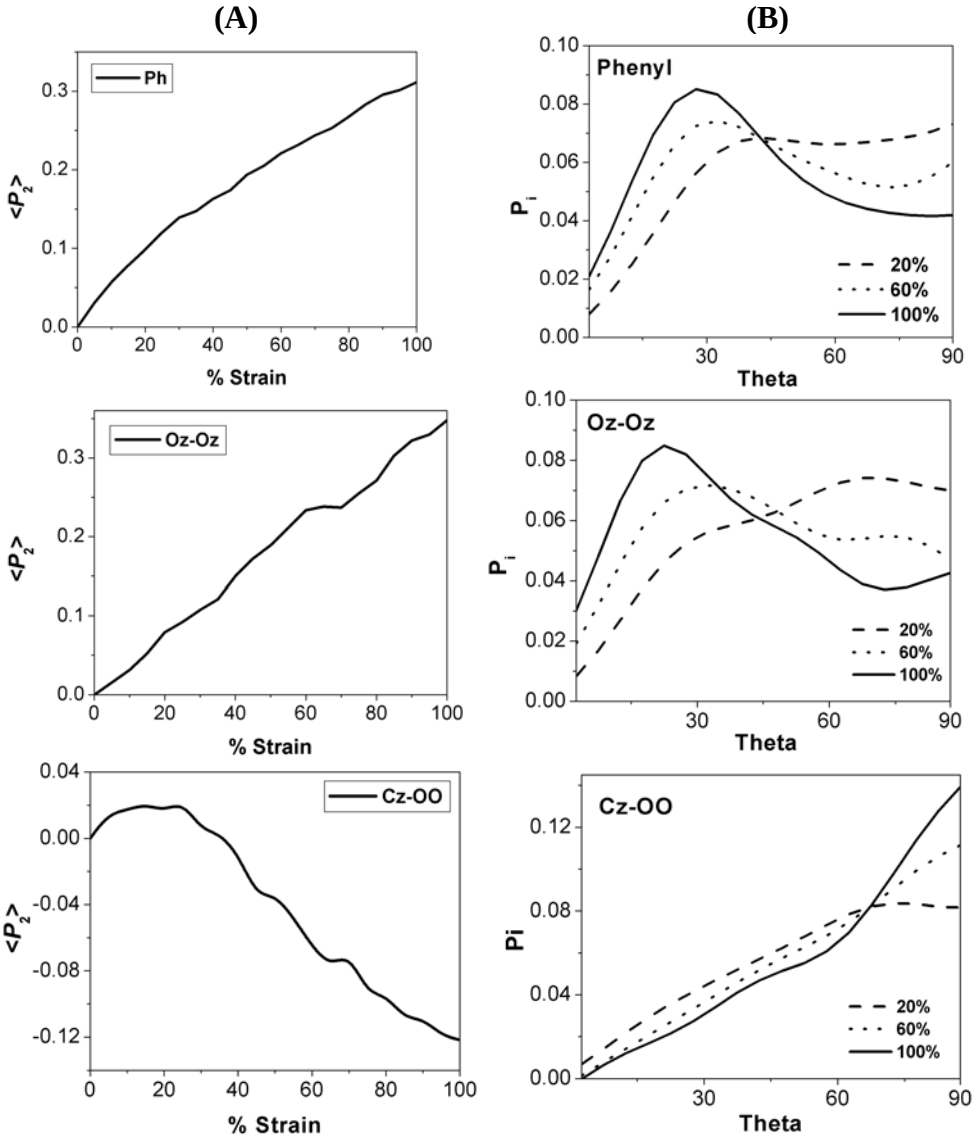

Figure 7.17. **(A)** Orientation functions of individual group vectors in DMPC as a function of strain. Vectors are defined in Figure 7.4. **(B)** Probability distribution of the angle between specified vectors and the stretching direction at different % strain

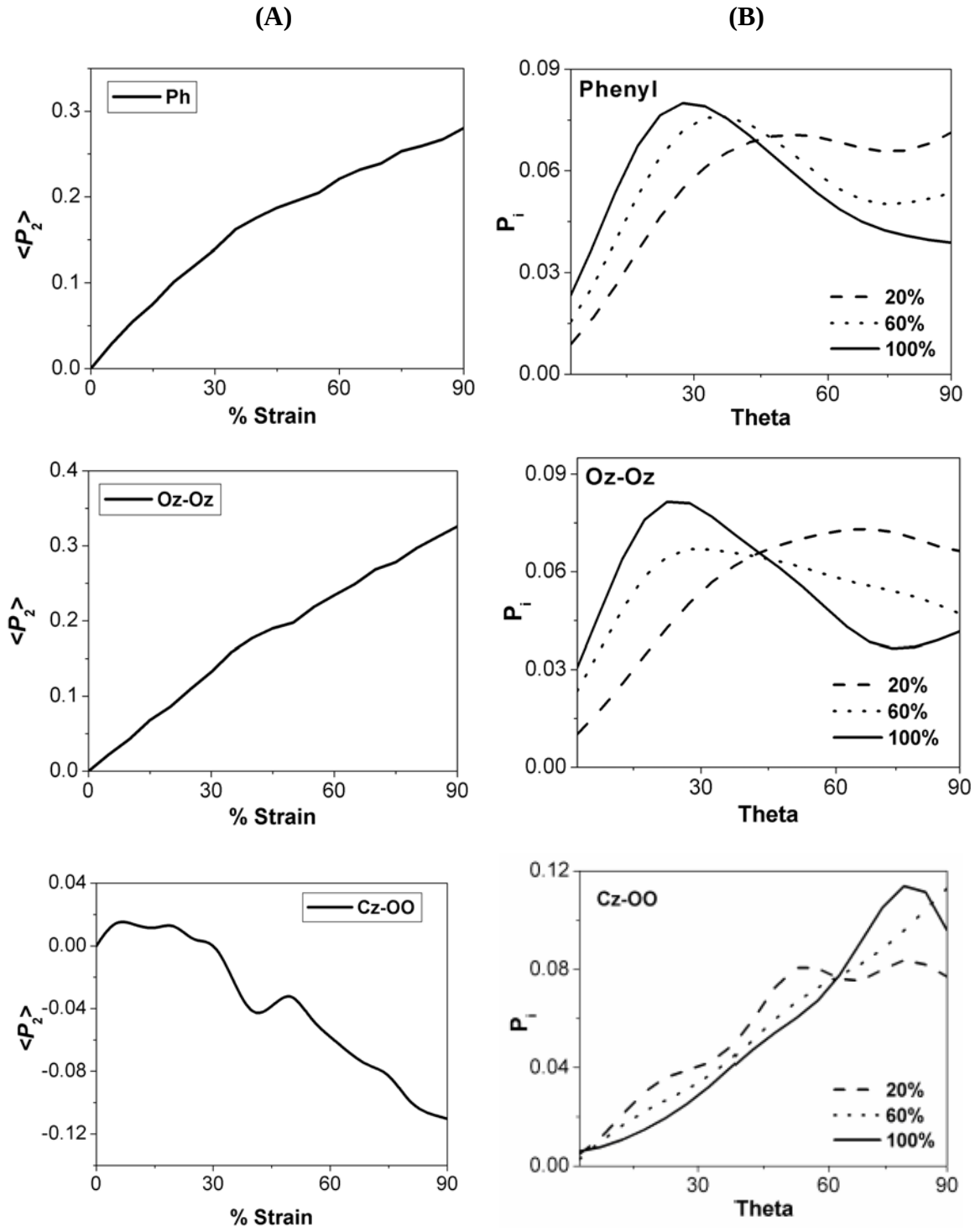

Figure 7.18. (A) Orientation functions of individual group vectors in DMBPC as a function of strain. Vectors are defined in Figure 7.4. **(B)** Probability distribution of the angle between the specified vectors and the stretching direction at different % strain

The probability distribution of the angle between the specified vectors in DMPC and DMBPC with respect to the stretching direction is also provided in Figures 7.17 and 7.18 respectively. The vectors that are parallel to the main chain, viz., the carbonate (Oz-Oz) and the phenylene 1-4 axis, exhibit a tendency to move towards a increasingly parallel orientation with respect to stretching direction with increasing levels of imposed strain. The peak maximum of distribution function shifts more and more to lower values of the orientation angles upon deformation. At 100% strain, prominent peaks with maximum probabilities are seen for angles in the range 25-30°. In addition, as the strain in the sample increases, probability for angles close to zero increases with a corresponding reduction in the probability for perpendicular orientation (angles close to 90°). For the carbonyl double bond vector, the angle between the vector and the stretching axis gets populated more in the range close to 90° with a concomitant reduction in the probability for angles close to 0°. These results suggest that in the case of DMPC and DMBPC, the polymer chain tends to align parallel to the stretching direction upon deformation, which is observed as described earlier in the case of BPAPC as well.

7.3.2.3. Torsion distribution accompanying deformation: DMPC

The torsional distribution plots as a function for deformation in DMPC is shown in Figure 7.19, Figure 7.20 and Figure 7.21. As was seen in the case of BPAPC, the distribution patterns are very much identical to those derived from conformational analysis of small chain fragments for the undeformed bulk sample and there are no appreciable differences in the distribution pattern during the course of deformation. The carbonate group torsions (ϕ_2, ϕ_3) are predominantly in the *trans* conformation in the undeformed sample and this conformation gets more populated with increase in strain, as seen from the increase in the probability density close to 0°. The RIS state for the phenyl-oxygen bond torsions (ϕ_1 and ϕ_4) were found to be near ±90° (section 3.3.1 in Chapter 3). In bulk undeformed sample, these torsions are disordered and spread out in the range from –120° to +120° with the lower probability density near 0°. For the oriented structures, the torsions get more scattered and spread out in the range from –150° to 150°. For BPAPC, ϕ_1 and ϕ_4 torsions are found to be distributed in the entire conformational space (-180° to 180°) in the oriented samples. The present torsion

data on DMPC indicates that the carbonate group undergoes appreciable reorientation (as also seen from the orientation curves) along with conformational changes. The *trans*, *trans* states of the carbonate group gets increasingly populated across the chain and this occurs together with the appreciable conformational changes taking place across the Ph-O bond (ϕ_1 and ϕ_4) which other wise in the single chain and bulk were restricted to a relatively narrow range. The distribution plot for the (ϕ_5, ϕ_6) torsion in the undeformed sample is identical to those derived from isolated chain fragments (section 3.3.1 in Chapter 3). It is seen that the distribution is rather unaffected by deformation even till 100% strain. Except for the fact that the torsions which were very well defined and were in a narrow range at the beginning of deformation gets more scattered in the same region thus leading to a broader distribution pattern. Therefore deformation leads to changes in conformation of the carbonate group, but the bisphenyl part remains relatively unaffected. This can be explained based on the effect of the *ortho* mehyl groups which is seen to be responsible for the conformational reorientation of the carbonate group in DMPC. BPAPC which is devoid of this kind of substitution, does not show much of a conformational rearrangement (except for an increase in the % of *trans*, *trans* conformations of the carbonate group which is observed in DMPC as well) for the carbonate torsions.

7.3.2.4. Torsion distributions accompanying deformation : DMBPC

The dihedral distribution patterns in DMBPC at various stages during deformation are provided below in Figure 7.22, Figure 7.23 and Figure 7.24. Overall, the general behavior of the torsions remains the same as discussed earlier for DMPC where appreciable changes were not observed for torsions ϕ_5 and ϕ_6 during deformation. Carbonate group torsions increasingly move towards the *trans, trans* conformation with an increase in strain. The Ph-oxygen torsions are flexible and respond to deformation by occupying a much broader conformational space with imposed strain. The torsions ϕ_5 and ϕ_6 in DMBPC are inequivalent. ϕ_6 torsions occupy the entire conformational range from –180 to 180° but the ϕ_5 torsions are restricted to narrow range (which is true for the single chain fragments and for the bulk undeformed sample as seen earlier). These torsion characteristics of the bisphenyl ring are retained during the entire course of deformation studied here.

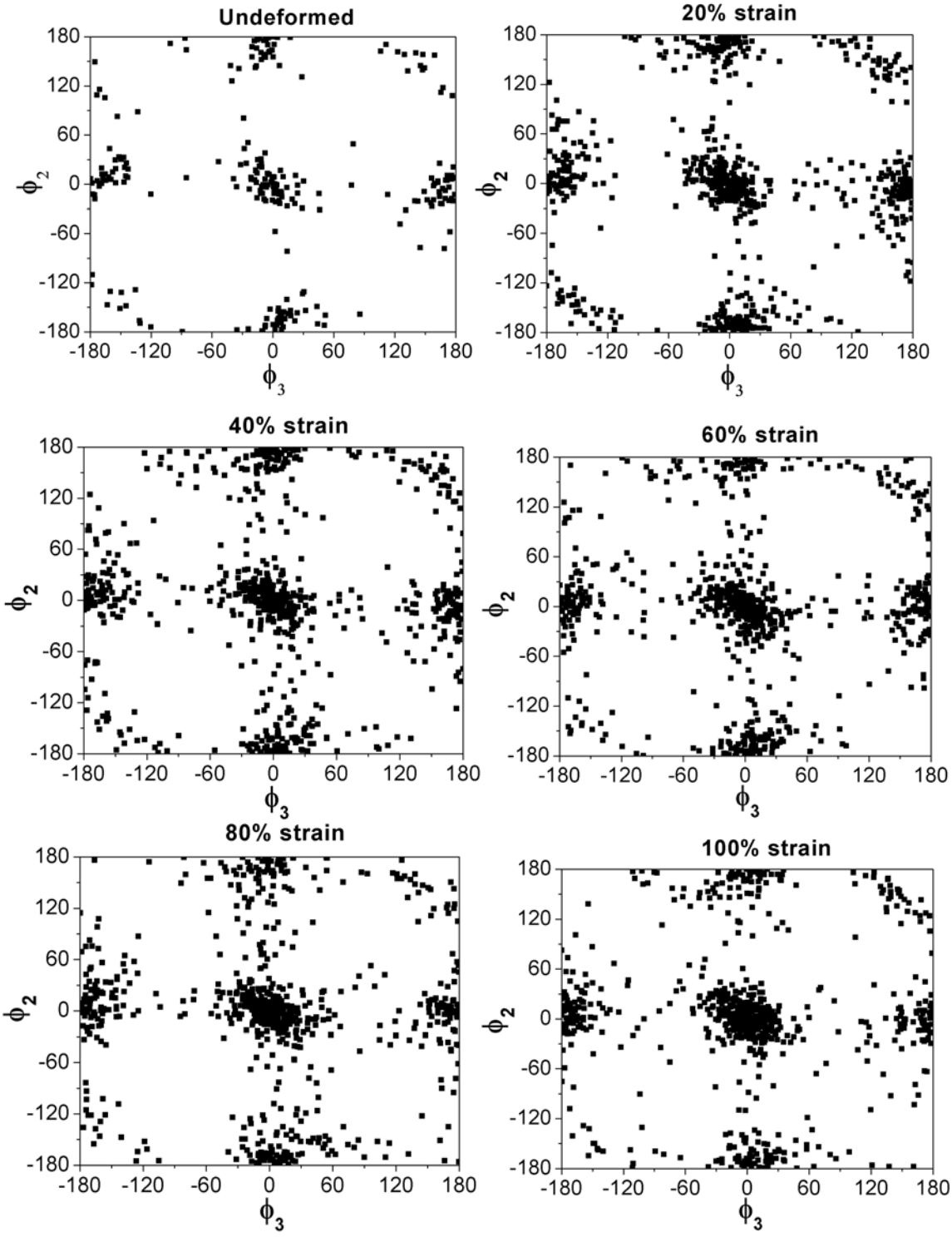

Figure 7.19. Torsional distributions ϕ_2 and ϕ_3 for the DMPC samples as a function of deformation

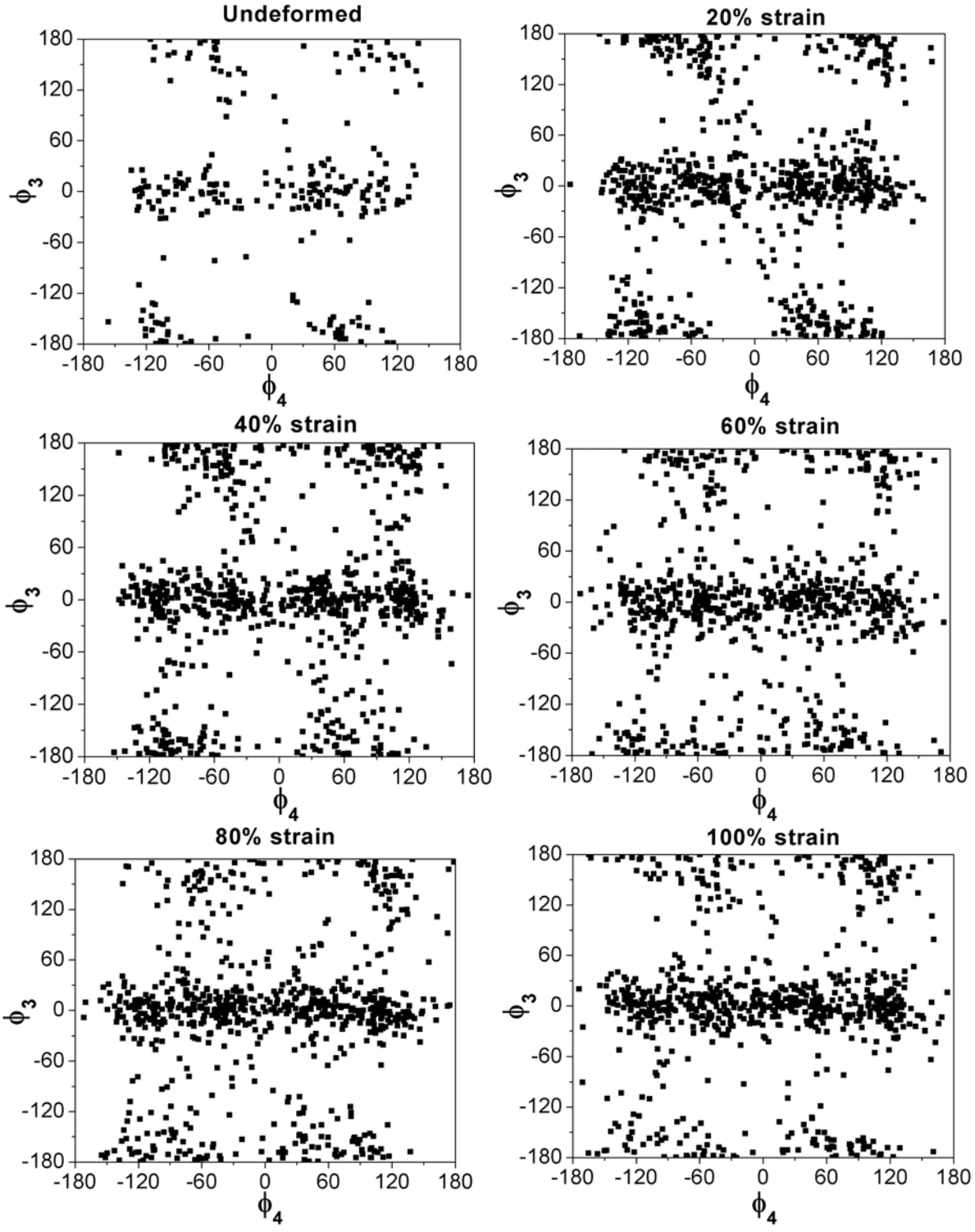

Figure 7.20. Torsional distributions ϕ_3 and ϕ_4 for the DMPC samples as a function of deformation

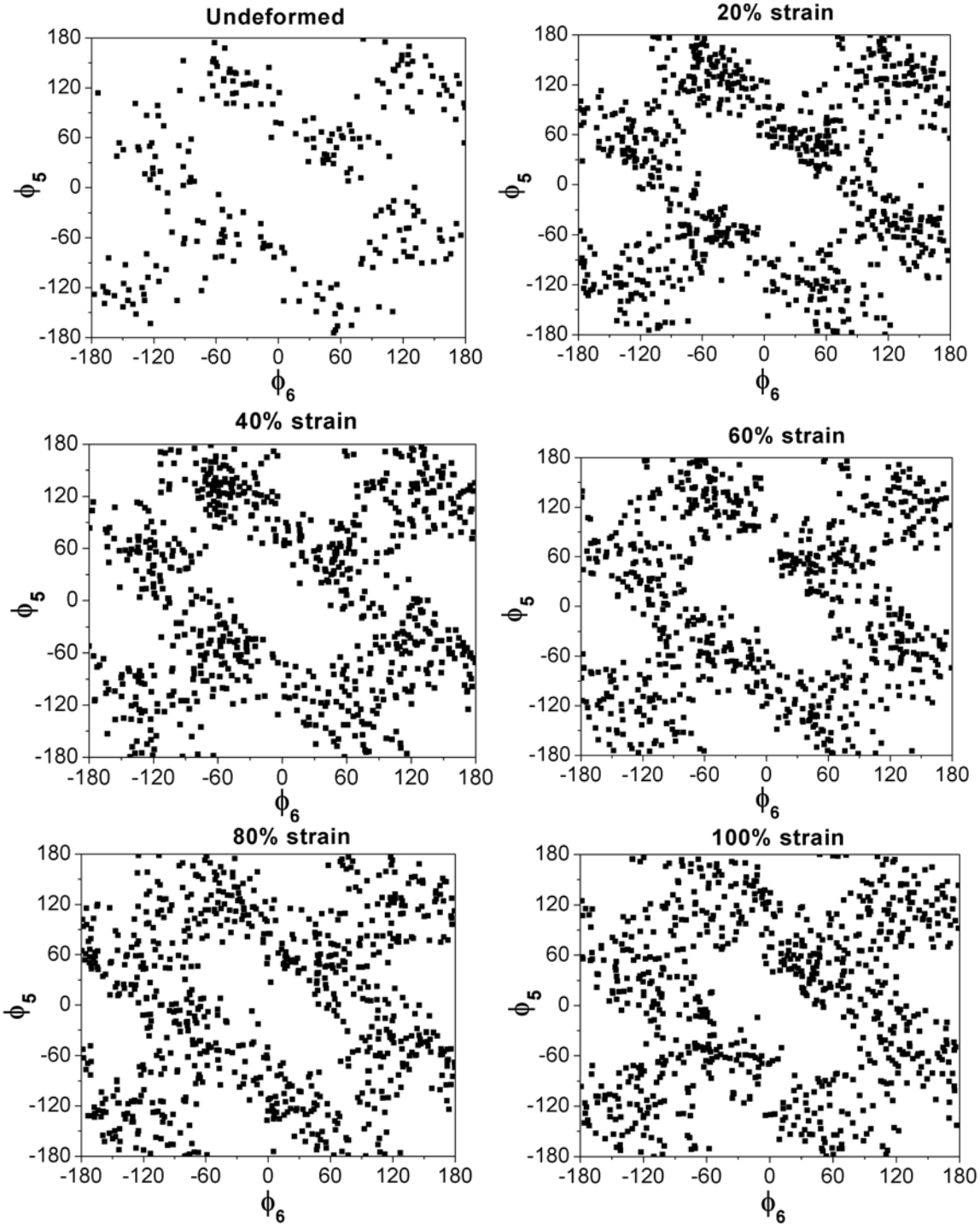

Figure 7.21. Torsional distributions ϕ_5 and ϕ_6 for the DMPC samples as a function of deformation

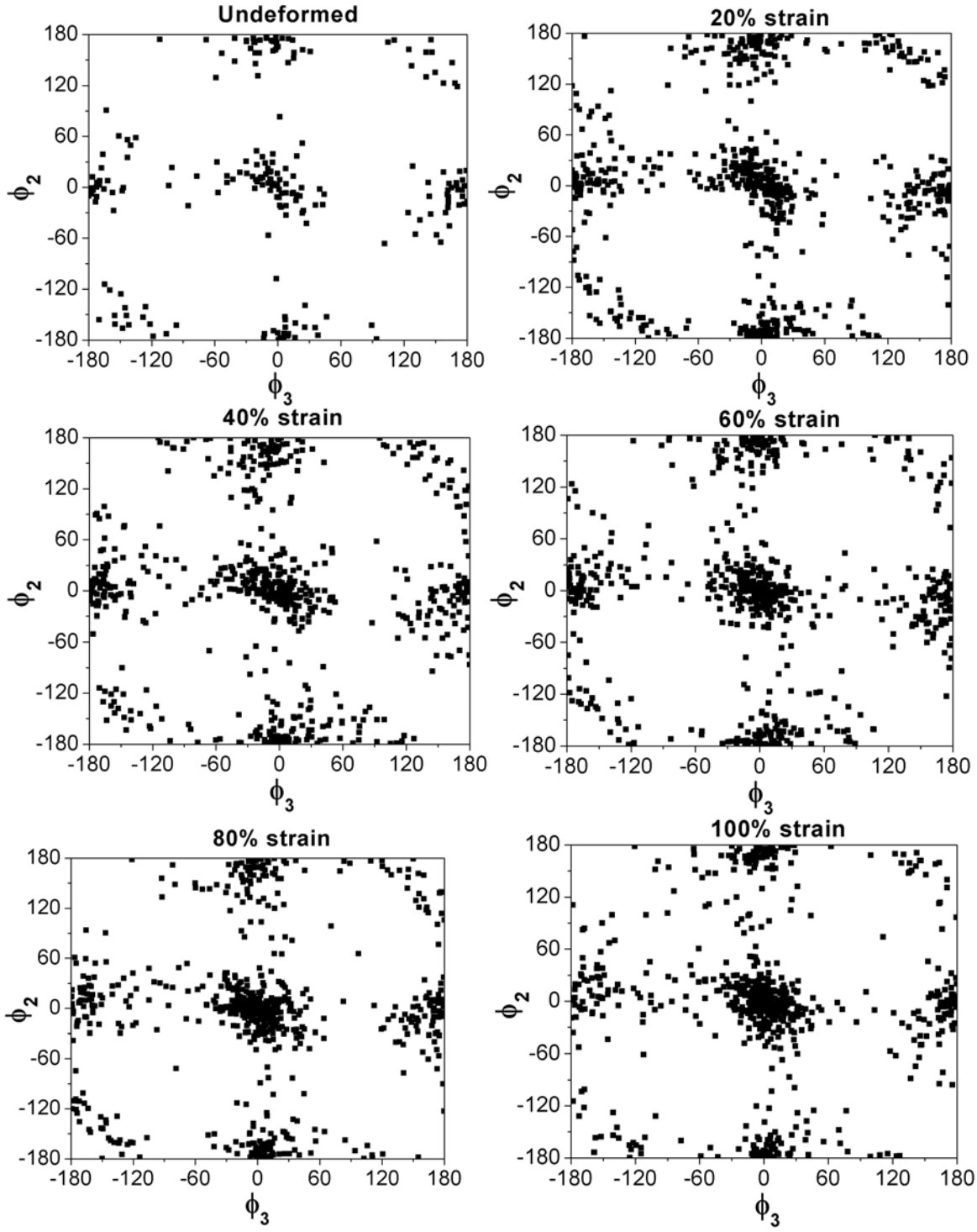

Figure 7.22. Torsional distributions ϕ_2 and ϕ_3 for DMBPC samples as a function of deformation

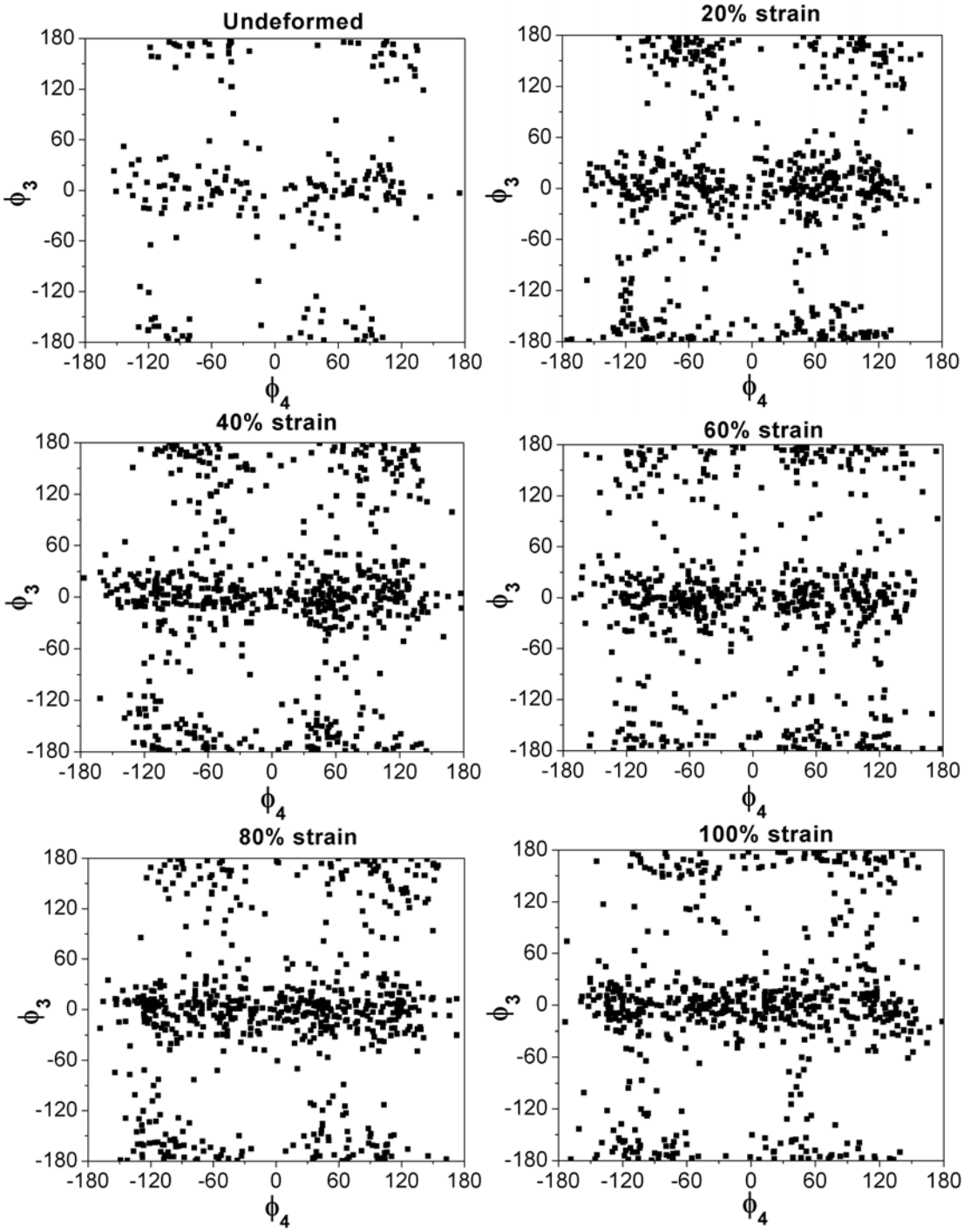

Figure 7.23. Torsional distributions ϕ_3 and ϕ_4 for the DMBPC samples as a function of deformation

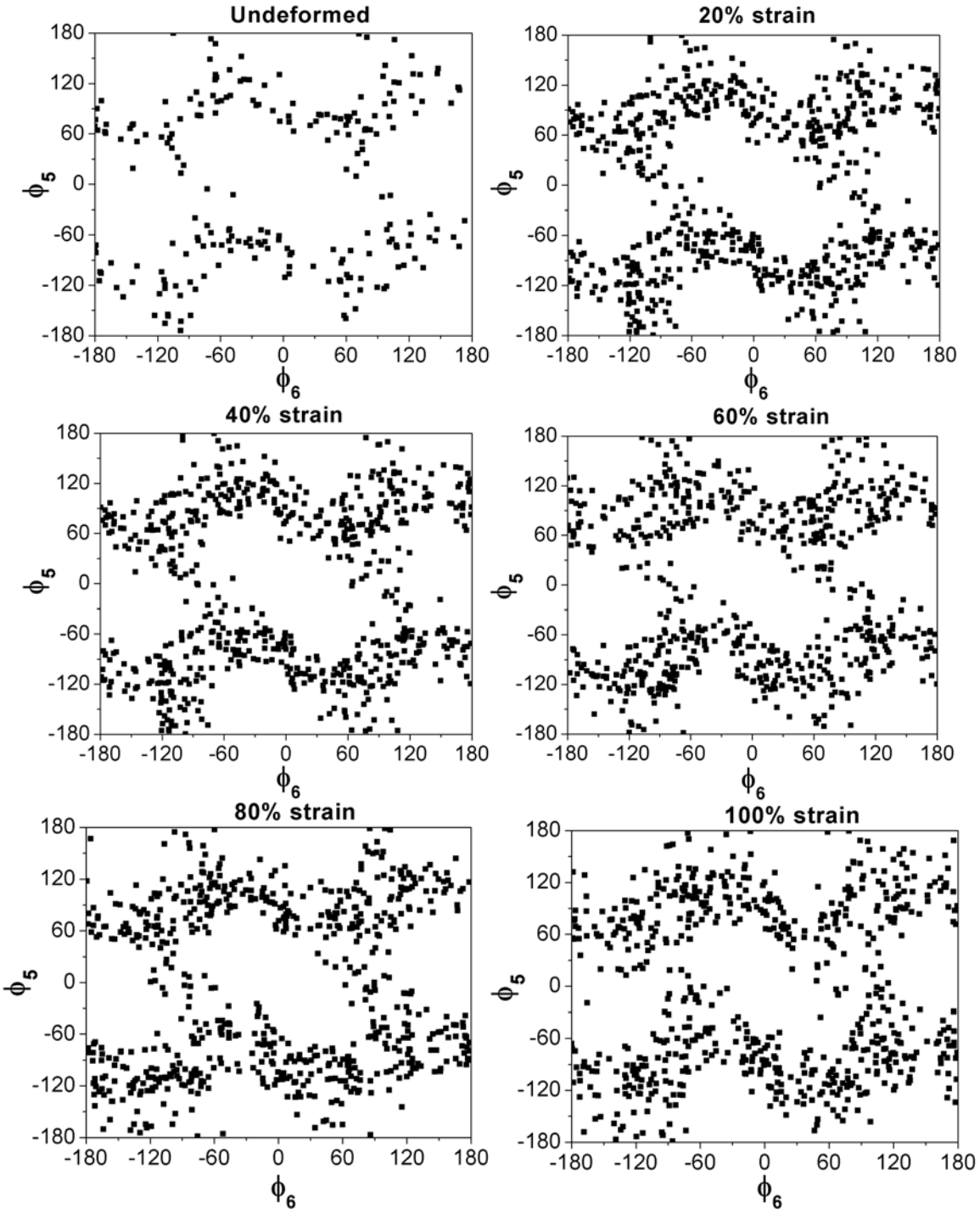

Figure 7.24. Torsional distributions ϕ_5 and ϕ_6 for the DMBPC samples as a function of deformation

7.3.2.5. Chain conformational properties of DMPC and DMBPC

The effect of deformation on chain dimensions in the case of DMPC and DMBPC are shown in Figure 7.25. Similar to BPAPC, the polymer chains in the case of DMPC and DMBPC

also show chain extension due to uniaxial deformation. For all the three polycarbonates chain dimensions increase as a function of deformation clearly indicating chain extension. Polymer chains thus respond to the imposed uniaxial strain by extension of the chains, orientation of the segments and the chain as a whole along the stretching direction. The end-to-end distance of the polymer chain increases by 36.6 Å (DMPC) and 35 Å (DMBPC) due to a total strain of 100%.

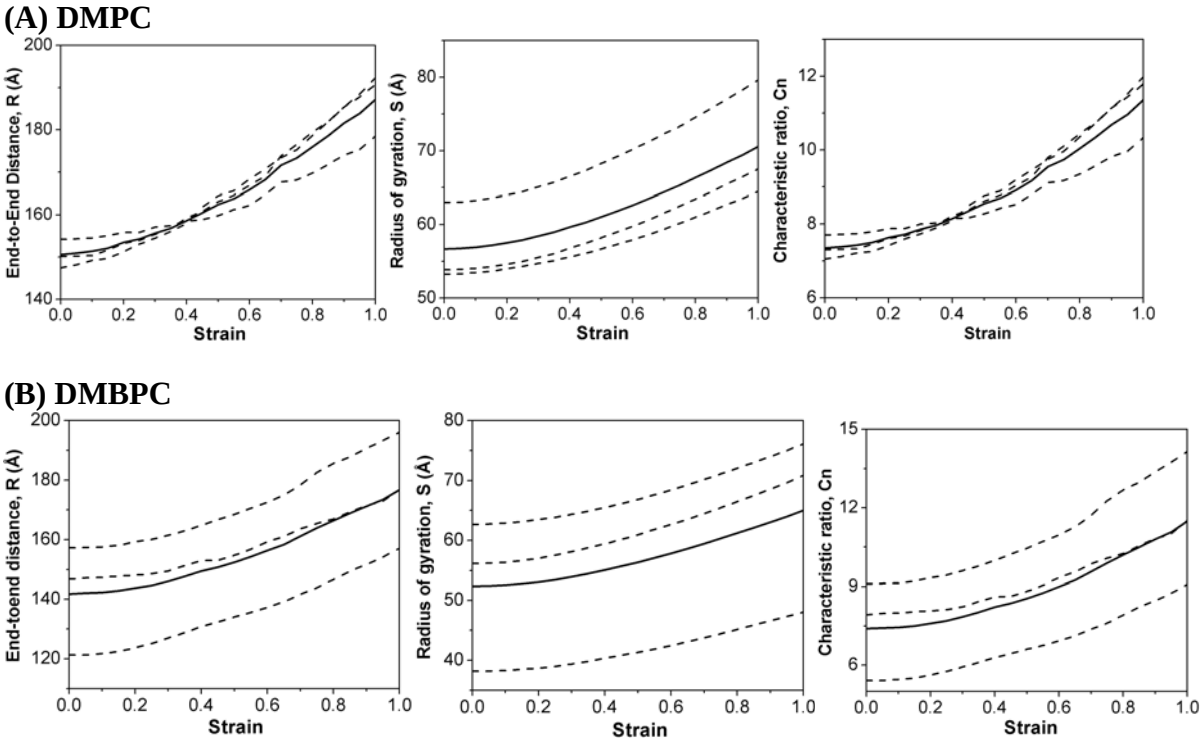

Figure 7.25. Chain dimensions of oriented (A) DMPC and (B) DMBPC samples due to deformation. The dotted curves represent the three samples each averaged over the three stretching direction simulations. Solid curve is averaged over all the three samples

7.3.3. Comparison of the orientation of BPAPC and substituted polycarbonates due to deformation

Figure 7.26 provides a comparison of the orientation characteristics of the phenyl and carbonate vectors due to deformation in the different polycarbonates studied in this work. The extent to which the phenyl groups orient during deformation is similar for all the three polycarbonates. This means that for the same amount of strain applied on the sample, there are no marked differences in the orientation behavior of the phenyl rings in these polycarbonates. Maximum value of the orientation achieved for the phenyl rings at 100%

strain is almost the same in these polycarbonates. For the Oz-Oz vector of the carbonate group, the PC's although follow the same trend of increasingly getting oriented towards the stretching direction, the extent to which these orientations happen during the course of stretching are different. At 100% strain, maximum orientation of this particular vector is achieved in the case of DMBPC followed by DMPC and then BPAPC. Considering the behavior of the carbonyl bond vector, appreciable differences are found between BPAPC and the other two substituted polycarbonates. The carbonyl bond vector is found to reorient by 3° in the case of BPAPC, whereas in the case of DMPC and DMBPC, this vector reorients by about 6.3° and 6.2° which is appreciable. Thus the orientation data derived in this work clearly brings out the differences in the response of the different groups to deformation in the various polycarbonates studied here.

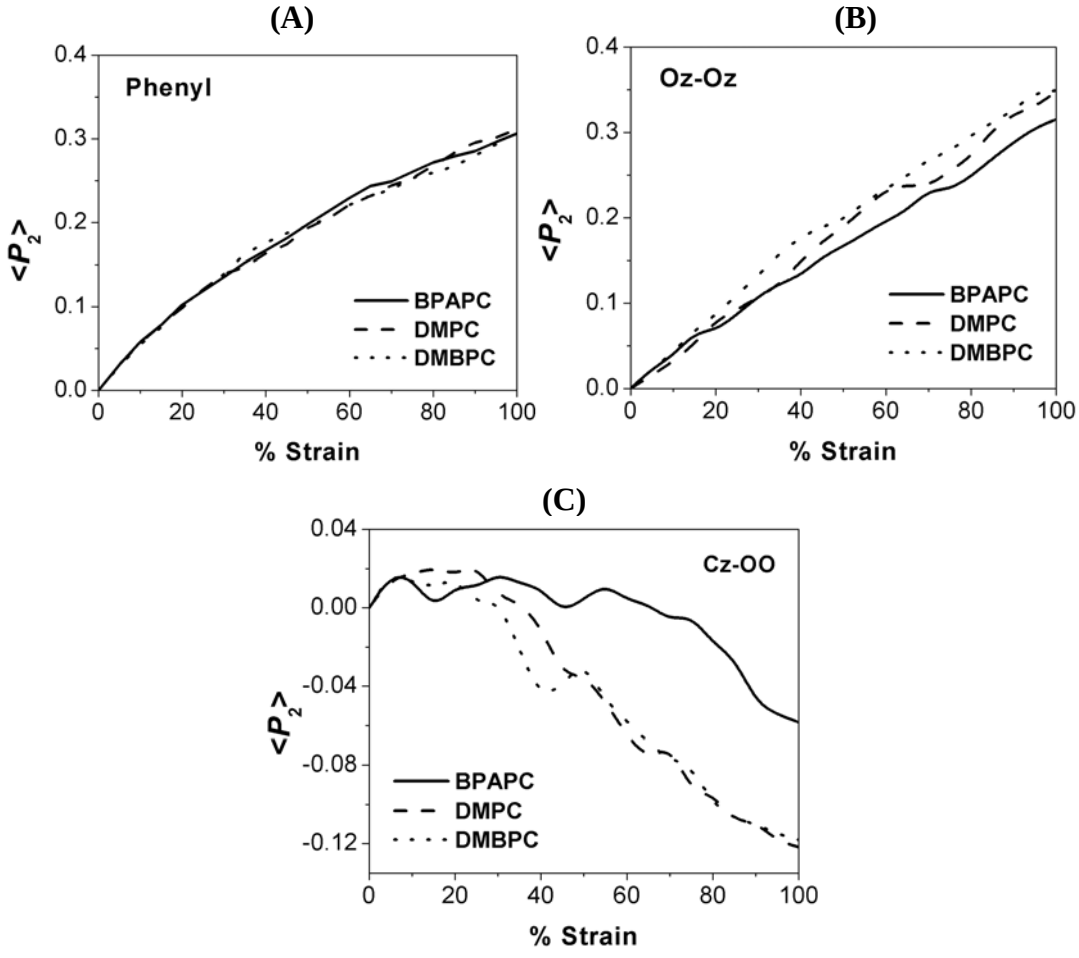

Figure 7.26. Comparison of the orientation functions of the **(A)** phenyl; **(B)** carbonate, Oz-Oz; **(C)** Cz-OO vectors for various polycarbonates studied

The phenylene rings orient in a similar fashion in all the three PC's. Whereas the orientation behaviour of the carbonate group (and specifically the carbonyl bond vector) for DMPC and DMBPC follow the same pattern and is markedly different from that of BPAPC. The extent to which the carbonate group reorients is more in the case of DMBPC than in DMPC. Thus, the *ortho* methyl groups or even the cyclohexyl group (DMBPC) do not have any effect on the orientation behavior of the phenyl rings. This is not true in the case of carbonate groups in which case its orientation is controlled by the *ortho* methyl groups, and which leads to appreciable differences in the vector orientation behavior between BPAPC on one hand and DMPC, DMBPC on the other. The difference in behaviour for DMPC, and DMBPC in comparison to BPAPC is due to the *ortho* methyl groups, which lead to an appreciable reorientation of the carbonate groups.

Orientation of the chain end-to-end vector as a function of deformation is shown in Figure 7.27. It can be clearly seen that the end-to-end vector is reorienting in a direction parallel to the stretching direction due to deformation in the case of all three polycarbonates. This behaviour is similar to that observed for the main chain vectors, viz., phenyl and carbonate groups. The difference in the orientation behaviour among the three polycarbonates clearly emerges as shown. The imposed deformation results in reorientation of the polymer chain in the substituted polycarbonates DMPC and DMBPC much better than in BPAPC. The polymer chain end-end vector reorients by 24.5º (DMPC) and 23.1º (DMBPC) where as in the case of BPAPC it is 17.5º. Structures in which the end-to-end vector is oriented perpendicular to the stretching direction (orientation function of about –0.5), uniaxial deformation does not bring about appreciable orientation of the vector parallel to the stretching direction and this is seen to be the case with BPAPC. For DMPC and DMBPC, in cases where the vector is aligned perpendicular to the stretching direction before deformation, reorientation towards the stretching direction occurs. Appreciable reorientation is observed for samples where the orientation of the end-to-end vector is fully random before deformation and this is the case with all three polycarbonates. In cases where the end-to-vector is aligned nearly parallel to the stretching direction (orientation function between 0.6 to 0.75) the vector moves towards a perfect parallel alignment at about 100% strain).

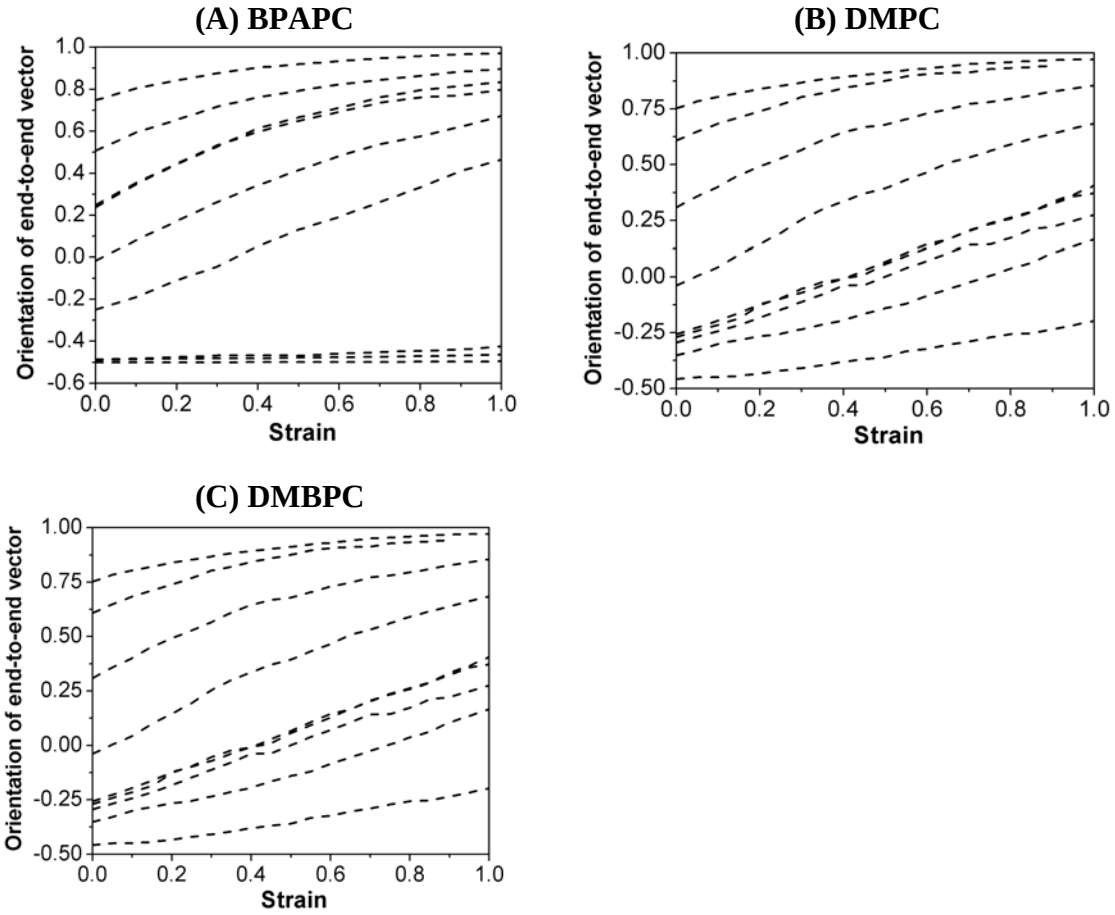

Figure 7.27. Comparison of orientation function of the end-to-end vector with respect to stretching direction as a function of deformation for (**A**) BPAPC; (**B**) DMPC and (**C**) DMBPC. Dotted curved correspond to the nine stretching simulations for each of the polycarbonate

7.3.4. Calculation of birefringence of oriented polycarbonates

7.3.4.1. Results using the direct method of polarizability transformations

Birefringence as calculated from the atomistic simulation of the uniaxial deformation of BPAPC and the two substituted polycarbonates, DMPC and DMBPC, as a function of strain is provided in Table 7.2. These results are obtained from the first method using transformations of individual group polarizability tensors into the laboratory reference frame of the bulk samples as a function of applied strain. The averaged orientation functions for the repeat units, which have been calculated from the orientation functions of the vectors constituting the backbone of the repeat units, are also given in Table 7.2. These are the averaged values over three independent samples and over three stretching directions. In

Figure 7.28 the birefringence calculated for BPAPC in the present study is compared with that experimentally measured by Wu[37] on glassy amorphous BPAPC at room temperature. Wu measured the birefringence of BPAPC samples stretched at room temperature, which were stretched above a draw ratio of 1.6 and these are provided in Figure 7.28 for comparison with the birefringence calculated for BPAPC in the present study.

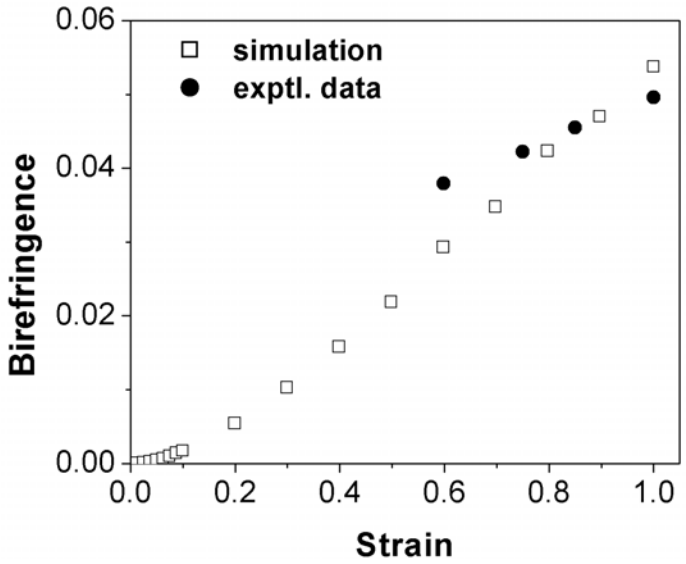

Figure 7.28. Comparison of calculated birefringence for BPAPC from the present simulation studies to that measured experimentally by Wu

As can be seen, the agreement between the calculated and the experimental birefringence values is fairly good especially above 70% strain. The experimental value for birefringence at a draw ratio of 2.03 is 0.0496. Te calculated value at 100% strain (draw ratio of 2) is 0.0537, which is within 8% of the experimental value. Wu's data showed that samples stretched below T_g exhibited slightly higher density than those samples stretched above T_g. DSC, density, XRD and IR measurements ruled out the possibility of stress induced crystallinity in the samples stretched below T_g. Higher density and higher birefringence in samples stretched below T_g were attributed to bond distortion during stretching. Thus when the BPAPC samples are stretched below T_g at room temperature there is an increase in density of the samples (0.15% increase in density at a draw ratio of 2.03), but in our calculations, density is maintained constant during the stretching simulations. Also Wu had observed that films stretched below T_g exhibited higher birefringence than those stretched above T_g and he attributed this to be due to the distortional birefringence in the

samples stretched below T_g. Data was corrected for this contribution and only the orientational part of the birefringence was used in turn for the calculation of intrinsic birefringence of BPAPC. The focus in the present work is not the calculation of intrinsic birefringence, but to understand and develop a methodology to calculate the birefringence of glassy amorphous polycarbonates from atomistic simulations and to elucidate the structural and conformational contributions to birefringence.

It can be seen that the comparison between the experimentally measured birefringence and the values calculated from the atomistic simulation approach outlined here is quite good. Below are a few points, which are discussed in some detail, and to be kept in mind while comparing the birefringence obtained from the atomistic simulation approach with the experimental values. The experimental measurements of birefringence are most often performed on polymer films using a light source at a particular temperature. The atomistic simulation methodology of the uniaxial deformation differs in many ways from the actual macroscopic experiments and these differences must be kept in mind when comparing simulations to experimental data. Experimentally, most studies dealing with uniaxial orientation are performed at constant deformation rates, which means that the stress increases as the material becomes more oriented and therefore harder to deform. This yields a linear relationship between draw ratio and time. In the simulation procedure for uniaxial orientation employed in the present study, samples are stretched by applying a strain on the periodic box and these are then relaxed to attain a configuration of lower energy in the potential energy surface. The temperature is included by using the amorphous bulk density of the polymer corresponding to room temperature, other than which there is no thermal activation, time also does not figure and therefore the rate of deformation is also undefined in this simulation procedure. The approach here is quasi-static in nature. In the present study, density is maintained constant during the deformation in the simulation procedure. In the case of BPAPC, experimental data shows that a simulation procedure with constant intrinsic poisson ratio assumption will not be valid at higher strains. In experiments stress is applied to the sample, which propagates throughout the sample through the chains and entanglements are thought to be playing a key role in this process. In the simulation procedure stress is applied to the polymer by deformation of the cell which defines the periodic boundary conditions. Although by using a constant stress MD algorithm, the rate of deformation and temperature

can be directly incorporated into the simulation protocol, and stress can be applied directly, the method is limited by the time scale of the simulations. Another aspect of the simulations is that, atomistic simulations generally are found to overestimate the orientation parameters as was seen in the case of uniaxially compressed BPAPC where the simulation order parameters were higher than the values obtained from NMR. Although there is qualitative agreement, simulations try to overpredict the orientation functions, this being attributed to either the finite size of the simulation cell or the absence of relaxation mechanism in the simulations.[6,7] The higher value of the birefringence derived from the simulated oriented BPAPC structure at 100% strain could be due to this overestimation of the orientation function in deformation simulations.

Coming to the calculation method for birefringence adopted here, first step of which involves tensorial addition of group polarizability tensors comprising the polymer chain via the valence optical scheme. In case of BPAPC, group polarizability tensors are employed, which have been derived from depolarized light scattering measurements of monomer fragments in CCl_4 solution. Thus these tensors, which have been determined from measurements in dense phases implicitly have contributions from the neighbouring inductive effects. When using these polarizability tensors for the calculation of birefringence, one thing to be noted is that the polarizabilities were measured at a wavelength of 632 nm. In Wu's measurement of birefringence the wavelength of light used was 546 nm which can lead to a 3% higher value than at the former wave length as was pointed out by Pietralla and Pieper[34]. Birefringence calculated as a function of strain contains contributions from the mechanical distortion of the conformation of the orienting chain units (fragments) as well as orientation of the chain segments themselves. Also we go with the assumption that the group polarizability tensors are unchanged (invariant) due to deformation, although changes in the conformation and geometry of the polycarbonate chains due to increasing strain in the sample are taken into account. Finally the geometry (bond length, angles and torsions) and conformation of the oriented BPAPC chain as obtained from the atomistic simulations using the PCFF force-field may not be the most accurate representation of the BPAPC chains in the amorphous phase while it is getting oriented, due to a lack of an adequate stress relaxation mechanism in the way simulations are conducted. But this approach can be considered

somewhere close to a real situation. Thus considering all these aspects pointing to the differences between the actual experimental conditions of birefringence measurement and the simulation protocol, the comparison obtained in the present work for the birefringence from atomistic simulation of uniaxial deformation of glassy BPAPC is extremely good.

Table 7.2. Calculated values of birefringence from atomistic simulations

% Strain	BPAPC		DMPC		DMBPC	
	$\langle P_2 \rangle$	Δn	$\langle P_2 \rangle$	Δn	$\langle P_2 \rangle$	Δn
10	0.054	0.00173	0.056	0.0014	0.050	0.0001
20	0.102	0.00544	0.098	0.0042	0.105	0.0028
30	0.146	0.01026	0.146	0.0084	0.147	0.0053
40	0.190	0.01580	0.189	0.0125	0.189	0.0079
50	0.225	0.02185	0.227	0.0174	0.223	0.0099
60	0.263	0.02929	0.271	0.0237	0.264	0.0123
70	0.293	0.03475	0.304	0.0286	0.294	0.0143
80	0.333	0.04232	0.333	0.0341	0.321	0.0172
90	0.359	0.04700	0.362	0.0405	0.347	0.0205
100	0.381	0.05370	0.386	0.0452	0.378	0.0238

Given in Figure 7.29 are the curves for the calculated birefringence as a function of the orientation function. In all the three polycarbonates birefringence varies in a linear fashion with the orientation function. Figure 7.30 provides a comparison of the calculated birefringence as a function of strain for all the three polycarbonates studied here. For BPAPC and DMPC, birefringence continuously increases with strain. Throughout the stretching region, BPAPC exhibits the highest birefringence followed by DMPC and then DMBPC has the lowest birefringence. The calculated birefringence values at 100% strain are 0.0537 (BPAPC), 0.0452 (DMPC) and 0.0238 (DMBPC). In Figure 7.31 and 7.32, the contribution by the phenylene and carbonate groups towards the total birefringence in case of each polycarbonate is given. As expected, predominant contribution to birefringence is from the phenylene rings for all the three polycarbonates. The differences in the birefringence among the three polycarbonates are also due to the phenylene rings. Birefringence contribution from the phenylene rings is highest in the case of BPAPC followed by DMPC and then DMBPC.

Carbonate group contribution towards the total birefringence is similar among the three polycarbonates.

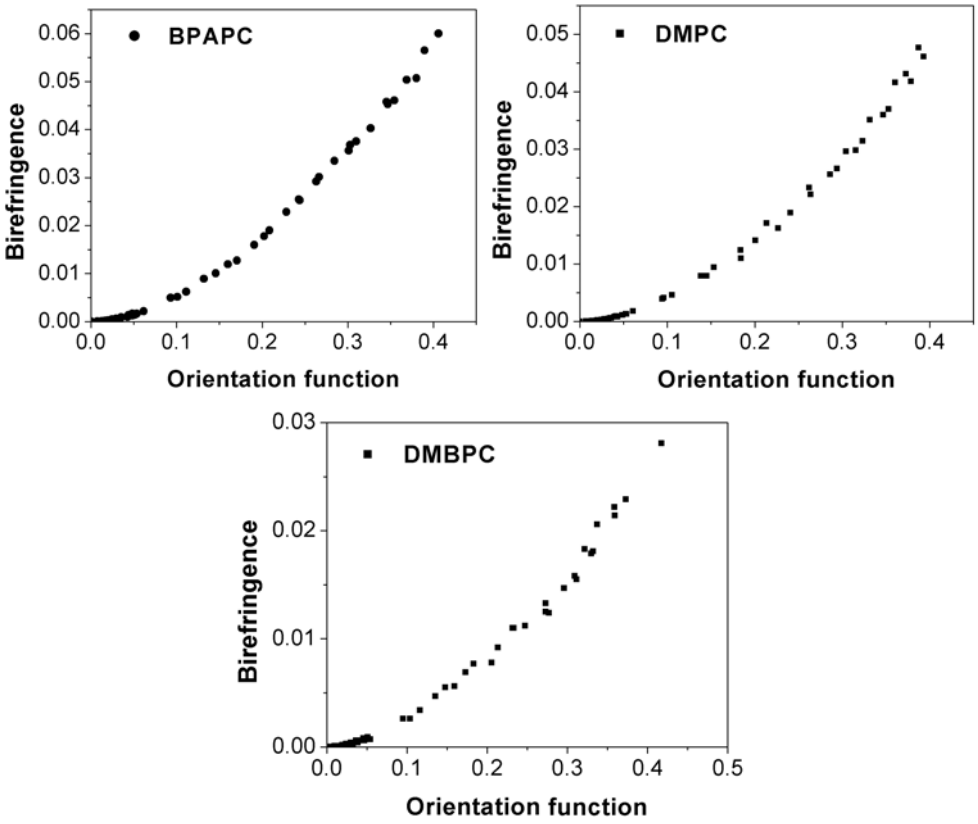

Figure 7.29. Calculated birefringence vs orientation function of the repeat unit in BPAPC, DMPC and DMBPC. Each point in a plot corresponds to one sample data, averaged over three stretching directions

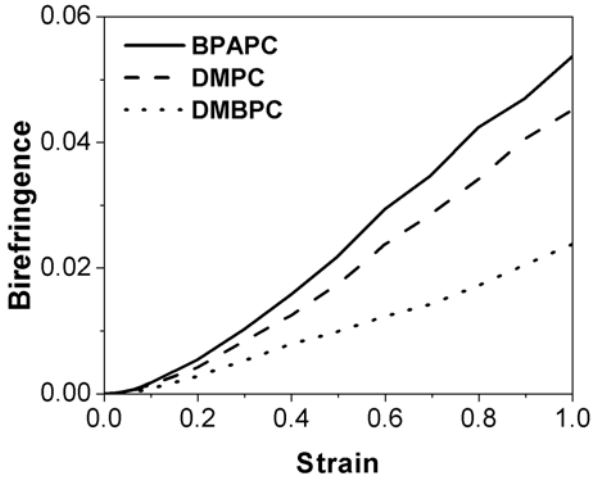

Figure 7.30. Calculated averaged value of birefringence as a function of strain for BPAPC, DMPC and DMBPC

(A) Total birefringence, Δ*n*

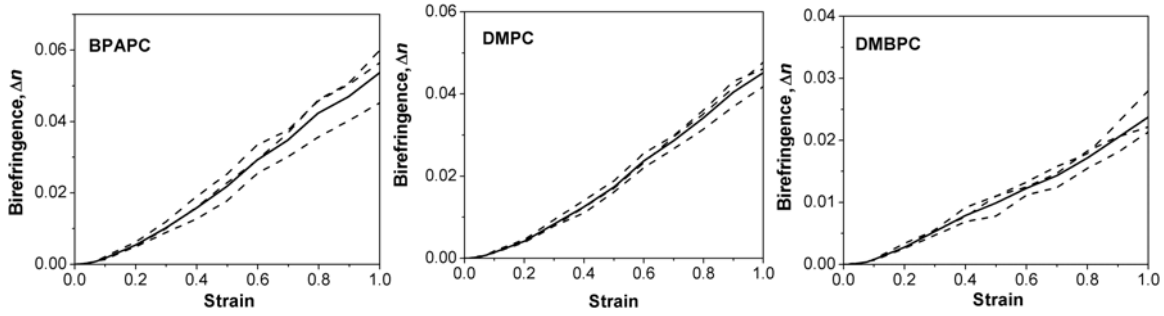

(B) Birefringence due to phenylene rings

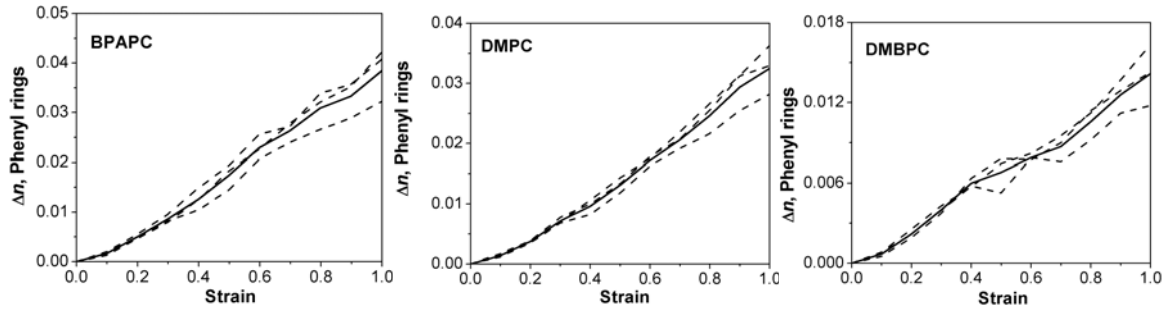

(C) Birefringence due to carbonate groups

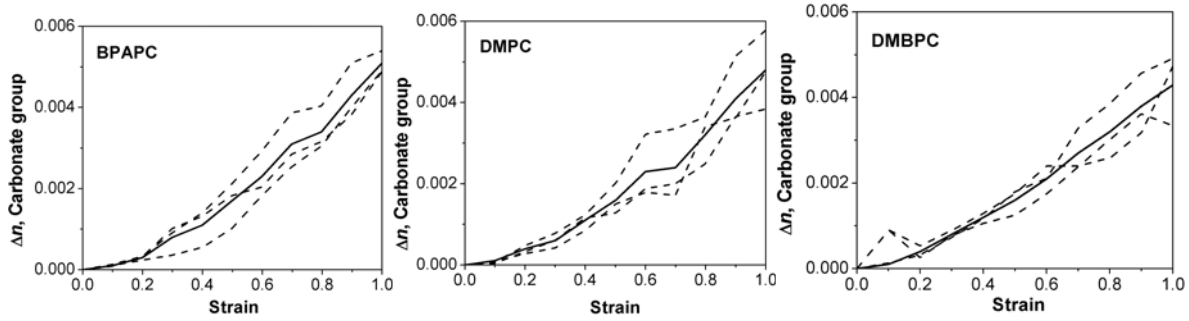

Figure 7.31. Calculated birefringence as a function of strain for BPAPC, DMPC and DMBPC. Corresponding to each plot, the solid curve is the averaged birefringence value for the polycarbonate and the dotted curves are for the 3 individual samples (each sample averaged over values for three stretching direction simulations). (A) Total birefringence, Δ*n*; (B) Δ*n* due to phenylene rings; (C) Δ*n* due to carbonate groups

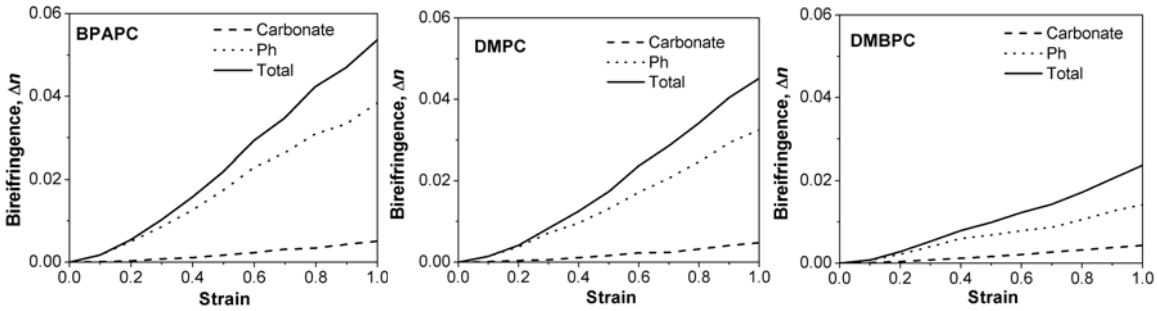

Figure 7.32. Calculated averaged birefringence as a function of strain for BPAPC, DMPC and DMBPC. Individual group contribution towards birefringence is also shown

The slope of the plot depicting birefringence vs strain (Figure 7.30) would correspond to the strain-optical coefficient (C_ε) of the polymer in the glassy state. This value when used along with the Youngs modulus can be used for the calculation of stress-optical coefficient in the glassy state (C_g). From a linear fit of these curves corresponding to each polycarbonate, in the entire strain range studied here, strain-optical coefficients were estimated. These values are 0.0546 (BPAPC), 0.0454 (DMPC) and 0.0234 (DMBPC). The experimental value for the strain-optical coefficient for BPAPC[24,47] is reported to be 0.1 and 0.15 and is 2-3 times higher than the value obtained from the simulated birefringence vs strain curve. Youngs moduli of DMPC and DMBPC estimated from the group contribution technique were 2.2×10^{10} dyn/cm^2 and 2.7×10^{10} dyn/cm^2 respectively.[68] The experimental value for the Youngs modulus of BPAPC is reported to be 2.2×10^{10} dyn/cm^2. From these, calculation of stress-optical coefficient was attempted. The estimated values were 25, 21 and 9 brewsters for BPAPC, DMPC and DMBPC respectively. The experimental values for these polycarbonates in the glassy state has been reported to be 82, 51 and 47 brewsters respectively.[24]

The poor comparison of the calculated stress-optical coefficients with the experimental values is thought to be due to the following issues. The direct calculation of the C_g from C_ε and a constant Youngs modulus is not an appropriate method and Isayev and co-workers[47] have described a methodology for this calculation from the master curves of the relaxation modulus and C_ε. The limitations of the simulation protocol employed in this work could also be one reason for underestimating the values of C_ε and C_g. The stresses are not applied to the polymer directly, but in terms of strain by stretching the periodic cell. The work described in this chapter is a first report on the calculation of birefringence of

polycarbonates in the glassy state and the comparison of calculated and experimental birefringence in the case of BPAPC is quite satisfactory.

7.3.4.2. Results using the indirect method with atomistic samples

Using this method the birefringence calculated for these polycarbonates is found to be 0.073 (BPAPC), 0.074 (DMPC) and 0.036 (DMBPC). In the case of BPAPC, the agreement between the calculated birefringence using this method with the experimental value is far from satisfactory (47% deviation). The behaviour in the variation of birefringence as a function of strain (details of the values at each strain in the elastic and plastic regions not provided here) is qualitatively similar by this method as compared to the first (direct) method discussed in previous section. This similarity is not unexpected since the indirect method owes its prediction to the orientation function which qualitatively behaves correctly as a function of strain in the atomistically deformed samples for all 3 polycarbonates. However by using the indirect method, the relative trend in the birefringence values among the 3 polycarbonates is not the same as that seen from experimental data in which case the birefringence of DMPC (from stress-optical coefficients) are lower than that of BPAPC. Therefore the indirect method of birefringence estimation is not a favourable one, not only for BPAPC but is also unable to distinguish the values for BPAPC and DMPC even though these polycarbonates are expected to provide very different values of the birefringence at any particular strain in the glassy state. In the indirect method, backbone orientation function along with fully stretched intrinsic birefringence per repeat unit of the polymer, are utilized. This method fails to address the contributions to the birefringence from bonds not part of the backbone in a correct manner; even though the use of only the backbone orientation function into eqs. (1) and (2) is the correct way since intrinsic birefringence is being employed to finally calculate bulk sample birefringence. In reality, experimentally the measurement of birefringence and derivation of orientation functions from birefringence measurements do take into account the self consistency between polarizabilities of backbone as well as side groups with proper corrections applied to the orientation function derivation such that the right values of “backbone orientation function” are obtained from measurement of “overall sample” (backbone + side groups) birefringence. In the in-direct method used here, we do not use the side-groups information during stretching. The first method of direct transformations

is better suited for the estimation of birefringence by its “ab initio” (direct) nature thus avoiding any ad-hoc representation of the physics of the situation and is therefore self-consistent in terms of the structure and optics.

7.4. Conclusions

Atomistic modeling of tensile deformation of BPAPC and two substituted polycarbonates, DMPC and DMBPC, in their amorphous glassy state has been performed. The methodology uses an isotropic starting sample of the polymer and performs repeated sequences of uniaxial extension in the tensile mode and relaxation using molecular mechanics. Stretching simulations for the polycarbonates were performed in their corresponding dense phases with full atomistic description and chemical details and thus taking into account all intra and interchain interactions in the system. Molecular level structural, conformational and orientational changes in the bulk phase accompanying the deformation are analyzed in detail. The probability distributions show that the vectors along the main chain orient parallel to the stretching direction in the case of all three polycarbonates studied here. The carbonyl double bond vector which is orienting perpendicular to the chain appreciable changes in orientation in the case of DMPC and DMBPC, but not for BPAPC. There is a marked increase in the population of vectors along the polymer chain and preference for lower angles with respect to the stretching direction in the case of main chain vector conforming to the earlier reported NMR results.

Neighbouring phenylene ring planes tend to align parallel to each other as the applied strain in the BPAPC sample increases. This tendency for nearly parallel orientation of phenyl ring planes is also observed in the case of phenyl rings which are far apart (distances between the phenyl rings any where between 6 to 10 Å). These results are in agreement with the NMR studies on plastically deformed BPAPC samples where a distinct tendency of the phenyl ring planes to orient parallel to one another upon deformation has been reported.[7] Nearest neighbour carbonate groups show a tendency for parallel orientation at about 100 % strain. Previously reported NMR measurements in the literature which were performed for BPAPC samples deformed by applying a compressive strain of 68%, carbonate groups did not show any preference for a particular type of orientation. The present results indicate that there is an

increased tendency for parallel orientation of nearest neighbour interchain phenylene rings and carbonate groups, and this response behaviour which results in better packing and ordering of these groups due to deformation. Torsion distributions of the deformed samples are found not drastically different from those of the undeformed samples. Population density of the various torsions in bulk deformed samples were found scattered around the maximum probable RIS states prevalent under theta conditions.

In the case of DMPC and DMBPC, the orientation of the main chain vectors follows the same pattern as shown by BPAPC. The orientation of the carbonyl bond vector is found to be negligible in the case of BPAPC, whereas this is not the case for DMPC and DMBPC. This response is ascribed to be due to the influence posed by the *ortho* methyl group substitutions near the carbonate group for substituted polycarbonates DMPC and DMBPC. Torsional distributions in the case of oriented DMPC and DMBPC are not appreciably different from that of the corresponding undeformed samples. The chain extension as a result of deformation is observed in all the three polycarbonates.

A new molecular simulation based approach accounting for the polarizability and anisotropy of the chain along with its geometry and conformation to calculate the birefringence of the oriented sample is presented. The polarizability tensors of individual groups in the strain deformation reference frame, during sequences of sample deformation, are used directly to calculate the sample birefringence. The comparison of simulated and experimentally available values for birefringence is in very good agreement for BPAPC. Calculated birefringence for DMPC and DMBPC are lower than that of BPAPC thus conforming to the trend in the experimental values of the stress-optical coefficients of the polycarbonates studied here. The effect of fundamental optical properties of the molecular groups in the chain on the birefringence properties, in conjunction with the orientational effects of the polymer segments, is brought forth in this work.

To summarize the results of this study, according to the different methods, the simulation on the birefringence of the three oriented polycarbonates in the amorphous bulk shows that DMBPC exhibit lower birefringence than DMPC and BPAPC. The orientations of the phenylene rings are very much similar in these polycarbonates irrespective of the

different types of substituents present. Contribution to birefringence is thought to mainly arise from the polarizable phenylene rings and therefore orientational contributions to birefringence from the constituting groups in the chain can be considered not very different from each other. It is the polarizability tensors and anisotropies of the groups and the geometry and conformation that the polymer chains adopt, which leads to such pronounced differences in the values of the birefringence being observed for these polycarbonates.

7.5. References

1. Hutnik, M.; Argon, A. S.; Suter, U. W. *Macromolecules* **1993**, *26*, 1097.
2. Qian, C.; Ludovice, P. J. *Makromol. Chem. Macromol. Symp*. **1993**, *65*, *123*.
3. Fan, C. F.; Cagin, T.; Chen, Z. M.; Smith, K. A. *Macromolecules* **1994**, *27*, 2383.
4. Fan, C. F. *Macromolecules* **1995**, *28*, 5215.
5. Utz, M.; Tomaselli, M.; Ernst, R.; Suter, U. W. *Macromolecules* **1996**, *29*, 2909.
6. Utz, M.; Atallah, A. S.; Robyr, P.; Widmann, A. H.; Ernst, R.; Suter, U. W. *Macromolecules* **1999**, *32*, 6191.
7. Utz, M.; Robyr, P.; Suter, U. W. *Macromolecules* **2000**, *33*, 6808.
8. Weiner, J. H.; Gao, J. *Macromolecules* **1994**, *27*, 1201.
9. Kroger, M.; Luap, C.; Muller, R. *Macromolecules* **1997**, *30*, 526.
10. Picu, R. C. *Macromolecules* **2001**, *34*, 5023.
11. Mavrantzas, V. G.; Theodorou, D. N. *Comput. Theor. Polym. Sci.* **2000**, *10*, 1.
12. Mavrantzas, V. G.; Theodorou, D. N. *Macromol. Theory Simul.* **2000**, *9*, 500.
13. Wilkes, G. J.; *Macromol. Sci.-Revs. Macromol. Chem*. **1974**, *10*, 149.
14. Treolar, L. R. *The Physics of Rubber Elasticity*; Oxford University Press: New York, 1967.
15. Read, B. E.; Duncan, J. C.; Meyer, D. E. In *Measurement Techniques of Polymeric Solids*, Brown, R. P.; Read, B. E. Eds., Elsevier Applied Science Pub., New York 1984.
16. Riande, E.; Saiz, E. *Dipole Moments and Birefringence of Polymers*; Prentice Hall: Englewood Cliffs, 1994.
17. Janeschitz-Kriegl H. *Polymer Melt Rheology and Flow Birefringence*; Springer: Berlin, 1983.

18. Ward, I. M. *Structure and Properties of Oriented Polymers*; Applied Science Publishers, Ltd.: London, 1975.
19. Wimberger Friedl, R. *Prog. Polym. Sci*., **1995**, *20*, 369.
20. Inoue, T.; Osaki, K. *Macromolecules* **1996**, *29*, 1595.
21. Osaki, K.; Okamoto, H.; Inoue, T.; Hwang, E. J. *Macromolecules* **1995**, *28*, 3625.
22. Osaki, K.; Inoue, T. *Macromolecules* **1996**, *29*, 7622.
23. Inoue, T.; Matsui, H.; Murakami, S.; Kohjiya, S.; Osaki, K. *Polymer* **1997**, *38*, 1215 and references cited therein
24. LeGrand, D. G. In *Handbook of Polycarbonate Science and Technology*; Le Grand, D. G.; Bendler, J. T., Ed.; Marcel Dekker, Inc.: New York, 2000.
25. Ito, K. *Exp. Mech.* **1962**, 1.
26. LeGrand, D. G. *J. Polym. Sci. A* **1964**, *2*, 931.
27. Champion, J. V.; Desson, R. A.; Meeten, G. H. *Polymer* **1974**, *15*, 301.
28. Biangardi, H. J. *Colloid Polym. Sci.* **1981,** *259*, 111.
29. Falkai, B. V.; Spilgies, G.; Biangardi, H. J. *Angew Makromol. Chem.* **1982**, *108*, 41.
30. Biangardi, H. J. *Makromol. Chem.* **1982**, *183*, 1785.
31. Pietralla, M.; Schubach, H. R.; Dettenmaier, M.; Heise, B.; *Progr. Colloid. Polym. Sci*. **1985**, *71*, 125.
32. Schubach, H. R.; Heise, B. *Colloid. Polym. Sci*. **1986**, *264*, 335.
33. Peetz, L.; Krueger, J. K.; Pietralla, M. *Colloid. Polym. Sci*. **1987**, *265*, 761.
34. Vogt, H. D.; Dettenmaier, M.; Spiess, H. W.; Pietralla, M. *Colloid. Polym. Sci*. **1990**, *268*, 22.
35. Pietralla, M.; Pieper, T. *Colloid. Polym. Sci*. **1990**, *268*, 797.
36. Jannson, J. -F.; Yannas, I. V. *J. Polym. Sci*. *Polym. Phys.* **1977**, *15*, 2103.
37. Wu, M. S. *J. App. Polym. Sci*., **1986**, *32*, 3263.
38. Lunn, A. C.; Yannas, I. V. *J. Polym. Sci*. *Polym. Phys.* **1972**, *10*, 2189.
39. Lundberg, L.; Stenberg, B.; Jansson, J. -F. *Macromolecules* **1996**, *29*, 6256.
40. Wimberger-Friedl, R. *Polym. Engg. Sci.*. **1990**, *30*, 813.
41. Wimberger-Friedl, R. *Rheol. Acta*. **1991**, *30*, 329.
42. Wimberger-Friedl, R. *Rheol. Acta*. **1991**, *30*, 419.
43. Nagai, T.; Kimizuka, Y.; Nito, K.; Seto, J. *J. App. Polym. Sci*. **1992**, *44*, 1171.

44. Inoue, T.; Okamoto, H.; Osaki, K. *Macromolecules* **1992**, *25*, 7069.
45. Hwang, E. J.; Inoue, T.; Osaki, K. *Polymer* **1993**, *34*, 1661.
46. Muller, R.; Pesce, J. J. *Polymer* **1994**, *35*, 734.
47. Shyu, G. D.; Isayev, A. I.; Li, C. T. *J. Polym. Sci. Polym. Phys.* **2001**, *39*, 2252.
48. Koenen, J. A.; Heise, B.; Kilian. H. -G. *J. Polym. Sci. Polym. Phys.* **1989**, *27*, 1235.
49. Heymans, N. *Polymer* **1987**, *28*, 2009.
50. Heymans, N. *J. Polym. Sci. Polym. Phys.* **1991**, *29*, 1193.
51. Buisson, G.; Ravi Chandar, K. *Polymer* **1990**, *31*, 2071.
52. Boyce, M. C.; Arruda, E. M.; Jayachandran, R. *Polym. Engg. Sci.*. **1994**, *34*, 716.
53. Spathis, G.; Kontou, E. *J. App. Polym. Sci*. **2001**, *79*, 2534.
54. Lee, S.; De La Vega, J.; Bogue, D. C. *J. App. Polym. Sci*. **1986**, *31*, 2791.
55. Wimberger-Friedl, R.; Hendriks, R. D. H. M. *Polymer* **1989**, *30*, 1143.
56. Wimberger-Friedl, R.; De Bruin, J. G. *J. Polym. Sci. Polym. Phys.* **1993**, *31*, 1041.
57. Wimberger-Friedl, R. *Polym. Engg. Sci.*. **2003**, *43*, 62.
58. Sun, H. *Macromolecules* **1994**, *26*, 5924.
59. Sun, H.; Mumby, S. J.; Maple, J. R.; Hagler, A. T. *J. Am. Chem. Soc*. **1994**, *116*, 2978.
60. Sun, H. *J. Comp. Chem*. **1994**, *15*, 752.
61. Sun, H.; Mumby, S. J.; Maple, J. R.; Hagler, A. T. *J. Phy. Chem*. **1995**, *99*, 5873.
62. Sun, H. *Macromolecules* **1995**, *28*, 701.
63. Cerius^2, San Diego, CA: Molecular Simulations 1996.
64. (a) Xie, L.; Gidley, D. W.; Hristov, H. A.; Yee, A. F. *J. Polym. Sci. Polym. Phys. Ed*. **1995**, *33*, 77; (b) Ruan, M. Y.; Moaddel, H,; Jamieson, A. M.; Simha, R.; McGervey, J. D. *Macromolecules* **1992**, *25*, 2407; (c) Powers, J. M.; Caddell, R. M. *Polym. Eng. Sci.* **1972**, *12*, 473.
65. Erman, B.; Marvin, D. C.; Irvine, P. A.; Flory, P. J. *Macromolecules* **1982**, *15*, 664.
66. Erman, B.; Wu, D.; Irvine, P. A.; Marvin, D. C.; Flory, P. J. *Macromolecules* **1982**, *15*, 670.
67. Floudas, G.; Lappas, A.; Fytas, G.; Meier, G. *Macromolecules* **1990**, *23*, 1747.

68. Bicerano, J, *Prediction of Polymer Properties*; Marcel Dekker: New York, 2002.
69. Robyr, P.; Gan, Z.; Suter, U. W. *Macromolecules* **1998**, *31*, 6199.
70. Brady, T. E.; Yeh. G. S. Y. *J. App. Phys*. **1971**, *42*, 4622.
71. Tomaselli, M.; Zehnder, M. M.; Robyr, P.; Grob-Pisano, C.; Ernst, R. R.; Suter, U. W. *Macromolecules* **1997**, *30*, 3579.
72. Robyr, P.; Utz, M.; Gan, Z.; Scheurer, C.; Tomaselli, M.; Suter, U. W.; Ernst, R. R. *Macromolecules* **1998**, *31*, 5818 and references cited therein
73. Davis, G. C.; Caruso, A. J.; Wetzel, J. R.; Hariharan, R.; Wisnudel, M. B. (General Electric Company) U.S. Patent 6,001,953, December 14, 1999.
74. Toshimasa, T. I.; Kuniyuki, H. M.; Tatsumi, H. I. (Teijin Chemicals Ltd.) U.S. Patent 5,633,060, May 27, 1997.
75. Shirouzu, S.; Shikuma, H.; Senda, N.; Yoshida, M.; Sakamoto, S.; Shigematsu, T.; Nakagawa, T.; Tagami, S. *Jpn. J. Appl Phys*., **1990**, *29*, 898.

Chapter 8: Summary and Conclusions

The work presented in this thesis represents an effort where different molecular simulation methods were judiciously and efficiently applied to study a series of structurally different polymers within one family of structures (i.e. polycarbonates) for the inter-relationship between molecular structure and physical properties with focus on optical properties.

Conformational features of BPAPC and four structurally modified polycarbonate chains, at the repeat unit level (backbone bond pairs), have been derived using force-field based conformational energy calculations. RIS models for these polycarbonates were formulated and then used to calculate averaged single chain dimensions such as $\langle R^2 \rangle$, $\langle S^2 \rangle$ and C_∞, as well as persistence lengths. The effect of different substituent groups in the polycarbonate chain on the local conformational characteristics of these polycarbonates is efficiently brought out in this comparative study.

The theoretical formulation applicable to calculation of polarizability tensors and optical anisotropy (γ^2) of molecular fragments constituting substituted polycarbonate chains is presented for the first time. The theoretical approach utilizes experimentally derived anisotropic polarizability tensors of molecular groups in order to be able to account for induction effects and interdependence of backbone conformational states. The valence optical scheme-rotational isomeric state method (VOS-RIS) is implemented to study the optical properties of several polycarbonates. The contribution of the different structural groups towards the optical anisotropy along with the effect of geometry and conformations is analyzed in detail.

Accurate geometries of the bisphenyl and carbonate fragments corresponding to the four structurally modified polycarbonates using ab initio quantum chemical calculations are being reported here for the first time. The conformational energy minimum states obtained from the quantum mechanical calculations are compared with those obtained from classical force-field based modeling.

Molecular dynamics simulations of bulk amorphous BPAPC and four structurally modified polycarbonates with full atomistic description are presented. Comparison of the

bulk amorphous structure of BPAPC and four structurally modified polycarbonates is presented. Detailed analysis covering various aspects such as conformational properties including the torsion distributions in the bulk, cohesive energy density and solubility parameters, radial distribution functions, static structure factors and free volume distributions were performed for the polycarbonates investigated. This study brings out the effect of different structural modifications on the amorphous structure and the associated intrinsic conformational properties of the polymer chains in the bulk phase.

Atomistic simulation of uniaxial tensile deformation of two substituted polycarbonates DMPC and DMBPC is being reported here for the first time. Detailed analysis of the various conformational, orientational and packing changes in the bulk amorphous structure of BPAPC and substituted polycarbonates due to deformation is presented. Simulations are conducted till a strain of 100 %, well into the plastic deformation region. Two methods for the calculation of optical birefringence from atomistic simulations is presented here. In the first method the group polarizability tensors for polycarbonates are directly transformed using the atomistic structure coordinates to the laboratory reference frame in order to follow the optical behavior during deformation. In the second method the intrinsic birefringence employed either from experimental data or RIS calculations is utilized along with the orientation functions from the atomistically simulated structures, in order to calculate the birefringence via the Lorenz-Lorentz equation. The results for different polycarbonates are compared and discussed. This is a first such attempt on any polymer other than poly(ethylene) in the condensed phase.

The important findings of the work presented in this thesis can be summarized as follows. The presence of a cyclohexyl group at the C_α carbon leads to heterogeneity of the phenyl rings of the bisphenyl fragment. The conformational characteristics about the C_α carbon remains unaffected by *ortho* methyl substituents on the phenyl rings, but these interactions strongly change the conformational states at the carbonate group resulting in almost perpendicular orientation of the phenyl rings with respect to the carbonate group. Chain dimensions of substituted polycarbonates are found to be slightly lower than that of BPAPC due to interactions posed by the substituting groups at C_α and on phenylene rings.

Presence of a cyclohexylidene group at the bisphenyl C_α carbon in polycarbonates significantly lowers $<\gamma^2>$ due to (i) low intrinsic polarizability of the cycloaliphatic substituent and (ii) conformation that the phenylene rings adopt due to the cyclohexyl group. Optical anisotropy of the polycarbonate containing *ortho* methyl substituents on phenylene rings is lower than the value for the polycarbonate devoid of this substitution. Reduction in $<\gamma^2>$ due to *ortho* methyl groups is found to arise predominantly due to the perpendicular orientation of the phenylene rings with respect to the carbonate plane in the repeat unit. Quantitatively, cyclohexylidene at C_α is more effective in lowering the optical anisotropy than methyl groups on backbone phenylene rings. Calculated $\langle\gamma^2\rangle/x$ of the repeat units follows a linear behavior with respect to experimentally observed stress-optical coefficient of these polycarbonates in the melt (C_m). Calculated $\langle\gamma^2\rangle/x$ of these structurally modified polycarbonate chains are all lower than that of BPAPC. The relative trend in the calculated values of $\langle\gamma^2\rangle/x$ is similar to that observed for C_m and C_g (glassy state) from experiments in literature.

Quantum chemical calculations of polarizability for polycarbonate model compounds have been carried out in vacuum. These calculations did not take into account the solvent effect and the absolute values of the derived mean-squared optical anisotropy of DPP and DPC were not in agreement with the condensed phased experimental values. Optical anisotropy of the different bisphenyl fragments derived from the ab initio calculations followed a similar trend as the results obtained from the RIS/VOS scheme and the experimentally derived group polarizabilities.

In the bulk amorphous state of these polycarbonates studied here, structural modification of the BPAPC repeat unit by aliphatic groups lowers the CED and solubility parameter. Population maxima of the various torsional distributions in the bulk are located at the various discrete rotational states as derived from conformational energy calculations under theta condition. However, bulk structures show torsion distributions that are not discrete resulting essentially from interchain packing constraints. The peak positions of the calculated neutron scattering curves are in agreement with the experimental reports in the literature, thus leading to a correct trend in the simulated neighboring chain distances for the various polycarbonates studied here. The distances between the neighboring chains

calculated from the scattering curves indicate a rather open structure with a higher free volume for TMCPC. On the contrary from the simulated bulk structures corresponding to DMBPC showed the lowest free volume indicating better packing. Thus a cyclohexyl substituent at the C_α carbon as well as methyl groups on phenyl rings lead to better packing than in the case of BPAPC.

The main chain orientation vectors tend to preferentially align parallel with respect to the stretching directions as the deformation progresses in polycarbonates. Orientation function of the phenylene rings varies in a similar fashion in all three polycarbonates whereas a much higher carbonate group reorientation towards the stretching direction is observed in the case of DMPC and DMBPC. There is an enhanced tendency for the phenylene and carbonate planes to align parallel to each other with increase in deformation and this is seen in BPAPC at shorter as well as longer distances till about 10 Å in BPAPC. The torsion distributions of the chain in the oriented samples are found to be not very different from that of the undeformed samples, although a tendency for the increase in population of the *trans*, *trans* conformation of the carbonate groups is clearly evident. For calculation of birefringence, in the first method, the group polarizability tensors for polycarbonates are directly transformed using the bulk atomistic structure coordinates to the laboratory reference frame to calculate polarizability anisotropy of the chain which is used along with the atomistically derived orientation function to calculate the optical birefringence. Calculated values of the birefringence from this method for BPAPC samples compares well and is within 8% experimentally reported value. This novel method of birefringence calculation of amorphous polymers undergoing deformation, in order to facilitate optical property prediction under glassy conditions at a particular strain, is shown to be very useful and may be applied to other polymers as well. Major contribution to the birefringence in these polymers is due to the phenylene rings. Calculated birefringence values for DMPC and DMBPC are lower than that of BPAPC in agreement with the experimental stress-optical behaviour of these polymers.

Future Perspectives

Molecular modeling and atomistic simulations are increasingly being applied to study various physico-chemical aspects of polymer behaviour. Although a large amount of

literature have accumulated which deal with investigations of different classes of polymers for various properties, systematic studies of a homologues series of polymers in the bulk phase or at various levels are scarce. The work presented in this thesis represents such an effort. Further studies of this kind with attention on other properties such as mechanical, heat resistance and other relevant properties would aid in a better understanding of the structural factors controlling the performance of these polymers. Such studies would provide valuable insights when applied to other types and classes of polymers as well.

The RIS/VOS scheme presented in this thesis can be applied to polycarbonates having cyclohexyl substituent at the C_α carbon as well as those having substitutions on the phenyl rings. The extension of this study to other structurally different polycarbonates would certainly aid in getting new insights into the effect and contributions of different structural groups in determining the polarizability and optical anisotropy of these polymers and also would lead to more quantitative structure-optical property relationships in these polymers.

Further studies on the geometry and conformation of the substituted bisphenyl and carbonate fragments can be used in developing a force-field for substituted polycarbonates.

Another aspect of importance in the study of atomistic simulation of uniaxial deformation is to apply a better simulation protocol for the study of polycarbonates and other polymers. The method for the calculation of birefringence in the glassy state needs to be improved. Also new methods have to be formulated for estimating the strain and stress-optical coefficients of polymers with complicated chemical structures, from atomistically simulated stress or strain derived orientations in glassy and melt states. It will also be interesting to simulate the orientation and birefringence of polycarbonates in the melt state. Another new aspect would be the simulation of optical properties such as refractive indices and birefringence of thin films of polycarbonates and other polymers because such properties assume unusual variations under thin film conditions with very important practical applications.

Appendix – I

Formulation of polarizability tensor and calculation of optical anisotropy of substituted bisphenyl fragment is described here. A sample calculation is also given.

The substituted bisphenyl fragment (BPC with a methyl group at the 4 position of the cyclohexylidene ring, BPC-5) can be considered to be formed from 1,1,4-trimethylcyclohexane (CYX-5) and two phenyl groups and the process in terms of fragment reorganization can be expressed as follows.

$C_6H_5\text{-}H + C_6H_{10}(CH_3)_3 + H\text{-}C_6H_5 \rightarrow (C_6H_5)_2C_6H_{10}\,(CH_3) + 2CH_4$

Polarizability tensor for CYX-5**:** CYX-5 has three methyl groups, wherein the methyl group at the para position can be either equatorial or axial. The polarizability tensor in the $X_0Y_0Z_0$ frame can thus be written as,

$$\hat{\alpha}_{CYX-5},E = \hat{\alpha}_{CYX-4} + 2\Gamma_{CC,E} + \Gamma_{CC,A}$$
$$\hat{\alpha}_{CYX-5},A = \hat{\alpha}_{CYX-4} + \Gamma_{CC,E} + 2\Gamma_{CC,A}$$

$$\left(\hat{\alpha}_{CYX-5},E\right)_{X_0Y_0Z_0} = \left(\frac{\Gamma_{CC}}{9}\right)\begin{bmatrix} 4 & 4\sqrt{2} & 0 \\ & -10 & 0 \\ & & 6 \end{bmatrix} + 2\left(\frac{\Gamma_{CC}}{9}\right)\begin{bmatrix} 6 & 0 & 0 \\ & -3 & 0 \\ & & -3 \end{bmatrix} + \left(\frac{\Gamma_{CC}}{9}\right)\begin{bmatrix} -2 & -2\sqrt{2} & 0 \\ & 5 & 0 \\ & & -3 \end{bmatrix}$$
$$= \left(\frac{\Gamma_{CC}}{9}\right)\begin{bmatrix} 14 & 2\sqrt{2} & 0 \\ & -11 & 0 \\ & & -3 \end{bmatrix}$$
$$\left(\hat{\alpha}_{CYX-5},A\right)_{X_0Y_0Z_0} = \left(\frac{\Gamma_{CC}}{9}\right)\begin{bmatrix} 4 & 4\sqrt{2} & 0 \\ & -10 & 0 \\ & & 6 \end{bmatrix} + \left(\frac{\Gamma_{CC}}{9}\right)\begin{bmatrix} 6 & 0 & 0 \\ & -3 & 0 \\ & & -3 \end{bmatrix} + 2\left(\frac{\Gamma_{CC}}{9}\right)\begin{bmatrix} -2 & -2\sqrt{2} & 0 \\ & 5 & 0 \\ & & -3 \end{bmatrix}$$
$$= \left(\frac{\Gamma_{CC}}{9}\right)\begin{bmatrix} 6 & 0 & 0 \\ & -3 & 0 \\ & & -3 \end{bmatrix}$$

By substituting the value of Γ_{cc} (0.53 Å^3), we derive the polarizability tensor, which in turn can be used in eq. (18) (Chapter 4) to obtain the squared optical anisotropy, 1.778 Å^6 and 0.281 Å^6 for ***E*** and ***A*** orientations respectively. Transformation of the polarizability tensor from $X_0Y_0Z_0$ to X'Y'Z' is carried out by making use of eq. (15) (Chapter 4), where the bond angle θ is 54.75°.

Polarizability tensor for BPC-**5:** The tensor is formulated according to the following group additivity,

$$\left(\hat{\alpha}_{BPC-5},E\right)_{X'Y'Z'}=\left(\hat{\alpha}_{Ph,b}\right)_{X'Y'Z'}+\left(\hat{\alpha}_{CYX-5},E\right)_{X'Y'Z'}+\left(\hat{\alpha}_{Ph,b}\right)_{X'Y'Z'}$$

The phenyl group polarizability tensor is *diag* [1.21 1.21 -2.42] when expressed in the xyz reference frame and this is transformed to the X'Y'Z' using eq. (5) (Chapter 4). The θ_b and θ_a torsions as obtained from conformational calculations for BPC-**5** (***E***) is (70°, 55°) and the bond angle 2τ' is 107.7°. Although there are eight minimum energy torsions, all correspond to a unique minimum and leads to the same value of squared optical anisotropy. The same procedure is followed for BPC-**5** (***A***), in which the case the polarizability tensor for CYX-**5** (***A***) is used. The torsions and the bond angle in this case are the same as that for BPC-**5** (***E***).

Appendix – II

In Table 1A, the results of the calculations of optical anisotropy of polycarbonate chains which were performed by considering lesser number of rotational states per bond is given. For BPAPC and BPCPC, two states per bond are used (instead of 4 for which results are given in the manuscript). For TMCPC, the ψ_b and ψ_a bonds originally have two states per bond and in the present set of calculations, only one state per bond is used. For DMBPC and DMPC, for ϕ_b and ϕ_a bonds two states per bond which are allowed are used in these calculations also. These calculations were done using equal statistical weights for the minimum energy conformational states.

Table 1A. Optical anisotropy per repeat unit in a chain considering lower number of rotational states per bond in the repeat unit

PC	ϕ_b	ψ_b	ψ_a	ϕ_a	$<\gamma^2>/x$ (Å^6)
BPAPC	50, -50	50, -50	50, -50	50, -50	168.20
	130, -130	130, -130	130, -130	130, -130	168.20
	50, -50	130, -130	130, -130	50, -50	68.10
	130, -130	50, -50	50, -50	130, -130	68.10
DMPC	95, -95	50, -50	50, -50	95, -95	64.79
	95, -95	130, -130	130, -130	95, -95	117.16
BPCPC	50, -50	70, -70	55, -55	50, -50	39.93
	130, -130	110, -110	125, -125	130, -130	39.93
	50, -50	110, -110	125, -125	50, -50	17.76
	130, -130	70, -70	55, -55	130, -130	17.76
TMCPC	50, -50	-70	-60	50, -50	43.76
	130, -130	110	120	130, -130	43.76
	50, -50	110	120	50, -50	23.18
	130, -130	-70	-60	130, -130	23.18
DMBPC	95, -95	70, -70	55, -55	95, -95	8.36
	95, -95	110, -110	125, -125	95, -95	49.20

For BPCPC, when ϕ =50º, -50º; (ψ_a, ψ_b) = (55º, 70º), (-55º,-70º), $\langle\gamma^2\rangle/x$ is 39.93 Å^6 whereas when ϕ =50º, -50º; (ψ_a, ψ_b) = (125º, 110º), (-125º, -110º), $\langle\gamma^2\rangle/x$ is 17.76 Å^6. For TMCPC-*e*, when ϕ =50º, -50º; (ψ_a, ψ_b) =(-60º,-70º), $\langle\gamma^2\rangle/x$ is 43.76 Å^6 whereas when ϕ =50º, -50º; (ψ_a, ψ_b) = (120º, 110º), $<\gamma^2>/x$ is 23.18 Å^6. For DMPC, when ϕ = 95º, -95º; (ψ_a, ψ_b) = (50º, 50º) and (-50º, -50º) γ^2/x is 64.8 Å^6 and when (ψ_a, ψ_b) = (130º, 130º) and (-130º, -130º), γ^2/x is 117.2 Å^6. For DMBPC, when ϕ = 95º, -95º; (ψ_a, ψ_b) = (55º, 70º) and (-55º, -70º), the γ^2/x is 8.36 Å^6, whereas calculations employing (ψ_a, ψ_b) = (125º, 110º) and (-125º, -110º) lead to 49.2 Å^6.

Appendix – III

Optical anisotropy per repeat unit, which is averaged over symmetric conformers in each polycarbonate, is given below.

In Tables 2A, the repeat unit optical anisotropy of the various conformers of the polycarbonates are given. These are grouped into various sets, for eg. for BPAPC, the 128 conformations possible for the repeat unit can be grouped into 10 sets and the number of conformers corresponding to each set is also given. The torsions for one of the representative conformers in each set are also given. The conformers in each set are symmetric and give the same value of $\langle\gamma^2\rangle/x$ for the repeat units. The $\langle\gamma^2\rangle/x$ given in the table correspond to the values of repeat unit anisotropy obtained by averaging over the symmetric conformers in each set.

Table 2A. Repeat unit optical anisotropy of polycarbonates obtained by averaging over the symmetric conformers. $\langle\gamma^2\rangle/x$ of a representative example of the repeat unit within each set with its torsional specification is given

a) BPAPC

	ϕ_b	ψ_b	ψ_a	ϕ_a	No. of conformers	$\langle\gamma^2\rangle/x$ (Å^6)
1	50	50	50	50	8	171.00
2	-50	50	50	-50	8	113.30
3	50	50	50	-50	16	108.09
4	50	50	50	130	16	105.93
5	50	50	50	-130	16	142.27
6	-50	50	50	130	16	77.17
7	-50	50	50	-130	16	76.92
8	130	50	50	130	8	71.75
9	130	50	50	-130	16	60.15
10	-130	50	50	-130	8	122.90

b) DMPC

	ϕ_b	ψ_b	ψ_a	ϕ_a	No. of conformers	$\langle\gamma^2\rangle/x$ (Å^6)
1	95	50	50	95	2	68.34
2	-95	50	50	-95	2	28.55
3	-95	50	50	95	4	38.00
4	95	50	-130	95	4	49.67
5	-95	50	-130	-95	4	136.55
6	-95	50	-130	95	4	71.24
7	95	50	-130	-95	4	97.57
8	95	50	-130	95	2	63.13
9	-95	50	-130	-95	2	196.26
10	-95	50	-130	95	4	76.70

c) BPCPC

	ϕ_b	ψ_b	ψ_a	ϕ_a	No. of conformers	$\langle\gamma^2\rangle/x$ (Å^6)
1	50	70	55	50	16	42.39
2	-50	70	55	-50	16	35.49
3	-50	70	55	50	16	23.19
4	50	70	55	-50	16	30.08
5	50	70	55	130	16	33.91
6	50	70	55	-130	16	32.24
7	-50	70	55	130	16	16.31
8	-50	70	55	-130	16	14.78
9	130	70	55	50	16	38.13
10	130	70	55	-50	16	8.70
11	-130	70	55	50	16	25.94
12	-130	70	55	-50	16	16.97
13	130	70	55	130	16	23.14
14	130	70	55	-130	16	15.99
15	-130	70	55	130	16	10.74
16	-130	70	55	-130	16	21.66

d) TMCPC

	ϕ_b	ψ_b	ψ_a	ϕ_a	No. of conformers	$\langle\gamma^2\rangle/x$ (Å^6)
1	50	-70	-60	50	16	32.10
2	-50	-70	-60	-50	16	45.63
3	-50	-70	-60	50	16	36.51
4	50	-70	-60	-50	16	22.26
5	50	-70	-60	130	16	14.39
6	50	-70	-60	-130	16	18.15
7	-50	-70	-60	130	16	42.08
8	-50	-70	-60	-130	16	38.54
9	130	-70	-60	50	16	15.47
10	130	-70	-60	-50	16	26.67
11	-130	-70	-60	50	16	9.91
12	-130	-70	-60	-50	16	34.32
13	130	-70	-60	130	16	27.63
14	130	-70	-60	-130	16	9.98
15	-130	-70	-60	130	16	14.69
16	-130	-70	-60	-130	16	26.44

e) DMBPC

	ϕ_b	ψ_b	ψ_a	ϕ_a	No. of conformers	$\langle\gamma^2\rangle/x$ (Å^6)
1	95	70	55	95	2	10.00
2	-95	70	55	-95	2	3.64
3	-95	70	55	95	2	3.03
4	95	70	55	-95	2	5.55
5	95	70	55	95	2	10.07
6	-95	70	55	-95	2	17.26
7	-95	70	55	95	2	16.98
8	95	70	55	-95	2	40.30
9	95	-110	55	95	2	11.38
10	-95	-110	55	-95	2	23.60
11	-95	-110	55	95	2	35.77
12	95	-110	55	-95	2	19.53
13	95	-110	55	95	2	52.88
14	-95	-110	55	-95	2	89.78
15	-95	-110	55	95	2	25.64
16	95	-110	55	-95	2	20.52

The arithmetic averaged $\langle\gamma^2\rangle/x$ from these calculations are 101.21 Å^6 (BPAPC), 77.23 Å^6 (DMPC), 24.35 Å^6 (BPCPC), 25.92 Å^6 (TMCPC-e) and 24.12 Å^6 (DMBPC). These values are slightly lower than those obtained from the RIS calculations by direct averaging through the *P* matrices over all the possible conformational states about the bonds in the repeat unit (Table 4.3 in Chapter 4).

Appendix – IV

Mean potential energies, individual energy components for each of the 10 amorphous cells in the case of all five polycarbonate will be given. This section will also present information on solubility parameter and chain dimensions of the all the equilibrated amorphous structures of the polycarbonates. In Table 3A the energetic and structural characteristics of the individual cells that have been obtained after sampling and subsequent minimization are given along with the averaged values. Also the time for which the total MD is performed is also shown.

Table 3A. Individual cell energies, bulk dimensions and solubility parameters

1. BPAPC

Name	ps[a]	E_{Bulk}[b] (kcal/mol)	*R* (Å)	*S* (Å)	$E_{single\ chain}$[c] (kcal/mol)	Cohesive energy density (cal/cm^3)	Solubility parameter $(cal/cm^3)^{1/2}$
BPAPC-1	160	-3849.1	147.7	50.9	-1891.5	98.28	9.91
BPAPC-2	185	-3804.8	146.9	48.7	-1889.5	96.13	9.80
BPAPC-3	150	-3799.5	143.4	52.6	-1877.2	96.51	9.82
BPAPC-4	190	-3796.9	156.6	57.8	-1839.4	98.25	9.91
BPAPC-5	150	-3833.90	138.3	52.5	-1796.1	102.3	10.1
BPAPC-6	160	-3817.1	163.4	53.5	-1812.3	100.6	10.0
BPAPC-7	160	-3814.2	164.5	55.9	-1841.7	99.02	9.95
BPAPC-8	180	-3829.4	173.6	47.0	-1820.7	100.8	10.0
BPAPC-9	160	-3813.7	189.0	72.3	-1797.7	101.2	10.1
AVG		-3817.6±17	158.2±16	54.6±7	-1840.7±37	99.2±2.1	9.96±0.1

[a] Number of picoseconds for which MD have been performed for each of the cells
[b] E_{bulk} corresponds to the minimized energy of the bulk cell after MD simulation
[c] E_{chain} is the energy of the polycarbonate chain devoid of periodic boundary conditions

2. BPCPC

Name	ps	E_{Bulk} (kcal/mol)	*R* (Å)	*S* (Å)	$E_{single\ chain}$ (kcal/mol)	Cohesive energy density (cal/cm^3)	Solubility parameter $(cal/cm^3)^{1/2}$
BPCPC-1	180	-3614.9	135.1	45.2	-1736.9	92.87	9.63
BPCPC-2	150	-3618.0	157.2	50.2	-1772.5	94.51	9.72
BPCPC-3	150	-3574.1	156.1	45.8	-1871.3	85.69	9.26
BPCPC-4	160	-3586.2	156.5	58.1	-1737.4	93.04	9.64
BPCPC-5	200	-3606.3	139.3	54.2	-1744.0	93.72	9.68
BPCPC-6	180	-3551.3	163.0	65.7	-1713.3	92.50	9.62
BPCPC-7	180	-3657.7	142.3	47.7	-1799.7	93.51	9.67
BPCPC-8	160	-3621.0	151.9	44.2	-1776.6	92.82	9.63
AVG		-3603.7±32.7	150.2±10	51.4±7	-1769.0±49	92.3±2.8	9.60±0.14

3. TMCPC

Name	ps	E_{Bulk} (kcal/mol)	*R* (Å)	*S* (Å)	E_{chain} (kcal/mol)	Cohesive energy density (cal/cm^3)	Solubility parameter $(cal/cm^3)^{1/2}$
TMCPC-1	190	-3622.6	143.94	57.0	-1944.0	77.79	8.82
TMCPC-2	250	-3654.5	133.04	46.6	-1983.4	77.44	8.80
TMCPC-3	160	-3596.0	154.01	50.9	-1940.2	76.73	8.76
TMCPC-4	250	-3646.3	131.68	41.9	-2022.7	75.23	8.67
TMCPC-5	190	-3648.7	140.01	53.7	-2102.4	71.65	8.46
TMCPC-6	240	-3643.2	125.25	52.9	-2057.4	73.49	8.57
TMCPC-7	160	-3636.0	146.04	49.3	-1941.7	78.51	8.86
TMCPC-8	200	-3660.4	119.04	52.3	-2062.7	74.04	8.60
TMCPC-9	170	-3588.9	138.01	51.0	-1971.1	74.97	8.66
AVG		-3633±25.4	136.8±10	50.6±4	-2002.8±60	75.54±2.2	8.69±0.13

4. DMBPC

Name	ps	E_{Bulk} (kcal/mol)	*R* (Å)	*S* (Å)	$E_{single\ chain}$ (kcal/mol)	Cohesive energy density (cal/cm^3)	Solubility parameter $(cal/cm^3)^{1/2}$
DMBPC-1	195	-3295.2	146.5	56.1	-1576.2	85.30	9.23
DMBPC-2	190	-3334.5	121.6	38.1	-1596.3	86.25	9.29
DMBPC-3	180	-3334.9	133.8	47.7	-1654.9	83.37	9.13
DMBPC-4	160	-3318.3	160.8	53.8	-1668.4	81.87	9.05
DMBPC-5	240	-3378.2	167.1	52.1	-1573.6	89.55	9.46
DMBPC-6	240	-3302.3	123.5	48.9	-1715.6	78.73	8.87
DMBPC-7	200	-3395.7	157.2	62.6	-1614.9	88.36	9.40
DMBPC-8	180	-3337.7	119.4	42.1	-1656.7	83.41	9.13
DMBPC-9	220	-3330.3	140.9	45.8	-1648.1	83.47	9.13
		-3336.3±32	141.2±17	49.7±7	-1636.9±47	84.48±3.31	9.19±0.18

5. DMPC

Name	ps	E_{Bulk} (kcal/mol)	*R* (Å)	*S* (Å)	$E_{single\ chain}$ (kcal/mol)	Cohesive energy density (cal/cm^3)	Solubility parameter $(cal/cm^3)^{1/2}$
DMPC-1	170	-3481.8	151.3	57.3	-1659.40	89.66	9.47
DMPC-2	220	-3521.2	150.9	53.8	-1762.75	86.52	9.30
DMPC-3	190	-3497.1	135.9	45.2	-1707.63	88.05	9.38
DMPC-4	150	-3476.9	153.9	53.3	-1668.50	88.97	9.43
DMPC-5	160	-3510.7	133.3	61.6	-1656.58	91.22	9.55
DMPC-6	160	-3464.8	130.1	46.6	-1686.26	87.51	9.35
DMPC-7	160	-3531.8	166.8	60.0	-1643.11	92.93	9.64
DMPC-8	250	-3524.0	169.0	45.4	-1721.45	88.68	9.42
DMPC-9	160	-3503.7	147.7	63.0	-1726.45	87.30	9.34
		-3501.3±23	148.8±13	54.0±7	-1692.5±39	88.98±2	9.43±0.11

Appendix – V

Intermolecular phenyl ring plane weighted distributions in bulk amorphous polycarbonates

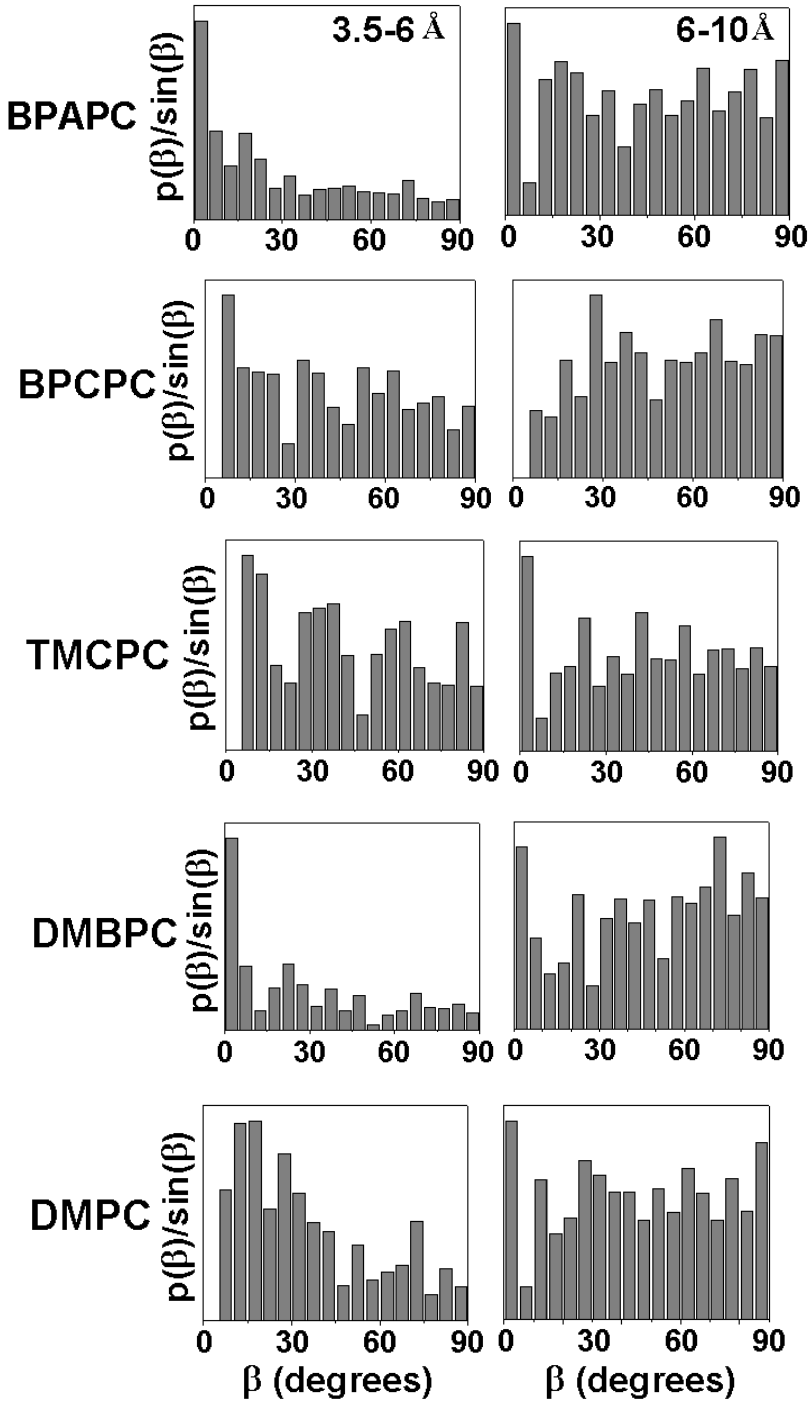

Figure 1A. Orientational distributions of the angle between the phenyl ring planes in bulk polycarbonates. The fractional contributions of the ring pairs from which the distributions were plotted for the distance intervals 3.5-6 and 6-10 Å in the order for various polycarbonates are (a) BPAPC, 0.256, 0.664 (b) BPCPC, 0.251, 0.682 (c) TMCPC, 0.185, 0.546 (d) DMBPC, 0.14, 0.684 and (e) DMPC, 0.20, 0.686.

Appendix – VI

Intermolecular phenyl ring and carbonate plane weighted distributions in oriented BPAPC samples

I. Packing of phenyl ring planes: 4-6 Å

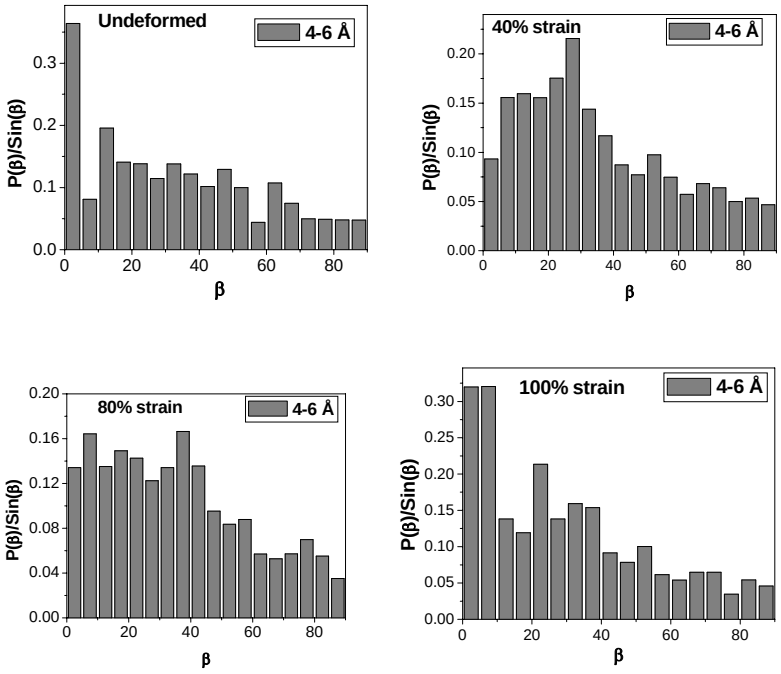

II. Packing of phenyl ring planes: 6-8 Å

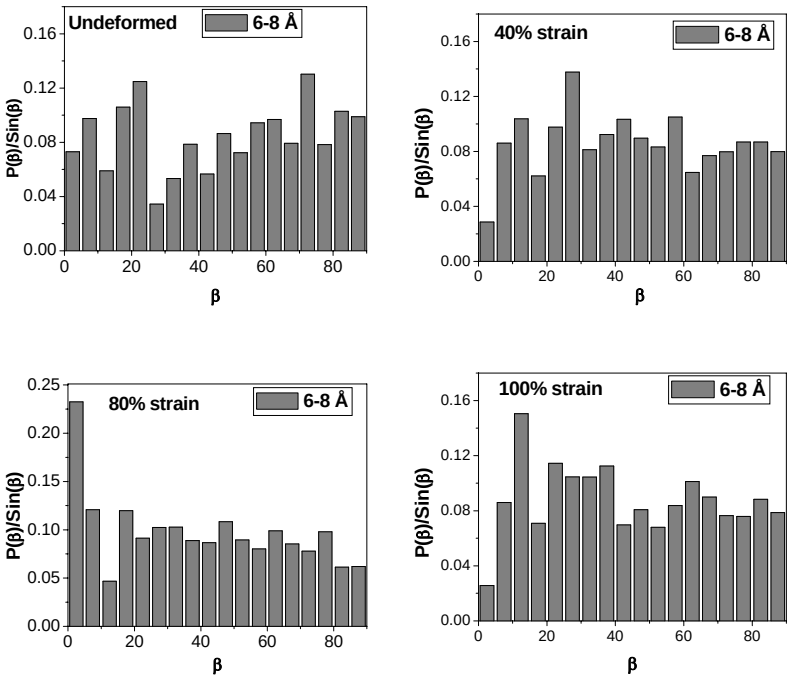

Figure 2A. Probability distribution of the intermolecular packing of phenyl ring planes in BPAPC samples as a function of deformation.

I. Packing of carbonate planes: 4-6 Å

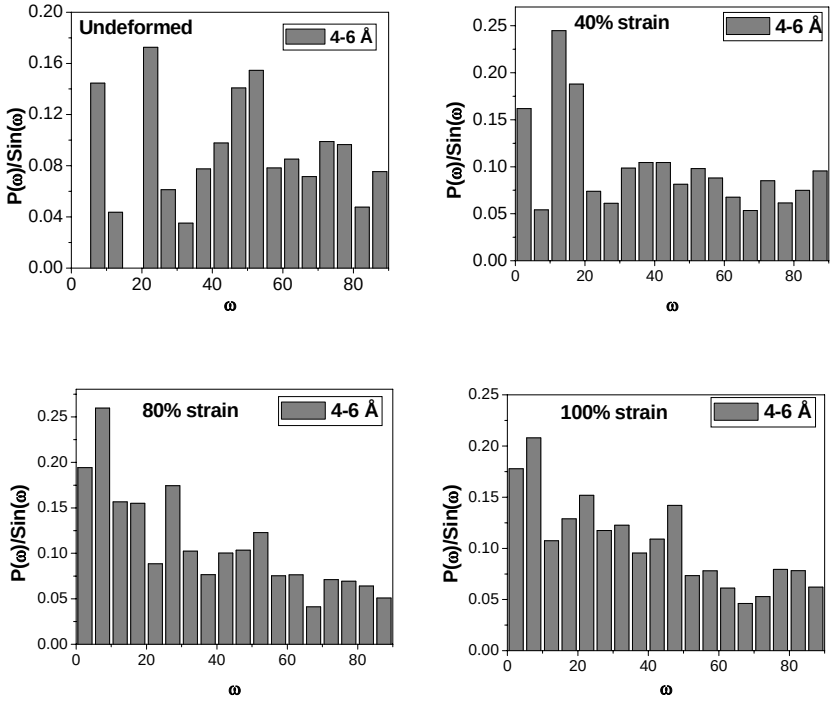

II. Packing of carbonate planes: 6-8 Å

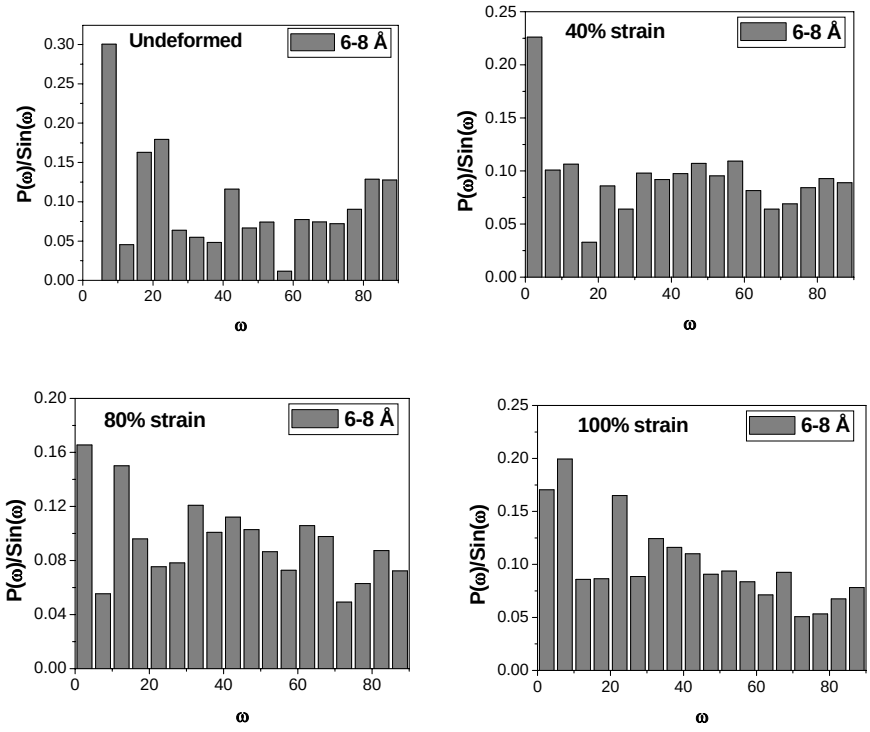

Figure 3A. Probability distribution of the intermolecular packing of carbonate planes in BPAPC samples as a function of deformation.

Synopsis

Molecular Modeling and Atomistic Simulations of the Structural and Optical Properties of Polycarbonates

Introduction

Molecular modeling techniques have proven to be a useful tool in the investigation of the physical properties of polymers. To judiciously and efficiently design materials, which have particular properties for specific applications, there is a need to understand the structural and dynamic behavior of polymer chains at the molecular level. Computer simulations assist in gaining an insight into the molecular and mesoscale structures and properties of polymers. Some of the physical properties of polymers at the macroscopic scale are also dictated by the structural aspects of single polymer chains and condensed polymer phases at the molecular length scales. Various computational modeling approaches such as molecular mechanics, molecular dynamics and Monte-Carlo simulations, have been applied to the study of polymers in order to determine their structure, conformations and physical properties. Quantum chemical calculations at different levels of accuracy have also been widely applied for determining the accurate geometry, conformation and energetics of relatively small fragments of polymer chains such as repeat units or monomers.

Optical properties of materials, especially polymers, are of importance in a variety of application areas including information storage systems and media.[1,2] Polymers are used as substrate material as well as memory layer in compact discs. As a material for magneto optical (MO) disc substrate, bisphenol A polycarbonate (BPAPC) is thought to be most suitable currently, because of its excellent thermal, mechanical and low hygroscopic properties. However, the large birefringence due to optical refractive index anisotropy of the phenyl rings in BPAPC renders the exact focus of the optical beam unsuitable for the purpose of reading and writing due to the anisotropic changes in the state of polarization of light in going through this material. The property “optical anisotropy” of polymer chains is, therefore, of considerable fundamental and practical relevance in providing an understanding of material behaviour and for the molecular design of materials with suitable properties. The chemical structure of the polymer chain repeat unit, conformations of the chain and the flow conditions which orient the chains during the processing of these materials, dictate their optical properties. Several experimental reports exist in literature where attempts have been made to lower the birefringence by structural modification of the bisphenol unit by various strategies. [3-5]

Conformational features of Bisphenol A Polycarbonate (BPAPC) have been the focus of considerable research since the pioneering work by Williams and Flory.[6] Various calculation methods have been utilized to investigate the conformational characteristics of BPAPC and the significant results have also been summarized.[7,8] The calculated chain dimensions of BPAPC from Rotational Isomeric State (RIS) models were in close agreement with the experimental values from light scattering and SANS measurements.[9-11] RIS models for various structural modifications of BPAPC were formulated from conformational energy calculations of the corresponding bisphenyl fragments neglecting torsional and coulombic interactions. The calculated

characteristic ratio of these polycarbonates (PC's) were insensitive to substitution of one or both of the methyl groups by either hydrogen atoms, phenyl rings or to substitution of the isopropylidene group by cyclohexyl group.[12,13]

The optical anisotropies (γ^2) of structural analogues as well as for BPAPC chains have been determined from Depolarized Rayleigh Scattering and electric birefringence experiments by Flory and co-workers.[14,15] The polarizability tensors of carbonate group and phenyl groups in BPAPC were deduced from the model compounds utilizing the Valence Optical Scheme (VOS). γ^2 calculated for BPAPC via the Rotational Isomeric State method using the derived polarizability tensors were in excellent agreement with the experimental values. Low-frequency DRS measurements by Floudas et al.[16] give results similar to those obtained from the earlier reports for BPAPC dilute solutions as well as for the bulk amorphous state, indicating only slight differences in this optical property between the single chain and the amorphous states. There are no reports in literature on theoretical as well as experimental studies on mean-squared optical anisotropy, $\langle\gamma^2\rangle$, of structurally modified polycarbonates.

Previous studies in literature on model compounds containing carbonate groups include ab initio calculations using a variety of basis sets such as STO-3G, HF-631G*, HF-631G**, 6-311G** and hybrid density functional theory (B3LYP, 6-311G** basis set) calculations in the gas phase.[17a-f] Polarizability anisotropies of a group of organic molecules dimethyl carbonate (DMC), methyl phenyl carbonate (MPC) and diphenyl carbonate (DPC) in solution in carbon tetrachloride were calculated by Sun and Mumby.[18] A direct approach that takes into consideration the solute molecular structure, liquid structure of the solvent and DFT techniques have been proposed to compute the apparent polarizabilities for molecules in dilute solution in non-polar solvents. Except for MPC and DPC, the results were in favorable agreement with the experimental data.

Simulations of structural properties of bulk amorphous BPAPC in the glassy as well as melt states have been reported.[19] The chain conformations in the bulk, radial distribution functions, static structure factor derived from simulations were compared with the experimental values. Bulk amorphous models have also been reported for BPCPC using atomistic simulations and for TMCPC via coarse-graining Monte-Carlo methods.[20-24] The scattering functions obtained from experiments were compared with those calculated from the generated bulk structures.

Although numerous experimental reports on birefringence of BPAPC and various structurally modified polycarbonates exists in literature,[25a-e] there have been no attempts till date on theoretical approaches for the estimation of this important property of polycarbonates. Stress optical coefficient of polyethylene melts have been determined via molecular dynamics and monte-carlo techniques.[26,27] The model used in both cases was relatively simple and reasonable agreement with the experimental data was obtained.

Objectives of the present work

1. To determine the conformational states and energetic information of model compounds of various structurally modified polycarbonates using force-field based energy minimization. To formulate the RIS models of these polycarbonates, by using the conformation and geometry derived from

conformational energy calculations and to calculate the unperturbed chain dimensions as a function of temperature and chain length.

2. To formulate a new methodology for the calculation of mean-squared optical anisotropy of structurally modified polycarbonates having two different types of substitution (a) cyclohexylidene group at the C_α carbon (b) methyl groups on the backbone phenyl rings. The parameters required for the calculation of the optical anisotropy of model analogues, monomer units as well as chains, will include the polarizability tensors of the constituent groups derived from experimental data and their geometry as obtained from force-field based conformational energy calculations, in each of these polycarbonates.
3. To determine the accurate geometry of the structural analogues of substituted polycarbonates by quantum chemical calculations. Polarizability tensors and optical anisotropies of the bisphenyl and carbonate fragments will be calculated from their corresponding energy optimized geometries.
4. To derive bulk amorphous models of structurally modified polycarbonates in the glassy state via detailed atomistic simulations. Structural properties of these amorphous models will be calculated and compared with available experimental data. Comparison between the different polycarbonates will be made in order to present the influence of chemical structure on the bulk properties.
5. To calculate the orientational optical birefringence of polycarbonates in the glassy state via atomistic simulations under a tensile load.

The thesis is organized into eight chapters as follows:

Chapter 1: Introduction

This chapter describes the application of various molecular modeling techniques for determining the conformationally dependent structural and optical properties of single chains and condensed amorphous phase of polymers. The literature status on the conformationally derived chain properties of polymers, studied using RIS theory will be presented. The detailed emphasis will be on the molecular modeling studies on polycarbonates till date.

Chapter 2: Scope and Objectives of the Present Work

The scope and objectives of the present thesis will be described in this chapter.

Chapter 3: Conformational Analysis, RIS models and Single Chain Properties of Structurally Modified Polycarbonates

This chapter describes the conformational features of BPAPC and structurally modified bisphenol polycarbonates studied using the PCFF force field by taking into consideration all possible intra and interatomic potential energy interactions. The polycarbonates with different chemical modifications include (1) cyclohexyl group at the C_α carbon, BPCPC (2) trimethylcyclohexylidene group at C_α, TMCPC, (3) cyclohexyl group at C_α and methyl groups on backbone phenyl rings, DMBPC (4) methyl groups on backbone phenyl rings, DMPC. The RIS models for these polycarbonates, formulated from the geometry, conformation and statistical weights will be developed. The conformational properties like the mean-squared end-to-end distance, radius of gyration, persistence length and characteristic ratio of polycarbonates will be presented. A comparison of the average

chain dimensions of these polycarbonates with respect to BPAPC will be given. The chapter will also present results on molecular dynamics calculations performed for a few of the structural moieties, to rationalize the some interesting unusual observations on the variation of chain dimensions for one of the polycarbonates. The influence of chemical structure on conformational properties is brought forth in this chapter.

Chapter 4: Optical Anisotropy of Structurally Modified Polycarbonates Having Cyclohexylidene and Methyl Substituents Using the Rotational Isomeric State Method

In this chapter, a new methodology for formulation of the polarizability tensors of polycarbonate molecular fragments will be described, which is applicable to substituted bisphenyl fragments, diphenyl carbonates and repeat units of various structurally modified polycarbonates having cyclohexylidene group at the C_α carbon and methyl groups on backbone phenyl rings. This theoretical approach utilizes polarizability tensors of constituent groups that have been derived from DRS measurements and the geometry from conformational energy calculations. The method is an extension of Flory's work on BPAPC. The optical anisotropy of bisphenyl and carbonate fragments, repeat units and single chains of structurally modified polycarbonates studied will be presented. The contribution of the various conformers towards the optical anisotropy is analyzed in detail. A critical evaluation of the various structural and conformational features responsible for lowering the optical anisotropy in structurally modified polycarbonates will be presented. A comparison of the calculated single chain optical anisotropy with the optical properties in the bulk state, for e.g. the stress optical coefficient in the glassy and melt states will be presented.

Chapter 5: Ab initio Calculations on Small Molecule Fragments of Structurally Modified Polycarbonates

This chapter will describe the results of quantum chemical calculations of model analogues of structurally modified polycarbonates using ab initio method. The optimized geometries of various bisphenyl and carbonate fragments of various structurally modified polycarbonates having cyclohexylidene group at the C_α carbon and methyl groups on backbone phenyl rings, calculated using HF/6-31G and HF/6-31G** basis sets will be presented. The polarizability tensors and optical anisotropy calculated from the optimized geometries of these fragments will be given. A comparison will be made between the optical anisotropies of bisphenyl and carbonate fragments calculated using the ab initio method and those calculated using the experimental group polarizability tensors via the VOS scheme.

Chapter 6: Detailed Atomistic Simulations of Structurally Modified Polycarbonates in the Glassy State

This chapter describes the generation of bulk amorphous structures of structurally modified polycarbonates in the glassy state via atomistic Monte-Carlo and molecular dynamics simulations in the NVT ensemble at 300 K. The polycarbonates studied here include BPAPC, BPCPC, TMCPC, DMBPC and DMPC. The conformations of polycarbonate chains in the bulk obtained from these simulations will be compared with the single chain conformational statistics derived using the RIS method, the results of which are presented in chapter 3. The

calculated cohesive energy densities and solubility parameters of these amorphous polycarbonates will also be presented. Also the radial distribution functions and the static structure factors will be given. Free volume distributions and ring plane orientations of these polycarbonates will be presented. The detailed interplay between the chemical structure of the polycarbonate, its packing in the bulk state, and the interatomic energy potentials will be brought forth.

Chapter 7: Atomistic Simulations of the Orientational Birefringence of Polycarbonates in the Glassy State

This chapter will describe a new theoretical approach based on fully atomistic molecular simulations, for the calculation of the orientation dependent birefringence of amorphous polycarbonates in their glassy state. The methodology uses an unstretched (unstressed or unstrained) starting sample of the polymer and performs repeated sequences of uniaxial extension in the tensile mode followed by molecular mechanics relaxation. The strain is applied till the inception of the plastic deformation. The birefringence and the instantaneous sample engineering stress at every strain step during the computer simulated creep experiment would be the outcomes of this simulation procedure. Results of the birefringence as a function of stress and strain and the stress optical coefficient will be presented and compared with available experimental data from literature. The accompanying molecular scale structural changes and their influence on the average orientation of the polymer chain segments will be discussed in relation to the birefringence. The effect of the fundamental optical properties of the molecular groups in the polymer chain, on the birefringence properties, in conjunction with the orientational effects of the polymer chain segments, will be understood and presented in detail.

Chapter 8: Summary and Conclusions

This chapter summarizes the results of the present thesis. The most important and significant conclusions from this work will be highlighted.

Appendix

Appendix – I: Formulation of the polarizability tensor and calculation of optical anisotropy of substituted bisphenyl fragment will be described in detail. A sample calculation will be given.

Appendix – II: Optical anisotropy per repeat unit in polycarbonate chain considering lower number of rotational states per bond in the repeat unit will be presented.

Appendix – III: Optical anisotropy per repeat unit, which is averaged over the symmetric conformers in each polycarbonate, will be presented.

Appendix – IV: Mean potential energies, individual energy components for each of the 10 amorphous cells in the case of all five polycarbonate will be given. This section will also present information on solubility parameter and chain dimensions of the all the equilibrated amorphous structures of the polycarbonates.

References

1. Kampf, G.; Mergel, D. In *Encyclopedia of Chemical Technology*; Howe-Grant, M., Ed.; John Wiley & Sons: New York, 1995; Vol. 14, p 277.
2. Mills, N. J. In *Encyclopedia of Polymer Science and Engineering*; Mark, H. F.; Bikales, N. M.; Overberger, C. G.; Menges, G., Eds.; John Wiley & Sons: New York, 1987; Vol. 10, p 493; Jones, R. S.; Kuder, J. E. In Supplement volume, p 554.
3. Schmidhauser, J.; Sybert, P. D. In *Handbook of Polycarbonate Science and Technology*, Legrand, D. G., Bendler, J. T., Eds.; Marcell Dekker Inc.: New York, 2000, p 73.
4. Kampf, G.; Freitag, D.; Fengler, G.; Sommer, K. *Polymers for Advanced Technologies* 1992, 169-178.
5. Werumeus Buning, G. H.; Wimberger Friedl, R.; Janeschitz-Kreigl, H.; Ford, T. M. In *Integration of Fundamental Polymer Science and Technology-2*; Lemstra, P. J., Kleintjens, L. A., Eds.; Elsevier: London, 1988; p 405.
6. Flory, P. J. *Statistical Mechanics of Chain Molecules*; Interscience: New York, 1969
7. Mattice, W. L.; Suter, U. W. *Conformational Theory of Large Molecules;* John Wiley & Sons: New York, 1994, p. 240.
8. Rehahn, M.; Mattice, W. L.; Suter, U. W. *Adv. Polym. Sci.* 131/132, 1995, p. 109.
9. Berry, G. C.; Nomura, H.; Mayhan, K. G. *J. Polym. Sci. A-2.* **1967**, *5*, 1.
10. de Chirico, A. *Chim. Ind.* **1960**, *42*, 248
11. Ballard, D. G. H.; Burgess, A. N.; Cheshire, P.; Janke, E. W.; Nevin, A.; Schelten, J. *Polymer* **1981**, *22*, 1353.
12. Sundararajan, P. R. *Macromolecules* **1989**, *22*, 2149.
13. Sundararajan, P. R. *Macromolecules* **1993**, *26*, 344.
14. Erman, B.; Marvin, D. C.; Irvine, P. A.; Flory, P. J. *Macromolecules* **1982**, *15*, 664-669.
15. Erman, B.; Wu, D.; Irvine, P. A.; Marvin, D. C.; Flory, P. J. *Macromolecules* **1982**, *15*, 670-673.
16. Floudas, G.; Lappas, A.; Fytas, G.; Meier, G. *Macromolecules* **1990**, *23*, 1747-1753.
17. (a) Laskowski, B. C.; Yoon, D. Y.; McLean, D.; Jaffe, R. L. *Macromolecules* **1988**, *21*, 1629. (b) Sun, H.; Mumby, S. J.; Maple, J. R.; Hagler, A. T. *J. Phys. Chem.* **1995**, *99*, 5873. (c) Bendler, J. T. *Comput. Theor. Polym. Sci.* **1998**, *8*, 83. (d) Meyer, H.; Hahn, O.; Muller-Plathe, F. *J. Phys. Chem. B* **1999**, *103*, 10591. (e) Montanari, B.; Ballone, P.; Jones, R. O. *Macromolecules* **1999**, *32*, 3396. (f) Dybal, J.; Schmidt, P.; Baldrian, J.; Kratochvil, J. *Macromolecules* **1998**, *31*, 6611.
18. Sun, H.; Mumby, S. *J. Chem. Phys*. **1996**, *104*, 1018.
19. Ballone, P.; Montanari, B.; Jones, R. O.; Hahn, O. *J. Phys. Chem. A* **1999**, *103*, 5387-5398 and references cited therein

20. Lamers, C.; Scharpf, O.; Schweika, W.; Batoulis, J.; Sommer, K.; Ritcher, D. *Physica B* **1992**, 180&181, 515-518.
21. Paul, W.; Pistoor, N. *Macromolecules* **1994**, *27*, 1249-1255.
22. Tschop, W.; Kremer, K.; Batoulis, J.; Burger, T.; Hahn, O. *Acta Polymer* **1998**, *49*, 61-74,
23. Tschop, W.; Kremer, K.; Hahn, O.; Batoulis, J.; Burger, T. *Acta Polymer*, **1998**, *49*, 75-79,
24. Eilhard, J.; Zirkel, A.; Tschop, W.; Hahn, O.; Kremer, K.; Scharpf, O.; Richter, D.; Buchenau, U. *J. Chem. Phys*. **1999**, *110*, 1819-1830
25. (a) Wimberger Friedl, R.; Schoo, H. F. M.; De Bruin, J. G. (U.S. Philips Corporation) U.S. Patent 5,424,389, June 13, 1995. (b) Shirouzu, S.; Shigematsu, K.; Sakamoto, S.; Nakagawa, T.; Tagami, S. *Jpn. J. Appl. Phys*., **1989**, *28*, 801-803. (c). Davis, G. C.; Caruso, A. J.; Wetzel, J. R.; Hariharan, R.; Wisnudel, M. B. (General Electric Company) U.S. Patent 6,001,953, December 14, 1999. (d) Toshimasa, T. I.; Kuniyuki, H. M.; Tatsumi, H. I. (Teijin Chemicals Ltd.) U.S. Patent 5,633,060, May 27, 1997. (e) Shigematsu, K.; Shirouzu, S.; Sakamoto, S.; Suzuki, T. (Idemitsu Kosan Company) Eur. Patent 0312 860 A2, April 26, 1989.
26. Gao, J.; Weiner, J. H. *Macromolecules* **1994**, *27*, 1201-1209
27. Mavrantzas, V. G.; Theodoru, D. N. *Comput. Theor. Polym. Sci*. **1998**, *10*, 1-13.